Dissertation

Design and Development of New Sensitive Materials in Fluorescence pH Sensors

DI Daniel Aigner

2014

Zur Erlangung des akademischen Grades
„Doktor der technischen Wissenschaften“
eingereicht an der
Technischen Universität Graz

Betreuer

Univ.-Prof. Dipl.-Chem. Dr.rer.nat Ingo Klimant
Institut für Analytische Chemie und Lebensmittelchemie
Technische Universität Graz

EIDESSTATTLICHE ERKLÄRUNG

Ich erkläre an Eides statt, dass ich die vorliegende Arbeit selbstständig verfasst, andere als die angegebenen Quellen/Hilfsmittel nicht benutzt, und die den benutzten Quellen wörtlich und inhaltlich entnommenen Stellen als solche kenntlich gemacht habe. Das in TUGRAZonline hochgeladene Textdokument ist mit der vorliegenden Dissertation identisch.

_____ _____

Date Signature

“I just can’t believe that it’s over”

James Blunt

Danksagung

Liebe Leute, liebe (Ex-)Büro- und AG-Kollegen, danke, Ihr wart das großartigste Arbeitsumfeld das ich mir vorstellen kann und Ihr wart wahrscheinlich der wichtigste Grund warum ich fast jeden Tag in den letzten vier Jahren zur Arbeit gekommen mit dem Gefühl – super mich dabei so gut fühlen zu können und so eine Gaude zu haben. Egal wie mein weiteres Leben verläuft, ich werde diese Jahre immer in glücklicher Erinnerung behalten.
Lieber Ingo, jemanden mit solchen fachlichen und menschlichen Qualitäten zum Chef zu haben wie Dich war sicher einer der Hauptgründe warum die letzten Jahre eine tolle Zeit für mich waren. Danke Sergey für deine unermüdliche Energie und große Hilfsbereitschaft ohne die ich wohl kaum hätte so produktiv hätte sein können.
Ein ganz besonderer Dank gebührt meinem privaten Umfeld das mir die Kraft gegeben hat, die vergangenen Jahre so gut zu meistern. Danke Lisa, ich bin glücklich über jeden Tag den ich mit Dir verbringen darf. Ich danke auch meinen Eltern und dem Rest meiner Familie, es ist schön Euch zu haben und mich immer auf Euch verlassen zu können.

Kurzfassung

Fluoreszenzbasierte pH-Sensoren werden für die zahlreichen Anwendungen in Forschung und Industrie, für die eine verlässliche pH-Messung benötigt wird, zunehmend attraktiver. Strategien für die Entwicklung leistungsfähiger Sensoren sind daher gefragt. In dieser Arbeit werden neue pH-Sensoren vorgestellt, die auf photoinduziertem Elektronentransfer (PET) beruhen. Sie beruhen auf Funktionalitäten, die Fluoreszenzlöschung durch PET nur bei basischem pH verursachen, wenn sie in ihrer deprotonierten Form vorliegen („PET-Gruppen“). Das PET-Konzept ist hochflexibel, wie an den verschiedenen Klassen von fluoreszenten Indikatorfarbstoffen (Perylen Bisimide, Rhodamine, Diketopyrrolo[3,4-c]pyrrole), PET-Gruppen (Amine, Phenolate) sowie Sensormaterialien (verschiedene organische Polymere sowie Silica werden zur Immobilisierung verwendet) und -formaten (Schichten und Partikel) ersichtlich ist. Spektraleigenschaften und Messbereich können durch Auswahl dieser Komponenten einfach eingestellt werden. Phenolate können auch Farbstoffe löschen die von Aminen unberührt bleiben und diese daher für die pH-Messung einsetzbar machen. Auch ein im Nahinfrarotbereich emittierender ((>700nm, Anregung bei ≈650nm möglich) Sensor der auf einem 1-Aminoperylen Bisimid basiert wird präsentiert. Darüber hinaus werden zwei Konzepte für die kovalente Bindung des Indikators an die Immobilisationsmatrix vorgestellt und die Wichtigkeit dieser Bindung wird experimentell belegt. Schließlich wird die praktische Anwendbarkeit der Sensoren anhand von Imaging sowohl in lebenden Zellen als auch in mikrofluidischen Systemen gezeigt.

Abstract

Fluorescence pH-sensors are becoming increasingly attractive tools for the abundant scientific and industrial applications requiring reliable pH-measurement and monitoring. Hence, tools useful to the design of high-performance sensors are clearly needed. In this thesis, new pH-sensors based on photoinduced electron transfer (PET) are presented. Those are accessible simply by attaching suitable functionalities (PET groups) capable of quenching fluorophores only in the deprotonated form. The versatility of the concept is demonstrated employing various classes of fluorescent indicator dyes (perylene bisimides, rhodamines, diketopyrrolo[3,4-c]pyrroles), PET groups (amines, phenoxides) and sensor matrices (several organic polymers and silica are used for immobilisation) and formats (layers and beads). It is shown how spectral properties and sensitive pH-range can be easily adjusted by the tools presented in this work. Phenoxide PET groups enable higher flexibility as they can effectively quench fluorophores which are not quenched by amines, as is pointed out. A sensor based on a 1-aminoperylene bisimide excitable in the deep red spectral range (≈ 650 nm) and emissive in the near infra-red (> 700 nm) is presented. Furthermore, two concepts for covalent grafting of the pH-indicator to the immobilisation matrix are successfully employed and the importance of covalent grafting is experimentally confirmed. Finally, practical applicability of the new sensors is exemplified not only by imaging in microfluidics, but also by live cell imaging.

TABLE OF CONTENTS

INTRODUCTION 1

Scope of this Thesis 2
Background 3
Basics 3
Luminescence 3
Fluorescence Sensors 4
pH-measurement 7
Fluorescence pH-sensors: Principles 8
Basics 8
Scope for Application 10
Referencing Techniques 10
Sensor Fabrication 12
Related Fluorescence Sensors for Other Analytes 13
State-of-the-art Fluorescence pH-sensors 14
Luminescent Probes 14
Immobilisation Matrices 20
Objectives: Design of High-performance pH-sensors 20
High-performance Fluorophores 20
Designing New High-performance pH-probes 22
Covalent Probe Coupling 23
Excitability at Long Wavelengths 23

RESULTS 25

NEW FLUORESCENT PERYLENE BISIMIDE INDICATORS – A PLATFORM FOR BROADBAND PH OPTODES 27
Preface to Chapter 1 28
New Fluorescent Perylene Bisimide Indicators – a Platform for Broadband pH Optodes 29
Introduction 29
Experimental 31
Results and Discussion 33
Conclusion 42
Acknowledgement 43
Supplementary Information 44

NOVEL NEAR INFRA-RED FLUORESCENT PH-SENSORS BASED ON 1-AMINOPERYLENE BISIMIDES COVALENTLY GRAFTED TO POLY(ACRYLOYLMORPHOLINE) 47
Preface to Chapter 2 48
Novel Near Infra-red Fluorescent pH-Sensors Based on 1-Aminoperylene Bisimides Covalently Grafted to Poly(acryloyl-morpholine) 49
Supplementary Information 54

NEW FLUORESCENT PH-SENSORS BASED ON COVALENTLY LINKABLE PET RHODAMINES 65
Preface to Chapter 3 66
New Fluorescent pH-Sensors Based on Covalently Linkable PET Rhodamines 67
Introduction 67
Experimental 68
Results and Discussion 72
Conclusion 78

Acknowledgement ... 79
Supplementary Information ... *80*

FLUORESCENT MATERIALS FOR PH SENSING AND IMAGING BASED ON NOVEL 1,4-DIKETOPYRROLO-[3,4-C]PYRROLE DYES ... 83
Preface to Chapter 4 ... *84*
Fluorescent Materials for pH Sensing and Imaging Based on Novel 1,4-Diketopyrrolo-[3,4-c]pyrrole Dyes ... *85*
Introduction ... 85
Results and Discussion ... 86
Conclusions ... 94
Experimental ... 94
Acknowledgement ... 97
Supplementary Information ... *98*

ENHANCING PHOTOINDUCED ELECTRON TRANSFER EFFICIENCY OF FLUORESCENT PH-PROBES WITH HALOGENATED PHENOLS ... 101
Preface to Chapter 5 ... *102*
Enhancing Photoinduced Electron Transfer Efficiency of Fluorescent pH-probes with Halogenated Phenols ... *103*
Introduction ... 103
Results and Discussion ... 105
Conclusion ... 109
Experimental ... 110
Acknowledgement ... 114

PERYLENE BISIMIDES FOR FLIM-BASED PH MEASUREMENTS IN 2D AND 3D CELL MODELS .. 115
Preface to Chapter 6 ... *116*
Perylene Bisimides for FLIM-based pH Measurements in 2D and 3D Cell Models ... *117*
Introduction ... 117
Results and Discussion ... 119
Conclusion ... 126
Experimental ... 127
Acknowledgement ... 130
Supplementary Information ... *131*

CONCLUSION AND OUTLOOK ... 133

APPENDIX ... 135

References ... *136*
Structure Analyses ... *152*
Chapter 1 ... 152
Chapter 2 ... 156
Chapter 3 ... 168
Chapter 4 ... 175
Chapter 5 ... 180
Chapter 6 ... 193

Part A

Introduction

Scope of this Thesis

pH, as one of the most fundamental parameters in medical research and diagnostics, life sciences, industrial process control, food industry and environmental science and monitoring, is an analyte of high social relevance. There is a high demand for effective measurement devices meeting the requirements given by the highly diverse applications in which pH plays a key role. Even though potentiometric pH-sensors such as the pH glass electrode are well established and feature convincing performance in many respects, fluorescence pH-sensors offer numerous advantages concerning miniaturisation, high sample-throughput, cost effectiveness or measurement with minimal contact to the sample. They clearly have a lot of potential for making up an attractive alternative in many applications. Furthermore, they enable imaging applications which have given rise to extensive application in biochemical and biomedical research.
Although numerous pH-probes and sensors have been presented, they are based on a limited number of fluorescent dye classes and only a few are potentially useful for long-term stable, high-resolution measurement at long excitation and emission wavelengths. This work aims on the design and development of new pH-sensors fulfilling those requirements. For this purpose, most importantly, a highly photostable pH-probe possessing bright fluorescence in the deep red or near infra-red range is needed. Photoinduced electron transfer (PET) is taken advantage of as it allows the preparation of pH-probes based on many fluorescent dye classes which are not intrinsically sensitive to pH, thus greatly extending the selection of available probes. PET is induced by attaching a suitable functional group ("PET group") the pK_A-value of which determines the sensitive pH-range of the resulting sensor. It will thus be evaluated as a tool for designing sensors with spectral characteristics and pH-ranges tuneable to match the range of interest for any particular application. Cross-sensitivity to ionic strength and narrow sensitive range are the main practical limitations of optical pH-sensors. PET-based concepts are expected to provide optimal premises for overcoming those limitations owing to their high flexibility and will be tested in this respect. Finally, covalent coupling of the pH-probe to the immobilisation matrix ("sensor bulk") is anticipated to improve the long-term performance of a pH-sensor. Grafting strategies will therefore be developed and evaluated.

Background

Basics

Luminescence

Luminescence is a powerful tool that allows detailed investigation of physicochemical and biological systems, from the macroscopic point of view down to the molecular level [1,2]. Because it can provide information with a high spatial and temporal resolution, it is suitable for mapping and imaging very different samples, as well as for following processes down to the nanosecond time scale. There is a large amount of information included in the luminescence of a sample which includes luminescence intensity, its spectral characteristics, its polarisation and its evolution over time. Therefore, luminescent probes are very flexible and can be useful for probing several parameters at once. Luminescence can be influenced by a large number of parameters such as sample composition, temperature, polarity, viscosity or its electrochemical properties. Though that enables all of those parameters to be probed by luminescence, it naturally also calls for a careful design of luminescence probes and experiments. Otherwise, the information given by them will be blurred and become misleading.

Luminescence is defined as the emission of light by an electronically excited system which, in turn, becomes partially or fully relaxed (figure 1). Luminescence can be emitted by many different species including organic and bioorganic molecules, organometallic complexes, atoms or inorganic crystals. This thesis will predominantly focus on organic luminophores. In those, luminescence is associated with relaxation from the first or second electronically excited state to the ground state. Since their electronic excitation is usually accompanied by vibrational and rotational excitation, luminescence emission is characterised by wide spectra, rather than narrow lines.

Fluorescence is a particular type of luminescence in which the excited state has been reached by the absorption of light and relaxation is a singlet-singlet transition. In phosphorescence, relaxation is a triplet-singlet transition. Because fluorescence is by far most important to this thesis, the term luminescence will from now on only be used for processes involving triplet-singlet relaxation. Notably, luminescence does not necessarily require the presence of light. Electronic excitation can be induced by electric fields [3] – this is of high importance in organic electronics – or can be the result of (bio)chemical reactions, which has not only been taken advantage of by nature (glow-worms, deep sea flora and fauna) but is also of increasing interest to luminescence research and technology [4].

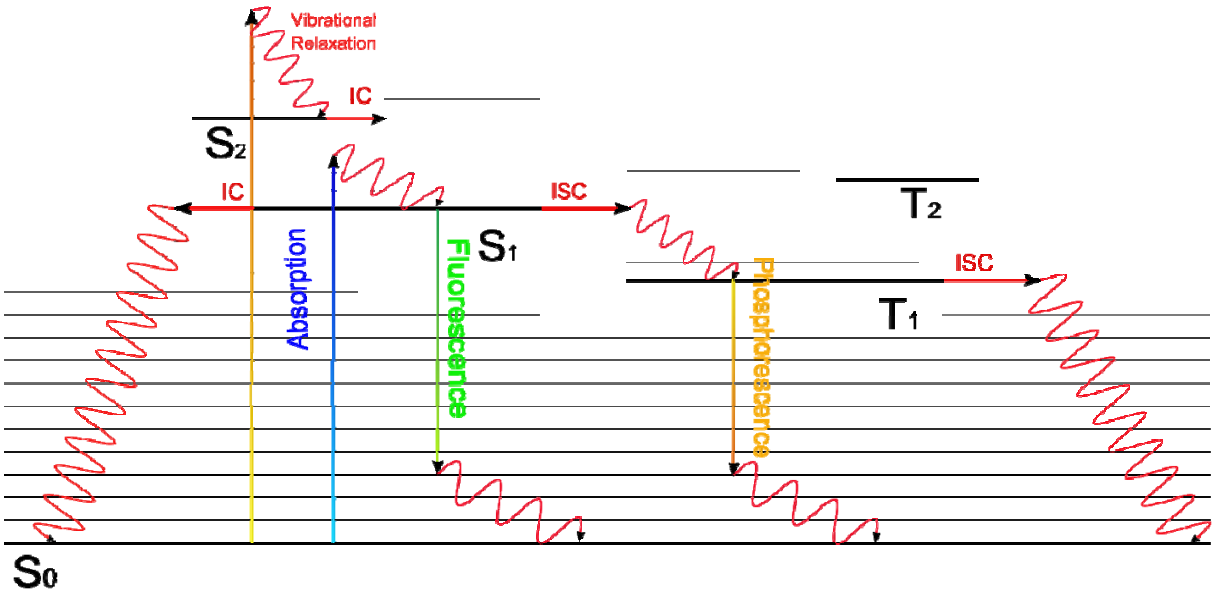

Figure 1: Jablonski diagram, visualising absorption of a molecule and its deactivation. S_0, S_1, S_2 – ground state, first and second excited states (all singlet); T_1, T_2 – first and second excited states (both triplet); IC – internal conversion, the vibrational deactivation effective without photon emission; ISC - intersystem crossing, the transition between states of unlike multiplicity.

Fluorescence Sensors

Sensors are devices permanently capable of generating a signal containing information about a sample when in contact to it. Chemical sensors are most frequently associated with probing sample composition, detecting particular chemical species (ions, molecules) by molecular recognition, though some of them have been designed to measure physical parameters such as temperature, polarity or viscosity. When biological components are detected, the sensor is referred to as biosensor [5]. Ideally, the sensors can be read out in real time, right where the sample is. This is in contrast to many methods in instrumental analytics in which samples are taken and measured in a different place later on, often after performing sample processing. Chemical sensors and biosensors are used on-line or in-line in fields and applications of high social and economic relevance such as process control in food and pharmaceutical industries or environmental monitoring (waste and sewage treatment, pollution control). On the other hand, diagnostics often intrinsically involve sample taking and require sample preparation to some extent. There, sensors help realising the high sample throughput demanded by social needs, featuring high compatibility with automatisation and miniaturisation techniques.

The most significant characteristics of a sensor are:

- Selectivity: Sensors are usually intended to be sensitive exclusively to a single analyte, although in some cases they are designed to measure a few analytes simultaneously. In reality, there always are unwanted cross-sensitivities, yet to a very different extent.
- Sensitivity: Defined as the increase of the generated signal with increasing analyte concentration, it is probably the most crucial parameter affecting working range, detection limit and measurement resolution. Though high sensitivity is in general

desirable and insufficient sensitivity is a highly abundant bottleneck, there are numerous applications calling for the measurement of high analyte concentrations, making systems with tuneable sensitivity most powerful.

- Reversibility: A sensor should not consume the analyte it is measuring and it should feature reversible response – devices with irreversible response are often called dosimeters.
- Response time: Fast response time is crucial for performing real-time analysis. While some applications demand fast response, it may be less critical for others so that optimisation of the response time becomes unnecessary and may compromise other benefits of the sensor.
- Stability: The measurement signal should be as stable as possible. Stability when in use is quantified by the operational life, the time after which a sensor no longer performs reliably and needs to be replaced. The shelf life specifies the time a sensor remains usable upon storage.

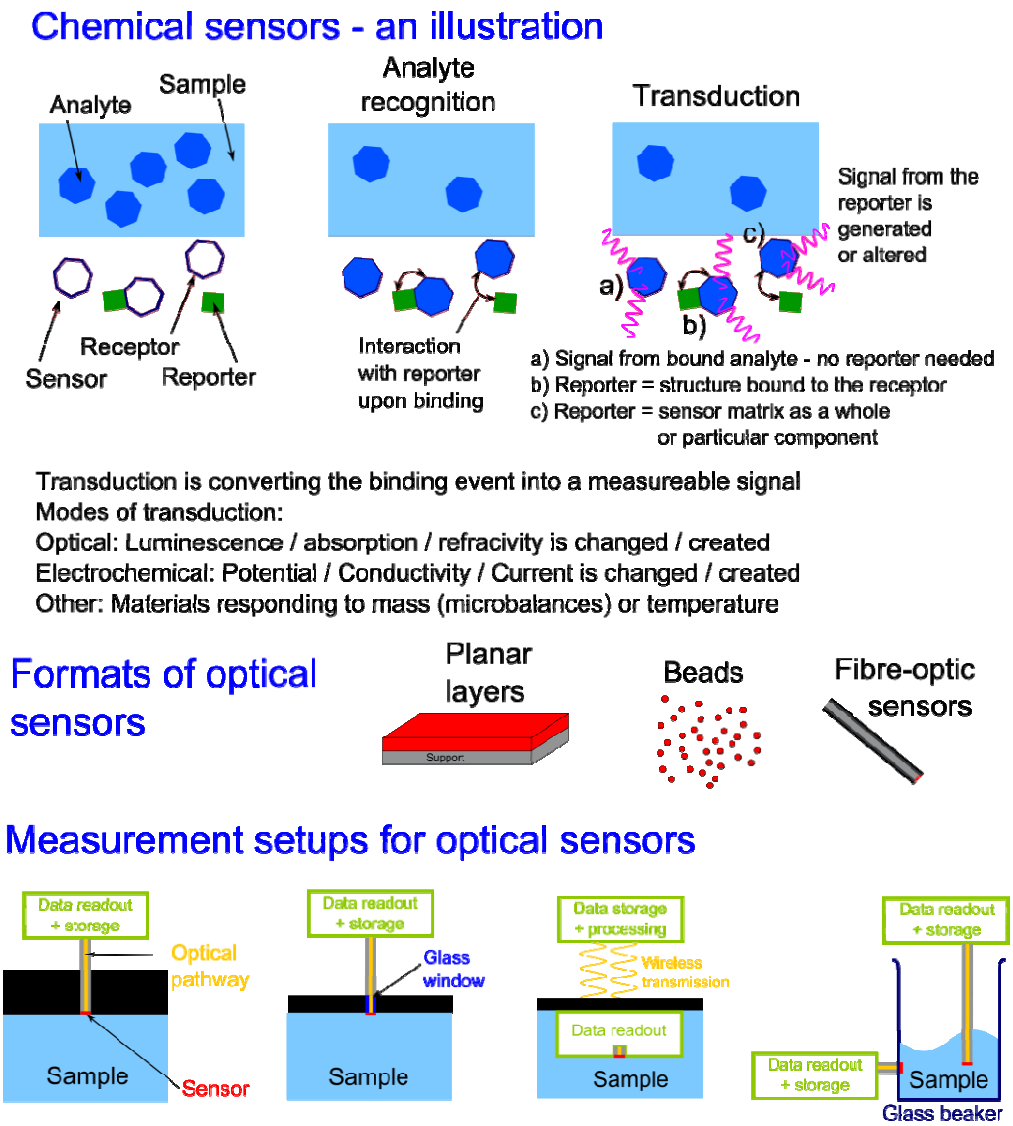

Figure 2: Schematic illustration of the basic principles of chemical sensing (top), formats of sensors and measurement for optical sensors (bottom).

In a chemical sensor, a binding event between the analyte and the sensor material always takes place (figure 2). The component responsible for analyte recognition is called receptor. The binding event then needs to be reported, that is, a measurable signal is generated or modified. That process is called transduction. In optical sensors, transduction is based on the change of absorptive, luminescent or refractive properties of a sensor component or the analyte itself [6].
Optical sensing constitutes, alongside with electrochemical sensing, one of two predominant concepts in chemo- and biosensors. Fluorescence sensing has become the most widely employed optical technique in optical chemical sensors owing to its high sensitivity and ease of measurement (figure 3) – fluorescence can be excited in a spot and measured in the same spot with a single fibre, separating excitation and emission light with optical filters. Absorption-based sensors [7] feature lower sensitivity but can be highly robust and are ideal when response needs to be visible with the eye. In biosensors, analyte recognition is often reported by fluorescent labels, though alternatives labelling techniques employing inorganic nanoparticles [8] are widely employed as well and label-free techniques - for instance based on refcratometry [9] or Raman scattering [10] - have become very popular.
Apart from their flexibility mentioned previously, fluorescence sensors offer a higher potential for miniaturisation and low-cost fabrication in comparison to electrochemical sensors, making prospects for more extensive future application bright. As of today, fluorescence sensors for molecular oxygen have been replacing their electrochemical counterparts in process and environmental monitoring. Optical sensors are applied in analysis of blood gas, pH and electrolytes, though electrochemical techniques remain popular in that field. Fluorescence detection plays an important role in commercially relevant tests for biological components such as hormones, enzymes and other proteins, for instance in the form of enzyme-linked immunosorbent assays (ELISA).

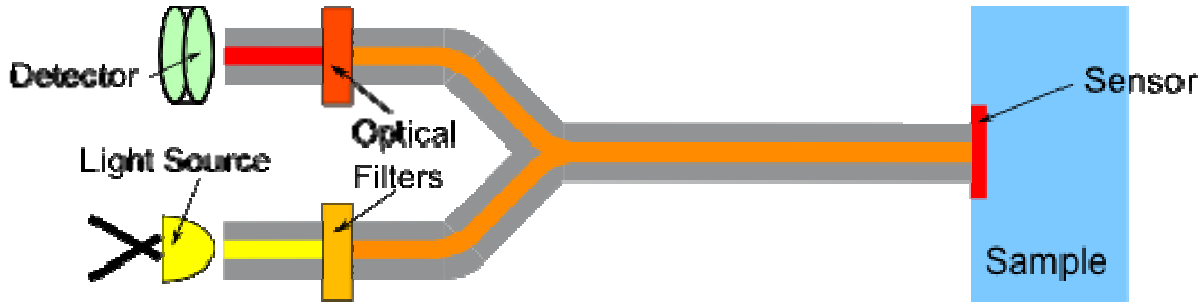

Figure 3: Schematic layout of a fibre-optic sensor.

The term fluorescence sensor can refer to both the sensitive material itself and to the entire measurement device based on it. In this thesis, “sensor” will generally refer to the sensitive material (figure 2). The fluorescence of the sensitive material is modulated upon interaction with the analyte in terms of fluorescence intensity, wavelength or decay time. Its readout (figure 3) requires an excitation source (e.g. a light-emitting diode, LED), the guidance of light to and from the sensitive material (usually accomplished by optical fibres), optical modules such as filters or dichroic mirrors and a detector (e.g. a photodiode). In contrast to electrochemical sensors, readout of the sensitive material does not necessarily require any physical contact, which can be highly beneficial with regard to sample perturbation and to the robustness of the readout unit required, for instance when measuring sterile samples or in applications involving high temperature, pressure or a chemically aggressive environment.

pH-measurement

pH – defined as the negative decadic logarithm of the H^+ ion activity in an aqueous solution - is one of the most fundamental analytes that exist. Because of its vital importance to biological systems, it is highly important in medicine, bioanalytics and life sciences, as well as in environmental and marine sciences. It is also a crucial parameter for many chemical, biochemical and physical processes that take place in aqueous systems and therefore more than relevant to biotechnological and chemical process control.
In human blood serum, even small deviations from the normal pH range (7.35 – 7.45) can be associable with severe crisis or illness. Examples are renal disease, hypoxia, intoxication or diabetes [11]. In cells, pH is inhomogeneous but strictly regulated [12]. The normal function of organelle pH regulation and the maintenance of intracellular pH gradients are crucial for vital processes such as oxidative phosphorylation in mitochondria or sorting and degradation of unneeded matter in endosomes and lysosomes. Because ATP-production in mitochondria by ATP-synthase requires a pH-gradient with respect to the more acidic cytosol, cell respiration is severely troubled in the case of pH-dysregulation. The normal function of many enzymes requires a certain pH. Those include the hydrolysing lysosomal enzymes which in case of abnormal pH would fail to break down metabolic waste or start digesting the cell itself. pH also plays an important role in many other cell physiological processes including proliferation, the regulation of ion transport and apoptosis. Many biochemical processes generate or consume acidic or basic compounds, which is often taken advantage of in enzyme activity screening or generally in biochemical assays. In environmental and marine science and analytics, pH can provide information about the level of pollution and the viability of an ecosystem. The presence of certain (micro)organisms is often accompanied by distinctive pH-changes, and a variation in pH can be an early sign for a fundamental change. In biotechnology, the proper function of organisms or enzymes commonly requires a certain pH which has to be carefully monitored and maintained. Considerable amounts of acidic or basic components can be formed in biotechnological fermentations or industrial chemical processes, calling for continuous pH-control.
pH is most frequently measured by the pH glass electrode, an ion-selective electrode used as potentiometric sensor. The potential of a silver / silver chloride electrode, which is in contact to the sample over a thin glass membrane, is measured. Protons cannot permeate the membrane, but bind to its porous surface which causes a migration of the natrium ions in the glass bulk and results in a linear decrease of the surface potential with increasing pH. Another silver / silver chloride electrode, which is in contact to the sample over a diaphragm and thus of pH-independent potential, is used as reference. Both electrodes are usually incorporated into a single glass body. The pH glass electrode is one of the best established chemical sensors due to its large working range of at least pH 0 to 12, its predictable and well-investigated susceptibility to cross-interferents and its accuracy. Drawbacks are in the fragility of the electrode and in the difficulty of miniaturisation. Safety concerns arise from the possible breaking of the glass body during in-vivo diagnostics or application in food industry, and small-scale or high-throughput applications are limited by relatively large size. Another frequently used electrochemical pH-sensor is the conductometric ion-sensitive field-effect transistor (ISFET). In contrast to a standard field-effect transistor, the gate (contact between source and drain) is not metallic but involves a thin layer of porous Si_3N_4, Al_2O_3 or Ta_2O_5 the conductivity of which is pH-dependent due to hydrolysis of surface groups. ISFETs can be manufactured in small dimensions by processes well-established in

semiconductor industry and have thus potential of overcoming the limitations of the glass electrode. However, they still require a reference electrode for readout. The usage of small semiconductor elements allows bypassing the need of glass-made reference electrodes which would bring the same limitations valid for the pH glass electrode but compromises the stability of sensor performance which makes frequent re-calibration necessary.
Despite the strong performance of electrochemical pH-sensors, fluorescence sensors offer a number of advantages relevant to many applications. They enable measuring without any direct contact to the sample, can be produced at lower cost and are easier to miniaturise which makes them more attractive for high-throughput applications. Furthermore, they are applicable in the presence of electromagnetic fields and, importantly, they enable imaging applications. Drawbacks include their non-linear response curve and their sensitive range which is often limited to 3 pH-units, though that can be accompanied by a higher resolution within that range. Moreover, like all optical sensors they measure proton concentration instead of activity which results in a cross-sensitivity to ionic strength, though that can be minimised by optimising the fluorescent sensor material, reducing its charge.

Fluorescence pH-sensors: Principles

Basics

Fluorescence pH-sensors in principle include no more than two components: a fluorescent pH-probe, sometimes called pH-indicator, and an immobilisation matrix. Most frequently, the pH-probe is a small organic molecule (i.e. a fluorescent dye), but fluorescent polymers or inorganic particles have also been employed. State-of-the-art pH-probes will be discussed in detail in later on. Obviously, the pH-probe needs to undergo a modulation in fluorescence quantum yield, spectral shape or decay time when exposed to variations in pH. That is associated with the equilibrium between an acidic (protonated) and a basic (deprotonated) form. As a result of the Henderson-Hasselbalch equation, pH-sensitivity is highest if pH = pK_A but in general limited to pH = $pK_A \pm 1.5$.

$$pH = pK_A + log\frac{[B^-]}{[HB]} + log\frac{f_{B^-}}{f_{HB}} - log\, a_{H_2O}$$ Equation 1

$[B^-]$,[HB] Concentrations of the acidic form HB and the basic form B^- (M)
f_{B^-},f_{HB} Activity coefficients of both forms
a_{H2O} Activity of water (constant)
$\log(f_{B^-}/f_{HB})$ quantifies the cross-sensitivity to ionic strength (zero if negligible)

Equation 1 provides the basis for the sigmoidal calibration of optical pH-sensors:

$$I = \frac{I_{\min} - I_{\max}}{1 + e^{(pH - pK_A)/dx}} + I_{\max}$$ Equation 2

I	Measured fluorescence intensity
I_{max}	Numerical coefficient expressing maximal
I_{min}	Numerical coefficient expressing minimal intensity
pK_A	Numerical coefficient expressing the (apparent) pK_A value (point of inflection)
dx	Numerical coefficient expressing the width of the sensitive range

The immobilisation matrix is to provide an environment in which the pH-probe is finely and homogeneously distributed without aggregating. Organic polymers are most common, but sol-gels or other silicon based materials have also been used. It should feature suitable water uptake to make sure the sensor equilibrates to sample pH as fast as possible. Beyond facilitating a suitable probe concentration and distribution, the immobilisation matrix plays a key role in optical sensors because it can exclude unwanted species in the sample from the sensor bulk, hence reducing cross-sensitivities. Exclusion of cross-interferents is most effective in gas sensors which essentially extract volatile compounds from the sample. In pH-sensors, components of a certain size and hydrophobicity can be kept out, above all in biological samples. A protective layer that acts as a filter, for instance a dense hydrogel, may additionally be applied between sensor layer and sample. Mechanical and adhesive properties of the sensor are governed by the immobilisation matrix, which makes up the bulk material. A good pH-sensor requires optimisation of both pH-probe and immobilisation matrix.

Optimisation criteria can be summarised as follows:

Desirable features of the pH-probe:

- High brightness (high molar absorption coefficient and fluorescence quantum yield)
- Tuneable pK_A value, which allows adjusting the sensitive range of the sensor
- Good chemical stability and photostability
- Long excitation and emission wavelengths
- Large Stokes' shift
- Spectral compatibility with common optical modules (light sources, filters, detectors)
- Good solubility and stability in the immobilisation matrix
- Commercial availability or easy synthetic accessibility
- Low charge for minimising cross-sensitivity to ionic strength in the sensor
- Functionalities for covalent coupling to the immobilisation matrix

Desirable features of the immobilisation matrix:

- Suitable water uptake
- Mechanical stability in the dry state as well as in contact with water
- Commercial availability or synthetic accessibility
- Negligible absorption of visible and near infra-red light
- Chemical stability in a wide pH range
- Low charge for minimising cross-sensitivity to ionic strength of the sensor
- For layers and fibres: good adhesion on suitable supports; compatibility with coating procedures
- For beads: simple and reliable bead fabrication; stability in dispersion
- Solubility in solvents needed for sensor fabrication
- Functionalities for covalent probe grafting

Scope for Application

The pH-range most relevant to optical sensors is given by the typical applications of interest. In diagnostics, maximum sensitivity should match the physiological pH (near 7.4) to enable a resolution as high as possible in this narrow range of interest. In life sciences, the same range may be desirable. However, due to the different pH in some tissues and cell compartments, slightly acidic (often pH 6 – 7, but pH can be as low as 4.5 in lysosomes [12]) or basic (pH 7.5 – 8 which is present in mitochondria [13]) pH may be targeted, depending on the particular application. The weakly acidic range is also of high interest to cancer research since cancerous tissue usually features an abnormally low pH as a result of glycolysis [14]. In biotechnological process control, pH between 5 and 7, depending on the fermentation, need to be detected. This range is therefore often also of interest in enzyme activity screening. Marine biology calls for measuring pH in seawater, which is in the range 7.8 -8.5 [15]. Applications outside these ranges are rare. A pH-sensing concept thus ideally should feature a sensitive range tuneable within pH 4.5 – 8.5 to allow for adaption of the sensitive range to the individual application, enabling optimal resolution.

Referencing Techniques

Like all fluorescence sensors, pH-sensors require a referencing technique for practical application in order to compensate for many effects and parameters which are not directly related to analyte concentration. Those include variations in local probe concentration and optical pathlength, unsteady efficiencies of the light source, the detector and the guidance of light to the detector or probe leaking, photobleaching and aggregation. Referencing can be performed by evaluating the ratio between the fluorescence intensities in two spectral windows, rather than in a single one (ratiometric measurement). Excitation can be kept constant and fluorescence can be observed at two windows (dual emission measurement), or one can use a fixed emission window and vary

excitation wavelengths (dual excitation measurement) [1]. Since dual emission measurement is applicable to devices equipped with a light source featuring narrow emission, such as many fluorescence microscopes and generally most systems employing lasers, it can be considered more useful. Probes featuring a pH-dependent shift in fluorescence spectra are called self-referencing as they do not require an additional fluorescent dye for referencing but their own fluorescence can be read out using two spectral windows (intrinsic referencing). Those are much more robust concerning variations in probe concentration due to leaking, photodegradation or aggregation since in sensors applying two fluorescent dyes the rate of those processes is usually unlike. ICT-based pH-probes (discussed in the following section) are generally self-referencing, though those undergoing PPT are only compatible with dual excitation measurement. For PET-based probes, a reference fluorophore is needed (extrinsic referencing).
Measurement of fluorescence decay time is much more robust against most of the mentioned perturbations and therefore is commonly considered self-referenced. However, decay times are not as simple to be measured as intensities. Perhaps the most relevant method for reading out luminescence sensors in the decay time mode is phase modulation fluorimetry. In this technique, fluorescence is excited by light of modulated intensity. The fluorescent emission signal is, with respect to the excitation light, shifted in phase and partially demodulated. Luminescence decay time is calculated from the phase shift measured:

$$\psi(ex) = A + Bcos(\omega t) \qquad \text{Equation 3a}$$

$$\psi(em) = a + bcos(\omega t - \phi) \qquad \text{Equation 3b}$$

Ψ(ex)	Wave function of the excitation light
Ψ(em)	Wave function of the emission light
A,a	Average intensity of excitation and emission light
B,b	Modulation amplitudes of excitation and emission light
ω	Angular modulation frequency (s^{-1})
ϕ	Phase shift of the emission light with respect to the excitation light

$$\phi = \arctan(\tau\omega) \qquad \text{Equation 4}$$

τ	Luminescence decay time (s)

While phase modulation fluorimetry is comparatively easy to perform for luminophores featuring decay times around or superior to 1 µs (those can feature phosphorescence, delayed fluorescence or fluorescence from lanthanoid centres), much more complex and costly instrumentation becomes necessary for organic fluorophores which typically feature decay times in the nanosecond range and therefore require very high modulation frequencies. Fluorescent dyes are predominantly used in pH-sensors as most luminophores featuring long luminescence decay times show cross-sensitivity to molecular oxygen which constitutes a severe limitation. Consequently, direct decay time measurement is not a good option in many applications for pH-sensors. An alternative is the dual lifetime referencing (DLR) technique in which the fluorescent indicator is combined with a pH-insensitive reference showing a significantly longer luminescence decay time [16,17]. The phase shift measured is then dependent on the

luminescence intensity ratio between indicator and reference, rather than the decay time of the reference which is ideally constant.

$$cot\phi = cot\phi_{REF} + \frac{1}{sin\phi_{REF}} \frac{I_{IND} M_{IND}}{I_{REF} M_{REF}}$$ Equation 5

ϕ	Phase shift measured
ϕ_{REF}	Phase shift measurable if only emission from the reference is observable
I_{IND}	Emission intensity of the indicator
I_{REF}	Emission intensity of the reference
M_{IND}	Demodulation of the indicator (defined as (b/a)/(B/A), parameters as stated in eqn. 3)
M_{REF}	Demodulation of the reference

Equation 5 is valid if $\tan\phi_{REF}$ is 1, which corresponds to an optimal modulation frequency. Because ϕ_{REF} and M_{REF} can be assumed as constant and M_{IND} is ≈1, $\cot\phi$ is dependent only on I_{IND}/I_{REF}, which for an ideal reference (I_{REF} = const.) is sigmoidally dependent on pH (eqn. 2).
When a high ratio of probe fluorescence is detected, a small phase-shift is observed and vice versa. Note that DLR is not a true measurement of luminescence decay time but constitutes a readout technique for fluorescence intensity based on phase modulation fluorimetry. It is therefore sensitive to changes in the signal brightness of both indicator and reference, as is the case in extrinsic ratiometric measurement. To deal with this limitation, reference materials very robust against photobleaching or leaking can be used. Nevertheless, the fluorescent indicator needs to fulfil equally high standards in order to obtain a highly robust pH-sensor.

Sensor Fabrication

Sensor fabrication in the simplest case involves dissolving pH-probe and matrix material in an organic solvent (figure 4). The resulting “cocktail” is then processed and left for solvent evaporation. Processing can consist in knife coating, screen printing, spin coating or spray coating of layers, while sensor fibres are often dip coated. Beads[18,19] can be prepared from “cocktails” by spray drying, precipitation or by dispersion followed by solvent evaporation. The probe can also be delivered into the beads by swelling with a probe solution (“staining”). Beads may also be entrapped into layers instead of or in addition to small molecules, particularly in sensors containing multiple sensitive components.
Alternatively, sensors can be made from the monomers by polymerisation [20] in bulk/solution (layers, fibres) or in emulsion (beads). Polymerisation is more complicated than the polymer processing methods mentioned beyond, but more versatile as it allows the preparation of self-made, optimised polymers. It also offers a direct access to cross-linked polymers and covalent probe coupling, though with some materials, cross-linking and probe coupling may be carried out after processing – a prerequisite for that is the presence of suitable functional groups. Some materials, such as sol-gels [21], are by definition made by polymerisation.
Some bead materials are compact and do not take up water. Examples are silica beads, though those are highly porous. In those cases, the probe is usually covalently linked to the bead surface. The beads are then dispersed in sensor layers or can be directly used. Properties of sensors may be different if the probe is bound to the surface than when it is located in the bulk as the probe is

exposed to a different microenvironment and is not shielded from interactions with the components in the sample.

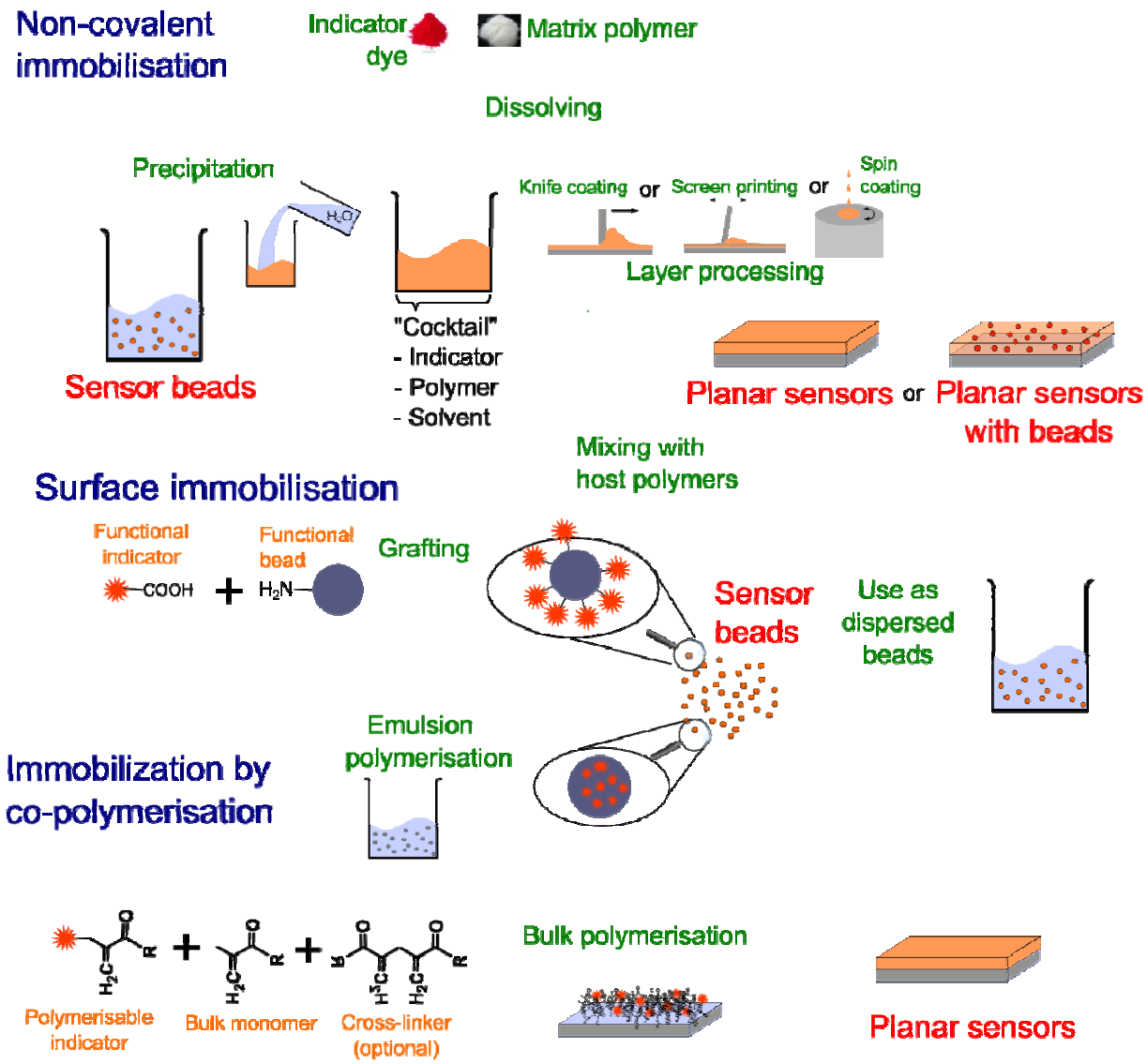

Figure 4: Schematic overview of sensor fabrication methods; this figure is not meant to ne complete but focuses on the methods most relevant to this thesis.

Related Fluorescence Sensors for Other Analytes

pH-sensitive systems are not limited to usage in pH-sensors, but can be modified to measure acidic and basic gaseous compounds and metal cations by minor adaptions of the sensor layout. If a pH-sensor is covered with a hydrophobic layer that excludes ions from it, ammonia or amines of low molecular weight can be detected [22]. The pK_A value of the pH-probe determines its sensitive range and needs to be carefully adjusted. The most common concept for fluorescence carbon dioxide sensors involves a pH-probe which, unlike in pH-sensors, is entrapped in a matrix that features low water uptake. Its basic form is usually negatively charged, and a bulky lipophilic cation is added for ion pair formation [23,24]. In some sensors for metal cations, both a pH-probe and a cation receptor are physically entrapped in the sensor layer. When cations are extracted from the matrix, protons in turn migrate out of the matrix to maintain charge neutrality, which

results in a measurable deprotonation of the pH-probe [25]. However, most fluorescence sensors for metal cations rely on different principles, including ICT or PET [26] (discussed in the following section). In PET-based probes, the PET group – most frequently an amine – is integrated into an ionophore and PET efficiency is modulated upon cation binding. Those probes principally are cross-sensitive to pH, though in many cases sample pH may be constant or outside the sensitive pH-range of the probe.

State-of-the-art Fluorescence pH-sensors

In this section, an overview about the most common fluorescence pH-sensors and -probes will be given. Some other concepts of particular relevance for this thesis will be discussed in the following section.

Luminescent Probes

The majority of pH-probes are organic fluorophores that bear a (de)protonisable group such as a hydroxyl, amino or imino group. Those usually feature large pH-dependent shifts in absorption and fluorescence spectra, often together with differing quantum yields and fluorescence decay times for acidic and basic form. That originates from the very different electron-donating properties of the protonated and deprotonated group and the different electron densities in the fluorophore resulting from them. The process is called intramolecular charge transfer (ICT). Because of the spectral shifts, such probes are suitable for dual-wavelength (ratiometric readout), as has been discussed in the previous section.
Probably the most well-known examples for ICT-based pH-probes are fluorescein derivatives (figure 5). The deprotonation of the phenolic group causes a strong bathochromic shift and an increase in fluorescence quantum yield so that the fluorescence of the basic form is interrogated in most cases. Emission of the basic form is often predominant even if the acidic one is excited. Fluoresceins are in equilibrium with a colourless lactone form, which is predominant in hydrophobic environment but also formed in a significant, for some derivatives in a dominating amount in water at low pH. Lactone formation can enhance the pH-sensitivity of fluoresceins by decreasing the brightness of the acidic form. However, it may be unwanted in some cases and can be prevented by esterification of the 3-carboxy group [15,27]. Bisacylated fluoresceins such as 2',7'-bis-(2-carboxyethyl)-(5,6)-carboxyfluorescein (BCECF) [28] are fluorogenic in the presence of esterases which has enabled their frequent application in live cells [29,30] and in enzyme activity screening. The biggest drawback of fluoresceins is their poor photostability which can be a severe limitation in pH-sensing and fluorescence imaging. Electron-withdrawing 2',7'-substitutents improve the photostability while simultaneously lowering the pK_A value to ≈ 5 [31], compared to 6.5 for the parent compound [32]. 2',7'-Difluorofluorescein ("Oregon Green") and 2',7'-dichlorofluorescein are frequently used pH-probes and derivatives bearing ion recognition moieties are widely applied in metal ion sensing [33,34]. 2'7'-Dialkylfluoresceins exhibit higher pK_A values principially enabling their application in marine science[15], but practical application is compromised by poor photostability. Fluoresceins with groups suitable for bioconjugation in the 5- and 6-positions are frequently applied as fluorescent labels. In those cases, their pH-sensitivity is often unwanted. Nevertheless, fluoresceins are among the most popular dyes in

fluorescence microscopy and available light sources and optical filters often match their spectral characteristics. Fluorescent dyes such as Alexa 488 have been made commercially available to provide highly photostable, pH-insensitive alternatives to fluoresceins in fluorescent labelling [35].

Rhodamines [36] (figure 5) are structurally similar to fluoresceins and also feature excellent brightness (product of molar absorption coefficient and fluorescence quantum yield, $\varepsilon^x\Phi_F \approx 100{,}000\ M^{-1}cm^{-1}$), while their photostability is usually significantly better. They are not intrinsically pH-sensitive, but the 1-amides and similar derivatives undergo lactame formation at basic pH. If suitable amide substituents are attached, the pK_A value can be tuned to enable measurement of weakly acidic to near-neutral pH [37-39]. The mechanism is very similar to lactone formation in fluoresceins and indeed, standard rhodamines bearing a 1-carboxy group undergo lactonisation, though unlike in fluoresceins the reaction is more favourable in basic media. In cases where lactonisation is unwanted, the 1,5-sulfo derivatives, called sulforhodamines, may be used. Fewer examples exist of pH-sensitive rhodamines and related compounds employing a PET (discussed below in this section) mechanism [40]. Those include compounds with other heteroatoms replacing oxygen in the xanthene core [41] and compounds lacking the 1-carboxy group (called rosamines) [42]. In the latter case, other substituents than hydrogen are usually present in the 1-position to prevent rotation of the phenyl ring which would cause a significant decrease in fluorescence brightness. Rhodamines are applied as fluorescent labels [36], as cell staining agents in fluorescence microscopy, in single molecule spectroscopy [43] and as fluorescent standards [44].

Benzo[c]xanthenes dyes were presented by Whitaker et al. [45]. Since then, they have been extensively applied both as molecular pH-probes and as indicators in pH-sensors [46-48]. Beneficially for life sciences, they feature longer absorption (510 – 600 nm) and emission (540 – 650 nm) wavelengths than most other fluorescent pH-probes. They include seminaphtho-fluoresceins (SNAFL dyes) and seminaphthorhodafluors (SNARF dyes) carrying oxygen or nitrogen atoms at the 10-position, respectively. For those derivatives carrying hydroxyl groups in the 3-position of the acidic form (SNAFL and some SNARF dyes), their deprotonation results in a bathochromic shift and in a decrease in fluorescence quantum yield. In some other SNARF dyes, the tertiary amino group in the 10-position is protonated in the acidic form and the 3-position is chinoid in both forms. For those, the basic form is bathochromically shifted but of higher fluorescence quantum yield with respect to the acidic one. Most benzo[c]xanthenes offer high sensitivity at near-neutral pH which is in good accordance with the physiological studies they are most frequently applied in. Their brightness is significantly lower than the one of fluoresceins and rhodamines ($\varepsilon^x\Phi_F < 15{,}000\ M^{-1}cm^{-1}$, $< 8000\ M^{-1}cm^{-1}$ if emissive in the red spectral region [45]) and in our experience, photostability can be an issue [49].

In some ICT-based pH-probes, the excited state value pK_A^* is significantly lower than the ground state value pK_A which causes fast deprotonation of the fluorophore once it has been excited. That process is known as photoinduced proton transfer (PPT). As a result, only fluorescence emission of the basic form is observable, regardless of pH. On the other hand, absorption and fluorescence excitation spectra remain pH-dependent. A well-known pH-probe undergoing PPT is 8-hydroxypyrene-1,3,6-trisulfonate (HPTS), which has been widely employed for pH [50-52] and carbon dioxide [23] [53] sensing. The basic phenoxide form is brighter ($\varepsilon^x\Phi_F \approx 20{,}000\ M^{-1}cm^{-1}$) and excitable at longer wavelength (455 nm) than the acidic one ($\varepsilon^x\Phi_F < 10{,}000\ M^{-1}cm^{-1}$; 405 nm).

The high charge of the molecule causes high cross-sensitivity to ionic strength and covalent coupling is required to prevent leaking into the aqueous sample. Hydrophobic trisulfonamide derivatives overcome both of those drawbacks and are excitable at longer wavelengths (≈ 520 nm, emissive at ≈ 560 nm when immobilised) [54]. However, in our experience brightness and photostability are diminished in comparison to the trisulfonate.
Another example for pH-probes undergoing PPT are 7-hydroxycoumarines. Coumarins are also accessible to the design of PET-based probes [55] (the PET principle is discussed below). However, they are excitable in the UV spectral range and excitability with visible light is restricted to extended coumarins [56].

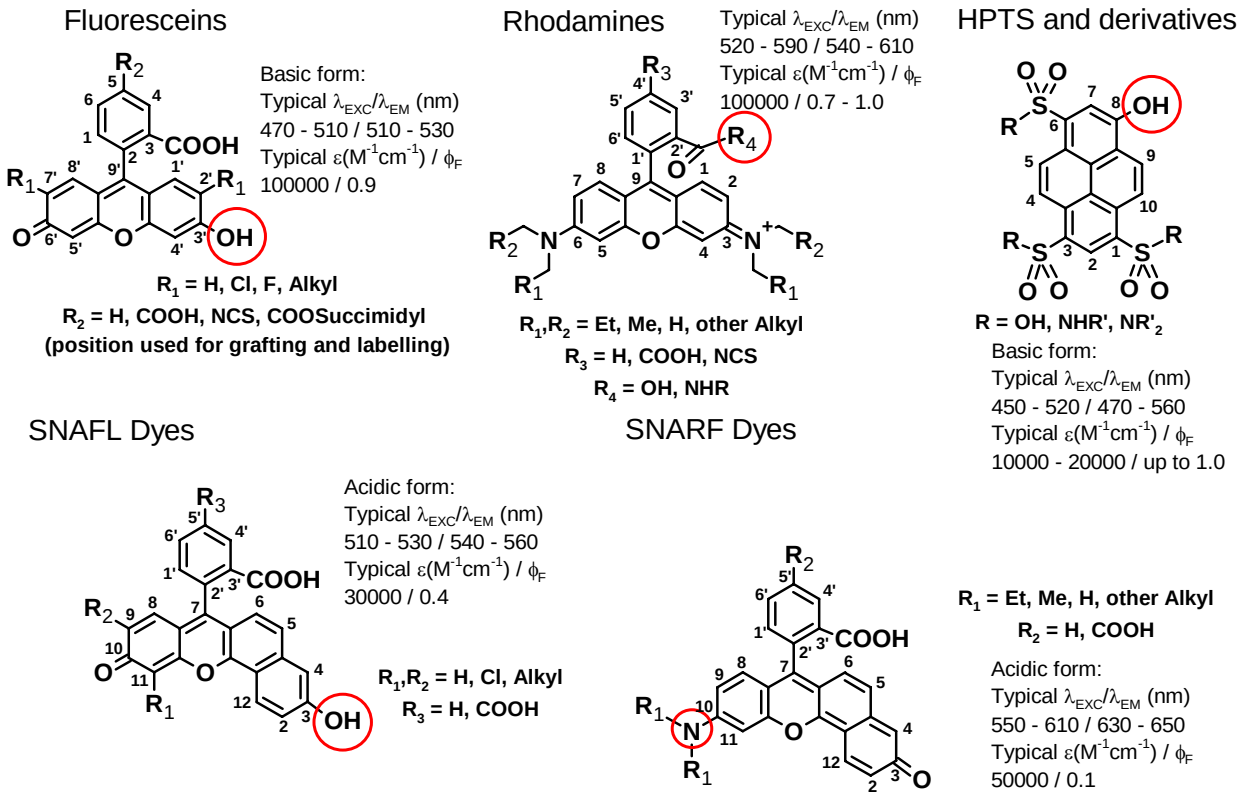

Figure 5: Structures and typical spectral properties of pH-probes undergoing ICT (sensitivity mechanisms for rhodamines are discussed beyond), with (de)protonable groups indicated by red circles. Spectral properties stated correspond to the form showing brighter fluorescence.

pH-probes can also take advantage of the photoinduced electron transfer (PET) process [57-62]. A functional group (the "PET group") is attached which results in a redox process between the PET group and the excited state fluorophore. In most cases, an electron is transferred from the PET group to fluorophore [63-65] and we will focus on that process, although there are also a few examples of excited state fluorophore oxidation [61]. The PET process is usually quickly reversible, the net result is thus fluorescence quenching, not fluorophore decomposition (figure 6). Amines are by far the most frequently employed PET groups, but phenoxides [66,67], carboxylates [68,69] or pyridine groups have been reported as well. All of those groups can undergo protonation, at which PET is no longer possible. Consequently, there is pH-sensitivity at pH-values close to the pK_A of the protonated PET group.

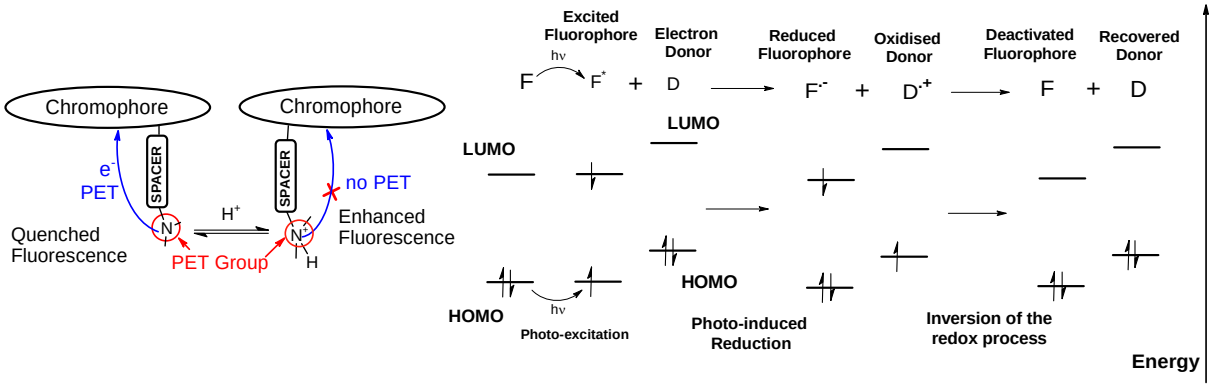

Figure 6: Schematic illustration of photoinduced electron transfer (PET). Left: Example with an amine donor - PET is prevented upon protonation as redox properties of the donor are dramatically changed. Right: Illustration of the redox process based on molecular orbitals.

The thermodynamic driving force for PET is given by Weller's equation[57]:

$$\Delta G_{Q,PET} = E_{Ox,Rec} - E_{Red,Flu} - \Delta E_{Exc,Flu} - E_{IP} \qquad \text{Equation 6}$$

$\Delta G_{Q,PET}$	Free enthalpy of the PET process (eV)
$E_{Ox,Rec}$	Oxidation potential of the receptor (eV)
$E_{Red,Flu}$	Reduction potential of the fluorophore (eV)
$\Delta E_{Exc,Flu}$	Singlet excitation energy of the fluorophore (eV)
E_{IP}	Ion pairing energy (eV)

PET is most effective with strongly electron-donating PET groups and electron-accepting fluorophores. Another important consequence of Weller's equation is that it is harder to obtain a PET-based pH-probe with fluorophores excitable at long wavelengths. One has to choose fluorophores and PET groups with beneficial redox potentials to compensate for the low transition energy then. Note that Weller's equation accounts for the thermodynamic favourability of the PET process and therefore defines the conditions under which PET in possible. Although PET often features a significantly higher rate than fluorescence if thrermodynamically favourable, there are also examples of kinetic inhibition [65]. Stereochemical parameters [70,71] may show considerable effects on the process. PET is also usually more likely in a polar environment, which can even enable the design of polarity probes [72].

PET is a quenching process that does not further influence the excited and ground state properties of the fluorophore. Therefore, only fluorescence intensity is affected, while there is no change in spectral shape and location and absorption is not affected at all. Although in some cases PET-based pH-probes may undergo changes in absorption spectra, those are caused by accompanying ICT effects, not PET. They can be described as effects of the charge of the PET group on the fluorophore, which may be located in close proximity. PET groups are typically not electronically connected to the fluorophore, but separated from it by covalent linkage over a spacer [59] . In systems where the PET group is directly bound to the fluorophore, but there is no conjugation concerning molecular orbitals, one speaks of a virtual C_0-spacer [41,66]. However, examples of PET groups integrated into the fluorophore are known as well [57,73,74]. There are few examples of PET groups non-covalently attached to the fluorophore or not attached to it at all [57,75]. That is understandable because the PET process requires contact between the molecular

orbitals of fluorophore and PET group to some extent. The distance between both should therefore be short.

PET offers high flexibility in pH-probe design, allowing to include intrinsically pH-insensitive fluorophores. Another major advantage of PET-based concepts is their modularity [62], which essentially allows tuning spectral properties and sensitive properties independently from each other by selecting fluorophore and PET group, respectively. Attaching PET groups of different structure generally facilitates simple tuning of the pK_A value of a pH-probe and can be applied to different fluorophores in the same way. Due to the lack of any pH-dependent spectral shifts, excitability and effects such as excitation energy transfer are independent on pH, which can make sensor behaviour less complicated. On the other hand, intrinsic dual wavelength referencing (section referencing techniques) is typically not possible for PET-based systems. Other referencing techniques may cause additional issues or require more sophisticated readout instrumentation.

Borondipyrromethene (BODIPY) (figure 7) dyes are among the most well-known PET-based pH-probes [66,76,77]. The BODIPY chromophore features excellent brightness ($\varepsilon^x\Phi_F \approx 80{,}000\ M^{-1}cm^{-1}$) and is frequently applied in studying biological systems [78,79]. Its pH-sensitive derivatives are often utilised as molecular probes, rather than in pH-sensors. Probes useful for different pH-ranges have been presented, making up an example for the flexibility of the PET concept. However, BODIPY dyes leave room for optimisation concerning photostability and are excitable at comparatively short wavelengths.

Naphthalene diimides and 1,8-naphthalimides feature good photostability and have been shown to be very effectively quenched by PET [80-82]. Such pH-probes are applied in cell imaging and commercially available as LysoSensors. They stain acidic cell compartments such as lysosomes where their fluorescence is enhanced and thus visible with good contrast to the surrounding, less acidic cytosol [83,84]. Interestingly, this advantage can be compromised by incomplete PET, even though 1,8-naphthalimides are known to feature highly effective PET in organic solvents where biological components are absent. PET-based anthracene probes [58,85] are also commercially available lysosomal stains. Significant drawbacks of naphthalene diimides and 1,8-naphthalimides include low brightness ($\varepsilon^x\Phi_F \approx 10{,}000 - 20{,}000\ M^{-1}cm^{-1}$) and short excitation wavelengths (< 450 nm) [86-88]. 2-Amino and 2,6-diaminonapthanlene diimides show strongly bathochromically shifted absorption (≈ 520 nm, ≈ 610 nm, respectively) [86] [89] but leave much room for optimisation in terms of brightness.

Cyanines are fluorophores offering excitability at rather long wavelengths. The chromophore is consisted of a chain of conjugated C-C double bonds terminated by nitrogen atoms. Increasing length of the conjugated chain correlates with increasing absorption and fluorescence wavelengths. Cyanines covering most of the visible spectrum are commercially available, for instance as Cy® dyes. Their extremely narrow, intense absorption brings high brightness (up to $\varepsilon^x\Phi_F \approx 100{,}000\ M^{-1}cm^{-1}$ which is exceptionally high for deep red emission) [83] [90]. There are two types of pH-probes. In PET-based probes, both nitrogen atoms are alkylated and a suitable PET group is attached [91,92]. If one or both nitrogen atoms are not alkylated, deprotonation of the cationic form results in a strong hypsochromic spectral shift and effective fluorescence quenching [93,94]. Cyanines have been the most relevant pH-probes emissive in the deep red and near infra-red, though alternatives are slowly being developed. Their biggest drawback is the limited chemical and photochemical stability of the polyolefinic fluorophore core, though the severity of this issue may considerably vary depending on probe structure and application.

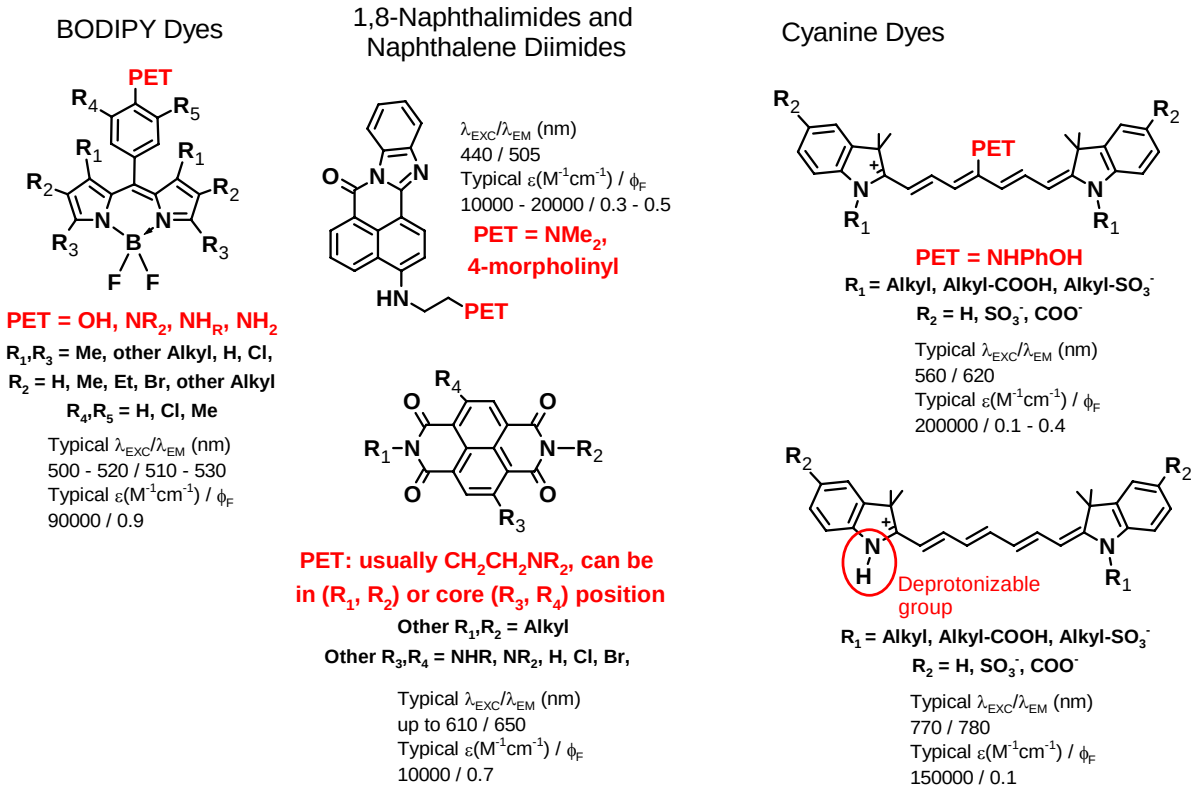

Figure 7: Structures and typical spectral properties of pH-probes undergoing PET.

Fluorescent probes exploiting the PET mechanism are much more common for detecting metal cations than they are for detecting protons. Though metal ion sensing is beyond the scope of this thesis, it has to be mentioned here that a large number of probes for calcium, sodium, magnesium, zinc and many other physiologically relevant metal ions has been presented [26,28,34,95-100]. Fluorescent cation probes have significantly contributed to understanding both intra- and extracellular physiological and biological processes.

Organic dyes are the most common luminescent pH-probes due to ease of preparation, rational design and handling, defined properties and the profound knowledge about them. Nevertheless, other sensitive materials are attracting increasing attention. Fluorescent micellar structures and organic polymers come in many different structures and are often applied as beads [101-103]. Upconverting nanoparticles [104,105] enable multiphoton excitation techniques which are characterised by the complete absence of fluorescent background. Research has so far only provided a coarse insight into their features. Quantum dots [106,107] feature broad, intense absorption while their emission wavelengths are dependent on their particle size and therefore tuneable. Toxicity is probably the biggest limitation of these interesting materials. Fluorescent proteins [108,109] have revolutionised live cell research. They are expressed in the cells and directly interrogated there, rather than being used in “conventional” pH-sensors with immobilised pH-probes which are discussed in most of this thesis. They can be engineered to become pH-sensitive [110,111] but are not designed for application outside of cells.

Immobilisation Matrices

The most common immobilisation matrices in pH-sensors are hydrogels based on organic polymers. The term hydrogel refers to those polymers which are swellable but not soluble in water. Examples for commercially available linear polymers of suitable hydrophobicity are poly(2-hydroxyethylmethacrylate) [81] or polyurethane hydrogels [27]. Cross-linked acrylamide gels were among the first materials used [20]. Cross-linked materials need to be polymerised during or after sensor preparation. Many of those would be water-soluble as linear polymers. Sol-gels [21,112] make up another important class of immobilisation materials and also involve sensor preparation staring from monomers. Silica beads are probably the most common examples for solid carriers the pH-probes is bound onto [113,114]. Even though suitable bulk materials for optical pH-sensors are commercially available, in many cases an individual immobilisation concept involving a self-designed immobilisation matrix and/or an individually developed grafting technique may provide the best solution for a certain pH-indicator or application. The individual design of immobilisation matrices may be more work-intensive but is also more flexible, yielding pH-sensors with particular properties that may not be accessible by the use of standard materials. A few of the numerous examples are [102,103,115,116].

Objectives: Design of High-performance pH-sensors

In order to meet the high demands of the diverse potential applications, tools for the design of high-performance pH-sensors are clearly needed. Among the numerous optimisation criteria mentioned earlier (section fluorescence pH-sensors: principles), high fluorescence brightness in combination with long excitation and emission wavelengths, tuneability of the sensitive range and highly stable sensor performance are probably the most crucial ones. Probe design is a logical starting point as those challenges are impossible to meet without an optimal pH-probe, though a well-suited immobilisation concept is necessary for exploiting the full potential of high-performance probes. Although it is of course desirable to fulfil all optimisation criteria perfectly, for some applications only some of them may be of high relevance while the optimisation of others may needlessly complicate sensor design or may compromise advantages which are of superior importance. The main objective of this thesis is therefore to demonstrate the value of tools applicable in sensor design. Those tools are not only intended to fulfil the mentioned optimisation criteria, but in particular to provide as much flexibility as possible in combination with ease of use, so that optimal pH-sensors for every application can be obtained in a simple way.

High-performance Fluorophores

The most widely employed pH-probes still feature individual drawbacks, as has been discussed. However, several high-performance fluorophores have so far not been employed in pH-sensing on a regular basis. Most of them have been presented very recently, often during the preparation of this thesis. However, the potential of some fluorophores known for a longer time still seems unexploited or largely unrecognised.

Perylene bisimides (PBIs) feature high brightness ($\varepsilon^x\Phi_F \approx 20{,}000 - 80{,}000$, $\approx 40{,}000$ $M^{-1}cm^{-1}$ for the derivatives most relevant in this thesis) and are known for excellent photostability, chemical and thermal stability [117]. They are widely applied in organic electronics [118,119], (supra)molecular signalling [120,121], single molecule fluorescence techniques [122,123] and fluorescent labelling of biomolecules such as enzymes or DNA [124-126]. Though PBI-based pH-probes employing PET were first presented in 1998 [59], their performance in sensors was modest owing to the high intrinsic aggregation tendency of the dyes. Although a few other examples of pH-sensitive PBIs have followed [103], much of their potential in this regard is still unexploited. PBIs offer great versatility concerning modification that allows tuning their spectral properties, to attach different PET groups in order to tune their pK_A values and to suppress aggregation. In particular, tetraphenoxy-PBIs offer fluorescence emission wavelengths of > 600 nm in combination with excellent photostability [69,119], while those bearing amino groups at the perylene core enable emission in the deep red to near infra-red range [127,128]. Near-infra red emission is even better accessible by enlarging the perylene core [119,129,130], but the resulting terrylene dyes are extremely hydrophobic and prone to aggregation. A class of PBI-based fluorophores with bright emission ($\varepsilon^x\Phi_F \approx 90{,}000$ $M^{-1}cm^{-1}$) in the deep red spectral region (≈ 650 nm) has recently been presented by Langhals et al [131]. None of those dyes has yet been utilised for pH-sensing.

Diketopyrrolo[3,4c]pyrroles have been widely applied as pigments [132], though strategies for solubilisation have been presented and the resulting dyes have found extensive application in organic electronics [133,134]. Though only featuring moderate brightness ($\varepsilon^x\Phi_F \approx 20{,}000$ $M^{-1}cm^{-1}$), they are attractive due to their high chemical stability and promising data concerning two-photon excitability has been presented [135]. Pyrrolopyrrole cyanine dyes [136,137] show excitability at long to extremely long wavelengths (≈ 850 nm, ≈ 950 nm for bis(pyrrolopyrrole) cyanines) together with exceptionally high molar absorption coefficients ($\approx 250{,}000$ $M^{-1}cm^{-1}$, $\approx 550{,}000$ $M^{-1}cm^{-1}$ for bis(pyrrolopyrrole) cyanines) and very high brightness for that emission range ($\Phi_F \approx 0.5$, resulting in $\varepsilon^x\Phi_F > 100{,}000$ $M^{-1}cm^{-1}$; $\Phi_F \approx 0.1$ for bis(pyrrolopyrrole) cyanines). Though their synthesis is demanding, the major challenge to their application in sensors may be solubility issues as the need for solubilising groups in order to provide at least some solubility has been reported. Despite the potential of the fluorophores, pH-sensitive diketopyrrolo[3,4c]pyrroles and pyrrolopyrrole cyanines have not yet been presented.

Squaraines are structurally unconventional fluorophores deriving from 3,4-dihydroxycyclobutene-1,2-dione ("squaric acid") which have found application in organic electronics [138-141]. There are structurally very different derivatives some of which possess extremely bright (up to $\varepsilon^x\Phi_F \approx 200{,}000$ $M^{-1}cm^{-1}$) red-light emission due to their remarkably high (up to > 300,000 $M^{-1}cm^{-1}$) molar absorption coefficients. The very poor photostability and the low stability against nucleophilic attack of some squaraines can be improved to some degree by structural modification, but poor solubility in our experience can be an issue. Nevertheless, their excellent brightness makes them promising candidates for fluorescence sensing, and a few squaraine-based pH-probes have already been presented [142,143].

Tetraarylazadipyrromethene (Aza-BODIPY) dyes are nitrogen-bridged analogs to BODIPY (discussed in the previous section) dyes featuring near infra-red emission (680 – 740 nm, absorption 660 – 710 nm). The deprotonation of phenolic or amino groups in a suitable position causes strong bathochromic shifts in absorption spectra. Though those shifts are caused by ICT,

the accompanying complete fluorescence quenching of the basic form clearly makes up evidence that PET plays a role in these dyes. While the pH-sensitive probes were presented by O'Shea and co-workers [73,144], the first pH-sensors based on Aza-BODIPYs were published more recently [145]. Excellent photostability and good brightness ($\varepsilon^x\Phi_F \approx 10{,}000\ M^{-1}cm^{-1}$ is an appreciable value for a dye featuring near infra-red emission) are significant advantages. The shift in absorption spectra brings a dependence of the calibration function on probe concentration originating from Förster resonance energy transfer while intrinsic referencing is not possible because the basic form is non-fluorescent. However, this limitation is not very critical as the calibration function remains predictable.
Aza-BODIPY derivatives conformationally restricted by ethylene bridges [146] promise significantly higher brightness ($\varepsilon^x\Phi_F \approx 40{,}000\ M^{-1}cm^{-1}$) in combination with slightly longer excitation (up to 740 nm) and emission (up to 750 nm) wavelengths. Even brighter (up to $\varepsilon^x\Phi_F \approx 140{,}000\ M^{-1}cm^{-1}$) near infra-red (absorption / emission 720 / 740 nm) have been reported for furane-condensed ("Keio Fluors") [147] and thiophene-condensed [148] BODIPY analogs. However, pH-probes based on those fluorophores have not yet been presented.

Designing New High-performance pH-probes

Despite the recent progress discussed, high brightness, excitability at long wavelengths and high photostability in combination are featured by very few pH-probes so far. We are therefore looking for a highly flexible concept suitable for introducing pH-sensors based on new fluorescent probes. Photoinduced electron transfer (PET) is clearly well suited to meet those challenges, and drawbacks such as difficulties in sensor referencing can be overcome. We also anticipated that PET is ideal for overcoming two of the most significant limitations of optical pH-sensors: their limited sensitive range and their cross-sensitivity to ionic strength. The first one can be overcome by combining several pH-probes in a single sensor which ideally should feature identical spectral properties but differing pK_A values. That can be accomplished by attaching different PET groups to the same fluorophore. Cross-sensitivity to ionic strength is caused by high charges of both pH-probe and immobilisation matrix. All common PET groups feature a single (de)protonation step and minimal indicator charge results when they are attached to a neutral fluorophore.

Covalent Probe Coupling

In the majority of pH-sensors reported in the literature, the pH-probe is physically entrapped in the immobilisation matrix, but not covalently bound to it. However, covalent linkage can improve the performance of fluorescence pH-sensors for several reasons. Firstly, there is no probe leaking from the sensor into the sample. If water-soluble pH-probes are used, leaking would lead to malfunction of the sensor very quickly. It has been shown that the attachment of hydrophobic anchors such as octadecyl groups can dramatically reduce leaking in such cases [27]. Still, covalent probe grafting can be beneficial, above all in biological systems where the toxicity caused by probe leaking is a concern. Secondly, above all for organic dyes, migration and aggregation can be dramatically reduced because the mobility of the dye is much lower when it is covalently attached. That is important because dye migration and aggregation can cause unwanted drifts in the fluorescence signal, above all for hydrophobic dyes and for long application times.

Excitability at Long Wavelengths

Low energy light causes less scattering and fluorescent background, lower levels of photodamage and has higher transmission in biological samples. Human tissue is significantly penetrated by red light and even more by near infra-red (NIR) light [149]. High levels of autofluorescence are generally only evoked by red light in the presence of chlorophylls, while even those cause minimal perturbations if NIR-excitation is employed.
The design of fluorescent probes suitable for interrogation at long wavelengths is a challenge because the small energy gap between ground state and excited state favours internal conversion, naturally decreasing fluorescence quantum yield. A quantum yield of 0.3 is a high value for fluorophores emitting in the NIR and in the case of emission at > 850 nm a value of 0.1 can be considered as exceptionally high. If probe design relies on PET, one has to consider that the thermodynamic driving force for PET decreases with the excitation energy. Fluorophore and PET group therefore have to be carefully selected to enable effective quenching.

Part B

Results

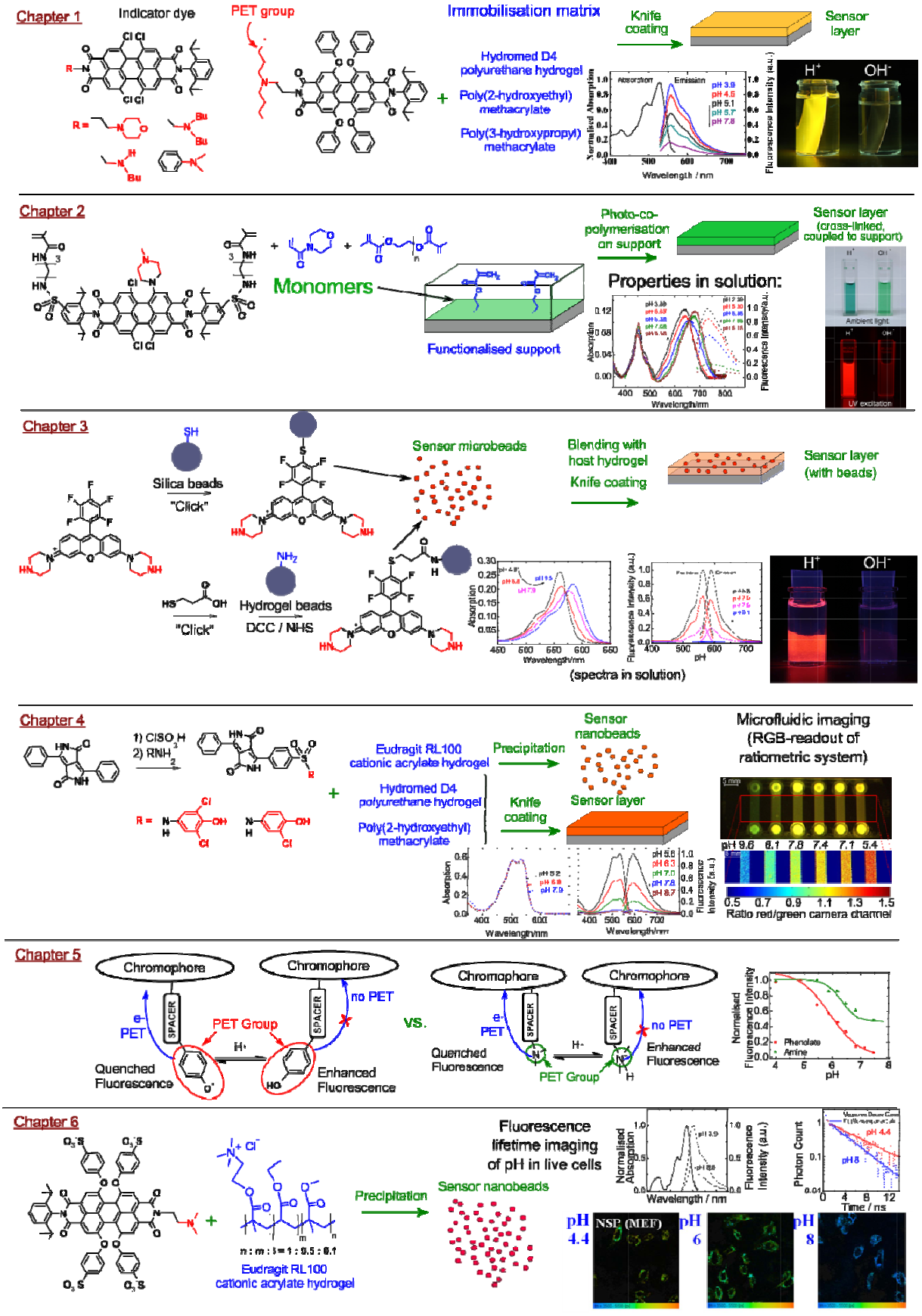

Figure 8: Overview of the fluorescence pH-sensors and probes presented in this thesis.

Chapter 1

New Fluorescent Perylene Bisimide Indicators – a Platform for Broadband pH Optodes

Preface to Chapter 1

Perylene bisimides (PBIs) were the first dyes of interest in this thesis. Their high brightness, excellent chemical stability and photostability and their versatility concerning chemical modification, which brings numerous possibilities for tuning spectral properties and attaching PET groups, indeed made them very promising. As is demonstrated in this chapter, asymmetric PBIs carrying an amino group causing PET in one imide position and a solubilising 2,6-diisopropylphenyl group in the other one are a good basis for very bright pH-sensors, as is shown both for 1,6,7,12-tetrachloroPBIs and 1,6,7,12-tetraaryloxyPBIs. That constitutes a significant progress since PBIs presented earlier [59] were used in polyvinylchloride containing very high levels of plasticiser, a material far from optimal for pH-sensing. Another system presented much more recently [103] allowed only a glimpse of their potential for pH-sensing. It is also confirmed that the sensitive pH-range can be tuned by attaching different PET groups and very similar calibration curves are obtained with chromophores featuring different spectral properties. Furthermore, combining several pH-probes with different pH-ranges is a feasible concept for the preparation of sensors with a broad sensitive range, as is experimentally verified. Those facts underline the high flexibility of the PET concept which is expected to be transferable to other fluorophores.

Though the presented sensors underline the high potential of PBI-based fluorescence pH-sensors, there are significant issues severely limiting their usefulness for application. Most importantly, their calibration curves are unstable. The sensors based on tetrachloro-PBIs indicators show a decrease in sensitivity over time, probably caused by dye aggregation, which implies the need of re-calibration after a few hours. The instability of sensors employing tetraphenoxy-PBIs is even more severe as is visible by shifting pK_A values, very long response times combined with incomplete response and poor signal reproducibility. Furthermore, while the expected excellent photostability is confirmed for the tetraphenoxy-PBIs, the tetrachloro derivatives surprisingly undergo a fast change in absorption spectra when intensely illuminated in the presence of water.

Consequently, sensors based on tetrachloro-PBIs are restricted to short application times and low light intensities while tetraphenoxy-PBIs do not seem suitable for practical application at all. To overcome those issues, referencing with another fluorophore is not suitable, but aggregation of the highly hydrophobic indicator dyes needs to be suppressed, for instance by covalent dye coupling. However, covalent linkage by grafting the perylene bisanhydride to amino-functionalised matrix materials turned out to be unsuccessful, probably due to the formation of amides that do not undergo full ring-closing to the imides. Furthermore, the excitation and emission wavelengths of the sensors are still shorter than desired, above all for the tetrachloro-PBIs. The most common strategies for increasing their absorption and fluorescence wavelengths are associated with further π-extension of the chromophore which is expected to further aggravate aggregation issues. Other concepts for making the sensors excitable at longer wavelengths therefore need to be found.

New Fluorescent Perylene Bisimide Indicators – a Platform for Broadband pH Optodes

This chapter was published in **Analytical and Bioanalytical Chemistry**, 2011, 400, 2475–2485; doi: 10.1007/s00216-010-4647-y

Authors: **Daniel Aigner, Sergey M. Borisov and Ingo Klimant**

Asymmetric perylene bisimide (PBI) dyes are prepared and are shown to be suitable for the preparation of fluorescence chemosensors for pH. They carry one amino functional substituent which introduces pH sensitivity via photoinduced electron transfer (PET) while the other one increases solubility. The luminescence quantum yields for the new indicators exceed 75% in the protonated form. The new indicators are non-covalently entrapped in polyurethane hydrogel D4 and poly(hydroxyalkylmethacrylates). Several PET functions including aliphatic and aromatic amino groups were successfully used to tune the dynamic range of the sensor. Because of their virtually identical spectral properties, various PBIs with selected PET functions can easily be integrated into a single sensor with enlarged dynamic range (over 4 pH units). PBIs with two different substitution patterns in the bay position are investigated and possess variable spectral properties. Compared to their tetrachloro analogues, tetra-*tert*butyl substituted PBIs yield more long-wave excitable sensors which feature excellent photostability. Cross-sensitivity to ionic strength was found to be negligible. The practical applicability of the sensors may be compromised by the long response times (especially in case of tetra-*tert*butyl substituted PBIs).

Introduction

Monitoring of pH is of vital importance in biotechnology, environmental analysis and marine science, as well as in medicine. Optical pH sensors based on fluorescence are attractive since continuous, real-time measurement can be performed in a virtually contactless way. Unlike electrochemical pH sensors, they are not subject to electromagnetic interferences and can feature higher sensitivity within their dynamic range. Although optical pH sensors show cross-sensitivity to ionic strength, this inconvenience has been overcome by employing a low-charged indicator dye embedded into an uncharged matrix [27]. Another drawback is their narrow dynamic range, compared to electrochemical sensors. Many fluorescence pH sensors that can be found in the literature are based on fluorescein derivatives [150,151], 8-hydroxypyrene-1,3,6-trisulfonate (HPTS) and its derivatives [50,152-154] or benzo[g]xanthene dyes [47,155-157]. However, most of the above sensors suffer from several drawbacks. Particularly, fluoresceins are commonly known for their limited photostability, especially in case of 2´,7´-alkyl-substituted derivatives [27]. Since HPTS is a highly charged molecule the cross-sensitivity to ionic strength is very high. Its lipophilic derivatives overcome these drawbacks but possess limited brightness. Benzo[g]xanthene dyes are long-wave excitable (> 600 nm) [45], but show moderate brightness and are prone to photobleaching [49]. The above-mentioned indicators possess considerably different spectral properties in the protonated and deprotonated state and therefore are limited to systems where a (de)protonisable function is located within the chromophore. However, pH sensitivity can also be introduced over photoinduced electron transfer (PET, figure 1-1). This process involves a redox

reaction between a chromophore in the excited state and another functionality that can be found within the same molecule or in its close vicinity but in most cases is not integrated into it [61]. As PET is usually fast and fully reversible, it essentially constitutes a quenching process. In most cases, the above-mentioned functionality is an amino group which is capable of quenching only in the non-protonated state so that pH sensitivity is found if the pH is close to the pK_A of the amino group.

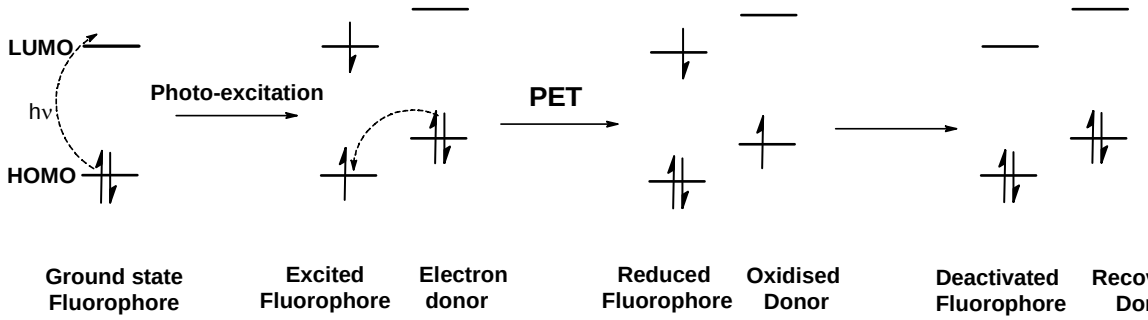

Figure 1-1: Schematic layout of photoinduced electron transfer (PET) between an electron donor and a fluorophore (electron acceptor). As a result of excitation, a MO higher in energy becomes populated (i.e. the HOMO is elevated) and electron transfer becomes possible. If the donor is an amine, its HOMO is located at much lower energy in the protonated state so that PET becomes impossible.

Various chromophors including polyaromatic hydrocarbons [58,64,96,113,158], coumarins [55] and particularly naphthalimides [82,159-161] have already been shown to be quenched via PET by aliphatic amines. Therefore, the field of available fluorescent pH indicators can be dramatically extended by attaching amino groups to not intrinsically pH-sensitive chromophores. Notably, PET has been widely used for the design of ion sensors [33,100,162-165]. An advantage of PET-based systems is their modularity [62], i.e. fluorophore and receptor can be selected independently to specifically design a fluorescent indicator. Spectral properties are determined by the chromophore, whereas proton affinity (i.e. pK_A) is much more specific for the amino function (fluorophore-spacer-receptor systems) [61]. Furthermore, an extension of the pH-sensitive range is much less complicated in the case of PET-based pH indicators since several dyes with different pK_A values but virtually identical spectral properties can be combined. The drawbacks of the chromophores commonly used to design PET-sensors include their short-wave excitation (resulting in higher levels of auto-fluorescence in biological media and stronger light scattering) and, particularly, moderate to low luminescence brightness (BS, defined as the product of molar absorption coefficient ε and luminescence quantum yield QY). For example, the BS for naphthalimide-based indicators is ~12,000.

Perylene bisimide (PBI) dyes are known for their relatively high molar absorption coefficients 30,000-90,000 $cm^{-1} M^{-1}$ [69,166], fluorescence quantum yields close to unity [167], and excellent photostability [117]. These features enable their application in OLEDs [168], photovoltaic cells [169], fluorescent solar collectors [167] and dye lasers [170], to state only a few. Furthermore, PBIs feature good versatility in respect to synthetic modification [59,103,127-129,171-176] which makes them promising candidates for the design of new PET pH indicators. In fact, the pH sensitivity of PBIs with amino functional substituents in both imide positions has already been demonstrated by De Silva and co-workers [59]. The application of those dyes in polymeric matrices was very limited due to their low solubility and high tendency to aggregation. Recently, Langhals and Pust [103] presented pH-sensitive nanomicells consisting of a PBI dye and sodium

dodecyl sulphate. However, the field of perylene-based fluorescent pH indicators is still in its infancy. Here we present a detailed study of various asymmetric PBI indicators that show appreciable pH sensitivity and bright fluorescence in different hydrogel matrices. As will be demonstrated, the pH sensitivity can be tuned by varying the amino functionality in the imide position whereas the substituents in the bay position influence the spectral properties.

Experimental

Materials

1,6,7,12-Tetrachloroperylene-3,4:9,10-tetracarboxylic bisanhydride and 1,6,7,12-tetra(4-*tert*-butylphenoxy)perylene-3,4:9,10-tetracarboxylic bisanhydride (technical grade) were purchased from Beijing Wenhaiyang Industry and Traiding Co.Ltd (http://china.zhaoteng.com). 1-Methyl-2-pyrrolidone and propionic acid were obtained from ABCR (www.abcr.de). All other solvents (synthesis grade) as well as NaCl and buffer salts were supplied by Carl Roth (www.roth.de). Deuterated chloroform $CDCl_3$ and anhydrous sodium sulfate were bought from Aldrich (www.sigmaaldrich.com). Silica gel (0.040-0.063 mm) was from Acros (www.fishersci.com). Polyurethane hydrogel (Hydromed™ D4) was purchased from CardioTech (www.cardiotech-inc.com). Poly(hydroxyproylmethacrylate) was obtained from Scientific Polymer Products (www.scientificpolymer.com). Poly(hydroxyethylmethacrylate) (MW=150000 g/mol) was from Polysciences Inc. (www.polysciences.com). Poly(ethylene glycol terephthalate) support (Mylar®) was from Goodfellow (www.goodfellow.com). Preparation of fluorescein octadecyl ester is reported elsewhere [27,177]. 1,6,7,12-tetrachloro-*N,N'*-(2,6-diisopropylphenylperylene-3,4,9,10-tertracarboxylic bisimide was synthesised in analogously to the literature procedure [69].

Syntheses

The synthetic concept is exemplified by the following synthesis of **2a**. The other dyes were obtained in a similar way. Their preparation is described in detail in the supplementary information.

*1,6,7,12-Tetrachloro-N-(2,6-diisopropylphenyl)-N'-(3-morpholinopropyl)perylene-3,4:9,10-tertracarboxylic bisimide (**2a**).* 1,6,7,12-Tetrachloroperylene-3,4:9,10-tetracarboxylic bisanhydride **1a** (1 g, 1.88 mmol) was dissolved in 1-methyl-2-pyrrolidone (=NMP) (150 ml), warmed to 35°C and a solution of 3-morpholinopropyl-1-amine (0.275 ml, 1.88 mmol) in NMP (20ml) was added dropwise under vigorous stirring. The reaction progress was monitored via thin layer chromatography on silica-gel and via UV-Vis spectroscopy. After TLC revealed total consumption of 1 and no further shift in absorption spectra of the mixture was observed, propionic acid (50 ml) and 2,6-diisopropylaniline (1.54 ml, 7.51 mmol) were added. The mixture was heated to 130°C for 21 h. After cooling to room temperature, it was poured onto 20% aqueous NaCl (1.4 l). The brown precipitate was separated by centrifugation, washed, re-dissolved in CH_2Cl_2, and dried with Na_2SO_4. Column chromatography with silica gel as the stationary and $CHCl_3$:MeOH as the mobile phase afforded 488 mg (32%) of **2a** as an orange powder. ^{1}H NMR (300MHz, $CDCl_3$, TMS): δ=8.75 (2H, s, Cl-C-C<u>H</u>-(1)); 8.71 (2H, s, Cl-C-C<u>H</u>-(2)); 7.53 (1H, t, iPr-C-CHC<u>H</u>-, J=7.6Hz); 7.37 (2H, d, iPr-C-C<u>H</u>-); 4.32 (2H, t, $(CO)_2NC\underline{H}_2$-, J=7.3Hz); 3.63 (4H, t, $OC\underline{H}_2$-, J=4.5Hz); 2.73 (2H, m, $PhC\underline{H}(CH_3)_2$, J=6.8Hz); 2.53 (2H, t, $NC\underline{H}_2C_2H_5N(CO)_2$, J=6.9Hz);

2.46 (4H, t, $NC\underline{H}_2CH_2O$ J=3.9Hz); 1.96 (2H, p, $NCH_2C\underline{H}_2CH_2N$, J=7.3Hz); 1.19 (12H, dd, $-CH(C\underline{H}_3)_2$, J_1=6.7Hz, J_2=4.1Hz). MALDI-TOF: m/z [MH^+] 814.1382 found, 814.1409 calcd.

Preparation of the sensor foils

A "cocktail" containing indicator dye (0.44 mg), hydrogel D4/pHPMA (44 mg) and tetrahydrofurane (500 µl) was knife-coated on a dust-free Mylar support to obtain a ~ 7 µm thick sensing layer after solvent evaporation. For pHEMA, the cocktail consisted of 55g·l^{-1} polymer and 550 mg·l^{-1} dye concentration in EtOH:H_2O (9:1 v/v).

Methods

Absorption measurements were performed on a Cary 50 UV-VIS spectrophotometer from Varian (www.varianinc.com). Fluorescence spectra were recorded on a Hitachi F-7000 spectrofluorimeter (www.hitachi.com). Relative fluorescence quantum yields were determined using rhodamine 101 (Fluka, www.sigmaaldrich.com) as a standard. NMR spectra were recorded on a 300MHz instrument (Bruker) in $CDCl_3$ with TMS as a standard. MALDI-TOF mass spectra were recorded on a Micromass TofSpec 2E. The spectra were taken in reflectron mode at an accelerating voltage of +20 kV.

pH calibration curves were obtained in a microplate reader (FluoStar Optima, BMG Labtech, www.bmglabtech.com). The "cocktail" containing dissolved polymer (5% w/w in THF or EtOH/H_2O mixtures) and dye (0.0125% w/w) was pipetted into 96-well polypropylene microtitreplates (Greiner Bio-one, www.gbo.com) and the solvent was allowed to evaporate. The obtained spots were incubated in the buffer solutions and interrogated using bandpass filters (475-490nm for excitation, 585-600nm for the PMT detector). The pH of the phosphate and phosphate-citrate buffer solutions was controlled by a digital pH meter (InoLab pH/ion, WTW GmbH & Co. KG, www.wtw.com) calibrated at 25 °C with standard buffers of pH 7.0 and 4.0 (WTW GmbH & Co. KG, www.wtw.com). The buffers were adjusted to constant ionic strength using sodium chloride as the background electrolyte.

Sensor response curves were recorded with a two-phase lock-in amplifier (SR830, Stanford Research Inc., www.thinksrs.com) equipped with a blue LED (λ_{max} 455nm) from Roithner (www.roithner-laser.com), a BG-12 short pass filter at the excitation side and a long-pass filter OG 550 (Schott, www.schott.com) before the PMT tube (H5701-02, Hamamatsu, www.sales.hamamatsu.com). The modulation frequency of 160 Hz was used.

For leaching tests, sensor foils (D4) were placed in a flow-through cell and the absorption of the films was monitored while aqueous buffers (IS 100 mM) were passed through it.

Photobleaching experiments were performed by irradiating the samples with the light of a 458 nm high-power 10W LED array (www.led-tech.de) focused through a lens purchased from Edmund optics (www.edmundoptics.de). Prior to the experiment a piece of the sensor foil (D4) was positioned in a quartz cuvette filled with the appropriate buffer. The photodegradation profiles were obtained by monitoring the absorption spectra. The absorption of the sensing layers and in the maximum of the light source was adjusted to 0.1.

Results and Discussion

Syntheses

As was mentioned above, perylene bisimides (PBIs) belong to photochemically robust molecules which possess high fluorescence brightness. However, solubility of many perylene derivatives is often rather low [167]. The commercially available 1,6,7,12-tetrachloroperylene-3,4,9,10-tetracarboxylic bisanhydride (figure 1-2) was chosen as a starting material since the chloro substituents in the bay position remarkably increase solubility compared to unsubstituted perylenes without significantly affecting spectral properties. The imide position was selected for attaching PET functionalities since spectral properties are usually not influenced by imide substituents due to nodes in the molecular orbitals located at the nitrogen atoms [178]. Preliminary experiments showed that symmetric tetrachloroperylene bisimides (TCPBIs) with two PET functionalities show excellent acid-base sensitivity in organic solvents, but application in a hydrogel matrix was compromised by severe leaching of the dicationic protonated form. Hence, it was envisioned that a single PET functionality is sufficient to render the molecule pH sensitive whereas the second position can be occupied by a solubilising group which enhances solubility and provides sufficient lipophilicity. Among such groups the bulky 2,6-diisopropylphenyl moiety is known to significantly enhance the solubility of perylene dyes and is present in highly soluble commercial Lumogen® Red dye. Several diamines were utilised for introducing the PET functionality, including aliphatic and aromatic ones (figure 1-2).

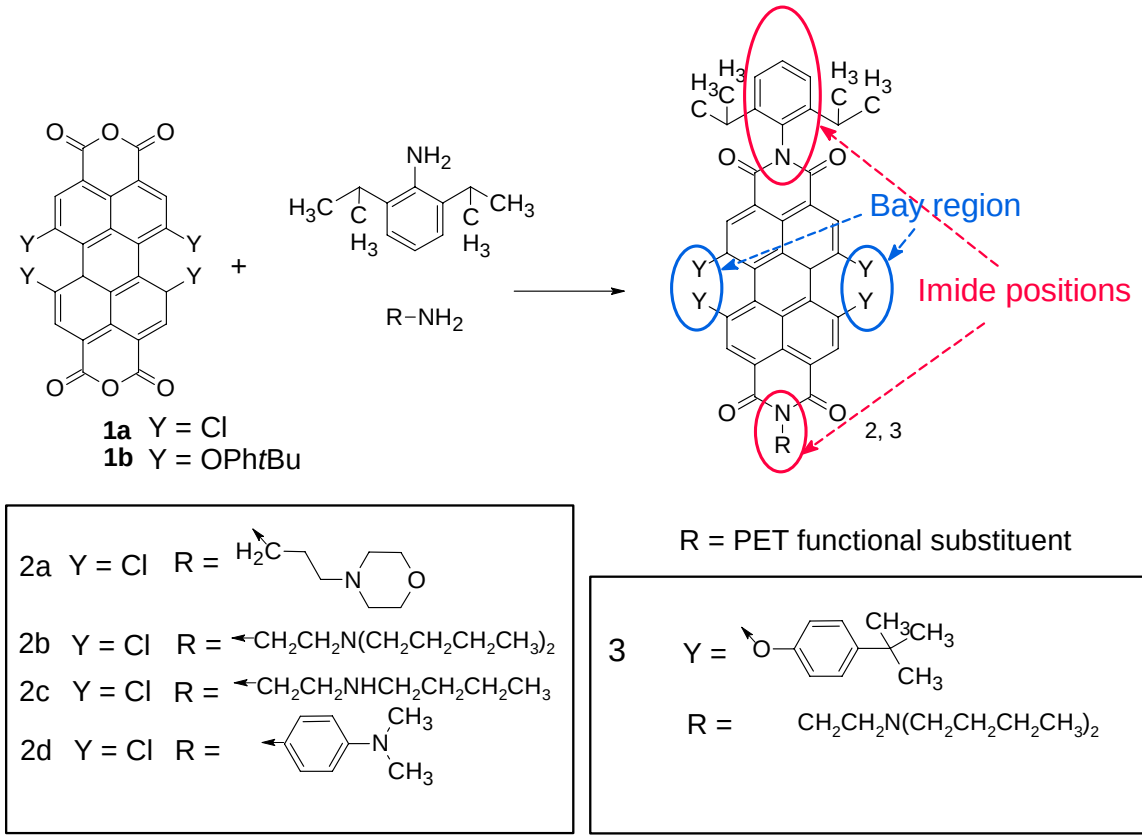

Figure 1-2: Reagents and conditions: 2a, 2b: *I)* R-NH_2 (1Eq.), NMP, 35 °C, 2h *II)* 2,6-diisopropylaniline (4 Eq.), NMP:EtCOOH (4:1), 130 °C, 18h; 2c: *I)* 2,6-diisopropylaniline (1.1Eq.), NMP:EtCOOH (4:1), 130 °C, 18h *II)* R-NH_2 (0.9Eq.), 35 °C; 2d: R-NH_2 (0.9Eq.), 2,6-diisopropylaniline (1.1Eq.), NMP, 130 °C, 24h; 3: *I)* 2,6-diisopropylaniline (3Eq.), NMP:EtCOOH (1:1), 130 °C, 24h *II)* R-NH_2 (2Eq.), 40 °C.

It was found that **1** can be reacted with aliphatic amines under mild conditions but reaction with aromatic amines requires elevated temperature and acidic catalysis. Notably, asymmetric PBIs are often prepared via a monoanhydride monoimide as an intermediate [179,180]. In the present case, however, this route is unpromising owing to poor stability of **1a** under the basic conditions that are usually employed for the preparation of the mentioned intermediate. The substantially different reactivities of aliphatic and aromatic amines did not allow simple coupling of an equimolar mixture with **1** (according to [181], for instance), but this concept was successfully employed for the preparation of bisaromatic compound **2d**. The indicators **2a-c** were prepared in a one-pot synthesis without isolation of the intermediate. Here the second amine was added to the reaction mixture after the reaction with the first amine was completed. The mixture of the asymmetric PBI and both symmetric PBIs was separable by column chromatography. The same concept was successfully employed also for the preparation of **3** starting from commercially available **1b**. The modest overall yields (7-36%) are explained by the formation of symmetric side products, naturally competing with the formation of the desired product. Nevertheless, all the products could be obtained in sufficient amount starting from reactants readily available at low cost.

Photophysical Properties

Table 1-1 provides an overview of photophysical properties of the new indicators. They possess good luminescence brightnesses BS. The molar absorption coefficients ε are found to be ~40,000 $M^{-1}cm^{-1}$ for all the indicators and the fluorescence quantum yields exceed 0.75. BS higher than 34,000 are obtained for all the dyes. These values are significantly higher than for the most common PET indicators based on naphthalimides (BS ~12,000). As expected, substitution of the chlorine atoms by 4-*tert*-butylphenoxy groups results in a pronounced bathochromic shift of the absorption and emission bands. Note the very similar spectral properties of **2a-d** which indicates extensive decoupling between the chromophore and the amino-functional substituent.

Table 1-1: P hotophysical properties of the perylene bisimide indicators in solution. Since pH-induced spectral shifts are small (< 5 nm in all cases), maxima are reported for acidic media only.

Dye	λ_{max} abs($\varepsilon \cdot 10^{-4}$)/nm ($M^{-1} \cdot cm^{-1}$) CH_2Cl_2	λ_{max} em/nm CH_2Cl_2	QY acidic $CHCl_3$	QY basic $CHCl_3$
2a	520(3.98); 486(2.76); 427(1.05)	552	0.95	0.044
2b	520(4.00); 486(2.78); 426(1.04)	552	0.95	0.015
2c	521(4.13); 487(2.88); 427(1.11)	554	0.84	0.055
2d	520(4.54); 487(3.16); 426(1.18)	559	0.81	<0.001
3	582(4.45); 542(2.70); 452(1.62)	624	0.76	0.11

Sensing Properties in Solutions

As expected, all the indicators possess much lower fluorescence quantum yields in the basic form compared to the acidic form (table 1-1). Table 1-2 shows the solvent dependency of the acid/base sensitivity for **2b** and **3** as representative examples. Efficient PET effect ($I_{acidic}/I_{bassic} > 10$) is observable in all the solvents tested, with only minor influence of solvent polarity on PET

efficiency and without a clear trend being recognisable. It should be mentioned here that the efficiency of a PET process can correlate with solvent polarity. For instance, for anthracence derivatives it was found to increase with polarity [72].

Table 1-2: PET efficiency of 2b ($8 \cdot 10^{-8}$ M) and 3 ($3 \cdot 10^{-8}$ M) in organic solvents, expressed as the ratio between fluorescence intensity in acidic (CF_3COOH, 0.05% v/v) and basic (ethyldiisopropylamine, 0.05% v/v) solvent.

Solvent	Dielectric constant	PET efficiency	
		2b	**3**
n-Hexane	1.9	41	1.9
Toluene	2.4	62	3.9
Methyl-*tert*butyl ether	2.6	42	3.5
Chloroform	4.7	47	4.6
Ethyl acetate	6.0	43	5.6
Tetrahydrofuran	7.4	42	5.5
Acetone	20	43	4.6
1-Propanol	20	32	4.6
Ethanol	24	39	4.9
Methanol	33	27	3.9

Sensing Properties in Polymeric Films

The pH sensors were obtained by non-covalently entrapping the indicators into hydrogels. D4 (a polyurethane hydrogel), poly(hydroxypropylmethacrylate) and poly(hydroxyethylmethacrylate) were used. Immobilisation has little effect on the absorption and the emission spectra of the indicators which shift bathochromically. For example, the absorption and emission in D4 were found to peak at 525nm and 558 nm, respectively, for **2a**, and at 589 and 622nm, respectively, for **3**. The sensing layers obtained show bright fluorescence which is visible with the naked eye at daylight. It should be mentioned that fluorescence of **3** in poly(hydroxyalkylmethacrylates) is weak which is likely to be caused by aggregation of the indicator. In agreement to the behaviour expected for a PET sensor, the fluorescence excitation and emission spectra are diminished in intensity but not altered in shape as pH is increased (figure 1-3). The absorption spectra remain almost unaltered and their pH-dependent spectral shift does not exceed 5nm in all cases. Such behaviour was found for all PBIs presented. As expected, fluorescence intensities of the indicators show typical sigmoidal shapes of the calibration plots (figure 1-4) from which the apparent pK_A values can be obtained. The apparent pK_A values as well as the intensity ratios for the acidic and the basic form of the dye are summarised in table 1-3.

Table 1-3: Calibration parameters of the indicators in hydrogels D4, poly(hydroxypropylmethacrylate) (pHPMA) and poly(hydroxyethylmethacrylate) (pHEMA): apparent pK_A values and the PET efficiency defined as the intensity ratio for the acidic and the basic forms of the indicator I_A/I_B.

Dye	Matrix					
	D4		pHPMA		pHEMA	
	Apparent pK_A	I_A/I_B	Apparent pK_A	I_A/I_B	Apparent pK_A	I_A/I_B
2a	5.1	5.5	5.6	47	4.9	26
2b	5.2	29	6.2	13	4.8	28
2c	6.5	12	—	8.6	6.8	38
2d	1.1	$4 \cdot 10^3$	1.9	$7 \cdot 10^3$	—	—
3	5.1	3.3	—	—	—	—

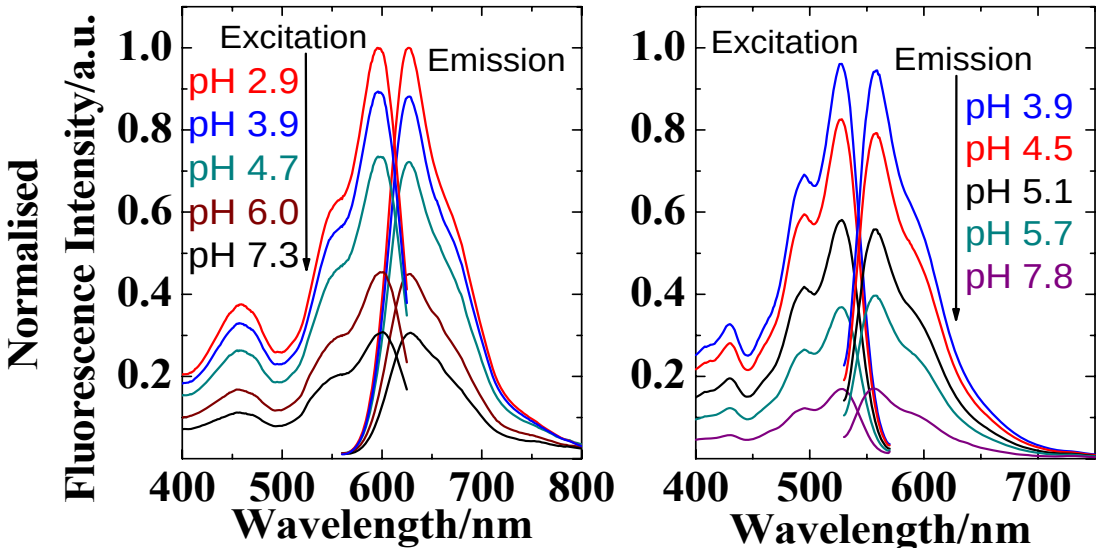

Figure 1-3: pH-dependent optical properties of 3 (left) and 2a (right) in hydrogel D4, IS = 100 mM. Fluorescence excitation were acquired at λ_{em}= 580nm and 640nm, fluorescence emission was excited at 515nm and 550nm for 2a and 3, respectively.

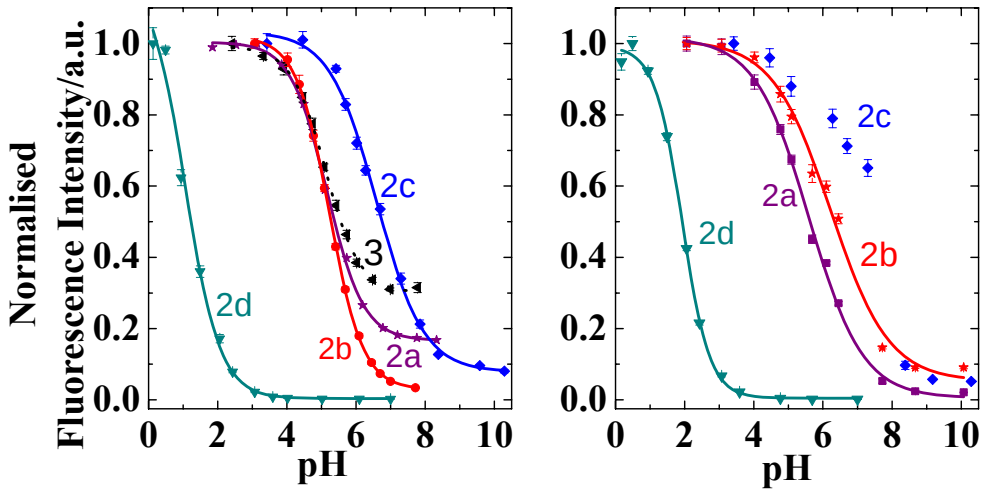

Figure 1-4: Calibration curves for the PBI indicators. Left – in D4 hydrogel; right – in poly(hyroxypropylmethacrylate). In poly(hyroxypropylmethacrylate), 2c does not show a typical sigmoidal calibration curve, therefore the apparent pK_A was not determined. Since 3 shows only weak fluorescence in the same matrix, the corresponding calibration curve is not displayed.

Table 1-3 demonstrates that the apparent pK_A values can be tuned by introducing amino groups with different basic character. The acidity of the protonated form decreases in the order 2d>2a≈2b>2c which corresponds to the general trend expected for aromatic, tertiary and secondary amines. On the other hand, the apparent pK_A values are also influenced by the polymer matrix. Significantly higher pK_A values (9.5-10) were reported for comparable compounds in solution [59]. Localisation in the less polar environment of the hydrogel matrix may decrease the apparent pK_A values since the charged acidic form is destabilised in these regions. This effect is opposite in case of anionic indicators (such as fluoresceins) which are known to have higher pK_A values in less polar environment. The generally higher pK_A values in pHPMA can be explained by higher hydrophilicity of the former compared to the hydrogel D4 which is a block copolymer containing both hydrophilic and hydrophobic domains. In this context, the pK_A values found in pHEMA are unexpectedly low, considering that pHEMA is even more polar than pHPMA. A possible explanation is partial aggregation of the lipophilc dyes in this relatively hydrophilic matrix. In fact, the brightness of pHEMA sensor films is lower than in the other polymer matrices which also suggests limited solubility of the dye in pHEMA.
It can be summarised that both the nature of the amino-group and the polymer can be used to tune the dynamic range of the sensor. Notably, the pK_A values obtained for **2b** and **3** are very similar despite their significantly different spectral properties. Therefore, the concept is likely to be transferable to other perylene-based indicators with different spectral properties. In terms of the dynamic range the sensors presented here are adequate for biotechnological applications. However, the pK_A values are generally too low for the sensors to be suitable for measurements at physiological conditions and in seawater. On the other hand, the indicator bearing an aromatic amine (**2d**) may find application for monitoring pH in strongly acidic media.
The PET efficiencies (defined as the ratio of the fluorescence intensities for the acidic I_A and the basic forms I_B of the indicator) are also collected in table 1-3. Generally, Weller´s equation [57] can be used to predict the PET efficiency [59,61] if the redox potentials of the fluorophore and the quencher are known:

$$\Delta G_{PET} = E^{ox}_{\mathrm{Re}c} - E^{\mathrm{Re}d}_{Fluo} - E^{S}_{Fluo} - E_{Ion} \qquad (2)$$

where ΔG is the thermodynamic driving force for PET, $E_{Ox,Rec}$ and $E_{Red,Fluo}$ are the oxidation/reduction potentials of amino function and fluorophore, respectively, is the energy of the singlet excited state of the fluorophore, and E_{Ion} is the ion pairing energy of the PET products.
As can be seen, the highest PET efficiency is observed for the aromatic amine (which is "switched off" in the basic form) and it is lower for the aliphatic amines. The sensitivity of **3** is significantly reduced compared to **2b** which bears the same PET functionality. The replacement of electron-withdrawing chlorine atoms by electron-donating aryloxy groups is expected to decrease the thermodynamic driving force for PET since (i) electron density in the chromophore is increased and its reduction, therefore, becomes less favourable and (ii) $E_{S,Fluo}$ decreases since **3** is excited at longer wavelength than **2b**. Nevertheless, a value of 3.3 still is sufficient for effective sensing. However, the above trend should be considered if bathochromically shifted pH indicators are designed since the PET efficiency may become too low for practical applications.

pH-sensor with Enlarged Dynamic Range

As was demonstrated above the spectral properties of the indicators **2a-d** are virtually identical (table 1-1) which provides the possibility of designing a pH sensor with enlarged dynamic range. To demonstrate the feasibility of the approach **2b** and **2c** were mixed together in the same sensor material. The absorption and the emission spectra of the hybrid material are virtually identical to the spectra of the individual probes (figure 1-5). The response of the sensor is also shown in figure 1-6. Indeed, the dynamic range of the new sensor is extended by ~ 2 units compared to the sensors based on single indicators. The calibration curve can still be fitted with eq. 1 (correlation coefficient > 0.998). In the same way, **2b** can be combined with **2d.** Since the pK_A values of both differ significantly, a two-step pH response is obtained (figure 1-S1, supplementary information). It should be emphasised here that the functionalities determining the pK_A value have very little influence on spectral and photophysical properties of the PBI indicators. Undesired effects caused by inner filter effects, Förster Resonance Energy Transfer between the probes or unlike photostabilities are therefore minimised. This is in contrast to other classes of pH indicators (e.g. fluoresceins) where the design of a broadband sensor is compromised by such effects. On the contrary, the PBI indicators presented here seem to be ideally suitable for the design of a broadband sensor. Such a sensor may represent an alternative to a glass electrode in various applications (e.g. environmental monitoring).

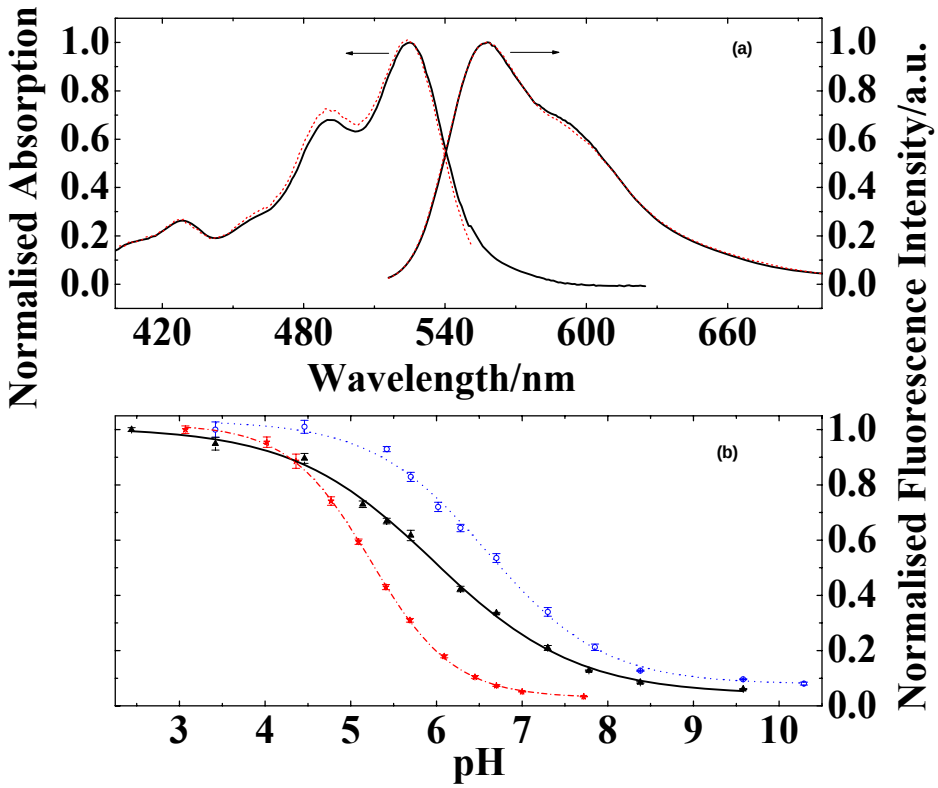

Figure 1-5: Characteristics of the broadband pH sensor containing 2b (0.08% w/w)) and 2c (0.16% w/w) in hydrogel D4: Top - spectral properties of the sensor (thick black line) compared to those of 2b (thin red line); bottom - the respective calibration curves (triangles - broadband sensor, stars - 2b, circles - 2c). Conditions: IS = 100mM, RT.

Cross-sensitivity to Ionic Strength

Cross-sensitivity to ionic strength (IS) is a common drawback of optical pH sensors. The effect of the ionic strength on the calibration plots can be rather small if the charge of the indicator is minimal. In fact, the lipophilic fluorescein derivatives (neutral in the protonated form and bearing a single negative charge in the deprotonated form) were demonstrated to possess very low cross-sensitivity to IS [27]. Figure 1-6 shows the response of a pH sensor based on an individual PBI (dye **3** in hydrogel D4) and the response of the broadband sensor based on the mixture of **2b** and **2c**. Evidently, both sensors exhibit virtually negligible cross-sensitivity to IS. In fact, the alteration of the IS from 50 to 500mM is accompanied by the increase of the apparent pK_A values by ≈ 0.1 units.

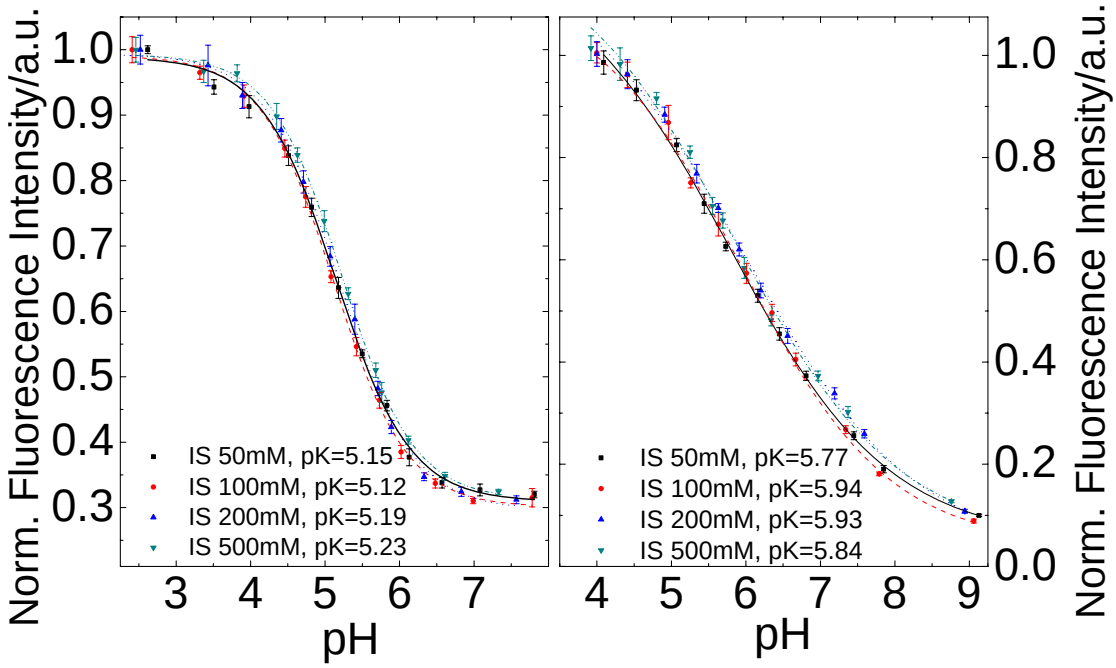

Figure 1-6: Ionic strength dependency of the calibration curves of the pH sensors. Left – for the sensor based on 3 (0.25% w/w) in D4; right - for broadband sensor containing 2b (0.08% w/w)) and 2c (0.16% w/w) in D4.

Leaching Tests

In case of **2a**, **2b**, **2d** and **3** no leaching into the aqueous solution is detectable after 24h in basic ($pH > pK_A + 2$) and acidic buffers ($pH < pK_A - 2$) which is in contrast to severe leaching observed for the indicators bearing two PET functionalities. In case of **2c** in D4, the absorption decreased by 7% within the first 6h at acidic pH but slowed after that (0.2%/h). No decrease was observed in basic buffer. Consequently, leaching is not critical for the investigated sensors due to pronounced hydrophobicity of the indicator dyes.

Photostability

Figure 1-7 demonstrates the photodegradation profiles for three pH indicators, namely perylene-based **2b** and **3**, and fluorescein octadecyl ester (FODE) which is used for comparison. Surprisingly, the photostability of the tetrachloro-PBI indicators **2a-d** was found to be rather

poor. In fact, the dyes bleach even faster than FODE. The rapid photodegradation is accompanied by the formation of a new dye which absorbs in NIR (700-800nm, figure 1-7, right). One of the possible bleaching pathways may be substitution of the chlorine atoms by hydroxide ions or water. This assumption is supported by the fact that the photostability of dissolved **2a-d** deteriorates in the presence of water, but it improves significantly in organic solvents such as tetrahydrofurane (THF). If water is added to THF the bleaching rate increases proportionally. Interestingly, the bleaching reaction is accompanied by an increase of fluorescence in unbuffered organic solvents which suggests the formation of HCl. The photobleaching rate of 1,6,7,12-tetrachloro-*N,N'*-(2,6-diisopropylphenylperylene-3,4,9,10-tertracarboxylic bisimide which bears no PET functionality was found to be similar which also suggests that the photobleaching pathway is determined by the presence of the halogens rather than the presence of a PET functionality.

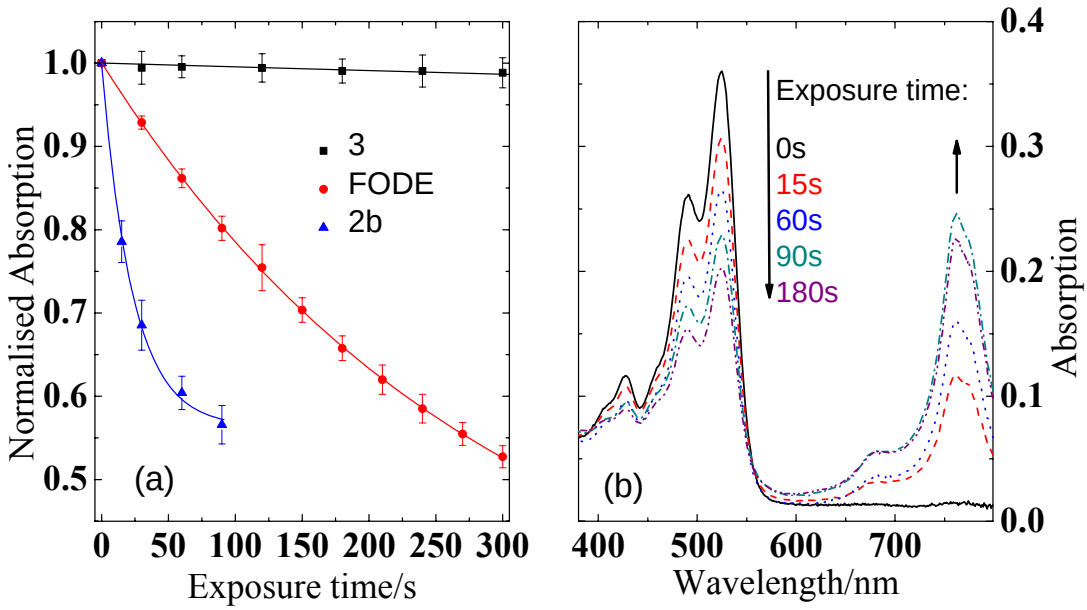

Figure 1-7: Photobleaching of perylene bisimide indicators in hydrogel D4: Left - decrease in absorption tetrachloro-substituted PBI 2b and tetraaryloxy-substituted PBI 3, and for fluorescein octadecyl ester (FODE); right - spectral changes accompanying the decomposition of 2b.

It is evident that substitution of the chlorine atoms in the PBI molecule by aryloxy groups renders the molecule highly photostable (figure 1-7, left). In fact, bleaching for **3** is several orders of magnitude slower than for FODE. For example, FODE degraded by almost 50% after 5min of irradiation whereas 3h of irradiation of **3** results in degradation of only 1.5% (pH 1.5) or 3% of the indicator (pH 9.6). Notably, the phototostability of **3** in organic solvent is not affected by the presence of water. Evidently, the aryloxy-substituted PBI is a platform of choice for designing pH sensors, but the tetrachloro-substituted derivatives are excluded from many applications due to their poor photostability.

Dynamic Response

Figure 1-8 demonstrates the response of the sensor based on **2b** in hydrogel D4 to an alteration of pH. As can be seen, the response is reversible and fairly fast (t_{90} is 5min on going from pH 6 to pH 4.3 and <30s in the reverse direction). The response time is a critical parameter if pHPMA is used

as immobilisation matrix. Significantly longer response times (>1h) are characteristic even for the thin (2 μm) sensing layers. In contrast to that, the sensors based on pHEMA are found to have significantly faster response which is comparable to the D4-based sensors. Generally, the sensors respond considerably faster to increasing pH than to its decreasing.
It was found that the sensors based on **3** embedded in hydrogel D4 responds much slower than the sensors based on **2a-d**. In freshly prepared foils, t_{90} can be ~10 min on going from pH 6 to pH 4 and ~5 min in the reverse direction. However, a considerable flattening of the curve causes significantly longer t_{95} (~60 and 15 min, respectively). It should also be noted that response times tend to significantly increase over storage time. That also results in worse reversibility for older foils. Evidently, very long response times for **3** indicate its localisation in hydrophobic domains of the hydrogel. Several strategies can be proposed for improving the response times of the indicators. For example, significantly less hydrophobic aryloxy substituents can be used to force the indicator into more hydrophilic regions. Covalent immobilisation (for instance via replacement of the 2,6-diisopropylphenyl substituent with a vinyl or acrylate moiety and subsequent co-polymerisation) may also help to provide a hydrophilic environment for the indicator.

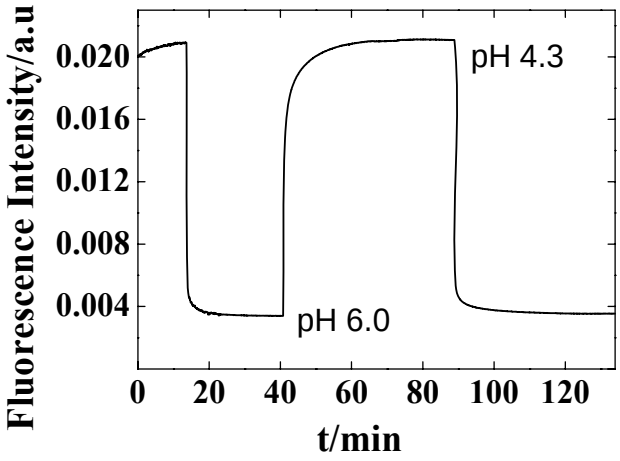

Figure 1-8: Response curves of 2b in D4 (dye content 1%, layer thickness 5μm) to dynamic changes of pH.

Long-term Stability

In hydrogel D4, the calibration curves show some drift towards lower I_A/I_B if the sensors are stored in buffer solution for several days (figure 1-9). For instance, in case of **2a**, I_A/I_B decreases from 5.5 to 2.9 within 4 weeks. Notably, the apparent pK_A values remain constant. Slow aggregation of the indicator is a possible reason for this phenomenon. Nevertheless, the drift is negligible within an interval of a few hours, but for longer measurements recalibration is required. On the other hand, virtually no drift was observed for the sensors based on pHPMA. Those sensors can be used for weeks without considerably changing their calibration plots.

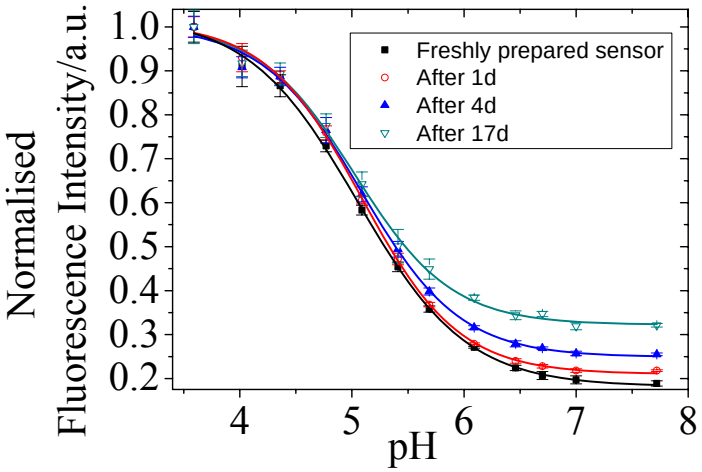

Figure 1-9: Calibration plots for 2a (0.25% w/w) in D4 followed over time. The sensors were stored in aqueous buffers (IS = 100 mM) in the darkness.

Referencing

Evidently, fluorescence intensity is a rather ambitious parameter which is affected by various factors such as light intensity of the excitation source, sensitivity of the detector, turbidity of the probe etc. Therefore, different referencing schemes are commonly employed. For the sensors presented above ratiometric measurements become possible by immobilising a fluorescent pH-insensitive dye in the same matrix (figure 1-S2). Other schemes such as Dual Lifetime Referencing are also possible.

Conclusion

pH-sensitive PET functional perylene bisimides (PBIs) were obtained in a single reaction step starting from commercially available compounds. The new indicators possess good luminescence brightness which is substantially higher that for common PET indicators such as naphthalimides. Two classes of PBIs with differing spectral properties were investigated: tetrachloroPBIs (**2a-d**) and a tetraaryloxyPBIs (**3**) which features bathochromically shifted absorption and emission spectra. Due to their small charge the sensing materials possess virtually negligible cross-sensitivity to ionic strength. The sensors based on tetrachloroPBIs possess good brightness in hydrogels D4, pHPMA and pHEMA and show excellent PET efficiencies. The pK_A value of the sensor can be tuned by attaching different amino groups to the PBI indicator. Virtually identical photophysical properties allow the preparation of a sensor for a broad pH range (> 4 pH units). Unfortunately, the sensors based on tetrachloroPBIs photodegradate readily. On the contrary, those based on the tetraaryloxy-substituted **3** possess unmatched photostability which is orders of magnitude higher than that of a common fluorescein-based indicator. As is demonstrated, the pK_A value is not considerably influenced by the nature of the chromophore. This suggests that tuneability of pK_A is applicable to tetraaryloxy-substituted PBIs and other perylene chromophores. The performance of the sensor based on **3** is compromised by long dynamic response which indicates localisation of the indicator in the hydrophobic domains of the hydrogel. It can be concluded that the PET-based perylenes represent a promising class of pH indicators

featuring excellent brightnesses, high photostabilities and tuneability of proton affinity and spectral properties. They constitute a platform for the future design of high-performance pH sensors that may outperform existing systems. However, all presented sensors still suffer from drawbacks. The poor photostability of those based on tetrachloroPBIs has been shown to be outstandingly improved by using tetraaryloxy-substituted **3**. To overcome the issues of slow dynamic response and signal drifts, optimisation in the indicator structure or/and covalent immobilisation into the polymer network are the most promising concepts.

Acknowledgement

The financial support from the Austrian Science Fund FWF (project P 21192-N17) is gratefully acknowledged. We thank Prof. Robert Saf (Graz University of Technology) for acquiring MS spectra.

Supplementary Information

to *New Fluorescent Perylene Bisimide Indicators – a Platform for Broadband pH Optodes*

Syntheses

*1,6,7,12-Tetrachloro-N-(2,6-diisopropylphenyl)-N'-(2-dibutylaminoethyl)perylene-3,4:9,10-tertracarboxylic bisimide (**2b**).*

1,6,7,12-Tetrachloroperylene-3,4:9,10-tetracarboxylic bisanhydride **1a** (1 g, 1.88 mmol) was dissolved in NMP (150 ml), warmed to 35°C and a solution of *N,N*-dibutylethylenediamine (0.403 ml, 1.88 mmol) in NMP (15 ml) was added dropwise under vigorous stirring. After the solution was stirred for 2 h the temperature was elevated to 50°C stirring continued for 1.5 h. Propionic acid (50 ml) and 2,6-diisopropylaniline (1.54 ml, 7.51 mmol) were added. The solution was cooled to room temperature and poured onto 20% aqueous NaCl (1,400 ml). The brown precipitate was separated by centrifugation, washed, re-dissolved in CH_2Cl_2:acetone 3:1, dried with Na_2SO_4 and purified by column chromatography with silica gel as the stationary and $CHCl_3$:MeOH as the mobile phase. **2b** was obtained as a deep orange powder (572 mg, 36%). ^{1}H NMR (300MHz, $CDCl_3$, TMS): δ=8.75 (2H, s, Cl-C-C<u>H</u>(1)); 8.71 (2H, s, Cl-C-C<u>H</u>(2)); 7.53 (1H, t, iPr-C-CHC<u>H</u>-, J=7.7Hz); 7.37 (2H, d, iPr-C-C<u>H</u>-); 4.33 (2H, t, $(CO)_2NC\underline{H}_2$-, J=7.0Hz); 2.66-2.83 (4H, m, PhC<u>H</u>$(CH_3)_2$; $(CO)_2NCH_2C\underline{H}_2$); 2.54 (4H, t, $NC\underline{H}_2C_3H_7$, J=7.3Hz); 1.44 (4H, p, $NCH_2C\underline{H}_2C_2H_5$, J=6.9Hz); 1.26-1.36 (4H, m, $NC_2H_5C\underline{H}_2CH_3$)1.19 (12H, dd, -CH($C\underline{H}_3)_2$, J_1=6.7Hz, J_2=4.0Hz); 0.87 (6H, t, $C_3H_7C\underline{H}_3$, J=7.2Hz. MALDI-TOF: m/z [MH^+] 842.2079 found, 842.2086 calcd.

*1,6,7,12-Tetrachloro-N-(2,6-diisopropylphenyl)-N'-(4-butylaminoethyl)perylene-3,4:9,10-tertracarboxylic bisimide (**2c**).*

1,6,7,12-Tetrachloroperylene-3,4:9,10-tetracarboxylic bisanhydride **1a** (1 g, 1.88 mmol) and 2,6-diisopropylaniline (0.350ml, 1.80 mmol) were dissolved in 300 ml of NMP:propionic acid (4:1 v/v) in a round bottom flask. The mixture was kept at 130°C for 16 h and after adding more 2,6-diisopropylaniline (0.050 ml, 0.26 mmol) and heating for 3h it was allowed to cool to 40°C. *N*-butylethylenediamine (0.245 ml, 1.71 mmol) in NMP (15ml) was added in portions and the solution was stirred at 40°C for 3 h. The deep brown reaction mixture was added to 30% aqueous NaCl (1.4 l), the precipitate was separated by centrifugation, washed, re-dissolved in CH_2Cl_2:acetone (3:1), dried with Na_2SO_4 and purified by column chromatography with silica gel as the stationary and toluene:EtOH as the mobile phase. **2c** was obtained as a deep orange powder (186mg, 14%). ^{1}H NMR (300MHz, $CDCl_3$, TMS): δ=8.75 (2H, s, Cl-C-C<u>H</u>-(1)); 8.71 (2H, s, Cl-C-C<u>H</u>-(2)); 7.53 (1H, t, iPr-C-CHC<u>H</u>-, J=7.7Hz); 7.37 (2H, d, iPr-C-C<u>H</u>-); 4.42 (2H, m, $(CO)_2NC\underline{H}_2$-); 3.09 (2H, m, $(CO)_2NCH_2C\underline{H}_2$); 2.68-2.80 (4H, m, PhC<u>H</u>$(CH_3)_2$; $NC\underline{H}_2C_3H_7$); 1.47-1.58 (2H, m, $NCH_2C\underline{H}_2C_2H_5$); 1.31-1.41 (2H, m, $NC_2H_5C\underline{H}_2CH_3$), 1.19 (12H, dd, -CH($C\underline{H}_3)_2$, J_1=6.7Hz, J_2=3.8Hz); 0.87 (3H, t, $C_3H_7C\underline{H}_3$, J=7.1Hz). MALDI-TOF: m/z [MH^+] 786.1456 found, 786.1460 calcd.

*1,6,7,12-Tetrachloro-N-(4-dimethylaminophenyl)-N'-(2,6-diisopropylphenyl)perylene-3,4:9,10-tertracarboxylic bisimide (**2d**).*

1,6,7,12-Tetrachloroperylene-3,4:9,10-tetracarboxylic bisanhydride **1a** (1 g, 1.88 mmol), 2,6-diisopropylaniline (0.424ml, 2.07mmol) and *N,N*-dimethyl-*p*-phenylenediamine (0.240mg, 1.69mmol) were placed in a round bottom flask and dissolved in 250 ml of NMP:propionic acid (4:1v/v). The mixture was heated to 130°C overnight. It was cooled to room temperature and

added to 20% aqueous NaCl (1.400ml). The precipitate was separated by centrifugation, washed, redissolved in CH_2Cl_2/acetone 6:1, dried with Na_2SO_4 and purified by column chromatography with silica gel as the stationary and toluene:acetone as the mobile phase to yield **2d** as an orange powder (140 mg, 10%). ^{1}H NMR (300MHz, $CDCl_3$, TMS): δ=8.76 (4H, d, Cl-C-C<u>H</u>-(1,2) Δδ=4.0Hz); 7.53 (1H, t, iPr-C-CHC<u>H</u>-, J=7.7Hz); 7.37 (2H, d, iPr-C-C<u>H</u>-); 7.16 (2H, d, $(CH_3)_2$NCCHC<u>H</u>, J=8.9Hz), 6.87 (2H, d, $(CH_3)_2$NCC<u>H</u>); 3.05 (6H, s, NC<u>H</u>$_3$); 2.74 (2H, p, PhC<u>H</u>$(CH_3)_2$ J=6.8Hz); 1.19 (12H, dd, -CH(C<u>H</u>$_3)_2$, J_1=6.7Hz, J_2=3.8Hz). MALDI-TOF: m/z [MH^+] 806.1136 found, 806.1147 calcd.

*1,6,7,12-Tetra(4-tert-butylphenoxy)-N-(2,6-diisopropylphenyl)-N'-(2-dibutylaminoethyl)perylene-3,4:9,10-tertracarboxylic bisimide (**3**).*

1,6,7,12-Tetra(4-tert-butylphenoxy)perylene-3,4:9,10-tetracarboxylic bisanhydride **1b** (2 g, 2.03 mmol) was dissolved in 300 ml of NMP)/propionic acid (1:1 v/v), the solution was flushed with N_2 and heated to 130 °C. 2,6-Diisopropylaniline (1.25 ml, 6.09 mmol) was added and the deep red mixture was stirred for 24 h. After cooling to 40°C N,N-dibutylethylenediamine (0.853 ml, 4.06 mmol) was added dropwise. The mixture was stirred overnight at RT. The violet crude product was precipitated with water, filtered, re-dissolved in CH_2Cl_2, dried with Na_2SO_4 and purified by column chromatography with silica gel as the stationary and ethyl acetate:methylene chloride as the mobile phase. Yield: 184 mg (7%) of **3**. ^{1}H NMR (300MHz, $CDCl_3$, TMS): δ=8.26 ((4H, d, ArO-C-C<u>H</u>-(1,2), Δδ=3.7Hz); 7.41 (1H, t, iPrCCHC<u>H</u>-, J=7.7Hz); 7.19-7.29 (10H, m, tBuCCHC<u>H</u>-; iPrCC<u>H</u>-); 6.84 (8H, dd, tBuCC<u>H</u>-(1,2), J=8.6Hz, Δδ=5.6Hz); 4.22 (2H, t, $(CO)_2$NC<u>H</u>$_2$-, J=7.0Hz); 2.64-2.77 (4H, m, PhC<u>H</u>$(CH_3)_2$; $(CO)_2NCH_2C$<u>H</u>$_2$); 2.51 (4H, t, NC<u>H</u>$_2C_3H_7$, J=7.2Hz); 1.37-1.52 (4H, m, NCH_2C<u>H</u>$_2C_2H_5$); 1.28 (40H, d, C(C<u>H</u>$_3)_3$ (1,2), Δδ=6.8Hz, NC_2H_5C<u>H</u>$_2CH_3$); 1.11 (12H, d, -CH(C<u>H</u>$_3)_2$, J_1=6.7Hz); 0.87 (6H, t, C_3H_7C<u>H</u>$_3$, J=7.2Hz). MALDI-TOF: m/z [MH^+] 1298.7321 found, 1298.7197 calcd.

Further Results

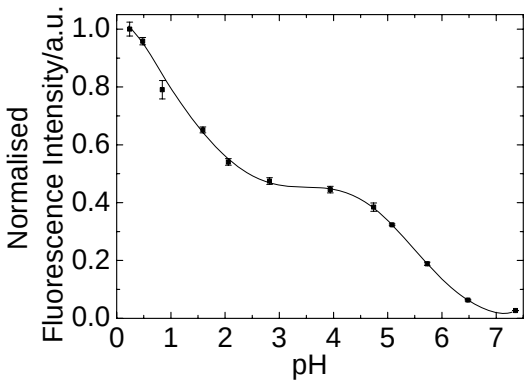

Figure 1-S1: Calibration curve a pH sensor containing 2b (0.0125% w/w) and 2d (0.0125% w/w) in hydrogel D4, conditions: IS = 100mM, RT. While the pH-response of both indicator dyes (2d: 0.5<pH<1.5; 2b: 5<pH<6) is clearly observable, their pK_A' values are too unlike to allow the design of a true broadband optrode with a single but broad dynamic range.

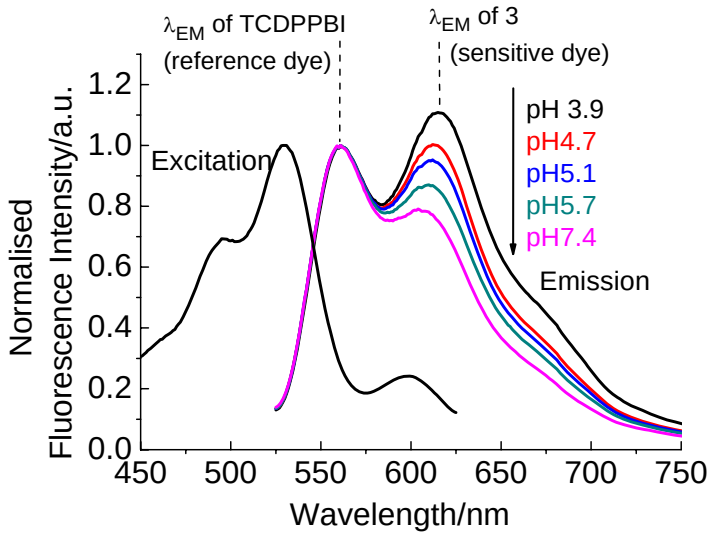

Figure 1-S2: A ratiometric pH sensor with 3 (0.5% w/w) as indicator dye and TCDPPBI (1.25% w/w) as reference dye in hydrogel D4. Emission spectra were taken with an excitation wavelength of 515nm, excitation spectra were observed at 635nm. Notably, TCDPPBI acts as donor in Föster resonance energy transfer, and 3 (the absorption spectrum of which perfectly matches the emission spectrum of TCPBI) is an acceptor. Since the absorption spectrum of the acceptor does not depend on pH, the efficiency of FRET (and the intensity of the donor) is constant in the whole pH range. On the contrary, the fluorescence intensity of 3 decreases if the pH is increased. Therefore, the ratio between the fluorescence in the emission maxima of both dyes allows pH calibration with a referenced signal.

Chapter 2

Novel Near Infra-red Fluorescent pH-Sensors Based on 1-Aminoperylene Bisimides Covalently Grafted to Poly(acryloylmorpholine)

Preface to Chapter 2

In this chapter, very important and significant improvements of the pH-sensors based on perylene bisimides (PBIs) are presented, making them highly promising for practical application.
Firstly, the absorption and fluorescence wavelengths of the PBI probes are dramatically increased without enlarging the chromophore core, thus without further provocating dye aggregation. A very simple reaction of the tetrachloro-PBIs with secondary cyclic amines yields the new 1-aminoPBIs which feature excitability in the deep red, near infra-red emission and large Stokes shifts due to their strong push-pull character. Though fluorescence brightness is reduced (to $\varepsilon^x\Phi_F \approx 5{,}000\ M^{-1}cm^{-1}$, compared to $\varepsilon^x\Phi_F \approx 40{,}000\ M^{-1}cm^{-1}$ for the tetrachloro-PBIs), it is still satisfying for a near infra-red-emissive dye and sufficient for high signal intensity.
Secondly, sensor dynamics are greatly improved to yield a pH-sensor which features fast and complete response, as well as excellent signal reproducibility and good long-term stability. That is accomplished by a concept for covalent dye coupling using the dye as cross-linker, which results in tight immobilisation of the dye in the matrix network. Coupling is carried out attaching acrylate groups followed by photo-co-polymerisation. The acrylate groups are grafted to the chromophore by chlorosulfonation of the 2,6-diisopropylphenyl substituents in the PBI, followed by reaction with *N*-aminopropylmethacrylamide. This is a flexible method that can be used to graft many different groups to various fluorophores – however, stability of the fluorophore against chlorosulfonic acid is a prerequisite. The co-polymerisation method used here yields very robust sensor layers with excellent adhesion and mechanical stability consisting of a material not yet employed in pH-sensors, poly(acryloylmorpholine).
Though the new concept for the preparation of new sensors with covalently coupled pH-probe is only tested with 1-aminoPBIs, it is likely that it would yield sensors with similarly good performance when the significantly brighter ($\varepsilon^x\Phi_F \approx 40{,}000\ M^{-1}cm^{-1}$) tetraphenoxy-PBIs are used for applications where long fluorescence wavelengths may be less important than strong signals.
Because this sensor shown near infra-red fluorescence, covalent dye coupling and good long-term stability, it makes up a key result to this thesis by which many objectives have been realised.

Novel Near Infra-red Fluorescent pH-Sensors Based on 1-Aminoperylene Bisimides Covalently Grafted to Poly(acryloyl-morpholine)

This chapter was published in **Chemical Communications**, 2013, 49, 2139–2141; doi: 10.1039/C3CC39151E

Authors: Daniel **Aigner, Sergey M. Borisov, Peter Petritsch and Ingo Klimant**

Novel pH sensors relying on 1-aminoperylene bisimide dyes covalently grafted to cross-linked poly(acryloylmorpholine) are presented. They feature fluorescence in the near infra-red range and a large Stokes shift (> 90 nm).

Fluorescence is a powerful tool for probing physical, (bio)chemical and biological (micro)environments as it allows highly sensitive mapping with excellent temporal and spatial resolution [1,2]. In the past decade, there has been a rapidly increasing interest in fluorescent dyes with near infra-red (NIR) emission since low energy light generates much lower fluorescent and scattering background and causes far less damage to biological samples. While NIR emitting fluorescent markers have become readily commercially available, pH probes are still scarce in that spectral range [73,91,107,145]. pH is one of the key analytes in biological and medical samples as well as in many biotechnological applications. This work focuses on a novel NIR fluorescent pH probe which is particularly useful in a solid matrix, *i.e.* in a pH sensor.

Perylene bisimides (PBIs) have been extensively investigated for numerous applications in molecular (opto)electronics and numerous other fields due to their exceptional optical and electrochemical properties, their remarkable ability to form supramolecular assemblies and their outstanding (photo)chemical stability [118-120,122,182,183]. While the PBI parent compounds emit yellow light, several strategies have been presented to increase their excitation and emission wavelengths. Extension of the π-system by elongation of the perylene core [184,185], attachment of unsaturated residues to the core via C-C bonds [171,186] or condensation with 1,2-diamines [187,188] are effective in this regard but result in very hydrophobic structures with a pronounced tendency towards aggregation in polar media which is highly unfavourable for the use in pH sensors. The attachment of electron-donating groups, in particular amines, can increase excitation and emission wavelengths by introducing a push-pull effect without an extension of the π-system. The concept has been successfully employed on the structurally related naphthalene diimides to obtain red-light emitting dyes and pH probes [81,86,89,189]. However, to the best of our knowledge, the corresponding NIR emissive pH indicators based on PBIs have never been reported.

In this work we present the PBI-based pH probes **1** and **2** (figure 2-1) and a pH sensor featuring covalent dye linkage, fluorescence emission in the NIR range (λ_{MAX} 735 nm) and a large Stokes shift (> 90 nm). pH sensitivity originates from Photoinduced Electron Transfer (PET) from the non-protonated amine (PET group) to the perylene chromophore, resulting in fluorescence quenching at basic pH [60,61]. In **1**, Intramolecular Charge Transfer (ICT) also contributes to pH sensitivity.

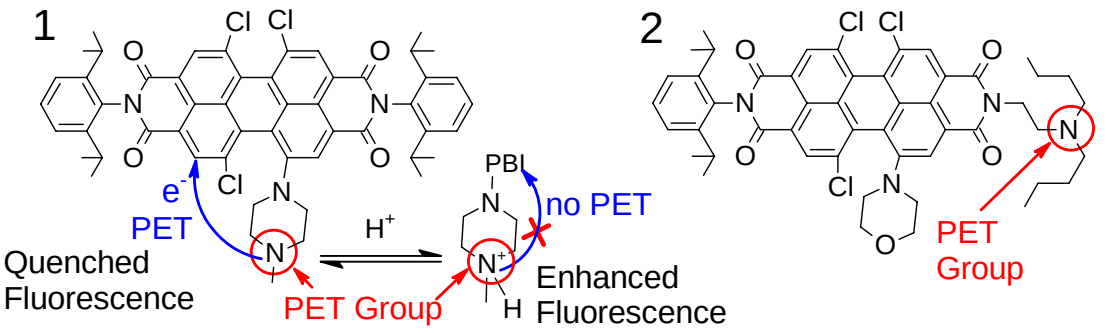

Figure 2-1: Structures of the PET (Photoinduced Electron Transfer) pH indicators 1 (PET group close to the perylene core) and 2 (PET group in the imide position).

Table 2-1: Spectral properties of 1 - 3 and the not amino-substituted pH indicator 4c[9] *N*-(2-(*N*,*N*-dibutylamino)ethyl)-(*N'*-(2,6-diisopropylphenyl)-1,6,7,12-tetrachloroperylene-3,4:9,10-tertracarboxylic bisimide (structure shown in the supplementary information)): ε - molar absorption coefficient, $\lambda_{max\ abs}$ absorption maximum wavelength, $\lambda_{max\ em}$ fluorescence maximum wavelength, Φ_F relative fluorescence quantum yield; n.d. not determined.

Dye	Medium	$\varepsilon \cdot 10^{-4}$ ($M^{-1}cm^{-1}$) acidic/ basic	λ_{max} abs (nm) acidic/ basic	λ_{max} em (nm) acidic/ basic	Φ_F acidic/ basic
1	THF	1.48/1.83 1.91/1.95	444/446 627/661	727/751	0.26/0.002
	D4	n.d.	447/450 631/672	706/n.d.	n.d.
2	THF	1.54/1.59 1.76/1.78	449/448 657/652	758/754	0.13/0.08
	D4	n.d.	451/449 666/659	740/736	n.d.
3	THF	1.54/1.69 1.99/1.95	445/448 630/666	732/755	0.23/0.003
	pAcMo[a]	n.d.	450/453 641/682	735/n.d.	n.d.
4c	CH_2Cl_2	1.04 2.78 4.00	426/426 486/486 520/520	552/552	0.95/0.015

[a] Poly(acryloylmorpholine)

The pH probes can be prepared starting from the corresponding 1,6,7,12-tetrachloroperylene bisimides in a simple step. The bisimides are accessible from the commercially available bisanhydride *via* standard procedures. The substitution of a single chlorine atom by a cyclic secondary amine (figure 2-2) results in a bathochromic shift of 100 - 140 nm, compared to the starting material. Several amino-PBIs have been described [127,186,190-194], however they have not yet been prepared over the substitution of chlorine. The remaining chlorine atoms reduce the electron density in the perylene core which enhances the push-pull effect and makes the chromophore a good acceptor for PET.

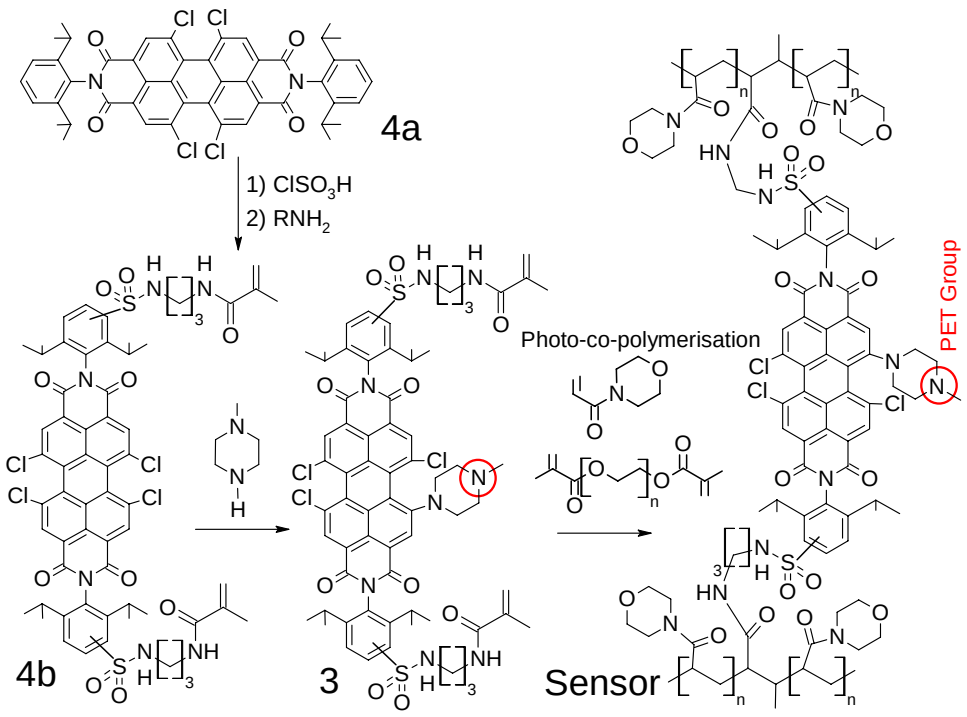

Figure 2-2: Preparation scheme for the pH sensor with covalent dye linkage. A detailed description of all synthetic steps can be found in the ESI.

1 and **2** show two very distinct absorption bands at 450 nm and > 627 nm which correspond to the $S_0 \rightarrow S_2$ and the $S_0 \rightarrow S_1$ transitions [192]. They possess lower fluorescence brightness (table 2-1; similar to literature values) [127] compared to the usually very bright PBIs without amino groups. However, brightness is still satisfying for pH probes with NIR emission. The photostability of **1** is better than the one of seminaphthorhodafluor (SNARF) decyl ester, which belongs to a frequently employed class of red light emitting pH probes. Exposed to the same illumination intensity, the SNARF ester is degraded by 30% in 1.5 h, **1** by 20% in acidic and 2% in basic solution (figure 2-S1 in the supplementary information).

Probe **1** carries the PET group close to the perylene core, in contrast to **2** where it is located in the imide position and thus is fully electronically decoupled. We found a strong effect of pH/acidity on fluorescence brightness of **1** both in solution and in a hydrogel film (D4®). Notably, the attachment of a secondary amino group by reacting **4a** with piperazine instead of *N*-methylpiperazine results in a dye which is equally pH sensitive but unstable in solution over time and shows broad, non-sigmoidal pH calibration curves. A possible reason is the higher reactivity of the secondary amine. For **2**, the effect of pH/acidity is much weaker and is largely dependent on the environment – **2** is 4.2 times brighter in acidic than in basic methylene chloride; in acetone/water 3:1 (V/V) the ratio 1.5 was found. In a D4 film, the pH induced signal change is 15%, too small for a reliable pH sensor (figure 2-3). Note that fluorescence quantum yields decrease in the order protonated **1** > (de)protonated **2** > deprotonated **1** while absorption and fluorescence spectra are bathochromically shifted. The electron-withdrawing effect of the nearby heteroatom (that is, NH^+ > O > N, respectively) weakens the push-pull effect in the 1-aminoperylenes. This ICT effect causes a pH-dependence in the absorption spectra of **1**. The low brightness of deprotonated **1**, compared to the protonated form, can be explained by the combination of ICT and PET. Since **1** proved to be the most stable and sensitive, this basic

structure (*i.e.* a tertiary amine bound closely to the perylene core) has been selected for the preparation of a NIR pH sensor.

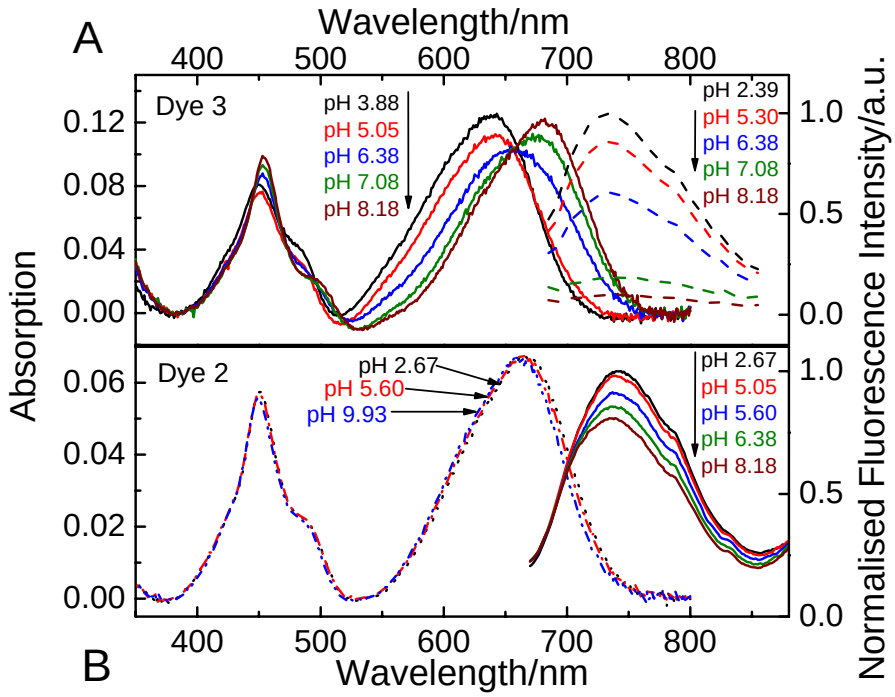

Figure 2-3: A: Absorption and fluorescence emission spectra (excited in the isobestic point) of 3 (0.2% (w/w)), covalently coupled to a cross-linked poly(acryloylmorpholine) layer (thickness 20 µm), measured at different pH (aqueous buffer, ionic strength 100 mM). B: Corresponding spectra for 2, physically entrapped in D4 hydrogel (0.5% w/w, 7 µm thick layer).

The immobilisation of pH probes in a solid matrix to yield pH sensors is of outstanding importance for many applications. From previous work, we know that the performance of pH sensors relying on physically entrapped PBIs can be unsatisfying in long-term measurements. We thus decided to prepare a pH sensor with covalent dye linkage to suppress migration and aggregation. This was achieved by the attachment of methacrylate groups and subsequent photo-co-polymerisation [195] into a cross-linked polymer layer which in turn is covalently linked onto a glass substrate upon polymerisation. Poly(acryloylmorpholine) was selected as bulk matrix polymer since preliminary experiments revealed that it provides suitable hydrophilicity (water content 50% in swollen condition, figure 2-S2) and good solubility of the pH probes in the monomer. This is the first time the polymer is reported as a matrix in an optical pH sensor. Methacrylate-modified **3** can be prepared from **1** by chlorosulfonation followed by reaction with an amino group (figure 2-2). This novel approach is not limited to tagging acrylates but can be extended to a large variety of functionalities, *e.g.* highly polar or charged groups in order to obtain water-soluble pH probes for biological imaging. Concerning spectral and pH sensitive properties, **3** is very similar to **1** (table 2-1, figures 2-S3,2-S5,2-S6).

The resulting pH sensor features very good reproducibility and signal stability in long-term measurement, together with a response time of < 90 s. It is much superior in this regard to sensors relying on **3** and **1** physically entrapped into D4 hydrogel (figure 2-4A and figure 2-S7, respectively). For those sensors the poor dynamic response is probably caused by pH-dependent dye migration between the hydrophilic and hydrophobic domains present in D4 which has an impact on fluorescence quantum yield. Poly(acryloylmorpholine), in contrast, is a more

homogeneous matrix and dye migration is strongly suppressed by covalent linkage. Note that **3** acts as a cross-linker, reducing its own mobility to a minimum.

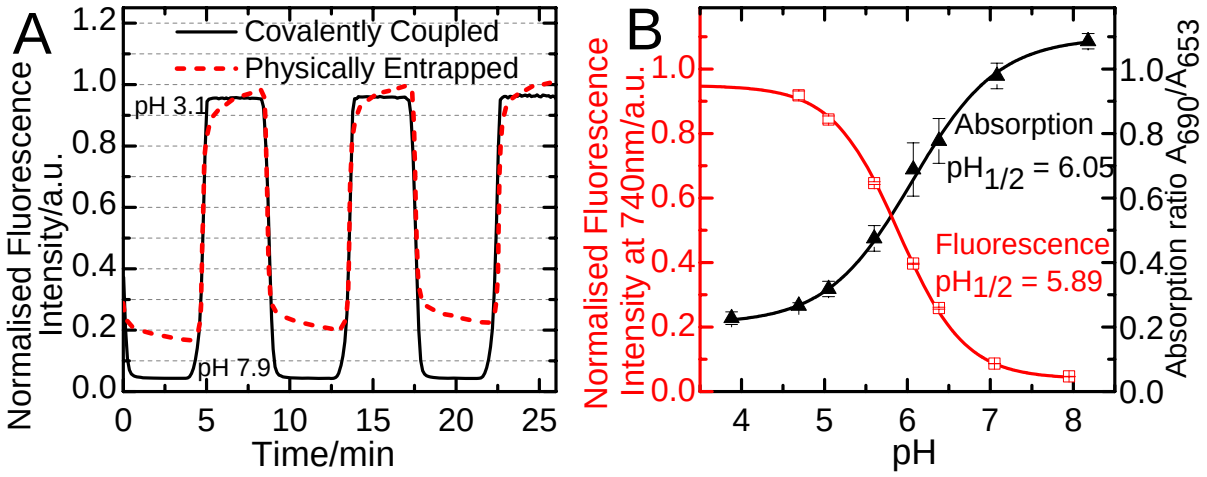

Figure 2-4: A: Dynamic response of the pH sensor with covalently grafted 3 (layer as specified below figure 2-3), compared to a D4 hydrogel sensor where 3 (0.5% w/w, layer thickness 7µm) is physically entrapped. B: pH calibration curves of the sensor with covalent dye linkage. $pH_{1/2}$ is the value at which half of the pH induced signal change is effective.

The sensor is very promising for biotechnological applications since its most sensitive range (pH 5 - 7) matches the pH region of interest in a wide variety of fermentation processes. This feature is particularly interesting since the recently presented NIR indicators [73,145] operate at higher pH. Photobleaching is not critical for the sensor, as displayed in figure 2-S1. Cross-sensitivity to ionic strength, a common problem in optical pH sensors, is small in the range 100 – 400 mM (error < 0.1 pH units, figure 2-S8; this is the range present in most biotechnological applications). To underline practical applicability, a referenced pH sensor employing the dual lifetime referencing (DLR) technique [17,22] has been prepared. The good performance of the referenced system is demonstrated in figure 2-S3.

In conclusion, we have presented a facile route to a novel NIR fluorescent pH sensor with covalent linkage of the indicator dye. The sensor is highly suitable for monitoring scientific and industrial biotechnological applications. In comparison to cyanine dyes which are the most frequently employed NIR emissive pH probes the presented indicator dye offers the advantages of good photostability and a large Stokes shift [91,107]. Current efforts are focused on indicators covering other pH ranges, as well as water-soluble derivatives for bioimaging.

This work was supported by the Austrian Science Fund FWF (project P 21192-N17). We thank Prof. Robert Saf (Institute for Chemistry and Technology of Materials) for acquiring MALDI-TOF spectra and the Institute of Organic Chemistry for their support in performing LC-MS.

Supplementary Information

to *Novel Near Infra-red Fluorescent pH-Sensors Based on 1-Aminoperylene Bisimides Covalently Grafted to Poly(acryloylmorpholine)*

Further Results

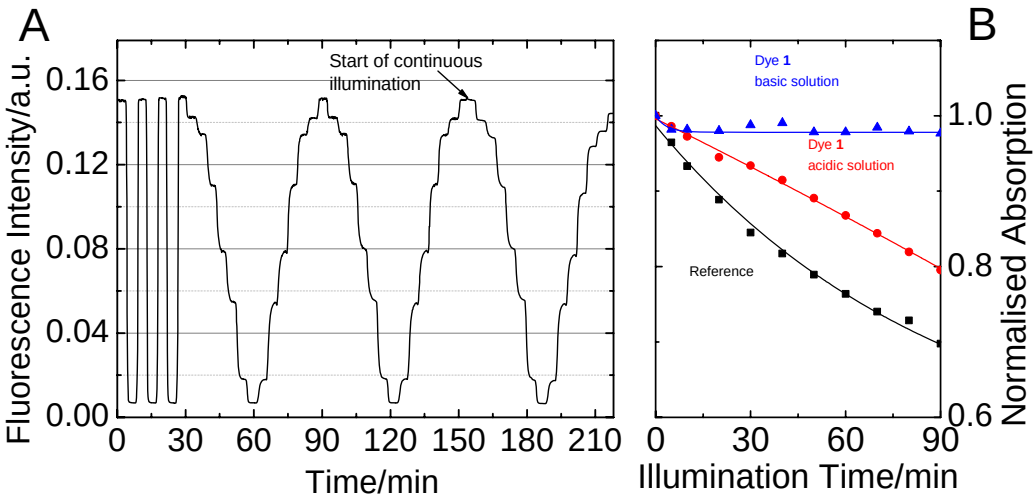

Figure 2-S1: A: Performance of 3 (0.2 % (w/w)), covalently coupled to a cross-linked poly(acryloylmorpholine) layer (thickness 20 µm) in long-term measurement and under varying illumination conditions – the LED used for excitation is switched to continuous illumination (until then illumination time was 14% of the total measurement time). > 1 h of continuous illumination causes an error of < 0.1 pH units, when calculated over the calibration curve. Note that in practical applications continuous illumination is not necessary and an interrogation time of 30 ms is typically sufficient to obtain a measurement point. Thus 1 h of continuous illumination equals about 100,000 measurement points which enables a long measurement time (days or weeks, depending on the application). B: Photodegradation profiles of 1 and SNARF decyl ester as a reference in *N,N*-dimethylformamide (acidic: 0.1% V/V trifluoroacetic acid; basic: 0.1% V/V ethyldiisopropylamine) when illuminated with a high-power LED array (645 nm). Absorption was observed in the respective maxima, *i.e.* 630 nm for acidic 1, 670 nm for basic 1, 657 nm for the reference. Initial absorptions were 1.1 at 645 nm.

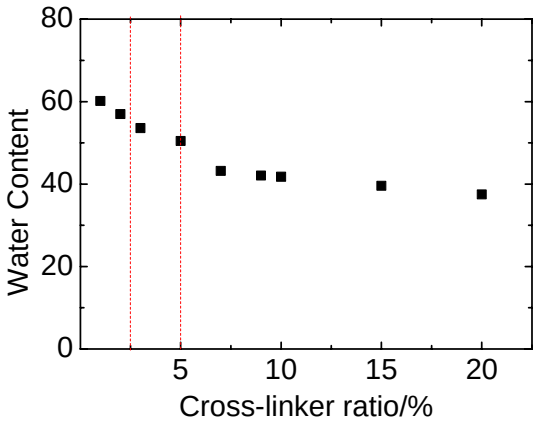

Figure 2-S2: Water content of poly(acryloylmorpholine) in the swollen state as a function of the cross-linker (polyethylene glycol diacrylate) ratio used (% w/w with respect to the total monomer weight). Water content was determined gravimetrically. The cross-linking degrees used in sensors in this work are 5 % for the intensity based sensor and 2.5 % for the dually lifetime referenced sensor (dashed lines).

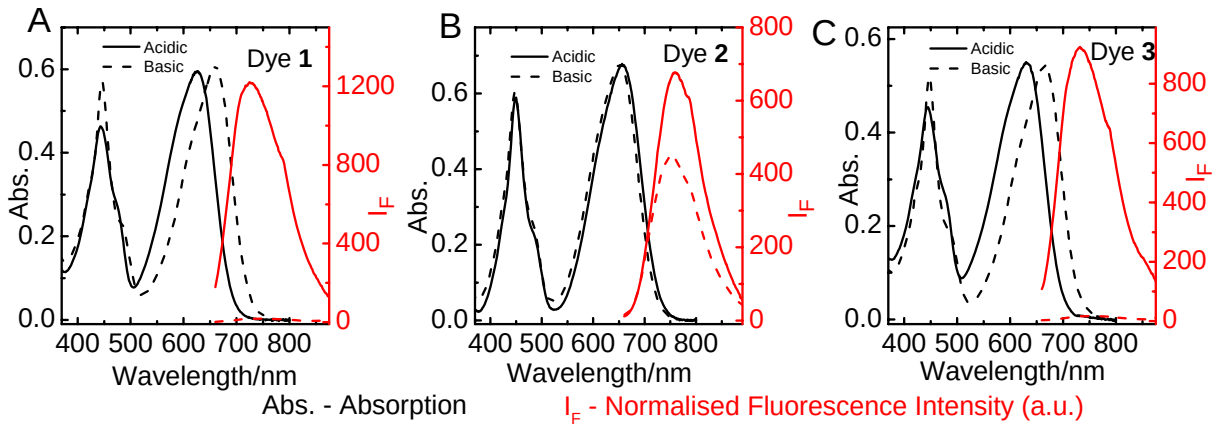

Figure 2-S3: Spectral properties of 1 (A), 2 (B) and 3 (C) in tetrahydrofuran/water 9:1 (V/V). Solutions were acidified with HCl (10 mM) and made basic with ethyldiisopropylamine (ratio 0.1 % V/V). Concentrations were 30 µM for measuring absorption and 3 µM for fluorescence. Fluorescence was excited in the respective isosbestic points.

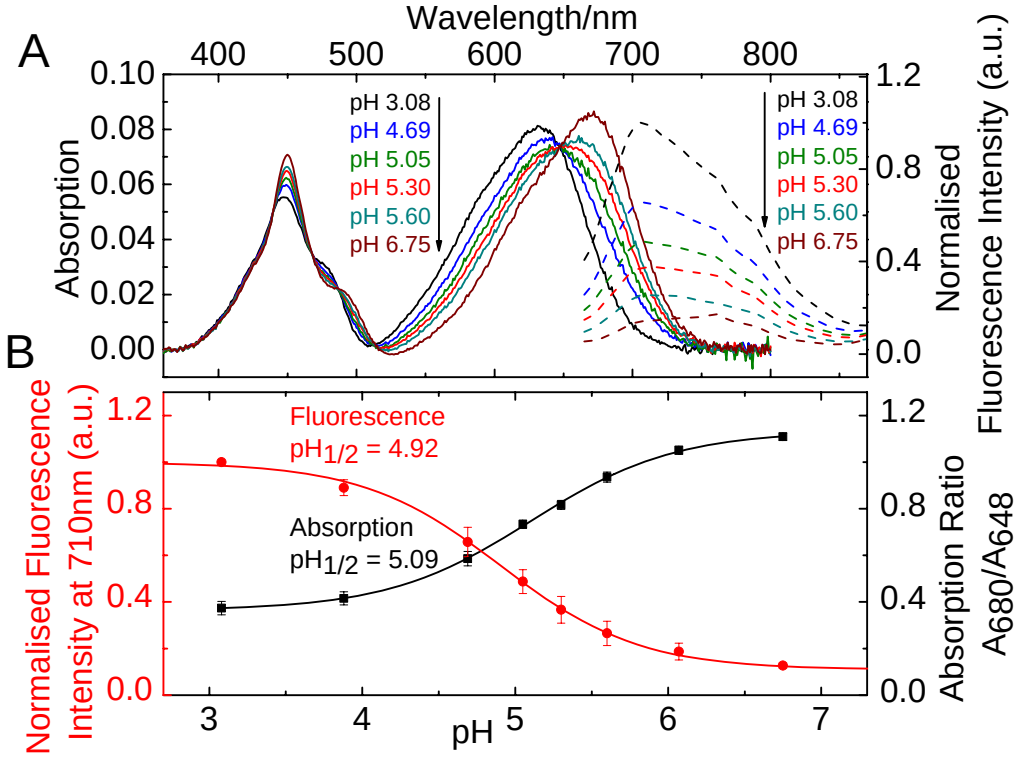

Figure 2-S4: A: Absorption (solid) and fluorescence spectra (dashed) of 1 in D4 hydrogel (dye content 0.5 % (w/w), layer thickness 7 µm) at different pH (aqueous buffer, ionic strength 100 mM). Fluorescence was excited in the isosbestic point (648 nm). B: Corresponding calibration curves. $pH_{1/2}$ is the value at which half of the pH induced signal change is effective.

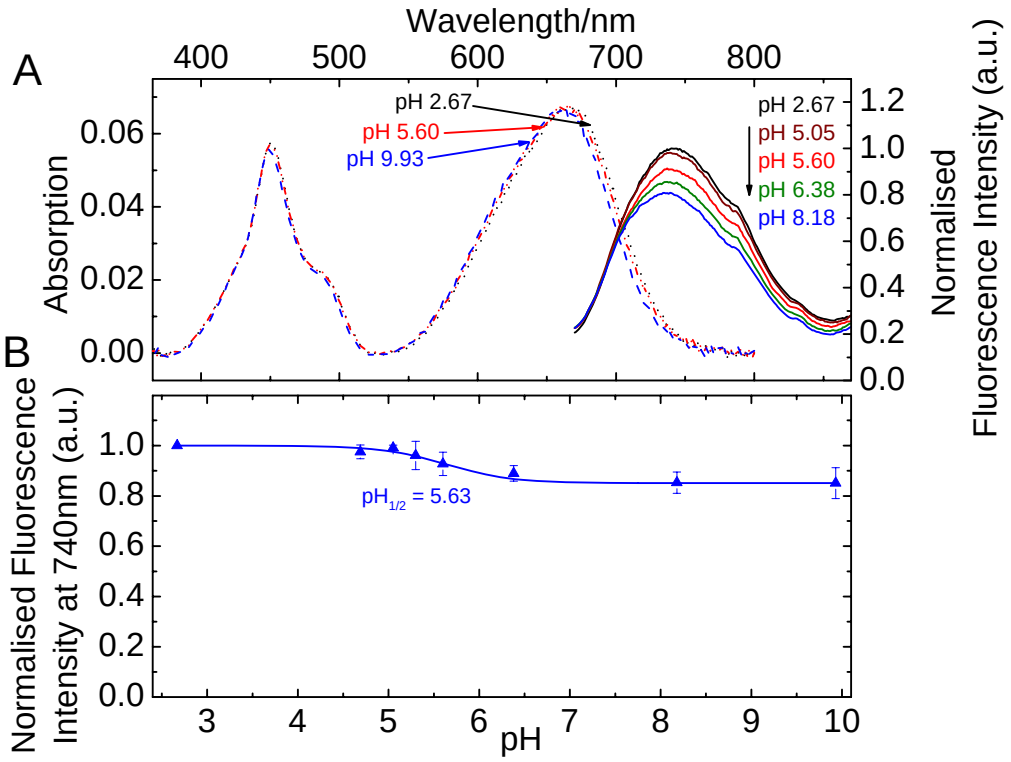

Figure 2-S5: A: Absorption (dashed) and fluorescence spectra (solid) of 2 in D4 hydrogel (dye content 0.5 % (w/w), layer thickness 7 µm) at different pH (aqueous buffer, ionic strength 100 mM). B: Corresponding calibration curve based on fluorescence emission in the maximum. $pH_{1/2}$ is the value at which half of the pH induced signal change is effective. Absorption is virtually independent on pH, calibration is not shown.

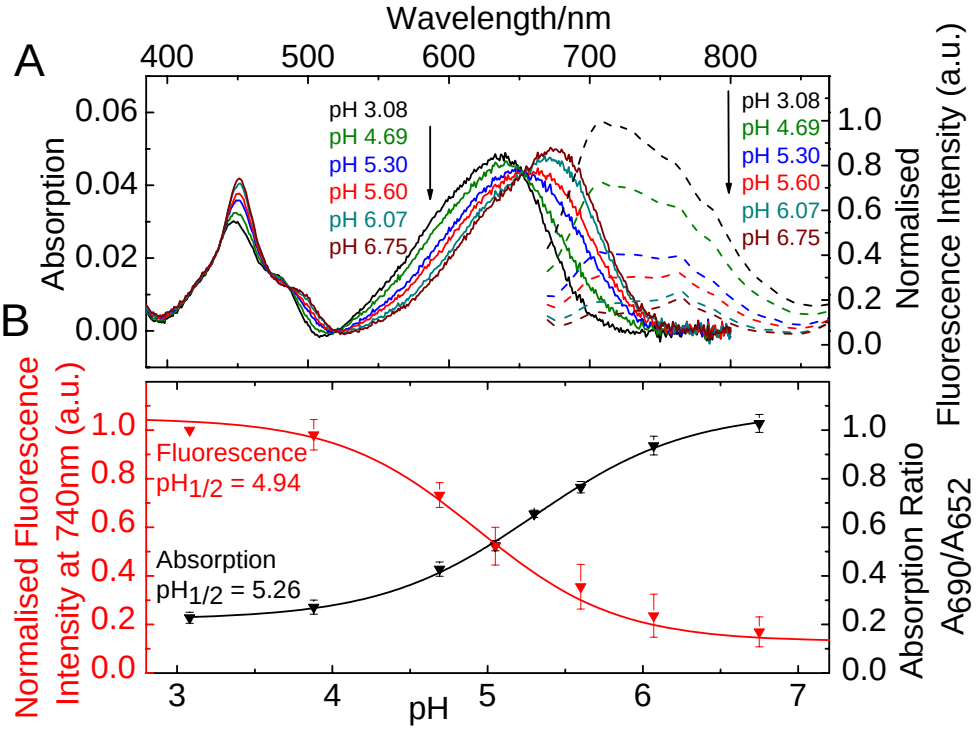

Figure 2-S6: A: Absorption (solid) and fluorescence spectra (dashed) of 3 in D4 hydrogel (dye content 0.5 % (w/w), layer thickness 7 µm) at different pH (aqueous buffer, ionic strength 100 mM). Fluorescence was excited in the isosbestic point (652 nm). B: Corresponding calibration curves. $pH_{1/2}$ is the value at which half of the pH induced signal change is effective.

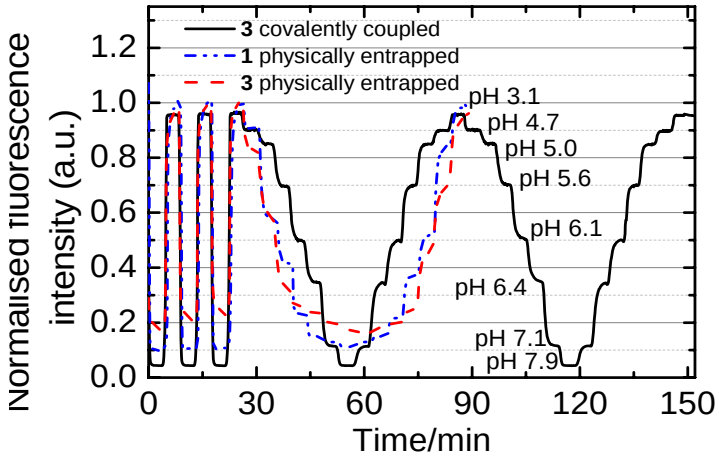

Figure 2-S7: Dynamic response of the pH sensor with covalently grafted 3 (layer as specified below figure 2-S1) in long-term measurement, compared to D4 hydrogel sensors where 3 and 1 are physically entrapped (dye content 0.5% w/w, layer thickness 7 µm).

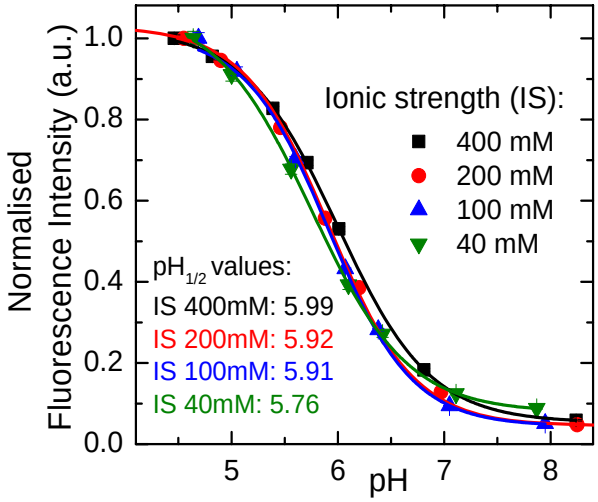

Figure 2-S8: Calibration curves of 3 (layer as specified below figure 2-S1), measured at different ionic strengths. $pH_{1/2}$ is the pH at which half of the pH induced signal change is effective.

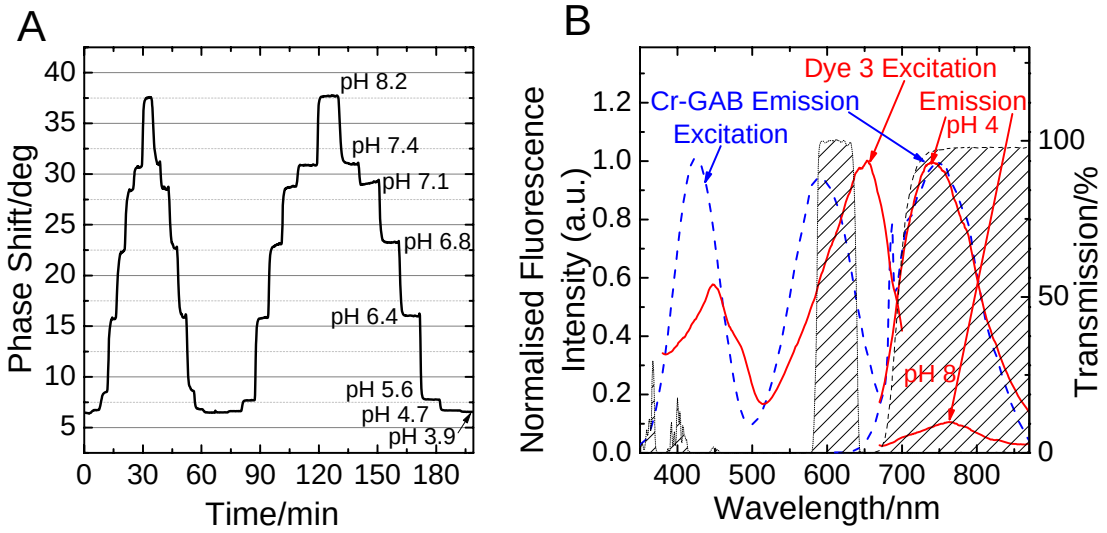

Figure 2-S9: A: Dynamic response of a dually lifetime referenced (DLR) sensor, *i.e.* 3 (0.1 % w/w), covalently coupled to a cross-linked poly(acryloylmorpholine) layer (thickness 20 µm) containing phosphorescent Cr^{3+}-doped gadolinium aluminium borate (Cr-GAB; 25 % w/w; molar Cr^{3+} content 2.5 % with respect to Al^{3+})) as reference material. B: Spectral properties of the components of the DLR sensor. The transmissions of the excitation filter (585 - 640 nm) and emission filter (> 695 nm) are visualised by striped areas.

Materials and Methods

Materials

1,6,7,12-Tetrachloro-*N,N'*-di(2,6-diisopropylphenyl)perylene-3,4:9,10-tertracarboxylic bisimide (**4a**) and 1,6,7,12-tetrachloro-*N*-(2,6-diisopropylphenyl)-*N'*-((2-dibutylamino)ethyl)perylene-3,4:9,10-tertracarboxylic bisimide (**4c**) were synthesised from 1,6,7,12-tetrachloroperylene-3,4:9,10-tetracarboxylic bisanhydride (purchased from Beijing Wenhaiyang Industry and Traiding Co.Ltd, http://china.zhaoteng.com) as reported in chapter 1. 1-Methyl-2-pyrrolidone was from TCI Europe (http://www.tcichemicals.com). Solvents used for work-up and purification (synthesis grade) and for LCMS (HPLC-MS grade) as well as NaCl, buffer salts and microscope slides were supplied by Carl Roth (www.roth.de). Deuterated solvents were obtained form eurisotop (www.eurisotop.com). Silica gel (0.040-0.063 mm) was purchased from Acros (www.fishersci.com), polyurethane hydrogel D4 from CardioTech (www.cardiotech-inc.com). Chrome(III)-doped gadolinium aluminium borate phosphors were prepared in analogy to a procedure described elsewhere [196]. All other chemicals were form Sigma-Aldrich (www.sigmaaldrich.com). Poly(ethylene glycol terephthalate) support (Mylar®) was from Goodfellow (www.goodfellow.com).

Methods

Absorption measurements were performed on a Cary 50 UV-VIS spectrophotometre from Varian (www.varianinc.com). Fluorescence spectra were recorded on a Hitachi F-7000 spectrofluorimetre (www.hitachi.com). Relative fluorescence quantum yields were determined at 25 °C using Nile Blue (Φ_F = 0.27 in ethanol) [197] as a standard. NMR spectra were recorded on a 300 MHz instrument (Bruker; coupling constants *J* will be stated in Hz) with TMS as a standard. MALDI-TOF mass spectra were recorded on a Micromass TofSpec 2E. The spectra were taken in reflectron mode at an accelerating voltage of +20 kV. For LCMS measurements, a Nucleodor 100-5 µm C18ec reversed phase column (Macherey Nagel; 130 x 8mm) was used; mobile phases were water/acetic acid 1000:1 (V/V) and acetonitrile (gradients are stated in tables A-1 and A-2, appendix). A HP/agilent G1315A diode array detector and a Shimadzu LSMS-2020 mass detector (www.shimadzu.de; electrospray ionisation) were employed.

Sensor response curves and pH calibration curves were measured in a home-made stainless steel flow-through cell, pumping buffer with a flow rate of 1 ml min^{-1} (except for the pH calibration curves of the sensors in D4 hydrogel which were measured with the spectrofluorimetre, sensors were incubated in a cuvette filled with buffer solution for 1min prior to measurement). Cell temperature was kept constant at 25 °C. The sensors were interrogated with a two-phase lock-in amplifier (SR830, Stanford Research Inc., www.thinksrs.com) equipped with a red LED (λ_{max} 629 nm) from Roithner (www.roithner-laser.com), a 620/50 nm bandpass filter from Edmund optics (www.edmundoptics.de) at the excitation side and a 695 nm long-pass filter (Schott, www.schott.com) before the PMT tube (H5701-02, Hamamatsu, www.sales.hamamatsu.com). The modulation frequency of 160 Hz was used for intensity measurement, while dually lifetime referenced sensors were measured employing a modulation frequency of 2.5 KHz.

The pH of the phosphate and phosphate-citrate buffer solutions was controlled by a digital pH meter (InoLab pH/ion, WTW GmbH & Co. KG, www.wtw.com) calibrated at 25 °C with standard

buffers of pH 7.0 and 4.0 (WTW GmbH & Co. KG, www.wtw.com). The buffers were adjusted to a constant ionic strength of 100 mM using sodium chloride as the background electrolyte.
Photostability measurements were performed by irradiating the samples with the light of a 645 nm high-power 10 W LED array (www.led-tech.de) focused through a lens purchased from Edmund optics. The photodegradation profiles were obtained by monitoring the absorption spectra.

Syntheses

*N,N'-di(2,6-diisopropylphenyl)-1-(4-methyl-1-piperazinyl)-6,7,12-trichloroperylene-3,4:9,10-tertracarboxylic bisimide (**1**)*

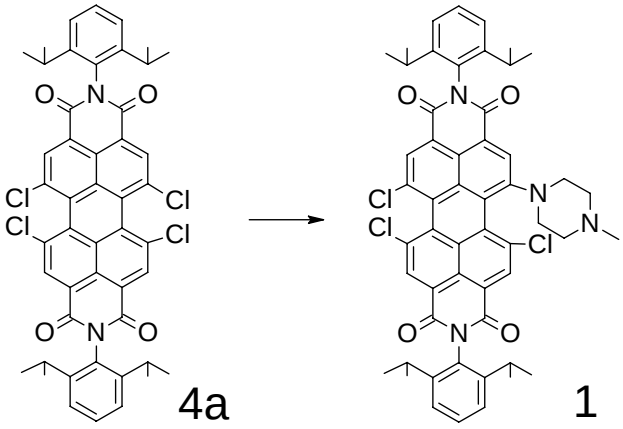

Figure 2-S10: Preparation of **1**.

4a (250 mg, 0.29 mmol) was added to a mixture of *N*-methylpiperazine (1.2 ml, 10.8 mmol) and 1-methyl-2-pyrrolidone (1.2 ml) at 40 °C. The mixture was stirred for 60 min, 0.1 M aqueous HCl/saturated aqueous NaCl 1:1 (V/V) (100 ml) was added, the green precipitate was washed with water/saturated aqueous $NaHCO_3$ 9:1 (V/V) (2 * 50 ml) and water (2 * 50 ml) and dried. Column chromatography with silica gel (40 – 63 μm) as the stationary and CH_2Cl_2:MeOH 70:1 (V/V) as the mobile phase afforded **1** (158 mg, 60 %). NMR spectroscopy: δ_H (300 MHz, $CDCl_3$) 8.75 (2 H, d, ArH (Core)), 8.59 (2 H, d, ArH (Core)), 7.53 (2 H, t, *J* 7.8, ArH), 7.38 (4 H, d, *J* 7.8, ArH); 4.29 (2 H, br s, NCH_2), 2.87-3.10 (2 H, m, NCH_2), 2.70-2.87 (4 H, m, ArCH), 2.48-2.70 (2 H, m, NCH_2), 2.38 (3 H, s, NCH_3), 2.25-2.34 (1 H, br s, NCH_2), 1.96-2.15 (1 H, br s, NCH_2), 1.21 (24 H, m, ArCHC<u>H</u>$_3$). δ_C (300 MHz, CDCl3) 163.6, 163.1, 162.9, 162.8 (C=O); 151.8, 145.9 (2 C), 145.7 (2 C), 135.6, 133.8 (2 C), 133.4, 133.3, 133.2, 132.3, 130.5, 130.4, 130.0 (2 C), 129.8, 129.7, 128.3, 124.6, 124.3-124.4 (4 C), 124.0, 123.8, 123.4, 122.1, 120.8, 119.6 (aromatic); 55.1, 54.6, 52.3, 47.5, 45.9 (NCH_2); 29.3-29.5 (multiple C, ArCH); 24.1-24.4 (multiple C, ArCH<u>C</u>H$_3$). MALDI-TOF *m/z* 911.2974 found, 911.2897 calculated.

*N-(2-(N,N-dibutylamino)ethyl-N'-(2,6-diisopropylphenyl)-1-(4-morpholinyl)-6,7,12-trichloroperylene-3,4:9,10-tertracarboxylic bisimide (**2**)*

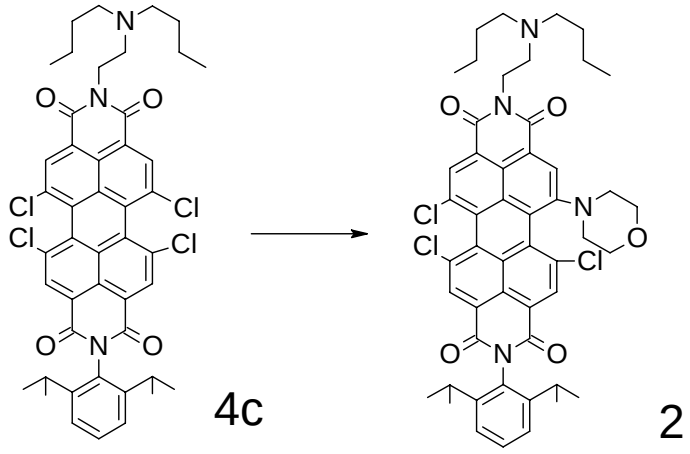

Figure 2-S11: Preparation of 2.

4c (65 mg, 0.077 mmol) was added to a mixture of morpholine (0.65 ml, 7.4 mmol) and 1-methyl-2-pyrrolidone (0.65 ml) at 40 °C. The mixture was stirred for 90 min, 0.1 M aqueous HCl/saturated aqueous NaCl 1:1 (V/V) (20 ml) was added and the green precipitate was washed with water/saturated aqueous $NaHCO_3$ 9:1 (V/V) (2 * 25 ml) and water (2 * 25 ml) and dried. The crude product was purified by column chromatography with silica gel (40 – 63 µm) as the stationary and CH_2Cl_2:MeOH (starting material was eluted with a ratio of 200:1 (V/V), product with 50:1) as the mobile phase to yield **2** (40 mg, 58 %). NMR spectroscopy: δ_H (300 MHz, $CDCl_3$) 8.70 (2 H, d, ArH (Core)), 8.52ppm (2 H, d, ArH (Core)), 7.51 (1 H, t, *J* 7.8, ArH), 7.37 (2 H, d, *J* 7.8, ArH), 4.40 (2 H, br s, $(CO)_2NCH_2$), 4.18-4.28 (1 H, m, $NC\underline{H}_2CH_2O$), 4.04-4.18 (2 H, m, $NC\underline{H}_2CH_2O$ (1 H) and OCH_2 (1 H)), 3.82-4.00 (1 H, m, OCH_2), 3.50-3.69 (1 H, m, OCH_2), 3.28-3.43 (1 H, m, OCH_2), 2.18-3.28 (9 H, m, $(CO)_2NCH_2C\underline{H}_2N$ (2 H) and $NC\underline{H}_2$ (4 H) and $NC\underline{H}_2CH_2O$ (1 H) and ArCH (2 H)), 2.06-2.18 (1 H, m, $NC\underline{H}_2CH_2O$), 1.38-1.69 (4 H, br s, $NCH_2C\underline{H}_2$), 1.30-1.38 (4 H, m, $NCH_2CH_2C\underline{H}_2$), 1.11-1.27 (12 H, q, *J* 5.9, $ArCHC\underline{H}_3$), 0.92 (6 H, t, $NCH_2CH_2CH_2C\underline{H}_3$). δ_C (300 MHz, CDCl3) 163.5, 162.9, 162.7 (2C) (C=O); 151.5, 145.7, 145.5, 135.4, 133.6, 133.1, 132.7, 132.6, 131.9, 130.3, 130.1 (2 C), 129.8, 129.7, 129.5, 128.1, 124.2, 124.1, 123.9, 123.7, 123.2, 123.1, 120.6, 119.8 (aromatic); 66.9, 66.0 (OCH_2); 53.9 (broad), 52.7, 50.8 (broad), 47.8 (NCH_2); 29.2 (ArCH); 24.0 ($ArCH\underline{C}H_3$); 20.4, 13.9 (Alkyl). MALDI-TOF *m/z* 893.3066 found, 893.3004 calculated.

*N-(3-([N-(3-(methacryloylamino)propyl)amino]sulfonyl)-2,6-diisopropylphenyl)-N'-(4-([N-(3-(methacryloylamino)propyl)amino]sulfonyl)-2,6-diisopropylphenyl)-1,6,7,12-tetrachloro-perylene-3,4:9,10-tertracarboxylic bisimide (**4b**)*

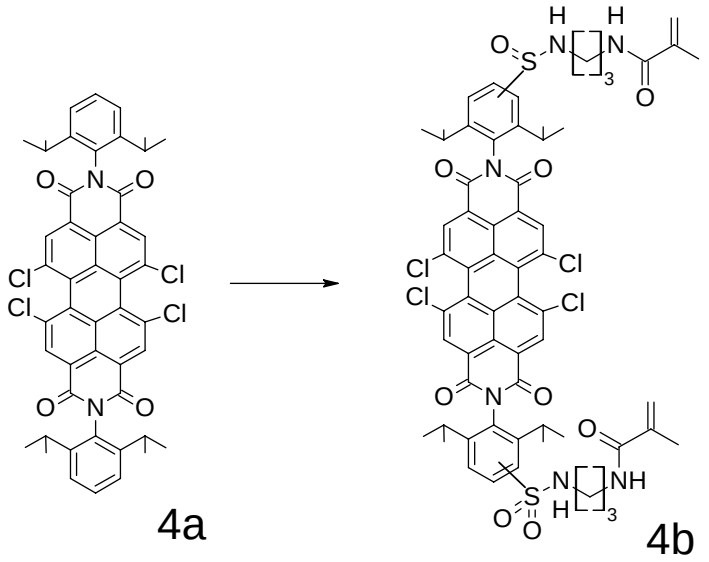

Figure 2-S12: Preparation of 4b.

4a (400 mg, 0.47 mmol) was heated to 60 °C in chlorosulfonic acid (4 ml) for 3 h. The reaction mixture was allowed to cool to RT and added dropwise onto crushed ice. The orange precipitate was transferred into a funnel, washed with ice water until neutral and dried applying a rotary vane pump. The dry disulfonyl dichloride was dissolved in anhydrous *N,N*-dimethylformamide (30 ml), *N*-(3-aminopropyl)methacrylamide hydrochloride (1.88 mmol, 336 mg) and triethylamine (4.71 mmol, 0.65 ml) were added. After stirring for 3 h at RT, the product was precipitated with 0.1 M aqueous HCl/saturated aqueous NaCl 1:1 (V/V) (200 ml), separated by centrifugation and washed with water (3 * 150 ml). The crude product was purified by column chromatography with silica gel (40 – 63 µm) as the stationary and $CHCl_3$:MeOH 97/3 as the mobile phase to yield **4c** (308 mg, 53 %). NMR spectroscopy: δ_H (300 MHz, $CDCl_3$) 8.67 (4 H, s, ArH (Core)), 8.18 (1 H, d, *J* 8.4, ArH)), 7.84 (2 H, s, ArH), 7.51 (1 H, d, *J* 8.4, ArH), 6.23 (2 H, q, *J* 6.7, SO_2NH), 5.55-5.80 (4 H, s and br s, C=CH (2 H) and CONH (2 H)), 5.37 (2 H, s, C=CH), 4.20 (1 H, p, *J* 6.2, ArCH), 3.47 (4 H, m, SO_2NCH_2), 3.13 (4 H, br s, $CONCH_2$), 2.79 (2 H, hex, *J* 6.6, ArCH), 2.63 (1 H, p, *J* 6.5, ArCH), 1.98 (6 H, s, $C=CCH_3$), 1.74 (4 H, p, *J* 6.9, $SONCH_2C\underline{H}_2CH_2N$), 1.20 (24 H, m, $ArCHCH_3$). MALDI-TOF *m/z* 1255.2783 found, 1255.2802 calculated.

*N-(3-([N-(3-(methacryloylamino)propyl)amino]sulfonyl)-2,6-diisopropylphenyl)-N'-(4-([N-(3-(methacryloylamino)propyl)amino]sulfonyl)-2,6-diisopropylphenyl)-1-(4-methyl-1-piperazinyl)-6,7,12-trichloroperylene-3,4:9,10-tertracarboxylic bisimide (**3**)*

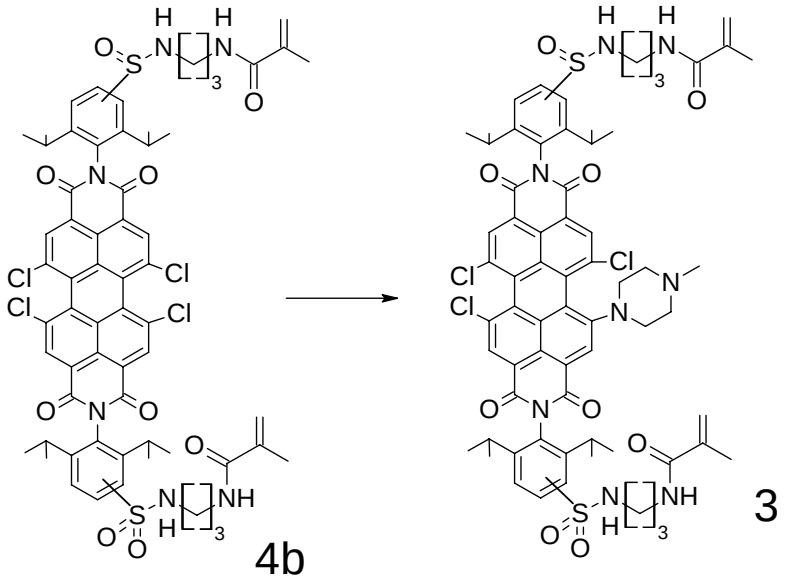

Figure 2-S13: Preparation of 3.

4b (300 mg, 0.239 mmol) was added to a mixture of *N*-methylpiperazine (2 ml, 18 mmol) and 1-methyl-2-pyrrolidone (3 ml) and stirred 40 °C for 45 min. The crude product was precipitated with 0.1M aqueous HCl/saturated aqueous NaCl 1:1 (V/V) (40 ml), washed with water/saturated aqueous $NaHCO_3$ 9:1 (V/V) (2 * 40 ml) and water (2 * 40 ml) and purified by column chromatography (silica gel, 40 – 63 µm), eluting with CH_2Cl_2:MeOH 25:1 (V/V), yielding **3** (136 mg, 43 %). NMR spectroscopy: δ_H (300 MHz, $CDCl_3$) 8.66-8.78 (2 H, m, ArH (Core)), 8.49-8.62 (2 H, m, ArH (Core)), 8.14 (1 H, d, *J* 8.2, ArH), 7.84 (2 H, s, ArH), 7.49 (1 H, d, *J* 8.2, ArH), 6.40 (2 H, br s, SO_2NH), 6.00 (2 H, br s, CONH), 5.75 (2 H, s, C=CH), 5.35 (2 H, s, C=CH), 4.32 (2 H, br s, $NC\underline{H}_2CH_2N$), 4.18 (1 H, m, ArCH(1)), 3.30-3.53 (4 H, m, SO_2NCH_2), 2.95-3.20 (5 H, m, $CONCH_2$ (4 H) and $NC\underline{H}_2CH_2N$ (1 H)), 1.99-2.95 (11 H, m, $NC\underline{H}_2CH_2N$ (5 H) and ArCH (3 H) and NCH_3 (3 H)), 1.87-1.99 (6 H, s, $C=CCH_3$), 1.71 (4 H, m, $SONCH_2C\underline{H}_2CH_2N$), 1.19 (24 H, m, $ArCHC\underline{H}_3$). MALDI-TOF *m/z* 1319.4100 found, 1319.4034 calculated.

Preparation of pH-sensors with covalently linked indicator dye

Microscope slides (76 mm x 2.6 mm x 1 mm) were functionalised with acrylate groups by covering them with a solution of methacryloxypropylmethyldichlorosilane (0.02 ml) in anhydrous tetrahydrofuran (THF; 1 ml). After incubating for 10 min in an inert atmosphere, the slides were washed with acetone and dried (60 °C, 10 min). A monomer mixture consisting of 1-acryloylmorpholine (95 mg), polyethylenglycol diacrylate (5 mg; average molecular weight 700 g mol^{-1}), photoinitiator 2-hydroxy-4'-(2-hydroxyethoxy)-2-methylpropiophenone (0.05 mg) and indicator dye **3** (0.2 mg) was added onto a functionalised microscope slide in an argon atmosphere and closed up tightly putting another microscope slide on top to yield a 26 mm x 26 mm layer of homogeneously distributed monomer mixture. Illumination with a 366 nm UV light source (4 * 9 W, Jolifin "Tunnel", www.jolifin.com) for 6 min afforded polymer layers which were

washed with THF/H_2O 1:1 (V/V) for 30 min prior to use. The layer thickness can be adjusted by attaching spacers of defined thickness onto the microscope slide used for closing up. In this work, the layer thickness of 20 µm was used.
For the preparation of dually lifetime referenced sensors, the following cocktail composition was used: 1-acryloylmorpholine (48 mg), polyethylenglycol diacrylate (2 mg), photo-initiator (0.06 mg), dye **3** (0.067 mg), chrome(III)-doped gadolinium aluminium borate (17 mg; composition: $GdAl_{2.925}Cr_{0.075}(BO_3)_4$).

Preparation of pH sensors with physically entrapped indicator dye
A "cocktail" containing indicator dye **1 - 3** (0.21 mg), hydrogel D4 (41 mg) and EtOH/H_2O 9:1 (V/V) (500 µl) was knife-coated on a dust-free Mylar support to obtain a sensing layer of 7.5 µm thickness after solvent evaporation.

Chapter 3

New Fluorescent pH-Sensors Based on Covalently Linkable PET Rhodamines

Preface to Chapter 3

Here, pH-sensors based on rhodamines quenchable by PET are presented. Among the numerous pH-probes based on rhodamines, this is one of the few employing PET and the only one with PET groups close to the xanthenes nitrogen atoms. Though not emissive in the near infra-red like the system presented in chapter 2, they are very bright pH-sensor with fast, highly reproducible response over a long time. Because the rhodamine probes are water-soluble, covalent dye coupling is absolutely necessary. That is facilitated by a pentafluorophenyl group available for "click" reaction with mercapto groups. In one immobilisation concept, the reaction is directly employed for binding onto silica particles which easily can be modified to carry mercapto groups. In the second concept, reaction with mercaptopropionic acid introduces a carboxy group which is then grafted to amino-functionalised hydrogel particles by the standard conjugation procedure involving activation with *N*-hydroxysuccinimide. Though both types of microparticles may be directly used in the particle form, they are embedded into hydrogel layers to yield planar optrodes in this work. While featuring almost identical pK_A values, the silica-based sensor shows a significantly wider working range.

The pentafluorophenyl intermediate shows high reactivity due to dimerisation and to another reaction resulting in reversible decolouring that could not be fully characterised. Although reactivity is much lower after reaction with mercapto groups, photostability of the sensors is not as high as expected, with photoreduction being the likely cause.

Nevertheless, the sensors are promising for practical applications and the strategies developed for covalent dye linkage may be useful also for other sensor systems. Because of their sensitive range at slightly acidic pH, they are most useful for application in biotechnology. Although high brightness and good long-term stability make the sensors a significant result for this thesis, they have not been selected of further optimisation since excitability at longer wavelengths is difficult to realise with the rhodamine-based system that lacks flexibility for further modification. Though related systems condensed with additional double bonds or benzene rings are known (red Alexa dyes, benzo[g]xanthenes) are known, high synthetic effort seems necessary to achieve only a moderate increase in excitation wavelengths and a decrease in photostability accompanying those modifications seems likely.

New Fluorescent pH-Sensors Based on Covalently Linkable PET Rhodamines

This chapter is the result of cooperation with **Universidad de Granada, Spain**, and was published in **Talanta**, 2012; 99, 194–201; doi: 10.1016/j.talanta.2012.05.039

Authors: **Daniel Aigner, Sergey M. Borisov, Francisco J. Orriach Fernández, Jorge F. Fernández Sánchez, Robert Saf and Ingo Klimant**

A new class of rhodamines for the application as indicator dyes in fluorescent pH sensors is presented. Their pH-sensitivity derives from photoinduced electron transfer between non-protonated amino groups and the excited chromophore which results in effective fluorescence quenching at increasing pH. The new indicator class carries a pentafluorophenyl group at the 9-position of the xanthene core where other rhodamines bear 2-carboxyphenyl substituents instead. The pentafluorophenyl group is used for covalent coupling to sensor matrices by "click" reaction with mercapto groups. Photophysical properties are similar to "classical" rhodamines carrying 2'-carboxy groups. pH sensors have been prepared with two different matrix materials, silica gel and poly(2-hydroxyethylmethacrylate). Both sensors show high luminescence brightness (absolute fluorescence quantum yield $\Phi_F \approx 0.6$) and high pH-sensitivity at pH 5-7 which makes them suitable for monitoring biotechnological samples. To underline practical applicability, a dually lifetime referenced sensor containing Cr(III)-doped Al_2O_3 as reference material is presented.

Introduction

pH is a key parameter for a wide range of applications in the medical field, in environmental and life sciences or for regulation and routine monitoring in industrial processes and in sewage purification plants, to mention only a few areas. Although electrochemical pH sensors are well-established and reliable tools for a large number of analytical tasks, optical pH sensors offer unmatched advantages in many other challenging applications, in particular for high-throughput screening, for applications where minimal contact to the sample is preferable, where a high degree of miniaturisation is required or in systems that do not allow the application of potentiometric sensors due to a strong electromagnetic field.

A number of fluorescent pH sensors have already been established in which derivatives of 8-hydroxypyrene-1,3,6-trisulfonate (HPTS) [50,51,198], fluoresceins [27,115,199,200] and benzo[g]xanthene dyes [45,48,49,201] have been the most common pH-sensitive indicator dyes. Most of these indicators, however, still are subject to limitations. Fluoresceins are commonly known for their limited photostability. HPTS derivatives are excitable at relatively short (< 500 nm) wavelengths which results in high levels of autofluorescence and scattering background. Benzo[g]xanthene dyes are long-wave excitable, but offer only limited brightness (defined as the product of molar absorption coefficient ε and fluorescence quantum yield, Φ_F) $\leq 12 \cdot 10^3$ $M^{-1}cm^{-1}$ [45] , which is at least 5 times lower than for the dyes presented in this work, and are prone to photobleaching [49].

Rhodamines are xanthene dyes featuring outstanding brightness (high ε in the order of $100 \cdot 10^3$ $M^{-1}cm^{-1}$ and Φ_F of 0.7-1 for most derivatives), generally good solubility in water and good

photostability [36]. These properties have enabled their application in cell imaging [202,203] and single molecule imaging [43,204], for the characterisation of micelles [205] and polymer beads [206] , as standards for fluorescence quantum yield [44] or as molecular switches [43,207] and fluorescence thermometers [208], to state only a few. Numerous rhodamine-based fluorescent probes for cations - most importantly Hg^{2+} [203,209,210], Cu^{2+} [211], Fe^{3+} [212], Pb^{2+} [213] - and thiols [214] have been presented. On the other hand pH-sensitive systems relying on rhodamines as pH probes [37,39,40,215-219] are less common. Most of these systems take advantage of the cyclisation equilibrium in rhodamines leading to non-fluorescent lactames.
Here we present a new class of amino-functional rhodamines the pH-sensitivity of which originates from the intramolecular photoinduced electron transfer process (PET, [59,60,61,65,77,96]) between non-protonated amino groups and the excited chromophore (figure 3-1). To the best of our knowledge, only very few examples for pH-sensitive PET rhodamines [41,102] can be found in the literature and those focus on application as probes in solution, not in a solid sensor matrix. The new dye class is accessible by a straightforward one-step synthesis. It carries a pentafluorophenyl group in the 9-position of the xanthene core which is employed for simple and effective covalent coupling by “click” reaction with mercapto groups. Covalent indicator linkage can be highly beneficial for pH optrodes since it suppresses migration and aggregation processes. Nucleophilic substitution in pentafluorophenyl groups has recently been presented as a versatile tool for grafting [220-224] . The suitability of the new fluorinated PET-rhodamines as indicators in pH sensors will be demonstrated.

Experimental

Materials and Methods

3-(1-Piperazinyl)phenol, pentafluorobenzaldehyde, methanesulfonic acid and (3-mercaptopropyl)trimethoxysilane were purchased from ABCR (www.abcr.de). Urea was from Acros (www.acros.com). All other reagents were obtained from Aldrich (www.sigmaaldrich.com). All reagents were of synthesis grade. Deuterated solvents were purchased form eurisotop (www.eurisotop.com). Anhydrous pydridine and *N,N*-dimethylformamide were bought from Aldrich. All other solvents (synthesis grade, HPLC gradient grade), as well as potassium persulfate, sodium chloride and buffer salts, were supplied by Carl Roth (www.carlroth.de). Hydroxyethylmethacrylate and ethyleneglycoldimethacrylate were filtered over aluminium oxide prior to use. Water used for HPLC chromatography was deionised using a Barnstedt NANOpure system. Dowex® 1-8 cation exchange resin was freshly charged with chloride prior to use.
Absorption measurements were performed on a Cary 50 UV-VIS spectrophotometer from Varian (www.varianinc.com). Fluorescence spectra were recorded on a Hitachi F-7000 spectrofluorimetre (www.hitachi.com). Relative fluorescence quantum yields Φ_F were determined using rhodamine 101 (Φ_F=0.96 [225]; Fluka, www.sigmaaldrich.com) as a standard. Absolute fluorescence quantum yields were determined on a Fluorolog 3 spectrofluorimetre equipped with an integrating sphere (Horiba Scientific, www.horiba.com). ^{1}H-NMR spectra were recorded on a 300 MHz instrument (Bruker) with TMS as a standard. ^{19}F-NMR spectra were taken on a Mercury Inova 300 instrument (Bruker) at a frequency of 282.47 MHz. MALDI-TOF masses were determined on a Micromass TofSpec 2E in reflectron mode at an accelerating voltage of +20 kV. pH calibration curves and sensor response curves were obtained by passing buffer solutions (1

ml·min^{-1}) by a sensor foil placed in a home-made flow-through cell. Cell temperature was kept constant at 25 °C. The luminescent signal was interrogated with a two-phase lock-in amplifier (SR830, Stanford Research Inc., www.thinksrs.com) equipped with a green LED (λ_{max} 525 nm) from Roithner (www.roithner-laser.com), a XR3080 bandpass filter (500-540nm; Horiba, www.horiba.com) at the excitation side and a long-pass filter (Schott, www.schott.com; OG 580 (> 580 nm), unless otherwise stated) before the PMT tube (H5701-02, Hamamatsu, www.sales.hamamatsu.com). The modulation frequency of 160 Hz was used, unless otherwise stated. The pH of the phosphate and acetate buffer solutions was controlled by a digital pH meter (InoLab pH/ion, WTW GmbH & Co. KG, www.wtw.com) calibrated at 25 °C with standard buffers of pH 7.0 and 4.0 (WTW GmbH & Co. KG, www.wtw.com). The buffers were adjusted to constant ionic strength using sodium chloride as a background electrolyte. LCMS measurements were performed on a Shimadzu LCMS system equipped with a LSMS-2020 mass detector and a SPD-M20A diode array detector (www.shimadzu.de).

Preparation of Dyes and Sensors

*N,N'-di(3-azapentane-1,5-diyl)-2',3',4',5',6'-pentafluororhodamine acetate (**1**)*

A mixture of 3-(1-piperazinyl)phenol (2.7 g, 15.15 mmol), pentafluorobenzaldehyde (1.5 g, 7.65 mmol) and methanesulfonic acid (20 ml) was heated to 210 °C under vigorous stirring. Temperature was maintained for 4.5 h, pentafluorobenzaldehyde (500 mg, 2.5 mmol) was added in two equal portions during the first 2.5h. The deep red mixture was allowed to cool to RT and was added dropwise into THF (250 ml). The sticky solid formed was re-dissolved in MeOH (50ml) and again precipitated with THF (250 ml). The procedure was repeated six times until a black powder was obtained. The powder was dissolved in H_2O (100 ml) and passed over Dowex® 1-8 cation exchange resin (Carl Roth) charged with chloride. The deep red solution was dried to yield 3.8 g of crude product. Purification was performed by HPLC chromatography on an Agilent 1100 station (www.chem.agilent.com) employing a Nucleodor 100-5 µm C18ec reversed phase column (Macherey Nagel; 200x15mm) and MeOH/0.1% aqueous acetic acid (gradient is stated in table A-3, appendix) as the mobile phase. Upon purification, 37 mg crude product yielded 12 mg pure **1.** Owing to the limited size of the available HPLC facility, not all crude **1** was purified. If up-scaling is performed, 1.23 g (2.14 mmol, 28%) of pure **1** can be isolated. ^{1}H NMR (300 MHz, CD_3OD containing 0.1% HOAc and 0.1% CF_3COOH, TMS): δ = 7.65ppm (2H, d, Ar-H(positions 1,8), $J_{ArH12,78}$ = 9.6 Hz); δ = 7.46 (2H, dd, Ar-H(2,7), $J_{ArH24,57}$ = 2.5 Hz); δ = 7.42 (2H, d, Ar-H(4,5)); δ = 4.13 (8H, t, $ArNCH_2$, J = 5.2 Hz); δ = 3.48 (8H, t, $HNCH_2$); δ = 1.99 (3H, s, $H_{acetate}$). ^{19}F NMR (282.5 MHz, D_2O): δ = -139ppm (2F, d, J = 20 Hz); δ = -150 (1F, t, J = 21 Hz); δ = -160 (2F, dt, J_1 = 6 Hz, J_2 = 21 Hz). MALDI-TOF: m/z [MH^+] 515.1847 found, 515.1870 calcd.

*N,N'-di(3-azapentane-1,5-diyl)-4'-(2-carboxyethylmercapto)-2',3',5',6'-tetrafluororhodamine acetate (**2**)*

Crude **1** (328 mg, containing 157 mg, 278 µmol of pure **1**[1]), *N,N*-dimethylacetamide (8 ml) and triethylamine (248 µl, 1.78 µmol) were heated to 50 °C and 3-mercaptopropionic acid (34.4 µl, 390 µmol) was added dropwise. Temperature was maintained for 3 h and the mixture was washed with hexane until a solid residue was obtained (4x100 ml). The residue was dissolved in MeOH/1 M aqueous HCl 1:1 (3x10 ml) and precipitated with THF (3x150 ml). Crude **2** was obtained as a black powder (130 mg). Purification was performed similarly to **1** (different gradient is stated in table A-4) and yielded 19 mg of pure **2** (35 mg crude product; 71 mg (0.11 mmol, 39%) if up-scaled). ^{1}H NMR (300 MHz, CD_3OD containing 0.1% CF_3COOH, TMS): δ = 7.55ppm (2H, d, Ar-H(positions 1,8), $J_{ArH12,78}$ = 9.6 Hz); δ = 7.32 (2H, dd, Ar-H(2,7), $J_{ArH24,57}$ = 2.3 Hz); δ = 7.26 (2H, d, Ar-H(4,5)); δ = 4.06 (8H, t, $ArNCH_2$, J = 4.9 Hz); δ = 3.48 (8H, t, $HNC\underline{H}_2$); δ = 3.32 (2H, t, $ArSCH_2$, J = 6.7 Hz); δ = 2.76 (2H, t, $C\underline{H}_2COOH$); δ = 2.06 (4.7H, s, $H_{acetate}$). ^{19}F NMR (282.5 MHz, D_2O): δ = -132ppm (2F, q, J = 11 Hz); δ = -139 (2F, q, J = 11 Hz). MALDI-TOF: m/z [MH^+] 601.1923 found, 601.1896 calcd.

*N,N'-di(3-azapentane-1,5-diyl)-2',4'-dicarboxyrhodamine acetate (**3**)*

Trimellitic anhydride (1.62 g, 8.42 mmol), 3-(1-piperazinyl)phenol (3 g, 16.83 mmol) and methanesulfonic acid (25 ml) were heated to 165 °C. Temperature was maintained for 3.5h, the deep red mixture was allowed to cool to RT and was added dropwise into THF (100 ml). The sticky black precipitate was re-dissolved in MeOH and precipitated by adding THF. The procedure was repeated six times to yield crude **3** (1.8 g) as a black powder. Purification was performed similarly to **1** (different gradient is stated in table A-5) and yielded 14 mg of pure **3** (44 mg crude product; 890 mg (1.74 mmol, 21%) if up-scaled). Both the 4'-carboxy and the 5'-carboxy regioisomer could be isolated in pure form and identified by NMR spectroscopy (figures A-36, A-37). Although the 5'-carboxy isomer was formed in comparable amounts (figure A-45) and is equally suitable for the present application, only pure 4'-carboxy isomer was used for characterisation. ^{1}H NMR (300 MHz, D_2O, TMS): δ = 8.32ppm (1H, s, Ar-H(position 3')); δ = 8.00ppm (1H, d, Ar-H(5'), $J_{ArH5'6'}$ = 7.5 Hz); δ = 7.27 (3H, d, Ar-H(6',1,8), $J_{ArH12,78}$ = 9.3 Hz); δ = 7.06 (2H, d, Ar-H(2,7)); δ = 6.97 (2H, s, Ar-H(4,5)); δ = 3.85 (8H, broad s, $ArNCH_2$); δ = 3.35 (8H, broad s, $HNC\underline{H}_2$); δ = 1.90 (3H, s, $H_{acetate}$). MALDI-TOF: m/z [MH^+] 513.2101 found, 513.2138 calcd.

Mercapto-functionalised silica gel beads

Li Chrospher 60 silica gel beads (Merck, average size 5 µm; 1 g) were dispersed in EtOH/H_2O 19:1 (40 ml) in a polypropylene vessel. (3-Mercaptopropyl)trimethoxysilane (26.8 µl, 0.144 mmol) and

[1] Crude **1** was used for the synthesis of **2**. The assay of **1** in the crude product can be easily calculated. The total rhodamine content is equal to the ratio of the molar absorption coefficients of crude and pure product (which is $4.3 \cdot 10^4 M^{-1}cm^{-1}/8.9 \cdot 10^4$=0.48). Figure S13 shows that there are no other rhodamines contained in the crude product (no impurities absorbing at 540 nm). Therefore, the assay of **1** in the crude product is 48% (w/w). For calculation, chloride was the assumed counter ion for crude **1**, while pure **1** is the acetate salt.

acetic acid (2 ml) were added and the mixture was stirred overnight at RT. The beads were separated by centrifugation (2450·g), washed with EtOH (6x50 ml) and dried (60 °C, 1 bar).

Amino-functionalised poly(hydroxyethylmethacrylate) (poly(HEMA)) beads
Poly(HEMA) beads were prepared adapting a method reported in the literature [226]. Poly(vinyl alcohol) (86000 g·mol^{-1}, 99% hydrolysed) (3 g) was dissolved in refluxing H_2O (300 ml). The mixture was allowed to cool to 40 °C and flushed with nitrogen for 30 min. 2-Hydroxyethylmethacrylate (3.26 ml, 27.3 mmol), ethylene glycol dimethacrylate (0.36 ml, 1.91 mmol), 2-aminoethylmethacrylate hydrochloride (80 mg, 0.48 mmol) and potassium persulfate (3 mg, 0.01 mmol) were added, the mixture was heated to 70 °C and stirred under a gentle nitrogen stream for 18 h. The precipitated beads were separated by centrifugation (2450·g), washed with H_2O (4x100ml) and EtOH (3x100ml) and freeze-dried (1 mbar, -90 °C, 18 h) to yield 1.6 g of a white powder.

pH-sensitive silica gel beads
A mixture of mercapto-functionalised silica gel beads (250 mg), rhodamine dye **1** (1 mg, 1.74 μmol), triethylamine (2.7 μl, 0.019 mmol) and *N,N*-dimethylacetamide (1 ml) was heated to 60 °C under vigorous stirring for 6 h. The beads were separated by centrifugation (2450·g), washed with 10 mM HCl (6x5 ml), EtOH (2x5 ml) and H_2O (6x5 ml) and dried (60 °C, 1 bar).

pH-sensitive poly(HEMA) beads
2 (1 mg, 1.5 μmol) was dissolved in anhydrous *N,N*-dimethylformamide(DMF; 0.5 ml) and dicyclohexylcarbodiimide (DCC; 1.37 mg, 6.6 μmol) was added. The solution was stirred at RT for 15 min and *N*-hydroxysuccinimide (NHS; 1 mg, 8.7 μmol) was added. After 45 min, a dispersion of amino-functionalised poly(HEMA) beads (100 mg) in anhydrous pyridine (1 ml) and a catalytic amount of 4-(dimethylamino)pyridine (DMAP) were added. The mixture was stirred overnight. The beads were separated by centrifugation (2450·g), washed with DMF (2x5 ml), CH_2Cl_2 (2x5 ml), EtOH (3x5 ml), 10 mM HCl (5x5 ml) and H_2O (3x5 ml) and freeze-dried (1 mbar, -90 °C, 18 h).

Preparation of Cr(III)-doped Al_2O_3 (ruby)
$Al(NO_3)_3{\cdot}9H_2O$ (16.54 g, 44 mmol), $Cr(NO_3)_3{\cdot}9H_2O$ (0.36 g, 0.90 mmol) and urea (18 g, 0.3 mol) were dissolved in H_2O (100 ml). The mixture was concentrated until a turquoise gel was obtained. The gel was heated to 500 °C and kept at this temperature for 10 min. After cooling to RT, the green solid was ground in a mortar and sintered for 24 h at 1100 °C in air. The pale pink powder obtained was ground in a ball mill to yield 1.9 g of fine Cr-doped Al_2O_3.

Preparation of the sensor foils
pH-sensitive silica gel beads in D4 hydrogel: A "cocktail" containing silica gel beads (28 mg), hydrogel D4 (41 mg) and EtOH/H_2O 9:1 (500 μl) was knife-coated on a dust-free Mylar support to obtain a sensing layer of about 12.5 μm thickness after solvent evaporation.
pH-sensitive cross-linked poly(HEMA) beads in linear poly(HEMA): Linear poly(HEMA) (MW=150000 g·mol^{-1}) was dissolved in EtOH:H_2O (9:1 V/V), insoluble residues were separated by centrifugation and discarded. Cross-linked poly(HEMA) beads (10 mg) were added to the

obtained solution (29 mg polymer in 500 µl) and the "cocktail" was knife-coated on a dust-free Mylar support to give a sensing layer of about 7 µm thickness after solvent evaporation.

Results and Discussion

Structures and syntheses of the new pH indicators and sensors are shown in figure 3-1. They are based on **1** which, unlike other rhodamines, does not carry a 2'-carboxy group. For comparison, compound **3** bearing a 2'-carboxy group is also investigated. pH-sensitive rhodamines have been covalently coupled to two different sensor matrices, i.e. silica gel beads and cross-linked poly(2-hydroxyethylmethacrylate) (poly(HEMA)) beads. Polymer hydrogels like poly(HEMA) are the most common matrices in pH sensors. Silica gel represents an interesting alternative material with very different properties. **1** was linked by direct reaction with mercapto-functionalised silica gel beads, while another route involving **2** was employed for the attachment to amino-functionalised poly(HEMA) beads.

Photophysical Properties

The photophysical properties of the synthesised rhodamines and commercially available rhodamine B are displayed in table 3-1. The electron-withdrawing highly fluorinated phenyl substituent causes a bathochromic shift of ≈ 30 nm for both acidic and basic form in compounds **1** and **2** in comparison to **3**. They are therefore excitable at > 70 nm longer wavelength than such widely used pH indicators as fluorescein or pyrene derivatives. Luminescence brightness is often expressed as the product of molar absorption coefficient ε and fluorescence quantum yield Φ_F. Both are comparable to the high values known for rhodamines.

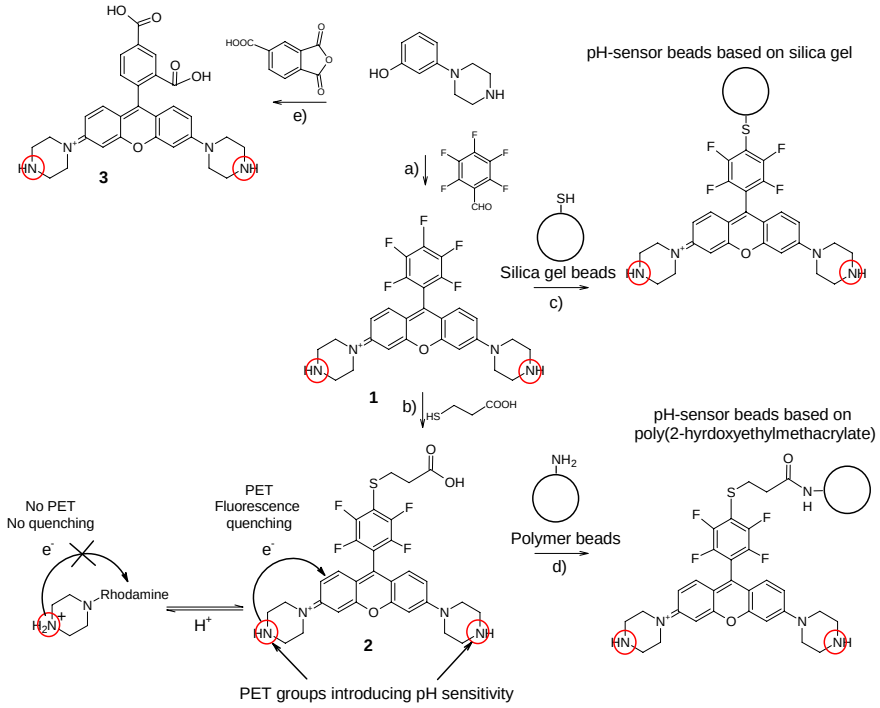

Figure 3-1: Preparation of the pH-indicators 1-3 and the two types of pH-sensor beads. Reagents and conditions: a) pentafluorobenzaldehyde, CH_3SO_3H, 210 °C (28%); b) 3-mercaptopropionic acid, Et_3N, *N,N'*-dimethylacetamide, 50 °C (39%); c) mercapto-functionalised silica gel beads, Et_3N, *N,N'*-dimethylacetamide, 60 °C; d) amino-functionalised poly(HEMA) beads, DCC, NHS, DMAP, *N,N'*-dimethylformamide; e) trimellitic anhydride, CH_3SO_3H, 165 °C (21%).

A somewhat lower Φ_F was found for **1**, while **2** shows almost equal Φ_F to **3** and rhodamine B. Note that mercapto-substituted **2** rather represents the rhodamine structures present in the sensors and is therefore more valid for comparison.
Similar Φ_F around 0.6 were found for the presented sensor materials (table 3-2). ε are even higher for **1** and **2** than for **3**. Consequently, luminescence brightness of a mercapto-substituted pentafluorophenyl-rhodamine such as **2** is as high as in the case of rhodamines carrying a 2'-carboxy group. Note that in table 3-1, lower ε are accompanied by broader absorption peaks (higher half-widths at half maximum, HWHM) so that the integral absorptions of all rhodamines are similar.

Table 3-1: Photophysical properties of 1-3 and rhodamine B: absorption maximum (λ_{max} *abs*) and corresponding molar absorption coefficient (ε); half-width at half maximum in absorption (HWHM); fluorescence emission maximum (λ_{max} *em*); relative fluorescence quantum yield (Φ_F). Values were determined in aqueous buffer solution, unless otherwise stated. Organic solvents were acidified with CF_3COOH (0.1% V/V) and made basic with Et_3N (0.1% V/V).

Compound	λ_{max} *abs*(ε 10^{-4})/nm ($M^{-1}\cdot cm^{-1}$) acidic/basic	HWHM/nm acidic/basic	λ_{max} em/nm acidic	Φ_F acidic/basic
1	560(8.82)/ 584(7.62)	40/57	588	0.40/<0.01
2	561(10.2)/583(8.17)	39/54	591	0.67/0.02
3	533(8.46)/554(8.38)	42/43	562	0.69/<0.01
Rhodamine B[a]	543(10.6)	35	565	0.70

[a] All values in EtOH, without any acid or base added

pH-sensitive Properties in Aqueous Solution

Absorption and fluorescence spectra of **2** together with pH calibration curves of **1-3** are shown in figure 3-2. pH sensitivity is caused by a strong decrease in emission intensity due to photoinduced electron transfer (PET). The sensitive range is around pH = 7 so that all dyes are potentially useful for fluorescence imaging in physiological samples. Fluorescence is essentially turned off as deprotonation of the piperazonium groups occurs. A hypsochromic shift of about 20 nm is observed for the absorption spectra of **1-3** upon protonation (table 3-1). This effect is not related to PET. It can be attributed to the electron-withdrawing effect of the positively charged piperazonium groups located in proximity of the rhodamine core. Note that fluorescence spectra are not bathochromically shifted with increasing pH. This indicates that the highly fluorescent acidic form is in equilibrium with a non-fluorescent basic one quenched by PET.

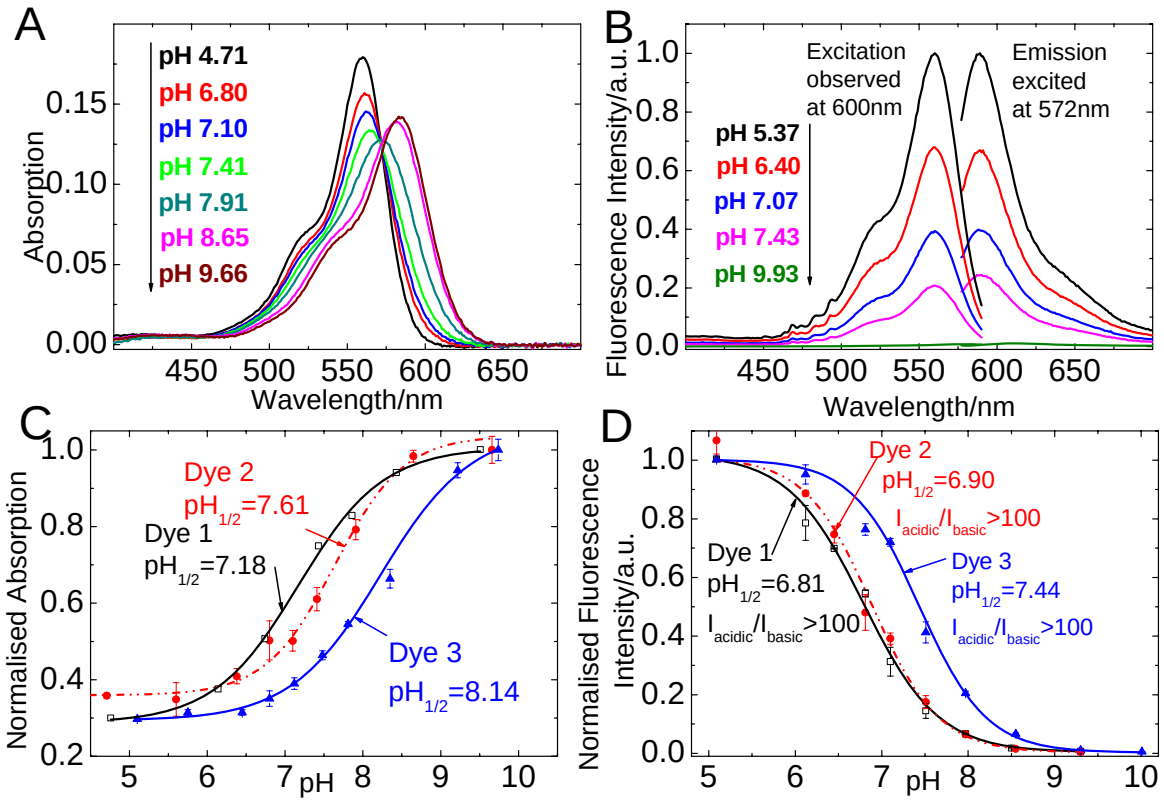

Figure 3-2: pH-sensitive properties of 1-3 in aqueous buffer solution (ionic strength 100 mM). Absorption spectra (A) and fluorescence spectra (B) of 2, dye concentration was 2 µM when recording absorption and 0.05 µM when recording fluorescence spectra. Spectra of 1 and 3 are similar and can be found in the supplementary information. C: pH calibration curves of 1 (squares), 2 (circles) and 3 (triangles) based on absorption, observed in the absorption maximum of the basic form. D: corresponding curves based on fluorescence emission, observed in the emission maximum of the acidic form. $pH_{1/2}$ is the pH at which half of the overall pH-dependent signal change is observed.

The sensitive range of **1** and **2** (figure 3-2) is found at lower pH than the one of **3**, which illustrates the incomplete decoupling between the piperazinyl groups and the chromophore. The acidic form of **1** and **2** is more strongly destabilised by the vicinity of the rhodamine core that carries a strongly electron-withdrawing fluorinated substituent. Absorption calibration shows response at considerably higher pH than fluorescence calibration. This can be attributed to the fact that shifts in absorption are related to the deprotonation of both piperazonium groups, whereas the deprotonation of the first group may already cause highly efficient PET.

Figure 3-3 emphasises that **1** does not undergo lactonisation under conditions where **3** is almost completely present in the lactone form. Lactame formation, a very similar process, has been taken advantage of to introduce pH sensitivity into rhodamines [37,39,40,215-217]. In the present system, however, preliminary experiments showed that lactonisation causes almost complete decolouring of PET rhodamine **3** as soon as it is linked to a sensor matrix. Therefore, the sensors presented in this work rely exclusively on the PET mechanism and employ dyes that do not undergo lactonisation.

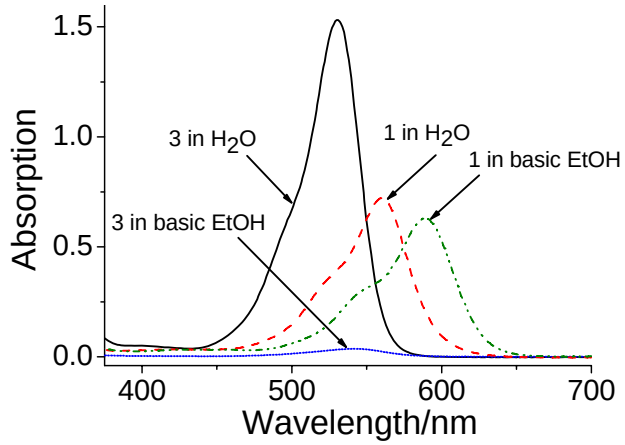

Figure 3-3: Lactonisation of 3, visualised by absorption spectra in H_2O and basic EtOH (containing Et_3N, 0.1% V/V). Due to lactonisation, virtually no absorption is observed in basic EtOH. On the other hand, 1 shows a shift but no attenuation of absorption in basic EtOH compared to H_2O. The slight decrease in the absorption maximum is due to peak broadening, not lactonisation.

Sensors with Covalent Dye Linkage

Covalent attachment of pH-sensitive rhodamine to both silica gel and cross-linked poly(2-hydroxyethylmethacrylate) (poly(HEMA)) beads was successful, yielding pH sensor beads. For characterisation, the beads were dispersed in polyurethane hydrogel D4® (for the silica gel beads) or in linear poly(HEMA) (for the cross-linked poly(HEMA) beads) to yield planar optrodes. Bright orange fluorescence of the obtained sensors is clearly visible for the acidic form (figure 3-4) and absolute fluorescence quantum yields were found to be rather high (table 3-2). Both sensor types exhibit excellent sensitivity and are most useful for measuring pH 5-7 which fits the pH range of interest in many biotechnological applications. The sensors respond at lower pH than the aqueous solutions of **1** and **2**. That is most likely due to the less polar environment in the sensor which destabilises the highly charged acidic form. Förster resonance energy transfer from the acidic to the basic form may also contribute to this effect, since the dye concentration is significantly higher in the sensors than in solution. Despite the high charge of the indicator dye, the sensors show small to moderate cross-sensitivity to ionic strength (figure 3-5). That is particularly true if the ionic strength (IS) is ≥100 mM, which is the case in the majority of biotechnological applications. For the silica gel sensors, errors are ≤ 0.1 pH-units if IS = 100-200 mM and ≤ 0.2 pH-units if IS = 100-500 mM. They are smaller for the sensor based on poly(HEMA) beads (≤ 0.05 pH-units if IS = 100-200 mM, ≤ 0.1 pH-units if IS = 100-500 mM), which is expected since poly(HEMA) is a less charged matrix than silica gel [27,227]. The response times are fairly fast (τ_{90} < 2 min for the sensor based on silica gel beads; τ_{90} = 2-3 min for the sensor based on poly(HEMA)). Reversibility and repeatability of the sensors are very good, as demonstrated in figure 3-7 and figures 3-S3, 3-S4 in the supplementary information.

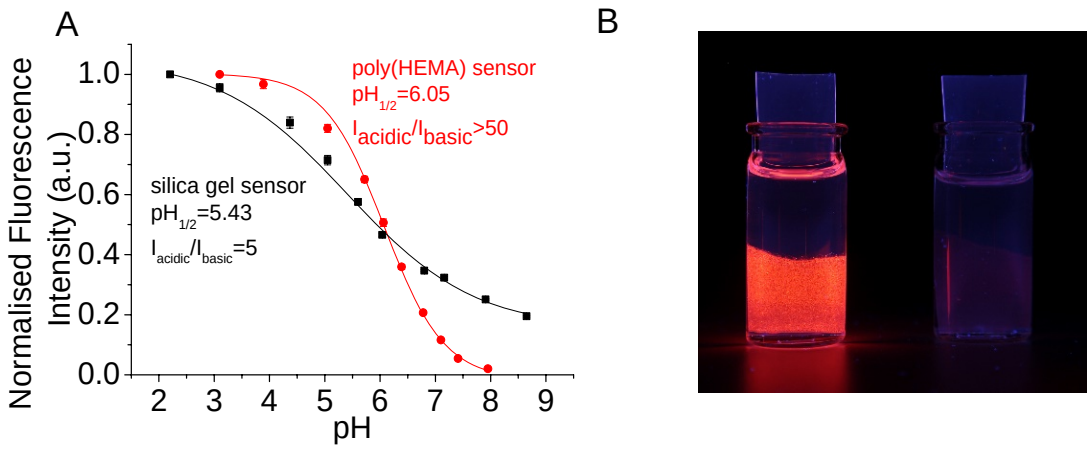

Figure 3-4: A: pH Calibration curves (ionic strength 100 mM) for the sensor foils based on silica gel beads in D4® hydrogel and cross-linked poly(HEMA) beads in linear poly(HEMA), both carrying covalently linked PET rhodamine. $pH_{1/2}$ is the pH at which half of the overall pH-dependent signal change is observed. B: Photographic image of the poly(HEMA) sensor foils in acidic (pH 4) and basic (pH 9) buffer.

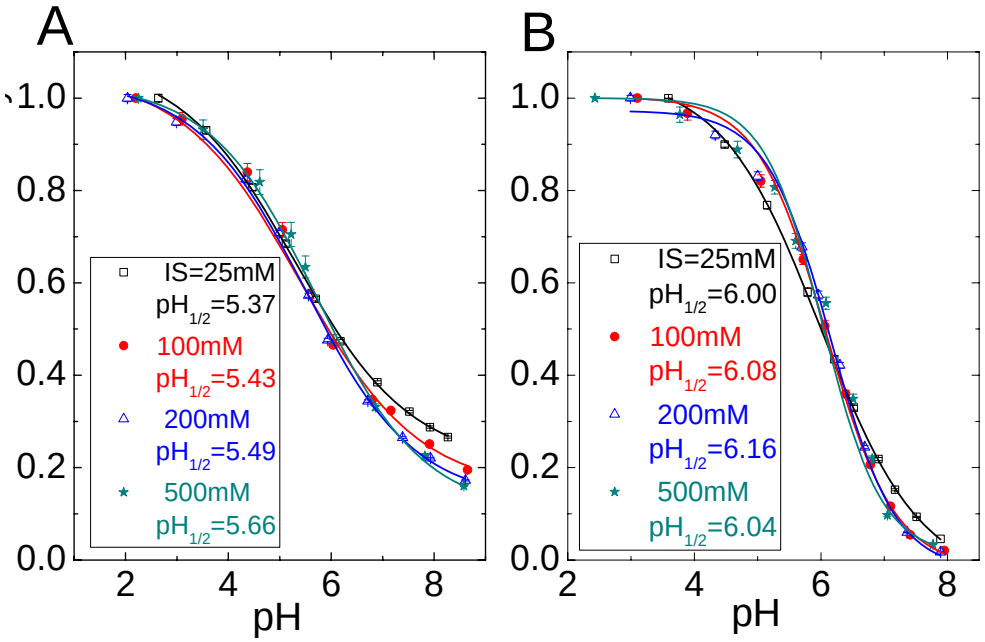

Figure 3-5: Calibration curves of the sensor based on silica gel beads (A) and on poly(HEMA) beads (B), measured at different ionic strengths (IS), and corresponding $pH_{1/2}$ values (pH value at which half of the overall pH-dependent signal change is observed).

Table 3-2: Photophysical properties of the sensing materials. The sensor foils were treated with acidic/basic buffer solution, pH 4/9. Prior to measuring Φ_F, the foils were acidified with HCl vapour.

Sensor	λ_{max} exc/nm acidic/basic	λ_{max} em/nm acidic/basic	Φ_F acidic
Silica gel beads in D4 hydrogel	572/583	598/609	0.65
Cross-linked poly(HEMA) beads in linear poly(HEMA)	576/592	601/612	0.61

Detailed calibration curves are shown in figure 3-4. The silica gel sensor beads are applicable over a broad range (pH 3-8). Measuring at pH > 8 (which is essentially outside the sensitive range) is not recommended and leads to irreversible signal decrease. That is probably caused by hydrolytic

cleavage of the Si-O bonds that attach the indicator to the silica gel surface. At pH ≤ 7.5, no signal decrease was observed over many hours. Notably, pH response is broader and quenching at basic pH is less effective than in solution or in the poly(HEMA) beads. This may be related to stabilisation of the cationic acidic form by the negatively charged silica gel surface. Other effects may also contribute to the observed phenomenon. In fact, Gao et. al. [228] demonstrated that fluorescence of a rhodamine dye bound to a silica gel surface can be enhanced at increasing pH.
The sensor based on poly(HEMA) beads shows very strong quenching at basic pH and a sharper response at pH 5-7, thus offering excellent sensitivity in this range. It is highly suitable for probing biotechnological samples.

Photostability

We expected the electron-withdrawing pentafluorophenyl group to suppress photooxidation and therefore improve the photostability of the rhodamines **1** and **2**, compared to **3**. However, the opposite effect was found for **1-3** in aqueous solution (figure 3-6) where 1 and 2 showed measureable photodegradation when illuminated with a high-power 525nm LED (3W). This suggests a non-oxidative mechanism as main photodegradation pathway. Therefore, worse photostability can be a drawback in the current system based on pentafluorophenylrhodamines, compared to the "classical" rhodamines carrying 2'-carboxyphenyl substituents. However, the sensors based on **1** and **2** are still very robust under the employed measurement conditions. In fact, continuous illumination with a standard 5 mm 525 nm LED over > 5 h caused no changes in the fluorescence signal. Note that for practical applications, continuous illumination is often not necessary so that measurement can be carried out for a much longer time before recalibration is required. Indeed, if long-time application and high light densities are required, the photostability of the sensors might become an issue.

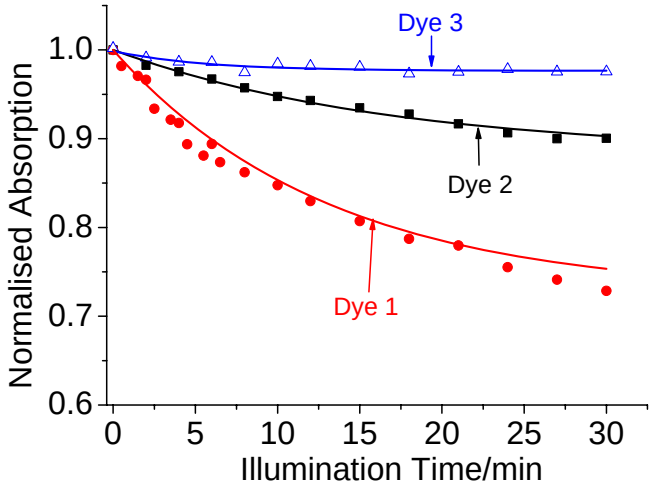

Figure 3-6: Photodegradation profiles (approximated with monoexponential decay) of 1-3 in aqueous buffer solution (100 mM; pH = 7.5) when illuminated with a 525 nm high-power LED (3 W). The solutions (3 ml) were placed in a glass cuvette and irradiated in a fixed position with respect to the light source. The photodegradation profiles were obtained by monitoring the absorption spectra in the absorption maximum of each dye. Dye concentration was adjusted so that A_{525} = 0.4 for all dyes.

Dually Lifetime Referenced pH-sensor

For practical applications, an optical sensor based on fluorescence intensity requires referencing. One possibility is the combination with a luminescent reference material and interrogation by phase fluorimetry (dual lifetime referencing, DLR) [16,17]. The observed phase shift is then a function of the ratio between luminescence intensity of the fluorescent indicator and the luminescent reference material. Cr(III)-doped Al_2O_3 ("ruby") was chosen as a reference material because it is spectrally compatible with the sensor particles and the light source (525 nm LED; figure 3-7A) and features good chemical stability and photostability. A typical measurement with pH-sensitive silica particles as sensitive material is shown in figure 3-7B. The referenced sensor shows excellent response and reversibility.

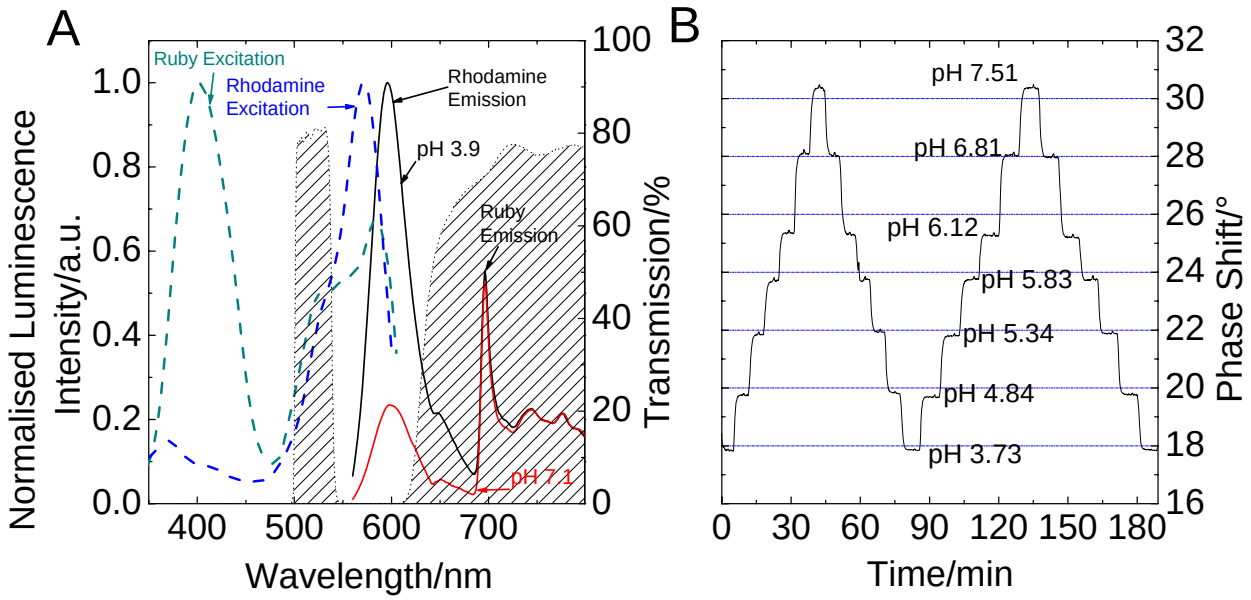

Figure 3-7: Properties of the DLR pH sensor (pH-sensitive silica gel beads:ruby 1:6 w/w in a 10 µm thick D4 hydrogel layer): A: Normalised luminescence excitation (dashed lines) of the rhodamine linked to silica gel particles and of ruby; luminescence emission (solid lines) of the DLR sensor at two different pH (both spectra were normalised dividing by the largest intensity count measured at pH 3.9), recorded with a spectrofluorimeter (λ_{EXC} = 525 nm). The transmission of the excitation filter (500-540 nm) and emission filter (> 630 nm) are visualised by striped areas. B: pH-response curve recorded by phase modulation fluorimetry (550 Hz).

Conclusion

A new class of pH-sensitive rhodamines has been presented. Their pH-sensitivity originates from photoinduced electron transfer (PET) from non-protonated amino groups to the excited chromophore. Concerning synthetic accessibility and performance as pH-indicators, they at least equal to the pH-sensitive rhodamines employing lactame-formation which have been extensively studied [39,40,215-217]. The dyes are suitable for pH monitoring not only in the dissolved state, but also as indicators in pH sensors. In contrast to the rhodamine bearing a 2,4-dicarboxyphenyl group (dye **3**), the new indicators carry a pentafluorophenyl group which enables facile and effective grafting via "click" chemistry. Furthermore, the sensitive properties of the new indicators are not affected by pH-dependent lactonisation, while almost complete lactonisation in the same

environment was detected for **3**. Sensors with covalent indicator linkage have been successfully prepared based on two matrix materials, silica gel and poly(2-hydroxyethylmethacrylate). Both sensors feature bright fluorescence ($\Phi_F \approx 0.6$) and their sensitive range perfectly matches the pH range of interest for many biotechnological applications (i.e. pH 5-7). They also show good response times, repeatability and long-term stability. For practical applications, a dually lifetime referenced sensor has been presented. Cross-sensitivity to ionic strength causes small to moderate errors (generally 0-0.1, at most 0.2 pH units), provided that the ionic strength is 100-500 mM, which is the case in most biotechnological applications. Although photostability is impaired by the pentafluorophenyl group, it does not compromise the applicability of the sensors under the tested conditions which can be used for a long time without a measurable signal decrease.

Acknowledgement

Financial support from the Austrian Science Fund FWF (project P 21192-N17) and from the Spanish Ministry of Education (joint project AT2009-0019) is gratefully acknowledged. The authors thank the Institute of Organic Chemistry, Graz University of Technology, particularly Jana Rentner, MSc for kind support in performing LC-MS. Furthermore, we thank Johann Pichler, Institute of Inorganic Chemistry, Graz University of Technology, for acquiring ^{19}F-NMR spectra, as well as Sarah Schiller and Stefan Schobesberger.

Supplementary Information

to *New Fluorescent pH-Sensors Based on Covalently Linkable PET Rhodamines*

UV/Vis Spectra

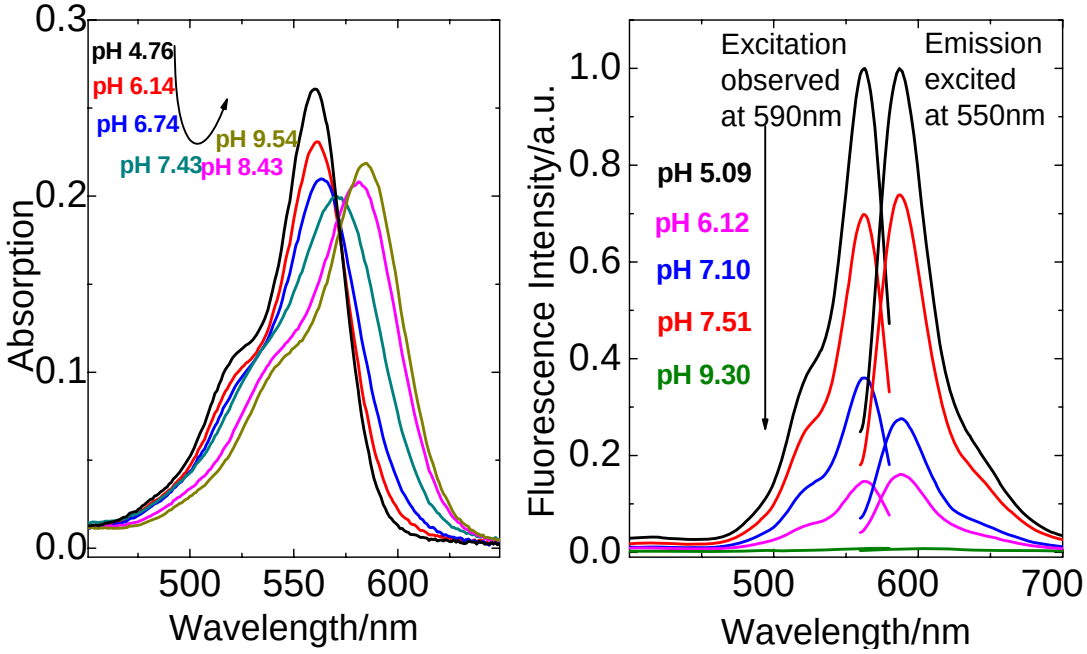

Figure 3-S1: Absorption spectra (left) and fluorescence spectra (right) of 2 in aqueous buffer solution (ionic strength 100mM) at different pH. Dye concentration was 2µM when recording absorption and 0.05µM when recording fluorescence spectra.

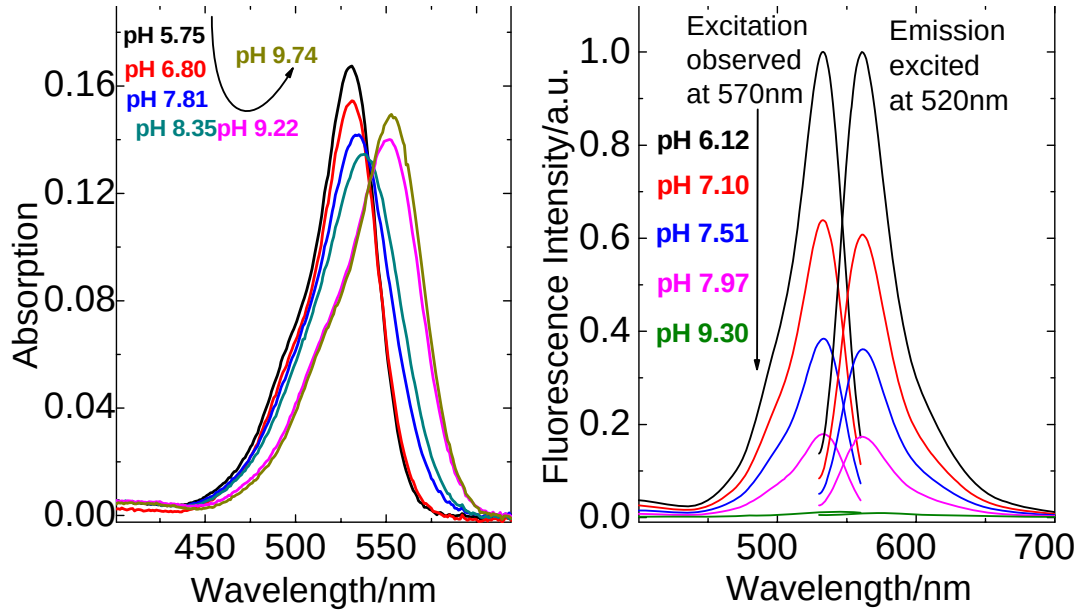

Figure 3-S2: Absorption spectra (left) and fluorescence spectra (right) of 3 in aqueous buffer solution (ionic strength 100mM) at different pH. Dye concentration was 2µM when recording absorption and 0.05µM when recording fluorescence spectra.

Sensor Response Curves

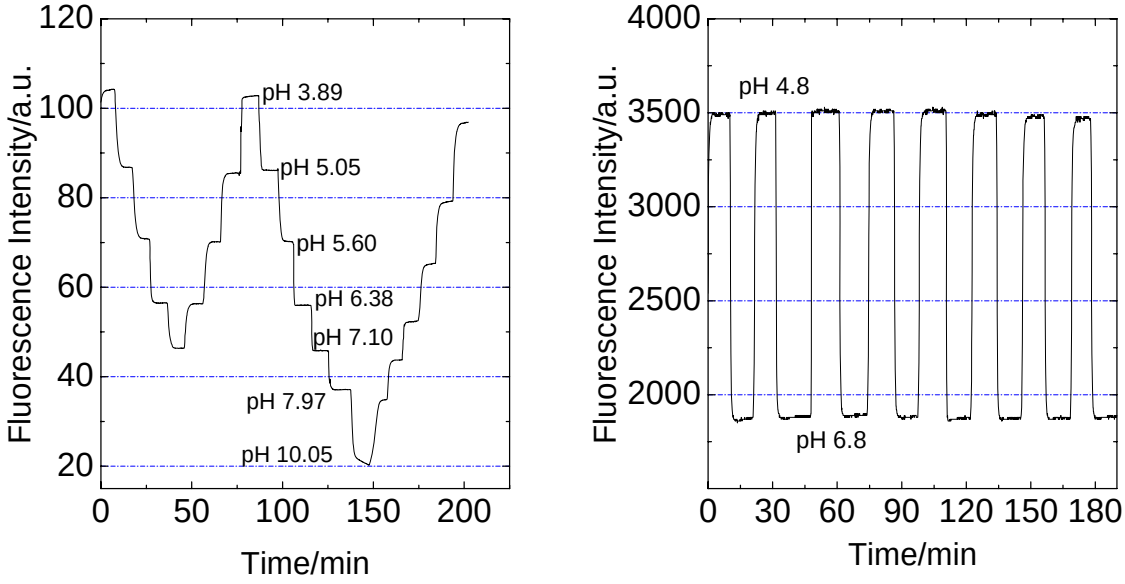

Figure 3-S3: Reversibility and repeatability of the sensor based on silica gel beads in D4® hydrogel. Signal drift and irreversible response are only observed at high pH values (>8) which are essentially outside the sensitive range.

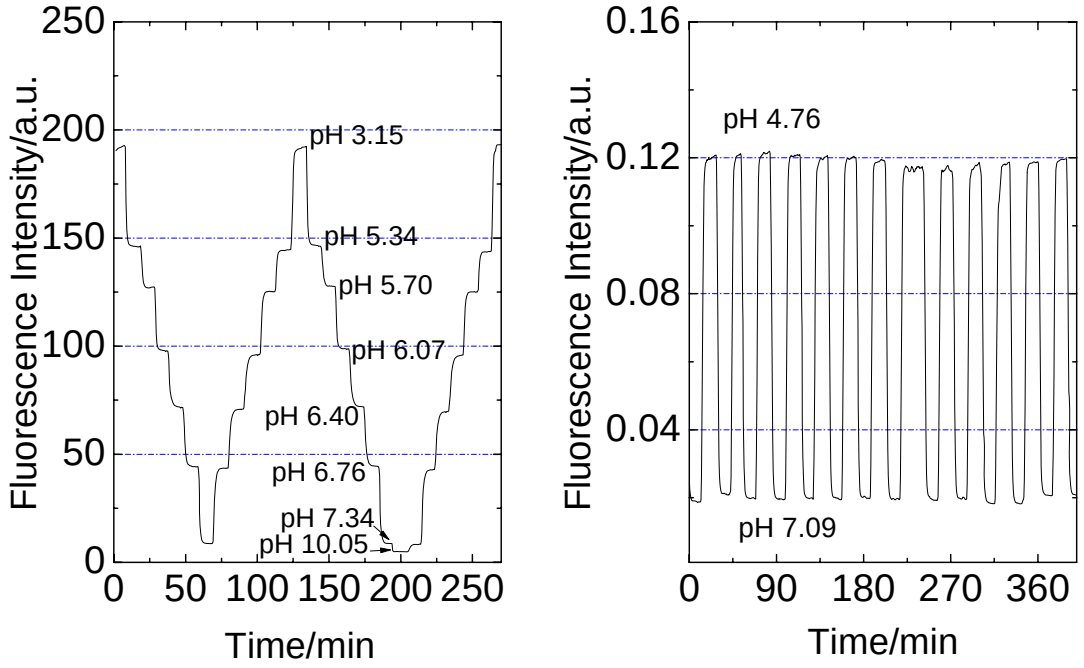

Figure 3-S4: Reversibility and repeatability of the sensor based on cross-linked poly(HEMA) beads linear poly(HEMA). They are good over the whole investigated pH range (pH 3-10).

Chapter 4

Fluorescent Materials for pH Sensing and Imaging Based on Novel 1,4-Diketopyrrolo-[3,4-c]pyrrole Dyes

Preface to Chapter 4

The pH-sensors based on diketopyrrolo[3,4-c]pyrroles (DPPs) presented in this section bring above all two new elements to this thesis:
Firstly, phenoxides are used as PET groups instead of amines. Interestingly, amines were found not to cause quenching of DPPs, while very effective quenching is caused by the phenoxides. The use of phenoxides, together with the employment of three different immobilisation matrices (Hydromed D4® polyurethane hydrogel layers, poly(2-hydroxyethylmethacrylate) layers and Eudragit RL100® nanoparticles) allows covering a broad pH-range of pH 4 – 10, while only pH < 7 are well measurable with the sensors presented in chapters 1 – 3. Sensitive range tuning is possible by varying the PET group and the immobilisation matrix and therefore expected to be applicable in the same way with the fluorophores presented in sections 1 – 3. In the absence of a PET group, there is another pH-dependent equilibrium in DPPs associated with deprotonation of the lactam nitrogen at pH > 10, making the sensors even more flexible and potentially applicable at strongly basic pH for which few pH-probes are available.
Secondly, when DPPs are combined with reference fluorophore Macrolex® Fluorescence Yellow, a ratiometric pH-sensor suitable for readout with a simple RGB camera is obtained. The nanoparticle-based sensors were successfully employed for fluorescence imaging in (micro)fluidic systems. That makes up the first demonstration of practical applicability of the pH-sensors developed in this thesis. Because the reference dye is used as donor in Förster resonance energy transfer (FRET), excitation efficiency and therefore brightness of the sensor are significantly improved, overcoming the moderate intrinsic brightness of DPPs.
The drawback of the DPP-based sensors is in their poor signal reproducibility and in drifting measurement signals. That is probably caused by modest photostability of the sensors and by migration and aggregation of the indicator dye which is not covalently coupled. Notably, significantly better photostability was found for similar DPPs in non-aqueous systems. Even when measured at very low light intensities, the DPP-based sensors show unstable behaviour over time, with signal drifts similar to those observed for tetraphenoxy-PBIs (chapter 1). Though not critical for the short application times typical for many fluidic applications, signal instability still constitutes a very significant limitation. This is therefore another example for non-covalent entrapment of highly hydrophobic or poorly soluble dyes resulting in poor sensor performance. Solubility of the DPP-probes is limited due to interactions involving hydrogen bonds at the lactam units. However, preliminary experiments with *N*-alkylated DPPs showed that they cannot be made pH-sensitive by the same method as non-alkylated DPPs. Hence improving solubility and covalent probe coupling are difficult as there are no functional groups available. Further optimisation of the DPP-based sensors was therefore not carried out.

Fluorescent Materials for pH Sensing and Imaging Based on Novel 1,4-Diketopyrrolo-[3,4-c]pyrrole Dyes

This chapter was published in **Journal of Materials Chemistry C**, 2013, 1, 5685–5693; doi: 10.1039/c3tc31130a.

Authors: **Daniel Aigner, Birgit Ungerböck, Torsten Mayr, Robert Saf, Ingo Klimant and Sergey M Borisov**

New optical pH-sensors relying on 1,4-diketopyrrolo-[3,4-c]pyrroles (DPPs) as fluorescent pH-indicators are presented. Different polymer hydrogels are useful as immobilisation matrices, achieving excellent sensitivity and good brightness in the resulting sensor. The operational pH can be tuned over a wide range (pH 5 – 12) by selecting the fine structure of the indicator and the matrix. A ratiometric sensor in the form of nanoparticles is also presented. It is suitable for RGB camera readout, and its practical applicability for fluorescence imaging in microfluidic systems is demonstrated.
The indicators are available starting from the commercially available DPP pigments by a straightforward concept employing chlorosulfonation and subsequent reaction with amines. Their sensitivity derives from two distinct mechanisms. At high pH (> 9), they exhibit a remarkable alteration of both absorption and fluorescence spectra due to deprotonation of the lactam nitrogen atoms. If a phenolic group is introduced, highly effective fluorescence quenching at near-neutral pH occurs due to photoinduced electron transfer (PET) involving the phenolate form.

Introduction

pH is one of the key parameters in medical, environmental and life sciences. Despite the strong performance of electrochemical pH-sensors, optical pH-sensors have proved invaluable in numerous important applications. They possess numerous advantages including for example greater ease of miniaturisation and the possibility of contactless measurement. Moreover, optical probes enable imaging applications [17,99,229-231]. These features are particularly attractive in high-throughput screening and for probing small samples such as living cells or sub-cellular structures [83,101].
Optical pH-sensors typically consist of a pH-sensitive dye (*i.e.* a pH-indicator) immobilised in a polymer matrix which has to provide suitable mechanical and adhesive properties, together with sufficient water uptake. Although most optical pH-indicators are essentially (de)protonable chromophores [20,45,152], those with proton receptors separated from the chromophore have also found numerous applications. They are the most flexible in terms of rational dye design since the chromophore and the receptor can be selected independently. Most frequently, they take advantage of the photoinduced electron transfer (PET) [60,62] process. Though PET is an extensively investigated effect, in most publications it is introduced by amine functionalities [64] [55,77,102], while phenolic groups have attracted comparatively little attention. In 1997, Gareis et al. [66] presented a boron-dipyrromethene (BODIPY) pH-indicator with a phenolic proton receptor. Most comparable systems have relied on the BODIPY chromophore since then [76,78,232].

Derivatives of 1,4-diketo-3,6-diphenylpyrrolo[3,4-c]pyrrole, often referred to as DPPs, are chemically stable, brightly fluorescent [233] molecules that have found a variety of applications. While the parent compounds are commonly used pigments, the attachment of suitable substituents yields readily soluble fluorescent dyes. Alkylation of the lactam nitrogen atoms is most effective in this regard since hydrogen bonding interactions are suppressed. DPP-based dyes and pigments have been used as high-performance colorants in prints and inks, as components of solid-state dye lasers [132,234-237] and more recently in the field of organic optoelectronics. Particularly, DPP-containing conjugated polymers [133,238,239] and small molecules [134] have found extensive use in Organic Field Effect Transistors (OFETs) [240,241] and Organic Solar Cells [242,243]. DPP dyes are also particularly promising for the design of two-photon excitable fluorophores [135,244]. A few DPP-based fluorescent probes and sensors for fluoride [245], cyanide [246], thiols [247] and molecular hydrogen [248] have been developed. The DPP-based probe presented by Yamagata et al. [249] is suited for detecting strong acids in organic solvents, rather than measuring near-neutral pH in aqueous solution. Recently, we presented carbon dioxide sensors that exploit the deprotonation of the lactam nitrogen atoms in DPPs [24]. The same mechanism is useful for the determination of comparatively high pH (> 9), as will be demonstrated in this work. Furthermore, we present – to the best of our knowledge for the first time – DPP-based pH-sensors that operate at near-neutral pH. They rely on PET from phenolate groups to the chromophore.

Results and Discussion

The preparation of the new pH-indicators and sensors is shown in figure 4-1. The indicators **2** and **3** feature phenolic PET groups. **4** carries a morpholino group for solubilisation and is an example of a DPP pH-indicator relying on deprotonation of the lactam nitrogen.

Indicator Syntheses

The indicators **2** - **4** can be easily prepared in a single step starting from commercially available 1,4-diketo-3,6-diphenylpyrrolo[3,4-c]pyrrole. Notably, the reaction conditions applied afforded only monosulfonated products. Doubly sulfonated products are formed under harsher reaction conditions [24]. The intermediate, a sulfonyl chloride, can yield a large variety of sulfonamides, depending on the amine it is reacted with. The synthetic concept employed is simple and versatile as it is applicable for any class of chromophore that can withstand chlorosulfonation. It is useful for tagging a large variety of structures and is not limited to the preparation of pH-indicators, which has been the main focus of this work.
The modest yields (13 – 22%) are due to difficulties in purifying the products by column chromatography. They strongly bind to the stationary phase and are hard to elute completely. Nevertheless, all products could be easily isolated in sufficient amounts starting from the cheap commercial pigment.

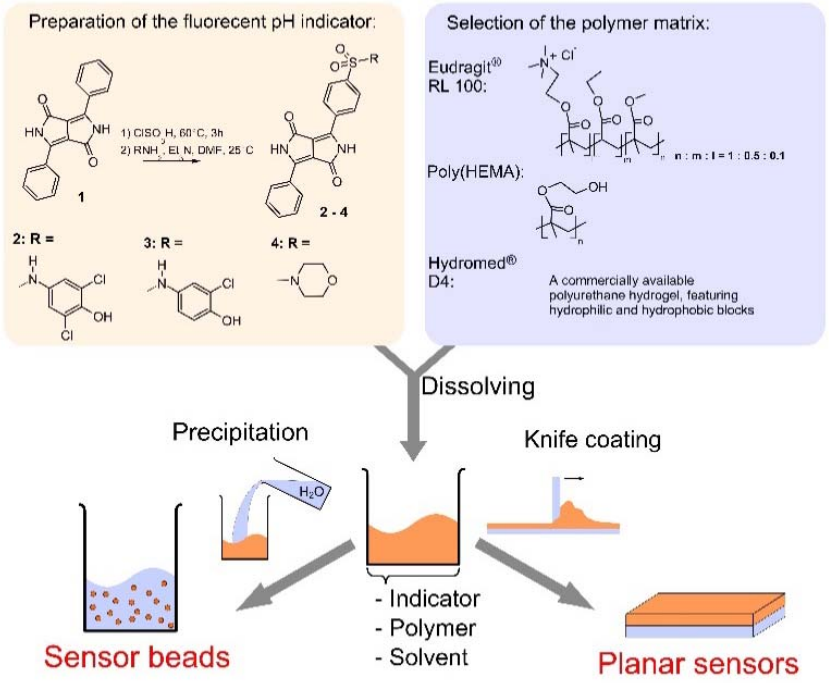

Figure 4-1: Scheme for the preparation of the fluorescence pH-sensors in this work.

Indicator Properties

Spectral properties of the DPP sulfonamides **2** - **4** in comparison to the starting material are listed in table 4-1. The attachment of a sulfonamide group results in bathochromically shifted and less structured absorption bands, while the Stokes shifts are significantly enlarged. Despite that **2** – **4** are not *N*-substituted their solubilities exceed 2 g / l in *N,N*-dimethylformamide and tetrahydrofuran. This is dramatically higher than for pigment **1** which is virtually insoluble in these solvents at 25 °C. Note that for the majority of applications requiring soluble DPPs, *N*-substituted derivatives are used. However, our preliminary experiments indicated that chlorosulfonation of a *N,N'*-dialkylated DPP (*N,N'*-di(2-ethylhexyl)-1,4-diketo-3,6-diphenylpyrrolo[3,4-c]pyrrole) and subsequent reaction with 4-amino-2,6-dichlorophenol did not yield a pH-indicator.

Table 4-1: Spectral properties of the DPP dyes in tetrahydrofuran: λ_{max} abs – wavelengths of the absorption maxima; ε - molar absorption coefficients; λ_{max} em - wavelengths of the fluorescence emission maxima; Φ_F - relative fluorescence quantum yield; n.d. - not determined; n.m. – not measureable (2 and 3 are virtually non-fluorescent in the phenolate form). Acidic/basic denotes 0.1% (V/V) trifluoroacetic acid / 1 mM tetrabutylammonium hydroxide.

Dye	λ_{max} abs($\varepsilon \cdot 10^{-4}$) / nm ($M^{-1} \cdot cm^{-1}$) acidic / basic	λ_{max} em / nm acidic / basic	Φ_F acidic/basic
1	468(2.95), 502(3.91)	514, 552	n.d.
2	509(2.23), 543(2.40) / 575(1.88), 606(2.16)[a]	580 / n.m.	0.70 / n.m.
3	508(1.74), 541(1.86) / 575(1.60), 606(1.86)[a]	577 / n.m.	0.66 / n.m.
4	509(2.02), 541(2.14) / 391(0.95), 584(1.89), 619(2.39)	576 / 679	0.71 / 0.08

[a] The bathochromically shifted spectra correspond to the dianionic form (both phenol and lactam are deprotonated). The absorption of the monoanionic form (only phenol is deprotonated) is not shifted with respect to the acidic form (figure 4-3).

The pH-sensitivity of the DPP indicators is associated with two distinct mechanisms, as illustrated in figure 4-2. **2** and **3** are subject to photoinduced electron transfer (PET) when the phenolic group is deprotonated. The result is fluorescence quenching around the pK_A of the phenolic group (that is, pH 5.9 – 9.3, table 4-2). No alteration of the absorption spectra at all is observed (figure 4-3), indicating that the effect is solely PET. Importantly, the quenching is extremely efficient (virtually no fluorescence from the deprotonated form is detected) which indicates that phenolates are suitable proton receptor groups for designing fluorescent pH-indicators. Thus they represent a very promising alternative to the much more common amino-based receptors.

Fluorescence quenching of **4** occurs at higher pH (9.7 – 11.6, figure 4-4) and is clearly accompanied by a bathochromic shift in absorption and fluorescence spectra. This effect is caused by deprotonation of the lactam nitrogen within the chromophore [24]. Similar changes in the absorption spectra can also be observed for **2** and **3** at higher pH. The absorption spectra shown in figure 4-2C correspond to the neutral and the monoanionic form of **4**. Note that the monoanion exhibits weaker but clearly detectable fluorescence. Under more basic conditions, a further bathochromic shift is observable, which originates from partial deprotonation of the second lactam nitrogen, resulting in the dianion.

Notably, the sulfonamide moiety itself can also undergo deprotonation. Typical pK_A values would be in the range 8 – 11 for structures comparable to **2** and **3** [250,251]. Such a deprotonation mechanism may contribute to their pH-sensitivity to some extent. The anion formed, a sulfonimide, is in protolytic equilibrium with the phenolate form shown in figure 4-2. Note that the sulfonamide group in 4 cannot be deprotonated and its pH-sensitivity is thus related exclusively to lactam deprotonation.

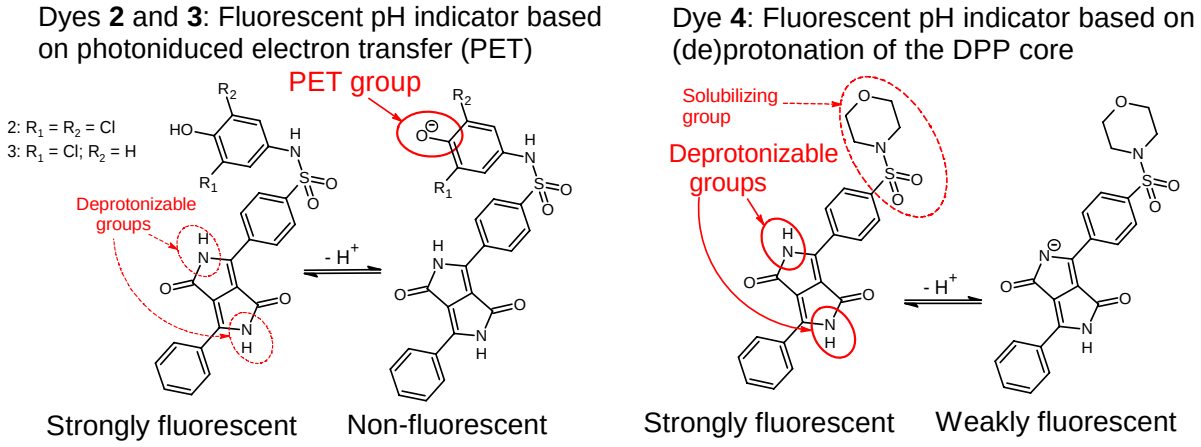

Figure 4-2: Mechanisms causing pH-sensitivity in the DPP-based indicators.

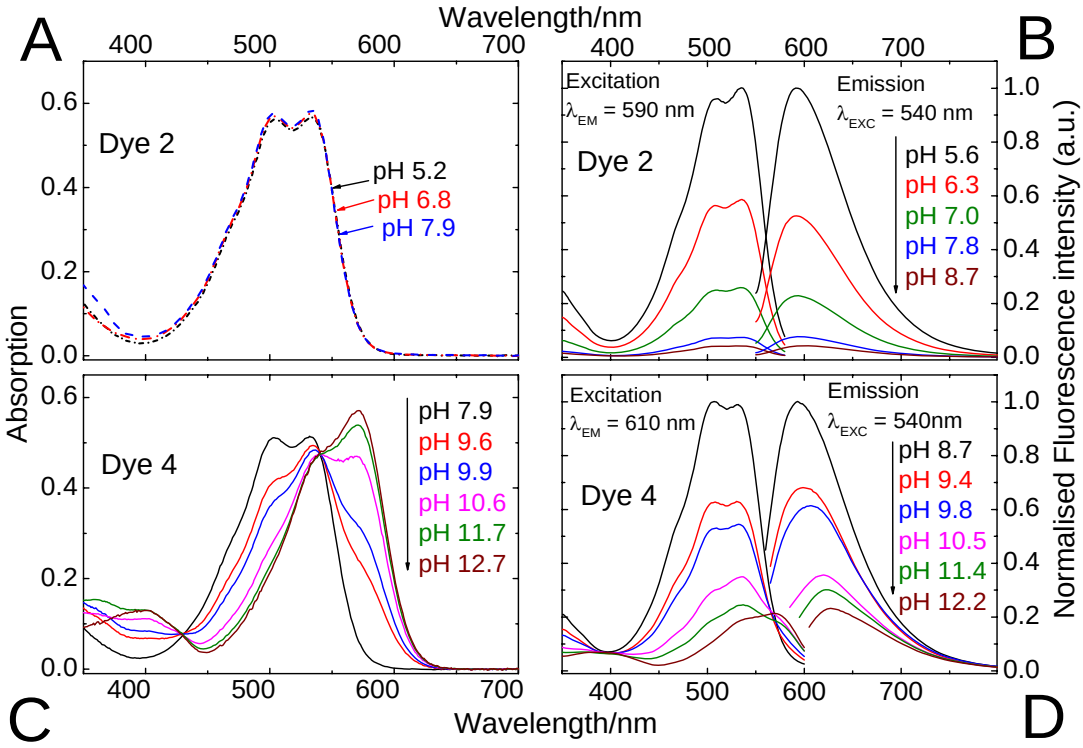

Figure 4-3: pH-dependent absorption (A, C) and fluorescence (B, D) spectra of the DPPs 2 and 4. Since 2 and 3 feature virtually identical spectral properties and differ only by their sensitive pH ranges, 3 has been included in the supplementary information (figure 4-S1) only. Spectra were recorded in ethanol/aqueous buffer (ionic strength 100 mM) solution 1:1 (V/V). pH values are those of the aqueous buffer used. DPP concentration was 20 µM for absorption and 4 µM for fluorescence measurements.

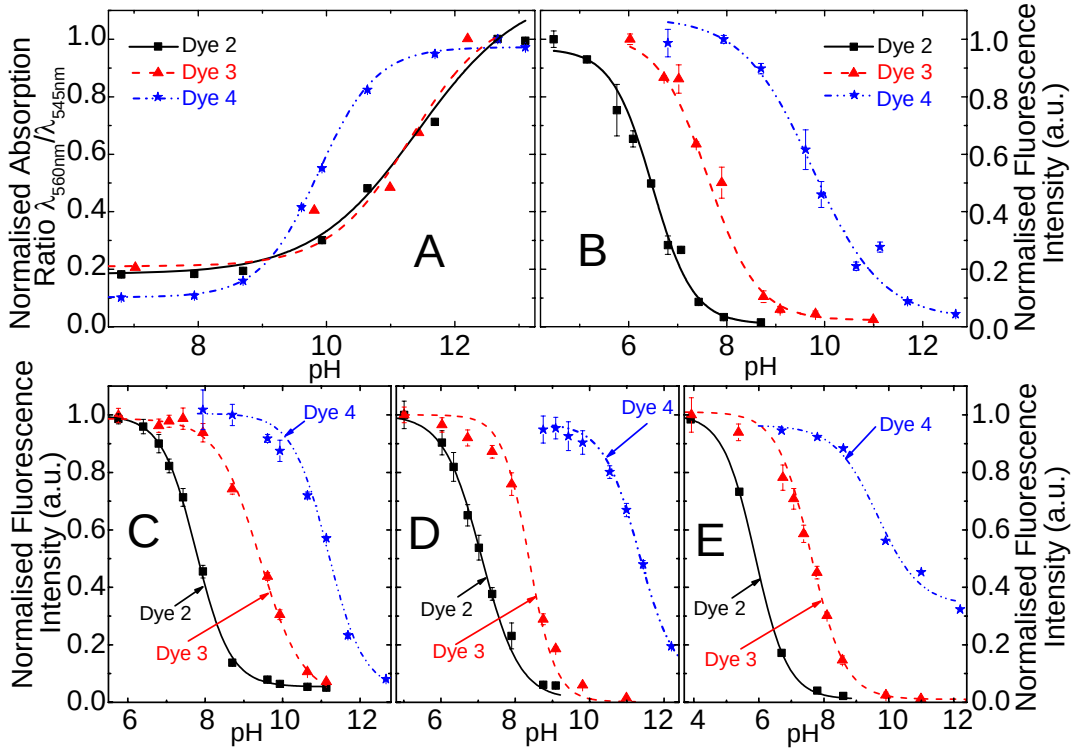

Figure 4-4: A: pH calibration curves of the DPP indicators in ethanol/aqueous buffer (ionic strength 100 mM) solution 1:1 (V/V); pH values are those of the aqueous buffer used. B: Corresponding fluorescence calibration curves for the solution (λ_{EXC} = 540 nm, observed at 595 nm); C, D: pH calibration curves based on fluorescence in planar sensors (dye content 0.25%; C in D4® hydrogel; D in poly(2-hydroxyethylmethacrylate), E: Calibration curves in RL100 sensors beads dispersed in aqueous buffer (dye content 0.5% (w/w), bead concentration 0.2 mg / ml).

Table 4-2: $pH_{1/2}$, the pH values at which half of the pH-dependent signal change is effective, based on absorption (Abs.) and fluorescence (Fluo.), corresponding to the calibration curves in figure 4-4. n.d. denotes not determined.

Dye	EtOH/H_2O 1:1 (V/V)		D4		poly(HEMA)	RL100
	$pH_{1/2}$ (Fluo.)	$pH_{1/2}$ (Abs.)	$pH_{1/2}$ (Fluo.)	$pH_{1/2}$ (Abs.)	$pH_{1/2}$ (Fluo.)	$pH_{1/2}$ (Fluo.)
2	6.49[a]	11.3[b]	7.76[a]	n.d.[c]	7.08[a]	5.88[a]
3	7.63[a]	11.3[b]	9.34[a]	n.d.[c]	8.36[a]	7.62[a]
4	9.75[b]	9.88[b]	11.1[b]	11.6[b]	11.1[b]	9.65[b]

[a] corresponds to deprotonation of the phenolic PET group
[b] corresponds to deprotonation of the lactam nitrogen
[c] The doubly charged basic form is quickly leached out of the sensor

The photostability of the DPPs has been investigated and compared to reference dyes which represent two of the most commonly used types of pH-indicators. It is vastly superior to that of fluorescein octadecyl ester (figure 4-5). Compared to HPTS (8-hydroxypyrene-1,3,6-trisulfonate), a highly photostable pH-indicator, DPPs are degraded 3 – 4 times faster under the same illumination conditions. Photostability is greatly increased (dye degraded > 20 times slower) in deoxygenated samples which implies an oxidative photo-degradation pathway or may involve photosensitised singlet oxygen. No degradation at all was observed for the phenolate form of **2**. That could be because PET causes fast quenching, leaving little time for degradation in the excited state.

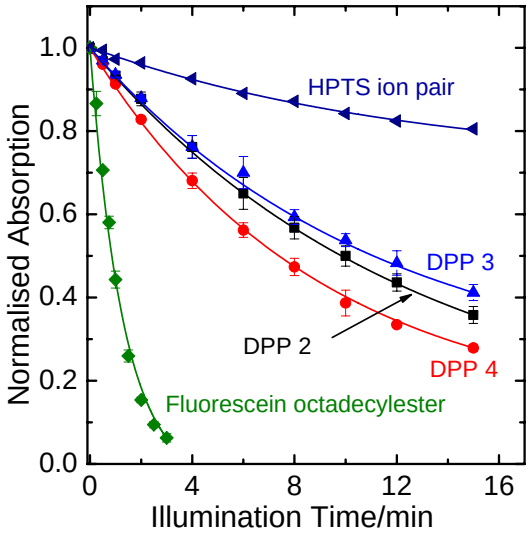

Figure 4-5: Photodegradation profiles of the DPP dyes, compared to fluorescein octadecyl ester and 1-hydroxypyrene-3,6,8-trisulfonate (HPTS) in the form of an ion pair with tetraoctylammonium. The solutions in tetrahydrofuran (for HPTS, 0.02 mM tetraoctylammonium hydroxide in the form of an 1 M methanolic solution was added) were illuminated with an 458 nm high-power LED array. The decay rates compared to 2 are 0.92 for 3, 1.12 for 4, 0.31 for HPTS ion pair and 6.1 for FODE.

pH-sensing Materials

The pH-indicators have been immobilised in polymer matrices to obtain pH-sensors. The host materials are Hydromed® D4 (a commercially available polyurethane-based hydrogel) and poly(2-hydroxyethylmethacrylate) (p(HEMA)) in the form of planar sensors and Eudragit® RL100 (a positively charged acrylate polymer) in the form of sensor nanobeads (typical average size 30 nm). The sensors are promising not only due to their high brightness and sensitivity, but in

particular because their sensitive range can be tuned by selecting the indicator structure and the matrix (table 4-2, figure 4-4). The PET-based indicators **2** and **3** can tackle pH 5 – 10. Monochlorinated **3** covers higher pH than dichlorinated **2**. The basic form of the indicator is negatively charged and thus most effectively stabilised by the cationic RL100 matrix and least effectively stabilised by the comparatively hydrophobic D4; this results in $pH_{1/2}$ values increasing in the same order. The pH-range covered by **2** and **3** in those matrices meets the one of interest to the most relevant applications for pH-sensors, namely medical applications (physiological pH 7 – 7.5), marine science (optimal pH 7.5 – 8.5) and biotechnological process monitoring (pH 5 – 7, depending on the process). **4** enables measurement at pH 9 - 12, a range that is more seldomly addressed but is of importance to applications such as concrete quality testing. In this pH-range, the choice of already available pH-indicators is rather limited.
In practical applications, not only the sensitive range of a fluorescence sensor is of importance but also referencing possibilities. Referencing can make the signal independent on the optical path length, the efficiency of the light source and the guidance of light to the detector. Therefore, a ratiometric pH-sensor employing the commercially available coumarin Macrolex Yellow (3-(5-chloro-2-benzoxazolyl)-7-(diethylamino)-2H-1-benzopyran-2-one) as a reference dye has been developed. In this approach, the reference dye is excited, its excitation energy is partially transferred to the DPP pH-indicator dye by Förster resonance energy transfer (FRET) and the emission ratio between both dyes is detected. The referenced system is particularly promising since it can be read out with a simple RGB-CCD camera (figure 4-S2 in the supplementary information). Imaging with RGB cameras is becoming increasingly popular [252-254]. Its sensitive range is very similar to the non-referenced analog, as demonstrated in figure 4-S3.

Planar Sensors
The usefulness of the planar ratiometric sensors is demonstrated in figure 4-6 – fluorescence imaging was successfully performed over an application time of > 0.5 h. However, limitations were revealed when the long-term performance of the planar sensors was examined in a fiber-optic measurement setup with a LED light source. A significant decrease of the indicator signal is observable if a sensor based on **2** or **4** is measured over several hours (6% per hour for **2**, 14% per hour for **4**; visualised in the ESI, figures 4-S4 and 4-S5, respectively). This signal drift is also present in the ratiometric system. It is strongly intensified when measurement is carried out under continuous illumination and it is accompanied by a diminishment in the DPP absorption band. That implies photo-degradation is an important factor for the signal drift. However, no significant dependence on illumination time was found if that time is generally short (a fraction of < 1% of the overall measurement time) and minimal emission intensity of the light source is applied. That suggests that other effects like dye aggregation or migration can also cause unwanted signal drift and become dominant at lower light intensities. Consequently, the DPP-based pH-sensors in the planar format are limited to applications requiring short times and low light densities.

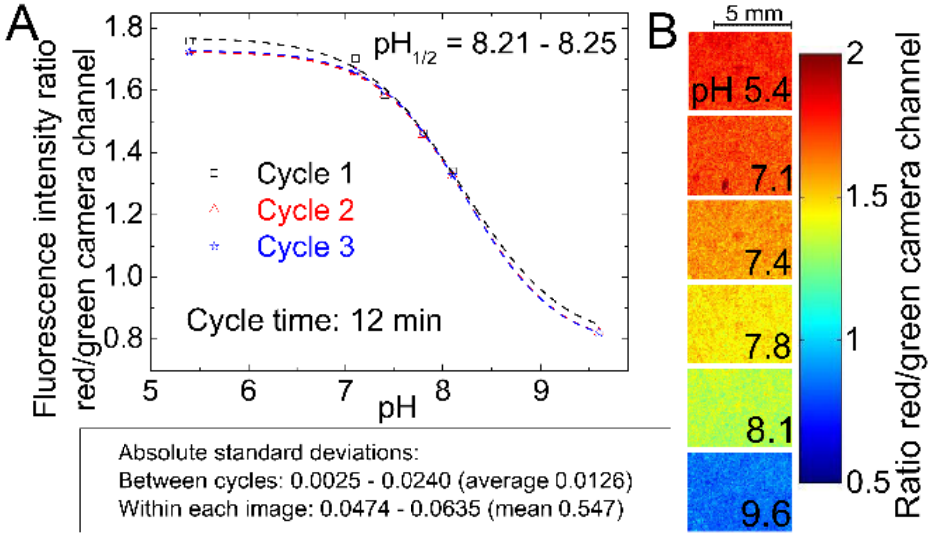

Figure 4-6: Fluorescence imaging with a planar ratiometric pH-sensor (7 µm thick) containing Macrolex yellow (1.5% (w/w)) and pH-indicator 2 (0.5% (w/w)), read out with a RGB-CCD camera. The sensor was placed in a home-made flow-through cell and buffer solutions (ionic strength 100 mM) were applied (flow rate 1ml / min, 2 min for each buffer). A blue (458 nm) LED array in combination with a Schott BG 12 bandpass filter (350 - 465 nm) was used for excitation. Excitation light was excluded from the camera employing a Schott OG515 nm long-pass filter. A: Calibration curve, based on the ratio between red and green color channel; B: Corresponding false color images.

Sensor Beads

In contrast to planar sensors which are static, sensor beads can be dispersed in the sample. Therefore, in all fluidic applications the beads are continuously renewed. When the residence time of each individual nanosensor is short, signal drifts within the sensor do not become noticeable even if the actual application time is long. As a result, photodegradation can be negligible in the case of sensor beads, while the same sensing materials used as planar sensors suffer from a signal drift. An example for this is given by figure 4-7A where the performances of DPP-based ratiometric pH-sensors in both formats are compared using a fluorescence microscope. Owing to the high light density typical for fluorescence microscopy, the signal of the planar sensor is dramatically affected by photo-bleaching and measurement is rendered essentially impossible. On the other hand, the performance of the RL100 sensor beads in a fluidic system remains unperturbed over the whole measurement time. Consequently, while the DPP-based planar sensors and sensor beads can both be useful for macroscopic fluorescence imaging (figure 4-6A), the use of beads is imperative in fluorescence microscopy. Figure 4-7 also demonstrates the applicability of the sensor beads in a microfluidic system. Note that imaging in microfluidic systems enables high-throughput measurements, for instance in medical applications. RGB cameras are generally simple readout systems available at low cost and were demonstrated to be suitable for pH-imaging in microfluidics [255]. To underline the suitability of the DPP-based sensor beads in this regard, they were used in a microfluidic system that allows parallelisation (figure 4-8).

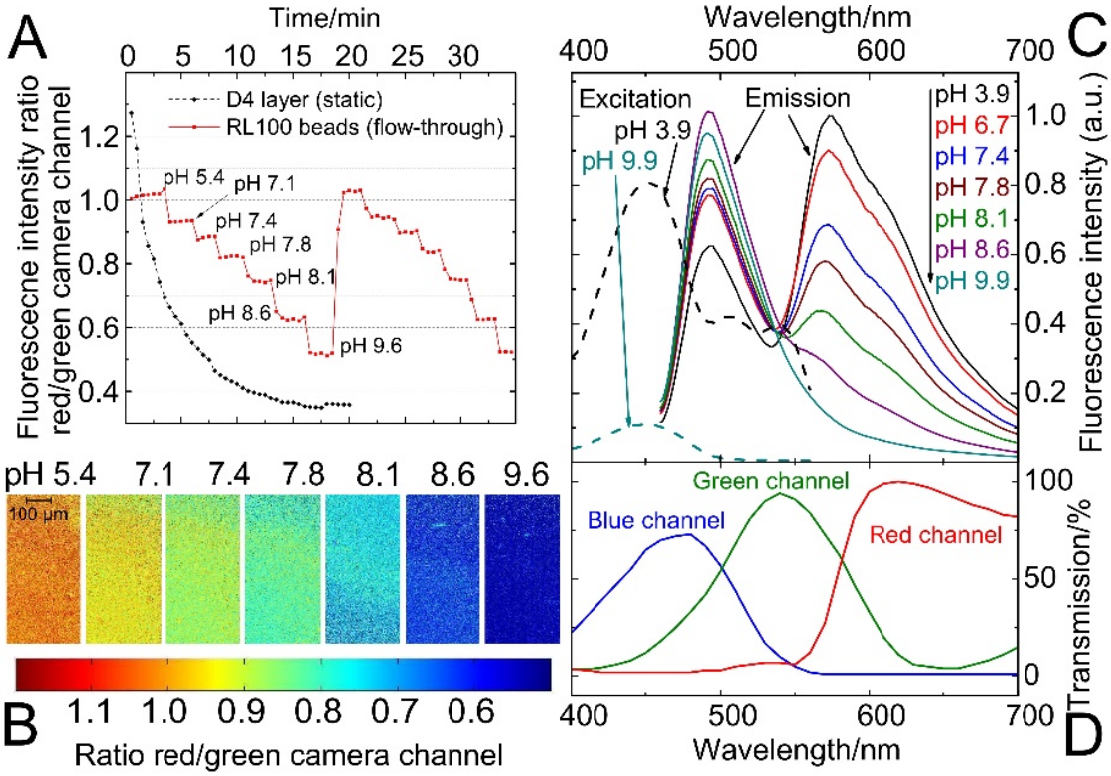

Figure 4-7: pH-imaging in a microfluidic system using a fluorescence microscope, employing ratiometric pH-nanosensor beads containing indicator 3 (1% w/w) and Macrolex® yellow (1.25% w/w) in RL100 polymer. The sensors were read out employing a RGB-CCD camera; A: Response curve of the bead suspensions, each measurement point was recorded illuminating for 2 s (the corresponding calibration curve can be found in figure 4-S6 in the ESI). They are compared to the performance of a planar sensor (static, placed on a microscope slide; composition as specified in figure 4-6) under the same measurement conditions; B: Images of the sensor bead suspensions corresponding to measurement A (cycle 1) - the ratio between red and green channel is visualised; C: pH-dependent fluorescence spectra (emission excited at 450 nm; excitation observed at 570 nm) of the sensor beads; D: Spectral characteristics of the RGB-CCD camera.

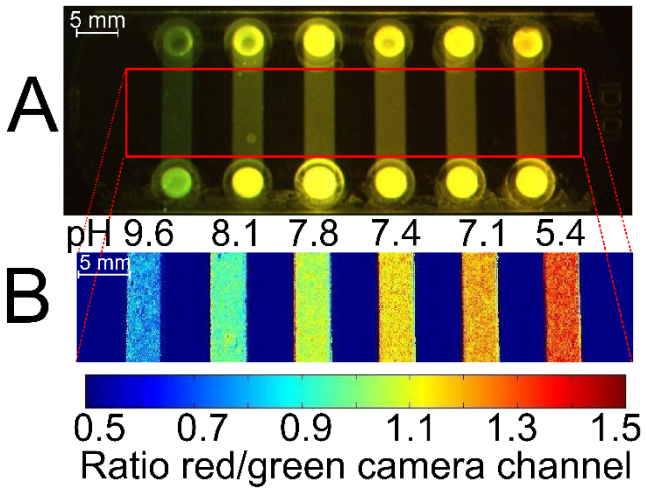

Figure 4-8: Example for a possible application of the DPP-based ratiometric pH-nanosensor beads in high-throughput measurement, using pH-imaging in a microfluidic system. pH can be determined simultaneously in every chip compartment. The pH-sensor beads (as specified near figure 4-7) in aqueous buffer of defined pH were read out employing a RGB-CCD camera. Excitation source and filters were the same as in figure 4-6. A: Photographic image; B: False colour image of the chip. At the channel inlets, locally higher optical pathlenghts cause deviations in fluorescence measurement due to overexposure. When red and green colour channels exhibit maximum intensities, the ratio of these channels is 1. For the sake of clarity, the inlets are not shown in B.

Conclusions

In conclusion, new pH-sensors have been presented that exclusively rely on fluorescent dyes and host polymers which are either commercially available or can be prepared from commercially available compounds in a single, simple reaction step. By properly selecting the sensor components, one can tune the sensitive pH-range of the material to cover a broad region (pH 5 - 12). This pH-region meets the requirements of a vast majority of pH-sensor applications. While sensors in the planar format are limited to short-time applications, sensitive nanobeads in Eudragit® RL100 polymer are most promising for practical applications in (micro)fluidic systems and even for fluorescence imaging and microscopy. By taking advantage of a ratiometric approach, good compatibility with a simple RGB camera for readout is accomplished.
Beyond the presented new pH-sensors, this work highlighted the usefulness of the tools employed for rational dye design. The phenolate proton receptors have been demonstrated to be very efficient quenchers operating via Photoinduced Electron Transfer and represent a promising alternative to the more commonly used amino-receptors. They can be used in combination with other fluorophores in order to match the requirements of a particular application considering spectral properties or indicator stability. The receptors have been attached by a simple concept, *i.e.* chlorosulfonation and subsequent reaction with amines. Following this concept, a variety of functionalities can be tagged to DPPs, making them suitable for probing analytes other than pH or targeting particular biomolecular structures.

Experimental

Materials and Methods

1,4-Diketo-3,6-diphenylpyrrolo[3,4-c]pyrrole (Irgazin Scarlet) was purchased from Kremer Pigmente (http://kremer-pigmente.de/en), Macrolex Fluorescent Yellow from Simon and Werner GmbH (www.simon-und-werner.de). 4-Amino-2-chlorophenol was from TCI Europe (www.tcichemicals.com), 4-amino-2,6-dichlorophenol from ABCR (www.abcr.de). Solvents used for work-up and purification (synthesis grade) as well as buffer salts were supplied by Carl Roth (www.roth.de). Deuterated solvents were obtained from Eurisotop (www.eurisotop.com), silica gel from Acros (www.fishersci.com). Polyurethane hydrogel D4® was from CardioTech (www.cardiotech-inc.com), poly(2-hydroxyethylmethacrylate) (MW = 150000 g / mol), from Polysciences Inc. (www.polysciences.com), Eudragit® RL100 from Evonik Industries (http://corporate.evonik.de). All other chemicals were form Sigma-Aldrich (www.sigmaaldrich.com). Poly(ethylene glycol terephthalate) support (Mylar®) was from Goodfellow (www.goodfellow.com).
NMR spectra were recorded on a 300 MHz instrument (Bruker) with TMS as a standard. MALDI-TOF mass spectra were taken on a Micromass TofSpec 2E in reflectron mode at an accelerating voltage of +20 kV. Absorption measurements were performed on a Cary 50 UV-VIS spectrophotometer from Varian (www.varianinc.com). Fluorescence spectra were recorded on a Hitachi F-7000 spectrofluorimeter (www.hitachi.com). Relative fluorescence quantum yields were determined at 25 °C using rhodamine 101 (Φ_F = 0.98 in ethanol [225]) as a standard. Photostability measurements were performed by irradiating the samples with the light of a 458

nm high-power LED array (10W input power, www.led-tech.de) focused through a lens purchased from Edmund optics. The photodegradation profiles were obtained by monitoring the absorption spectra.

pH-imaging was performed using a RGB-CCD camera (Marlin F201C, Allied Vision Technologies, http://www.stemmer-imaging.de) equipped with a Xenoplan 1.4/23 objective lens (http://www.schneiderkreuznach.com). For images taken on the fluorescence microscope (Zeiss Axiovert 25 CFL, http://corporate.zeiss.com), a blue ultrabright LED with emission maximum at λ = 450 nm (Luxeon lambert emitter, blue, 5 W) was applied as the excitation light source and combined with a filter set-up consisting of Linos DT blue/Linos DC blue/Schott OG 515 (LINOS Photonics, Göttingen, Germany; Schott, www.schott.com) as the excitation filter/dichromatic mirror/barrier filter, respectively. Image acquisition was performed with the software AVT SmartView (http://www.alliedvisiontec.com). Matlab R2008a (www.mathworks.com) was used for image processing. The color channels of the obtained images were separated and the ratiometric images were obtained by dividing the red by the green channel.

Microfluidic flow-through experiments were performed using a custom made flow cell or a 6 channel µ-Slide (ibidi µ-Slide VI $^{0.4}$, http://ibidi.com), which was connected to a syringe pump (model 540060, TSE systems, www.tse-systems.com).

The pH of the buffer solutions was controlled by a digital pH-meter (InoLab pH/ion, WTW GmbH & Co. KG, www.wtw.com) calibrated at 25 °C with standard buffers of pH 7.0 and 4.0. The buffers were adjusted to a constant ionic strength of 100 mM using sodium chloride as the background electrolyte.

Syntheses

*1,4-Diketo-3-((4-[N-(3,5-dichloro-4-hydroxyphenyl)amino]sulfonyl)phenyl)-6-phenylpyrrolo[3,4-c]pyrrole (**2**)*

1,4-Diketo-3,6-diphenylpyrrolo[3,4-c]pyrrole (500 mg, 1.73 mmol) was heated in chlorosulfuric acid (3 ml) to 60 °C. After 3 h, the mixture was allowed to cool to RT and was added dropwise onto ice cubes. The deep orange precipitate was filtered using a Büchner funnel, rinsed with cold H_2O (0 °C) until pH was neutral and dried by applying a rotary vane pump for 0.5 h. The obtained sulfonyl chloride was dissolved in dry *N,N*-dimethylformamide (30 ml) and 4-amino-2,6-dichlorophenol (1.25 g, 7.02 mmol, 4 equiv.) and triethylamine (1.94 ml, 13.9 mmol) were added. The mixture was stirred for 2.5 h at RT, then 1 M aqueous HCl (150 ml) was added. The precipitate was washed with water, dried and purified by column chromatography (silica gel, 40 – 63 µm) with ethyl acetate / chloroform 75 / 25 as eluent, yield 188 mg (21%). Mp.: Decomposition at > 260 °C. UV/VIS absorption: λ_{max}(tetrahydrofuran)/nm 246 (ε/dm^3 mol^{-1} cm^{-1} 37 000), 291 (32 100), 509 (22 300) and 543 (24 000). IR absorption: ν_{max}/cm^{-1} 3426 and 3320 (NH), 3222 (OH), 3030-3160 and 2800-2980 (CH), 1676, 1630 and 1595 (CO), 1555, 1488, 1395, 1331, 1283, 1219, 1156, 1088, 986, 893, 843, 811, 757, 726, 701, 645, 605, 552, 470. NMR (300 MHz, DMSO-*d6*, TMS): δ_H = 11.47 (1 H, s, Ar-H), 10.44 (1 H, s, ArOH), 10.11 (1 H, s, SO_2NH), 8.3 - 8.7 (2 H, br s, CONH), 8.33 (3 H, d, J = 8.4Hz, Ar-H), 8.26 (1 H, dd, J_1 = 7.7 Hz, J_2 = 1.1 Hz, Ar-H), 7.70 - 7.86 (4 H, m, Ar-H), 7.09 (2 H, s, Ar-H). δ_C = 175.67, 166.14 (C=O); 147.20, 146.29, 139.39, 139.02, 135.80, 133.54, 132.49, 131.34, 130.49, 130.16, 129.17, 127.65, 126.25, 124.73, 122.64, 120.99, 110.81, 100.35 (aromatic). MALDI-TOF: m/z [MH$^+$] 528.0190 found, 528.0188 calcd.

*1,4-Diketo-3-((4-[N-(3-chloro-4-hydroxyphenyl)amino]sulfonyl)phenyl)-6-phenylpyrrolo[3,4-c]pyrrole (**3**)*

3 was prepared according to the same procedure as **2**, 4-amino-2-chlorophenol (4 equiv.) was reacted with the sulfonyl chloride. Column chromatography was performed with ethyl acetate / ethanol / 25% aqueous NH_3 93 / 7 / 0.33 as eluent, yield 116 mg (14%). Mp.: Decomposition at > 270 °C. UV/VIS absorption: λ_{max}(tetrahydrofuran)/nm 245 (ε/dm³ mol^{-1} cm^{-1} 27 200), 291 (23 800), 508 (17 400) and 541 (18 600). ν_{max}/cm^{-1} 3407 and 3314 (NH), 3225 (OH), 3030-3160 and 2800-2980 (CH), 2360, 2339, 1677, 1635 and 1593 (CO), 1557, 1507, 1487, 1405, 1332, 1287, 1202, 1156, 1088, 1053, 953, 895, 843, 820, 757, 726, 701, 614, 597, 544, 496. NMR (300 MHz, DMSO-*d6*, TMS): δ_H = 11.45 (1 H, s, Ar-H), 10.10 (2 H, d, ArOH, SO_2NH), 8.3 - 8.7 (2 H, br s, CONH), 8.31 (3 H, dd, J_1 = 8.1 Hz, J_2 = 2.1 Hz, Ar-H), 8.26 (1 H, dd, J_1 = 7.7 Hz, J_2 = 1.4 Hz, Ar-H), 7.70 - 7.86 (4 H, m, Ar-H), 7.06 (1 H, d, J = 2.3 Hz, Ar-H), 6.89 (1 H, dd, J_1 = 8.7 Hz, J_2 = 2.4 Hz, Ar-H), 6.85 (1 H, d, J = 8.5 Hz, Ar-H). δ_C = 175.64, 166.15 (C=O); 150.50, 147.15, 139.79, 139.16, 135.81, 133.26, 132.46, 131.31, 130.48, 129.24, 128.99, 127.65, 126.67, 124.71, 123.23, 121.78, 119.54, 116.90, 110.75, 100.36 (aromatic). MALDI-TOF: m/z [MH$^+$] 494.0600 found, 494.0577 calcd.

*1,4-Diketo-3-((4-(1-morpholinyl)sulfonyl)phenyl)-6-phenylpyrrolo[3,4-c]pyrrole (**4**)*

1,4-Diketo-3,6-diphenylpyrrolo[3,4-c]pyrrole (300 mg, 1.04 mmol) was heated in chlorosulfuric acid (3 ml) to 60 °C. After 3 h, the mixture was allowed to cool to RT and added dropwise onto morpholine (10 ml). The deep red mixture was stirred for 10 min and H_2O (80 ml) was added. The precipitate formed was thoroughly washed with water, dried and purified by column chromatography (silica gel, 40 – 63 µm) with methanol / chloroform 95 / 5 as eluent, yield 170 mg (22 %). Mp. > 300 °C. UV/VIS absorption: λ_{max}(tetrahydrofuran)/nm 247 (ε/dm³ mol^{-1} cm^{-1} 28 000), 292 (27 900), 509 (20 000) and 541 (21 400). IR absorption: ν_{max}/cm^{-1} 3419 and 3309 (NH), 3030-3170 and 2780-2980 (CH), 2368, 2339, 1665, 1627 and 1597 (CO), 1554, 1486, 1449, 1436, 1340, 1325, 1284, 1260, 1161, 1114, 1095, 938, 839, 747, 701, 668, 612, 595, 536, 469. NMR (300 MHz, DMSO-d6, TMS): δ_H = 11.58 (1 H, s, Ar-H), 8.3 - 8.8 (2 H, CONH), 8.50 (2 H, d, J = 8.7 Hz, Ar-H), 8.36 (1 H, d, J = 7.8 Hz, Ar-H), 8.30 (1 H, dd, J_1 = 7.8 Hz, J_2 = 1.1 Hz, Ar-H), 7.85 (3 H, dt, J_1 = 8.4 Hz, J_2 = 1.9 Hz, Ar-H), 7.77 (1 H, t, J = 7.5 Hz, Ar-H), 3.67 (4 H, t, J = 4.2 Hz, OCH_2), 2.95 (4 H, t, J = 4.1 Hz, $ArNCH_2$). δ_C = 175.71, 166.19 (C=O); 147.27, 138.99, 135.81, 135.01, 133.76, 132.49, 131.34, 130.48, 129.15, 127.66, 127.26, 124.73, 110.90, 100.41 (aromatic); 65.29 (C-O); 45.92 (C-N). MALDI-TOF: m/z [MH+] 438.10 found, 438.11 calcd.

Preparation of planar sensors

A “cocktail” containing indicator dye (0.16 mg), hydrogel D4 / p(HEMA) (41 mg) and ethanol / water 9:1 (V/V) (500 µl) was knife-coated on a dust-free Mylar support to obtain a ≈ 7 µm thick layer after solvent evaporation. Ratiometric sensors were prepared in analogy, using 0.2 mg of **2**, 0.6 mg of Macrolex Yellow and tetrahydrofuran (461 µl) as a solvent.

Preparation of sensor nanoparticles

Eudragit RL100 (100 mg) was dissolved in acetone (50 ml), indicator dye (1 mg) and Macrolex yellow (1.25 mg) were added. Water (300 ml) was added quickly (5 s). Acetone was removed on a rotary evaporator and the particle suspension was concentrated to a volume of 50 ml.

Acknowledgement

Financial support from the Austrian Science Fund FWF (project P 21192-N17) is gratefully acknowledged. We thank Martin Thonhofer, Institute of Organic Chemistry, and Stefan Müller, Institute of Inorganic Chemistry, for their support in measuring melting points and IR spectra.

Supplementary Information

to *Fluorescent Materials for pH Sensing and Imaging Based on Novel 1,4-Diketopyrrolo-[3,4-c]pyrrole Dyes*

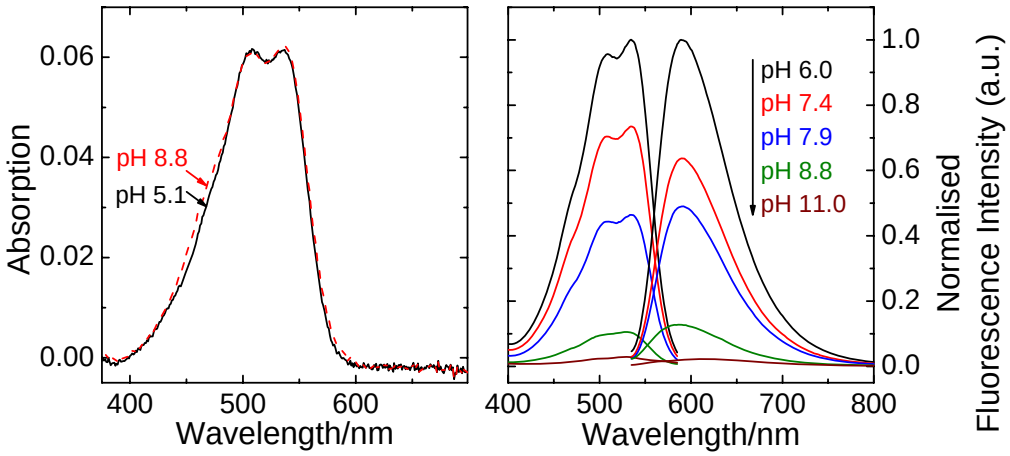

Figure 4-S1: pH-dependent absorption and fluorescence spectra of 3. Spectra were recorded in ethanol/aqueous buffer (ionic strength 100 mM) solution 1:1 (V/V). pH values are those of the aqueous buffer used. DPP concentration was 20 µM for absorption and 4 µM for fluorescence measurements.

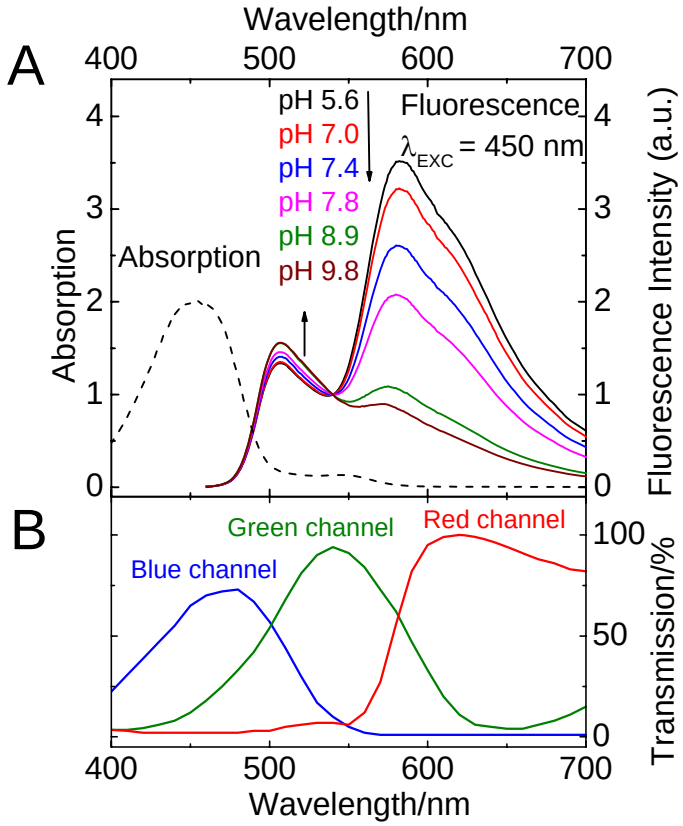

Figure 4-S2: A: pH-dependent fluorescence spectra a planar ratiometric sensor containing Macrolex Yellow (1.5% (w/w)) and DPP pH-indicator 2 (0.5% (w/w)). B: Spectral characteristics of the RGB CCD camera.

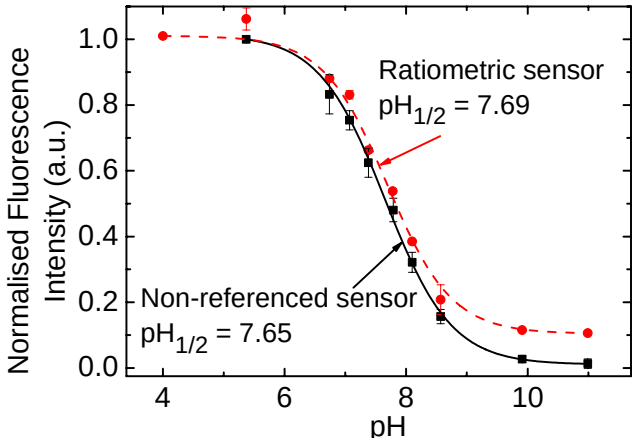

Figure 4-S3: pH calibration curve of the ratiometric sensor beads, *i.e.* dye 3 (1% w/w) and Macrolex Yellow (reference dye; 1.25% w/w) in RL100 (bead content 2 mg / ml in aqueous buffer of ionic strength 100 mM), compared to beads containing only 3 (0.5% w/w) – this non-referenced system is also included into figure 4-4 (main text).

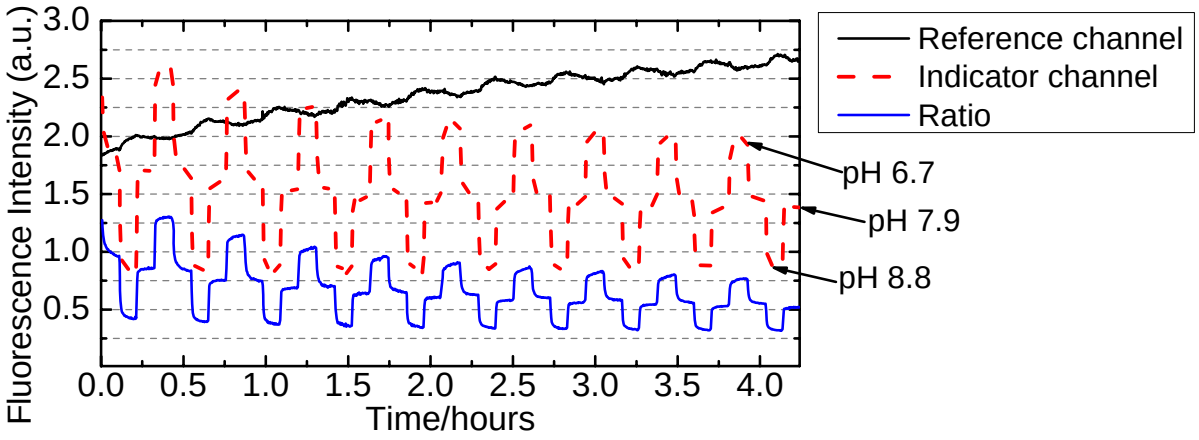

Figure 4-S4: Long-time performance of a planar ratiometric sensor containing Indicator 2 (0.5% w/w) and Macrolex Yellow (1.5% w/w) in D4 hydrogel, excited with a 450 nm LED (Roithner, www.roithner-laser.com) combined with a Schott BG 12 bandpass filter (350 - 465 nm). The reference channel was equipped with 520 / 40 nm bandpass filter, the indicator channel with a 600 / 50 nm bandpass filter (both from Edmund optics, www.edmundoptics.de). Both channels were equipped with separate PMT detectors, *i.e.* do not represent absolute brightness ratios. The planar sensor was placed in a home-made flow-through cell and 100 mM buffer was passed through the cell, flow rate 1ml / min. Cell temperature was kept constant at 25 °C. The sensors were interrogated with a two-phase lock-in amplifier (SR830, Stanford Research Inc., www.thinksrs.com) equipped with a PMT detector (H5701-02, Hamamatsu, www.sales.hamamatsu.com). Illumination time was 1% of the measurement time.

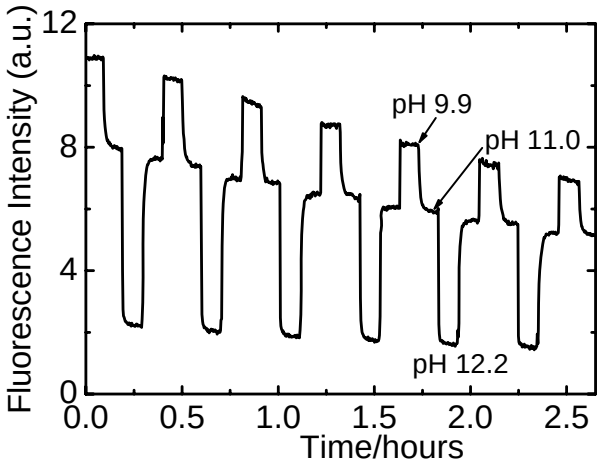

Figure 4-S5: Long-time performance of a planar sensor containing 4 (0.4% w/w) in D4 hydrogel, excited with a 525 nm LED combined with a 520 / 40 nm bandpass filter (Edmund Optics) and a Schott OG 550 nm longpass filter before the detector. Measurement was carried out as stated near figure 4-S4.

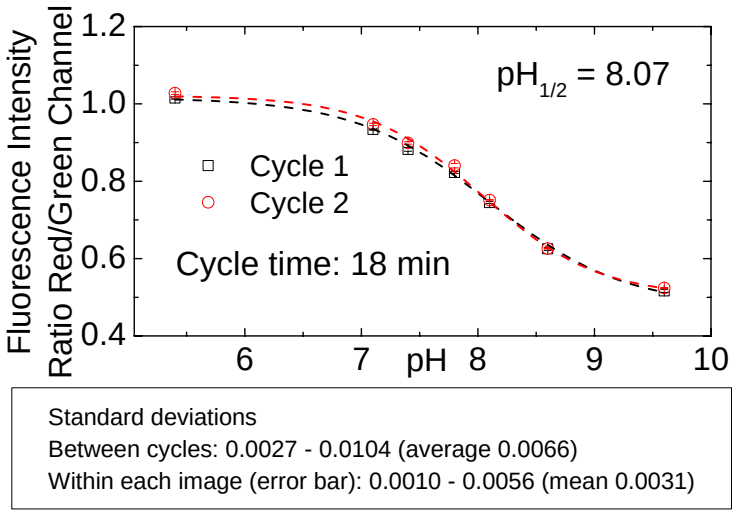

Figure 4-S6: -calibration curve of pH-nanosensor beads containing dye 3 (1% w/w) and Macrolex yellow (reference dye; 1.25% w/w) in RL100 polymer. The beads were read out under the fluorescence microscope employing a RGB-CCD camera. Response curve and images are shown in figure 4-7.

Chapter 5

Enhancing Photoinduced Electron Transfer Efficiency of fluorescent pH-probes with halogenated phenols

Preface to Chapter 5

In previous experiments, phenoxides proved highly flexible for tuning the sensitive range of optical pH-sensors and they turned out to quench some flurophores more effectively than amines. That was found not only for DPPs (chapter 4) but preliminary experiments also showed that 1-aminoPBIs and tetraphenoxy-PBIs are completely quechned by phenoxides but only partially quenched by amines located in the imide position. In this section is confirmed that phenoxides generally are more effective quenchers than the more frequently used amines and thus make a larger number of fluorophores accessible to pH-sensing. Fluorescent dyes with phenoxides and amines linked to the same fluorophore in a manner as similar as possible reveal more effective quenching by phenoxides in basic solution under defined conditions for fluoresceins, rhodamines, DPPs, tetraphenoxy-PBIs and 1-amino-PBIs. It is also confirmed that equal PET groups bring similar calibration curves even when linked to structurally very different fluorophores, indicating that assembling fluorophores and PET groups in a modular way is an effective, predictable method to obtain pH-probes with selectable spectral properties and sensitive pH-range. The PET groups are attached in the form of aminophenols which are compatible with many conjugation reactions and many of which are commercially available. A variety of simple reactions including coupling of activated carboxylic acids and sulfochlorides with amines is employed. Those reactions are typical for bioconjugation and fluorescent labelling and are easy to perform utilising bioconjugation “kits”. Consequently, a large number of tailor-made pH-probes is accessible by simple strategies which are convenient to perform and do not require a profound expertise in organic synthesis.

As electrochemical experiments reveal, the less positive oxidation potential of phenoxides compared to amines is probably not the sole reason for their higher effectiveness as quenchers, but kinetic aspects may play a significant role. Indeed, the low PET efficiencies of the 1-aminoperylene bisimdes and rhodamines carrying amines investigated in this chapter contrast the results in chapters 2 and 3 where very high efficiencies were found for the same fluorophores with amino groups attached in different positions.

In the majority of the cases where quenching by PET is partial, the basic form exhibits a shorter fluorescence decay time than the acidic one. Note that shorter decay times may not be observable if quenching is very effective as the fluorescent signal of the basic form is too weak and only residual fluorescence of the acidic form or background fluorescence is measurable.

Enhancing Photoinduced Electron Transfer Efficiency of Fluorescent pH-probes with Halogenated Phenols

This chapter has been prepared for publication in **Journal of the American Chemical Society**

Authors: **Daniel Aigner, Stefan A Freunberger, Robert Saf, Sergey M Borisov and Ingo Klimant**

Photoinduced electron transfer (PET), which causes pH- and environment-dependent quenching of fluorescent dyes, is more effectively introduced by phenoxide groups than by amino groups which have been much more commonly used so far. That is demonstrated in fluorescence and electrochemical measurements involving several classes of fluorophores. Consequently, the attachment of phenolic groups allows for fast and simple preparation of a wide selection of fluorescent pH-probes with tailor-made spectral properties, sensitive ranges and individual advantages, so that the needs of a large number of applications can be met. Fluorophores carrying phenolic groups may also be used for sensing analytes other than pH or molecular switching and signalling.

Introduction

Rational dye design is a key issue in molecular recognition, (super)molecular signalling and optoelectronics. “Modules” capable of a certain function such as interacting with an analyte [1] (pH, cations, carbon dioxide, glucose or complex biomolecules like proteins), molecular switching [256-258] or charge generation [259,260] are attached to or integrated into a chromophore. Photoinduced electron transfer (PET) [57,60,61] is a process that can enable all of these processes. A functional group capable of PET undergoes a redox process involving the excited state (but not ground state) of a chromophore. In fluorescent dyes, this results in fluorescence quenching as the process is quickly reversible. The charge separation implied is thus short-lived but can be taken advantage of in photovoltaics.

In this work, we focus on fluorescent dyes suitable for sensing pH (“probes”). We also aim on providing insights into the PET process in general which may be helpful for the design of dyes and materials applying PET for other purposes. PET-based fluorescent probes and sensors have been presented mostly for recognising ions [26,96,261-263], but also for measuring pH [41,55,59,83,189]. Those probes and sensors are of great potential for application in diagnostics, life sciences, environmental analytics or industrial process control. In most PET-based probes, fluorescence quenching is caused by an alkylamino group. Upon protonation of the amine or interaction with a cation, PET is impeded or prevented, which results in fluorescence enhancement. Consequently, there is a pH-response affiliated with the deprotonation of the phenolic form, thus characterised by the corresponding pK_A value, with a usual sensitive pH-range of $pK_A \pm 1.5$. Phenoxide groups can act in the exactly same way, as was first demonstrated by Gareis et al. by means of a phenol-modified boron-dipyrromethene (BODIPY) dye [66]. Yet, only a few examples of pH-probes carrying phenolic PET groups have been presented so far, most of which are BODIPY dyes [67,76,232,264,265]. Notably, dyes with phenolic groups fully

integrated into the chromophore are not commonly considered true PET probes since the redox properties of the chromophore itself are pH-dependent, even though PET may play a significant role in some [73,142].

Here we present, for the first time, a systematic comparison between fluorescent pH-probes carrying phenoxide PET groups and those bearing amines. We show, on the basis of various fluorophores, that halogenated phenoxide groups are generally more effective quenchers than amines, and they make up a great basis for designing fluorescent probes. Because many phenol derivatives are commercially available and they can be attached to numerous dyes by simple reactions, probes with tailored properties are available in a convenient way. Their spectral properties, sensitive ranges and stabilities can be selected to meet the variable and demanding requirements of life sciences and diagnostics.

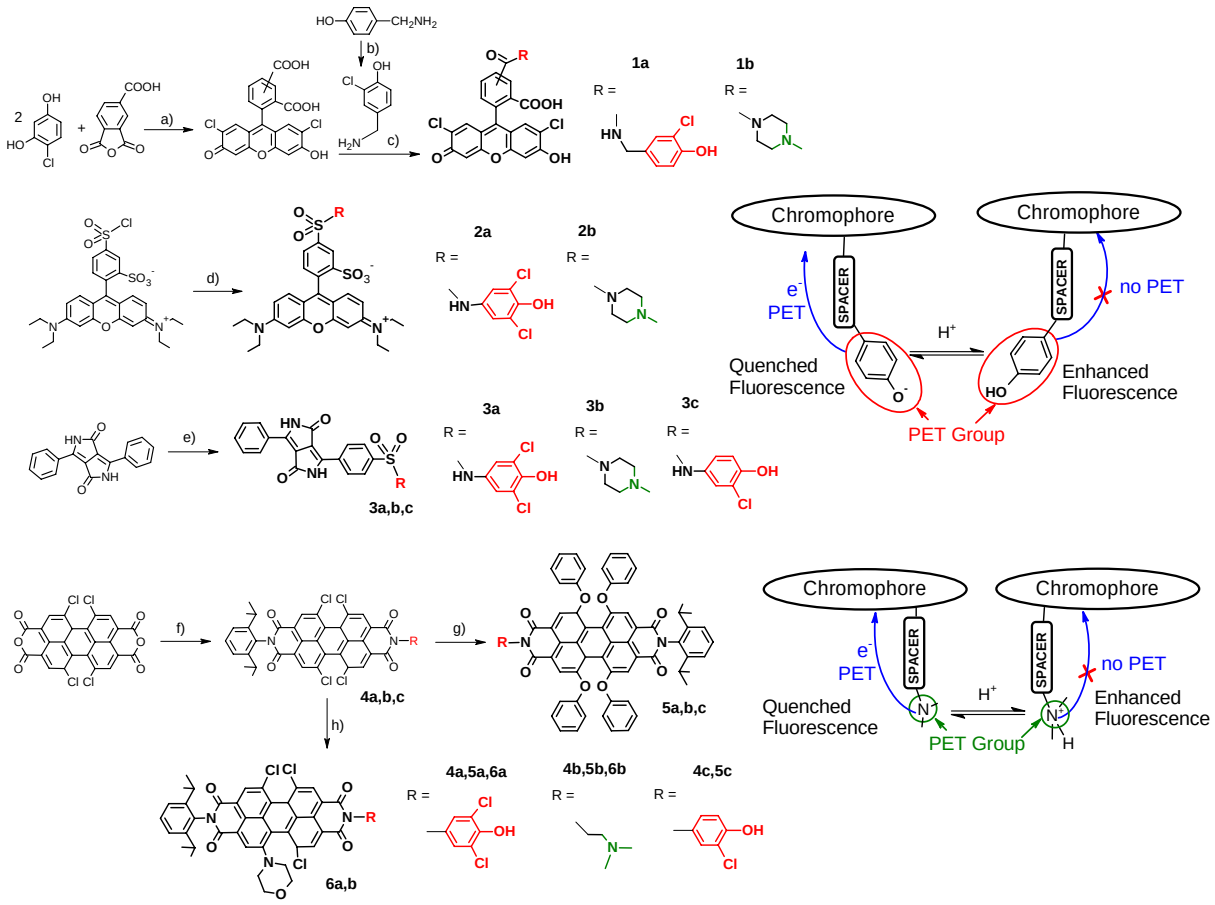

Figure 5-1: Structures and preparation of 1-6 and working principle of photoinduced electron transfer (PET). Synthetic conditions: a) CH_3SO_3H, 145°C, 1 h; b) SO_2Cl_2, RT, 2 h; c) EDC, NHS, DMF, RT, 1.5 h; R, Et(*i*Pr)$_2$N, 4 h; d) R, Et_3N, DMF, 16 h, 0 – 25°C; e) $ClSO_3H$, 60°C, 3 h; R; f) RNH_2, 2,6-diisopropylaniline, 1-methyl-2-pyrrolidone ("NMP"), C_2H_5COOH, 110°C, 22 h; g) PhOH, K_2CO_3, NMP, 110°C, 3.5 – 22 h; h) Morpholine, NMP, 40 °C, 2 h.

Results and Discussion

Several dye classes with very different spectral (figure 5-1, table 5-1) and chemical properties have been selected for this work, including xanthenes (fluoresceins and sulforhodamines), diketopyrrolo-[3,4-c]pyrroles (DPPs) and perylene bisimides (PBIs). To introduce PET, both halogenated (*o*-chloro and *o,o*-dichloro) phenols and tertiarty amines have been attached. Both groups are capable of introducing pH-sensitivity, as PET is prevented upon protonation. Fluorescence pH-calibration has therefore been selected as the primary evaluation method of the PET process. Calibration was carried out in mixtures of ethanol and aqueous buffer (1/1 (V/V)), to provide sufficient solubility for all the investigated dyes which include both water soluble and highly hydrophobic structures. To further suppress any potential aggregation and other effects perturbing the fluorescence measurement (dimerisation, self-quenching), calibration was performed in highly dilute ($6 \cdot 10^{-8}$ - $2 \cdot 10^{-6}$ M) solution. For all dyes, no or very little (≤ 3 nm) effect of buffer pH on maxima and shape of both absorption and fluorescence spectra was found which emphasises the absence of major pH-dependent effects other than PET. Only data measured in acidic solution is thus stated in table 5-1.

Table 5-1: Absorption and fluorescence maxima and individual advantages of the presented dyes in ethanol/water mixture, (5 – 10 mM buffer pH 4.0 added, pH 6.4 for 1A and 1B). Dye concentration was 2 – 20 μM for absorption, 0.05 – 2 μM for fluorescence measurement.

Dye	λmax abs (ε 10^{-4}) / nm ($M^{-1} \cdot cm^{-1}$) ($EtOH/H_2O$ 1:1 (V/V))	λ_{max} fluo / nm ($EtOH/H_2O$ 1:1 (V/V))	Individual advantages
1A	513 (8.58)	534	Very bright; two sensitive ranges
1B	514 (9.07)	535	Very bright
2A	564 (9.84)	589	Very bright
2B	567 (9.13)	590	
3A	502 (1.82), 533 (1.84)	591	Well suited for fluorescence imaging[266]
3B	505 (1.66), 535 (1.71)	594	
3C	504 (1.79), 533 (1.81)	589	Well suited fluorescence imaging[266]
5A	447 (1.44), 541 (2.80), 578 (4.24)	620	Outstanding photostability
5B	451 (1.30), 541 (2.77), 578 (4.19)	620	Outstanding photostability[267]
5C	452 (1.21), 543 (3.08), 578 (4.66)	620	Outstanding photostability
6A	461 (1.60), 662 (1.74)	756	Near infra-red emission
6B	449 (1.77), 658 (1.85)	761	Near infra-red emission[268]

Quenching caused by PET at basic pH was significantly stronger for the dyes carrying phenolic groups (dyes 1-6 a,c) than for those bearing amines (dyes 1-6 b) (figure 5-2, table 5-2). Indeed, quenching was almost complete for DPPs 3a and 3c and PBIs 5a, 5c and 6a, while it was partial for 5b and absent for 3b and 6b. In the case of xanthenes, partial quenching by phenoxide groups but no quenching by amino groups was found. Note that, even though PET is often associated with on-off fluorescence quenching [60], partial quenching by PET is not uncommon for certain systems in certain environments [267-269]. For tetrachloro-PBIs (such as 4a-c, which are

intermediates for the preparation of 5a-c), we had previously found strong quenching by amines [270].

All pH-probes are synthetically easily accessible, xanthene and DPP dyes via a single step, PBIs via two simple steps. In particular, the xanthene based-probes were prepared from commercially available dyes (Lissamine rhodamine B and 5(6)-carboxy-2',7'-dichlorofluorescein NHS ester). These and many other dyes, which have been designed to perform bioconjugation, are widely commercially available and easy to handle as "kits". In this way, pH-probes with selectable spectral properties are easily accessible also to the synthetically inexperienced user. This work clearly emphasises that phenoxide PET groups are better suited for creating a selection of new pH-probes since they can be combined with significantly more fluorophores to yield PET-based probes. The phenol-based probes presented here cover a wide range (excitable at 400 – 660 nm, emissive at 500 – 750 nm) of the visible spectrum. They feature individual advantages so that many applications can be addressed with them. For example, the xanthenes 1A and 2A are very bright and compatible with light sources and filters widely used in fluorescence microscopy. Both feature sensitivity at near-neutral pH while good photostability can be expected for rhodamines and dichlorofluoresceins, in contrast to non-chlorinated fluoresceins. 1A is an example for a probe featuring two sensitive ranges and can therefore be applied for measuring both near-neutral and acidic pH. Advantages of 3A,C, 5A,C and 6A have been discussed in previous publications, as listed in table 5-1.

Furthermore, since many aminophenols with different substitution patterns are commercially available, it is possible to select the pK_A value of the resulting pH-probe and thus its sensitive range. For instance, the di- and monochlorinated phenolic groups presented here are useful for slightly acidic and neutral to slightly basic values, respectively. The similar pK_A values for fluorophores featuring very different structure and hydrophilicity underline that the sensitive range can be selected beforehand depending on the application.

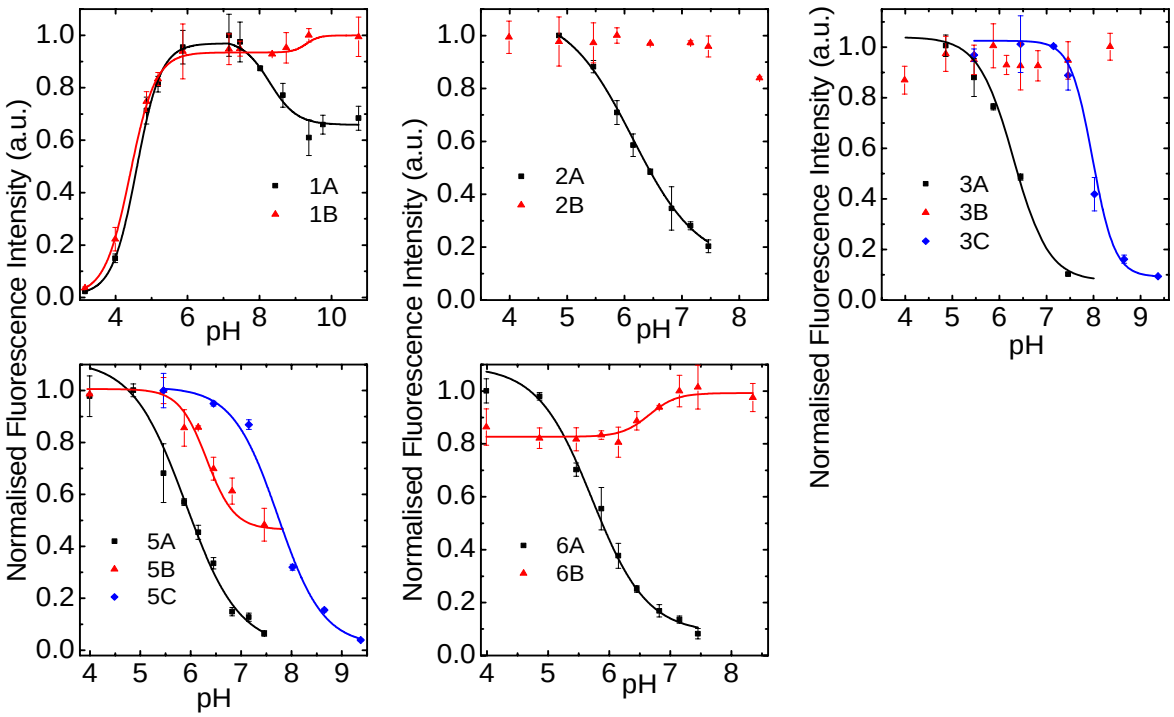

Figure 5-2: Fluorescence pH-calibration curves of fluorescent dyes ($6 \cdot 10^{-8}$ M in ethanol / aqueous buffer (ionic strength 100 mM) 1/1 (V/V)) modified with phenoxide (1-6 a,c) and amine (1-6 b) PET groups.

However, probes carrying phenolic groups are not limited to pH-sensing, but also potentially useful for measuring carbon dioxide and ions – since the sensitivity in most optical carbon dioxide probes is affiliated with the protonation of a phenoxide group [23,271] and PET-based indicators (mostly based on amines, so far) have been widely applied for optical sensing of metal cations [26,95,96,272].

Because PET is a quenching process, we expected that dyes undergoing PET may feature shorter fluorescence decay times than their acidic forms which are not affected by PET. While decay times are not expected to be pH-dependent in the case of complete quenching since the decay time of the basic form is not measureable, we anticipated that a shorter decay time should be detectable for dyes undergoing partial quenching. In fact, we found shorter decay times for 1B and 5B, indicating that PET is a quenching process that diminishes both fluorescence intensity and decay time. For 2B, a biexponential decay curve was found in basic solution and a diminishment in decay time could not be verified, indicating that in this case, there may be more than just two species contributing to the decay times. Still, pH-probes undergoing partial quenching by PET are potentially very useful for quantitative pH measurement and imaging as they enable decay time readout and do not require further referencing. Indeed, we have very recently applied that concept for live cell pH-imaging [267].

Table 5-2: pH-sensitive of the presented dyes: Φ_F – fluorescence quantum yield; τ – fluorescence decay time. Acidic/basic: pH of the buffer added to the ethanol/water mixture (buffer concentration 5 – 10 mM, ionic strength 50 mM); acidic – pH 4.0, basic – pH 9.4 (for 1A and 1B pH 6.4 and 11.7, respectively). In organic solvents, acidic solutions contain trifluoroacetic acid, basic ones ethyldiisopropylamine (0.1% (V/V) each). Dye concentration was 2 μM for 6a and 6b, 0.05 – 0.3 μM for all other dyes. n.m. – not measureable.

Dye	Φ_F ($EtOH/H_2O$ 1:1 (V/V))				Φ_F (CH_2Cl_2)		τ / ns ($EtOH/H_2O$ 1:1 (V/V))	
	Acidic	Basic	Ratio	pK_A	Acidic	Basic	Acidic	Basic
1A	0.72	0.48	1.50	4.6[a]; 8.3			3.9	2.2
1B	0.79	0.85	0.93	4.4[a]			3.9	3.9
2A	0.4	0.084	4.76	6.2			2.2	2.9; 0.6[d]
2B	0.37	0.35	1.06	--			2.0	2.2
3A	0.18	< 0.01	> 20	6.3	0.7[c]	< 0.01[c]	5.5	n.m.
3B	0.29	0.33	0.88	--	--	--	6.0	6.2
3C	0.26	< 0.01	> 20	8.0	0.66[c]	< 0.01[c]	3.4	n.m.
5A	0.16	< 0.01	> 20	5.9	0.99	0.025	5.4	n.m.
5B	0.38	0.18	2.11	6.3	0.9	0.16	5.8	2.8
5C	0.56	< 0.01	>50	7.7	--	--	4.6	n.m.
6A	0.052	< 0.01	> 20	5.8	0.17	0.038	1.1	n.m.
6B	0.043	0.051	0.84	(6.7)[b]	0.24	0.0055	1.6	1.5

[a] Intrinsic pH-sensitivity of the fluorescein derivative, not related to PET
[b] Slight enhancement of fluorescence at basic pH, not related to PET
[c] In tetrahydrofuran, according to [35]
[d] Biexponential fit was required, with 79% abundance for 2.9 ns

The thermodynamic driving force of the PET process, $-\Delta G_{Q,PET,}$ is given by Weller's equation: [57]

$$\Delta G_{Q,PET} = E_{Ox,Rec} - E_{Red,Flu} - \Delta E_{Exc,Flu} - E_{IP}$$

Where $E_{Ox,Rec}$ is the first oxidation potential of the PET group (receptor), $E_{Red,Flu}$ the first reduction potential of fluorophore, $\Delta E_{Exc,Flu}$ the singlet excitation energy of the fluorophore and E_{IP} the ion pairing energy. Consequently, a high rate for PET, resulting in effective quenching, will be observed if the PET group is easily oxidised, the fluorophore is easily reduced and the fluorophore is absorptive at short wavelengths [59,61,62]. PET is also more favourable in polar solvents [72]. Though kinetic aspects can play a significant role - in particular, PET becomes less effective with decreasing distance between fluorophore and PET group, and an adverse nature and orientation of molecular orbitals may inhibit the process [65,70,71] - these thermodynamic considerations generally enable a valuable estimation whether a PET process will take place.
We therefore measured the redox potentials of fluorophores and PET groups to determine $-\Delta G_{Q,PET}$ (table 5-3). Model compounds for fluorophore and PET group were used in some cases, as listed in table 5-3 and disussed in the following.

Table 5-3: Redox properties and calculation of PET driving force using model compounds. $\Delta E_{Exc,Flu}$ (singlet excitation energy) is calculated from the fluorescence spectra measured as stated for table 5-2. Redox potentials of the model compounds $\Delta U_{Ox,Rec}$ and $\Delta U_{Red,Flu}$ were determined from cyclic voltammograms (displayed in the appendix) measured in ethanol/water containing K_2CO_3 (5% w/w), except for DPP-MonoSA and 5A-C which were measured in tetrahydrofuran/water 9:1 (V/V) containing K_2CO_3 (0.2% w/w). (i) denotes irreversible reaction.

Dye	$\Delta E_{Exc,Flu}$ / eV	Model Fluorophore	$\Delta U_{Red,Fl}$ / V	Model PET Group	$\Delta U_{Ox,Rec}$ / V	$\Delta G_{Q,PET}$ / eV
1A	2.37	2,7-Dichlorofluorescein	-1.16	5C	0.64 (i)	-0.67
1B	2.37	2,7-Dichlorofluorescein	-1.19	Triethylamine	1.03	-0.25
2A	2.15	Sulforhodamine B	-0.99	5A	0.71 (i)	-0.55
2B	2.15	Sulforhodamine B	-0.99	Triethylamine	1.03	-0.23
3A	2.21	DPP-MonoSA[a]	-0.79 (i)	5A	0.71 (i)	-0.81
3B	2.21	DPP-MonoSA[a]	-0.79 (i)	Triethylamine	1.03	-0.48
3C	2.21	DPP-MonoSA[a]	-0.79 (i)	5C	0.64 (i)	-0.87
4A	2.29	Cl-DAPBI[b]	-0.21	5A	0.71 (i)	-1.47
4B	2.29	Cl-DAPBI[b]	-0.21	Triethylamine	1.03	-1.15
4C	2.29	Cl-DAPBI[b]	-0.21	5C	0.64 (i)	-1.54
5A	2.07	5A	-0.55	5A	0.71 (i)	-0.91
5B	2.07	5B	-0.55	Triethylamine	1.03	-0.59
5C	2.07	5C	-0.55	5C	0.64 (i)	-0.98
6A	1.75	MOP3Cl-DAPBI[c]	-0.37	5A	0.71 (i)	-0.77
6B	1.75	MOP3Cl-DAPBI[c]	-0.37	Triethylamine	1.03	-0.45

a) 1,4-Diketo-3-((4-[N-(2-ethylhexyl)amino]sulfonyl)phenyl)-6-phenylpyrrolo[3,4-c]pyrrole

b) 1,6,7,12-Tetrachloro-N,N'-di(2,6-diisopropylphenyl)perylene-3,4:9,10-tertracarboxylic bisimide

c) 1-(4-Morpholinyl-6,7,12-trichloro-N,N'-di(2,6-diisopropylphenyl)perylene-3,4:9,10-tertracarboxylic bisimide

In accordance to the method used by DeSilva and co-workers [59], model compounds available at low cost and with presumably very similar photo- and electrochemical properties were measured for most fluorophores. The redox potentials of the PET groups may be estimated measuring those

of amines and chlorophenoxide or *p*-aminochloropphenoxide ions. However, since in most of the obtained indicators the PET groups are located closely to electron-withdrawing groups (imide, sulfonamide, carboxamide), we decided to use 5A-C as model compounds. The oxidation potential found for the basic form of 5A (0.708 V) is indeed higher than the one of 2,6-dichlorophenol (0.56 V, irreversible oxidation) and significantly higher than the one of 4-amino-2,6-dichlorophenol (-0.09 V, reversible oxidation). Using 5A – in which the phenoxide group is substituted by a strongly electron-withdrawing imide group - as model compound should prevent an overestimation of $-\Delta G_{Q,PET}$ since the other phenoxide groups are not expected to feature significantly lower electron densities. In 5B, the oxidation potential cannot be reliably determined due to background oxidation. The literature value for triethylamine [59] was used instead. The true oxidation potantials of the indicators may be slightly higher due to the presence of β-nitrogen atoms carrying electron-withdrawing substituents. Singlet excitation energies were calculated form fluorescence spectra as outlined by Ford et al [273]. For the ion pairing energy, the value 0.1 can be assumed [59,274]

For all indicators, PET has been estimated to be thermodynamically favourable, even for the amines 1-3B and 6B in which no PET was experimentally found. The use of triethylamine as model compound may cause an overestimation of $-\Delta G_{Q,PET}$. However, in order to inverse thermodynamic favourability for PET in all indicators, the true oxidation potentials of the amines should be as high as ≈ 1.5 V (almost 0.5 V higher than for triethylamine), which seems highly impropable considering that the amines only differ by a β-amino substituent. Conqequently, even though the smaller thermodynamic driving force for PET may play a role in the much lower efficiency of the PET process observed with amines, it does not seem convincing as the sole explanation. Kinetic aspects may play an additional role and indeed, we had previously found highly effective PET both for rhodamines [275] and 1-aminoperylene bisimides [268] carrying amino groups in different positions than those investigated in this work. Thus we present here another example for how the PET process can be influenced by structural parameters. Effective PET requires certain proximity between the HOMO of the donor and the LUMO of the acceptor which may be easier to realise with phenoxide systems. Note that amino groups usually require a minimum spacer length of two atoms if attached by the easy-to-use techniques presented in this work. A single-carbon spacer would results in aminal structures which are unstable.

Conclusion

In conclusion, we have demonstrated that employing phenolic groups causing photoinduced electron transfer (PET), pH-probes derived from a wide range of fluorophores can be created, featuring selectable sensitive pH-ranges, spectral properties and individual advantages that can be selected to meet the requirements of many particular applications. In particular, phenoxide PET groups allow much higher flexibility than the much more commonly used amines as they can quench many fluorophores at basic pH which are not quenched by amines. The probes are accessible via simple reactions similar to those common in bioconjugation chemistry, which makes the concept applicable for a wide research field, without requiring a profound expertise in synthetic organic chemistry. Fluorophores carrying phenolic PET groups are not limited to pH-sensing, but can be applied for the numerous other application possibilities affiliated with PET such as ion sensing, molecular switching and signaling or organic electronics.

Experimental

Materials and Methods

1,6,7,12-Tetrachloroperylene-3,4:9,10-tetracarboxylic bisanhydride was purchased from Beijing Wenhaiyang Industry and Traiding Co.Ltd (http://china.zhaoteng.com), 1,4-diketo-3,6-diphenylpyrrolo[3,4-c]pyrrole (Irgazin Scarlet) from Kremer Pigmente (http://kremer-pigmente.de/en). The preparation of Cl-DAPBI and DPP-MonoSA is published elsewhere [24,270]. MOP3Cl-DAPBI was prepared according to a procedure described previously [268]. 1-Methyl-2-pyrrolidone was from ABCR (www.abcr.de), chlorophenols from TCI Europe (www.tcichemicals.com). Deuterated solvents were obtained form Eurisotop (www.eurisotop.com), silica gel from Acros (www.fishersci.com), solvents used for column chromatography from VWR (www.vwr.at). Inorganic salts were supplied by Carl Roth (www.roth.de). All other chemicals were from Sigma-Aldrich (www.sigmaaldrich.com).
Absorption measurements were performed on a Cary 50 UV-VIS spectrophotometer from Varian (www.varianinc.com). Fluorescence spectra were recorded on a Fluorolog3 spectrofluorimetre (www.horiba.com) equipped with a NanoLED 455 nm laser diode and controller for decay time measurement. Decay curves were subjected to monoexponential fit using DAS6 software supplied by the manufacturer. Relative fluorescence quantum yields were determined using rhodamine 101, rhodamine B and Nile Red as standards (quantum yields 0.96, 0.65 [225] and 0.27 [197] in ethanol, respectively). NMR spectra were recorded on a 300MHz instrument (Bruker) in $CDCl_3$ with TMS as a standard. MALDI-TOF mass spectra were recorded on a Micromass TofSpec 2E. The spectra were taken in reflectron mode at an accelerating voltage of +20 kV.
The pH of the buffer solutions (phosphate, acetate, TRIS) was controlled by a digital pH meter (Seven Easy, Mettler Toledo, www.mt.com) calibrated at 25 °C with standard buffers of pH 7.0 and 4.0 (WTW GmbH & Co. KG, www.wtw.com). The buffers were adjusted to constant ionic strength using sodium chloride as the background electrolyte.
Electrochemical measurements were performed using a VMP3 electrochemical workstation (Biologic) and a multi-necked, air-tight glass cell. The measurements were carried out at room temperature. A 1 mm diameter glassy carbon disk (BAS Inc.) was employed as the working electrodes. Prior to use the working electrode was polished with 0.05 μm alumina slurry in water and rinsed with copious amounts of water and ethanol followed by drying. A platinum wire served as the counter electrode. Measurements were performed using a Ag/AgCl reference electrode (BAS Inc.). Electrolytes were saturated with Ar prior to the measurements. $E_{1/2}$ was determined from the peak potentials for quasi-reversible processes. For irreversible processes the $E_{1/2}$ was estimated from the half peak potential Ep/2 via E½ = Ep/2 -1.09 RT/nF [276].

3-Chloro-4-hydroxybenzylamine
4-Hydroxybenzylamine (300 mg, 2.44 mmol) was dissolved in a mixture of 1M hydrochloric acid in acetic acid (5 ml) and *N,N*-dimethylformaide (0.5 ml). Sulfuryl chloride (414 μl, 5.12 mmol) was added and the precipitate formed upon stirring (RT, 2 h) was separated by centrifugation, washed with acetic acid and methylene chloride and left to dry. The product (containing ≈ 6 % impurity) was used without further purification, yield 264 mg (69 %). ^{1}H NMR (300 MHz, CD_3OD, TMS): δ = 7.44 (d, 1H, J = 1.9 Hz, H(1)); 7.22 (dd, 1H, J_1 = 8.3 Hz, J_2 = 1.8 Hz, H(2); 6.97 (d, 1H, J = 8.4 Hz, H(1); 4.00 (s, 2H, H(4)).

5(6)-Carboxy-2',7'-dichlorofluorescein
Trimellitic anhydride (1g, 5.21 mmol) and 4-chlororesorcinol (1.51g, 10.4 mmol) were stirred in methanesulfonic acid (25 ml) at 145°C for 1 h. The mixture was allowed to cool to RT and water (400 ml) was added. The crude product was washed thoroughly with water (1.5 l), dried and used without further purification, yield 2.36 g (98 %).

*5(6)-(3-Chloro-4-hydroxy-benzylaminocarboxy)-2',7'-dichlorofluorescein (**1a**)*
(5,6)-Carboxy-2',7'-dichlorofluorescein (350 mg, 0.62 mmol), 1-ethyl-3-(3-dimethylaminopropyl)carbodiimide hydrochloride (166 mg, 0.87 mmol) and *N*-hydroxysuccinimide (100 mg, 0.87 mmol) were stirred in dry *N,N*-dimethylformamide (5 ml) for 1.5 h at RT. To the solution of NHS ester obtained were added 3-chloro-4-hydroxybenzylamine (205 mg, 1.30 mmol) and ethyldiisoproylamine (301 µl, 1.73 mmol)). After 4 h, the crude product was precipitated and washed with water, dried and purified by column chromatography (silica gel, 40 – 63 µm) with methylene chloride / methanol / acetic acid 98 / 2 / 0.25 as eluent. Eluate containing product was concentrated to 5 ml, precipitated and washed with water, drying yielded 211 mg (46 %). ^{1}H NMR (300 MHz, CD_3OD containing 0.02 M NH_3, TMS): δ = 8.49 (d, 0.5H, J = 1.3 Hz, H(5a)); 8.01 – 8.15 (m, 1.5H, H(4a,4b,5b)); 7.69 (d, 0.5H, J = 1.0 Hz, H(3b)); 7.33 – 7.39 (m, 1H, H(3a,7)); 7.30 (d, 0.5H, J = 1.8 Hz, H(7)); 7.16 – 7.22 (dd, 0.5H, J_1 = 8.2 Hz, J_2 = 2.0 Hz, H(9)); 7.11 (d, 2.5H, J = 1.6 Hz, H(2,9)); 6.82 – 6.93 (dd, 1H, J_1 = 8.3 Hz, J_2 = 14.2 Hz, H(8)); 6.60 (s, 2H, H(1)); 4.43 – 4.56 (d, 2H, H(6)). MALDI-TOF: m/z [MH^+] 584.0069 found, 584.0071 calcd.

*5(6)-(4-Methyl-1-piperazinylcarboxy)-2',7'-dichlorofluorescein (**1b**)*
After preparing the NHS ester as described for **1a**, *N*-methylpiperazine (175 µl, 1.58 mmol) and ethyldiisoproylamine (301 µl, 1.73 mmol)) were added and the mixture was stirred for 4 h. Repeated washing with n-hexane afforded an oily residue which was purified by column chromatography with methylene chloride / methanol / concentrated aqueous HCl 85 / 15 / 0.375 as eluent, yield 163 mg (39 %). ^{1}H NMR (300 MHz, CD_3OD containing 0.02 M NH_3, TMS): δ = 8.09 – 8.17 (s + d, 1H, H(5a,5b); 7.65 (dd, 1H, J_1 = 7.8 Hz, J_2 = 1.1 Hz, H(4a,4b)); 7.27 – 7.39 (2d, 1H, J_1 = 7.7 Hz, J_2 = 1.2 Hz, H(3a,3b)); 7.10 – 7.19 (2s, 2H, H(2)); 6.59 (s, 2H, H(1)); 7.10 – 7.19 (2s, 2H, H(2)); 3.5 – 3.9 (m, 4H, H(6)); 2.44 – 3.64 (m, 4H, H(7)); 2.28 – 2.39 (2s, 3H, H(8)). MALDI-TOF: m/z [MH^+] 527.0756 found, 527.0776 calcd.

*Sulforhodamine B-4'-(N-(3,5-dichloro-4-hydroxyphenyl))sulfonamide (**2a**)*
4-Amino-2,6-dichlorophenol (17 mg, 0.096 mmol) and triethylamine (13.8 µl, 0.010 mmol) were dissolved in anhydrous *N,N*-dimethylformamide (0.3 ml), the mixture was cooled to 0°C and lissamine rhodamine B (50 mg, 0.087 mmol) was added. After stirring for 4h at 0°C and 12h at RT, the solvent was removed by repeated washing with n-hexane. The sticky crude product was purified by column chromatography with methylene chloride / methanol 96 / 4 1 as eluent, yield 28 mg (45 %). ^{1}H NMR (300 MHz, $(CD_3)_2SO$, TMS): δ = 10.43 (1H, s, H(9)); 10.20 (1H, s, H(8)); 8.43 (1H, d, J = 1.7 Hz, H(4)); 7.72 (1H, dd, J_1 = 8.0 Hz, J_2 = 1.8 Hz, H(5)); 7.43 (2H, d, J = 7.9 Hz, H(6)); 7.06 (2H, s, H(7)); 6.98 (2H, dd, J_1 = 9.5 Hz, J_2 = 1.8 Hz , H(2)); 6.93 (2H, d, J = 1.9 Hz, H(3)); 6.84 (2H, d, J = 9.3 Hz , H(1)); 3.63 (8H, q, J = 7.1 Hz , H(10)); 1.20 (12H, t, J = 6.9 Hz , H(11)). MALDI-TOF: m/z [MNa^+] 740.1034 found, 740.1035 calcd.

*Sulforhodamine B-4'-(N-(3-azapentane-1,5-diyl))sulfonamide (**2b**)*
N-Methylpiperazine (21.2 µl, 0.19 mmol) was dissolved in anhydrous *N,N*-dimethylformamide (0.3 ml), lissamine rhodamine B (50 mg, 0.087 mmol) was added. Reaction and work-up were carried out as described for **2a**. Column chromatography was performed used with methylene chloride / methanol / 25% aqueous ammonia 94.5 / 5 / 0.5 as eluent, yield 23 mg (41 %). ^{1}H NMR (300 MHz, D_2O, 0.1% HCl conc., TMS): δ = 8.49 (1H, d, J = 1.5 Hz, H(4)); 8.14 (1H, broad d, J = 7.8 Hz, H(5)); 7.57 (1H, d, J = 7.6 Hz, H(6)); 6.95 (2H, d, J = 9.7 Hz, H(1)); 6.92 (2H, dd, J_1 = 10.0 Hz, J_2 = 1.2 Hz , H(2)); 6.84 (2H, d, J = 1.1 Hz, H(3)); 4.03 (2H, d, J = 12.6 Hz, H(7)); 3.64 – 3.73 (2H, d, J = 12.3 Hz, H(7)); 3.53 – 3.64 (8H, q, J = 7.1 Hz, H(10)); 3.33 (3H, d, J = 12.6 Hz, H(8)); 2.92 – 3.06 (5H, m, H(8,9)); 1.24 (12H, 7, J = 6.9 Hz, H(11)). MALDI-TOF: m/z [MH^+] 641.2493 found, 641.2468 calcd.

*1,4-Diketo-3-((4-[N-(3,5-dichloro-4-hydroxyphenyl)amino]sulfonyl)phenyl)-6-phenylpyrrolo[3,4-c]pyrrole (**3a**)*
The preparation of **3a** is described in chapter 4.

*1,4-Diketo-3-((4-(4-methyl-1-piperazinyl)sulfonyl)phenyl)-6-phenylpyrrolo[3,4-c]pyrrole (**3b**)*
1,4-Diketo-3,6-diphenylpyrrolo[3,4-c]pyrrole (500 mg, 1.73 mmol) was heated in chlorosulfuric acid (5 ml) to 60 °C. After 3 h, the mixture was allowed to cool to RT and added dropwise onto *N*-methylpiperazine (10 ml, 90.1 mmol, pre-cooled to 0°C). The product was precipitated with H_2O (100 ml), washed thoroughly with water, dried and purified by column chromatography with ethyl acetate / ethanol / 25% aqueous ammonia 89 / 10 / 1 as eluent, yield 51 mg (7 %). ^{1}H NMR (300 MHz, $(CD_3)_2SO$, TMS): δ = 11.50 (1H, broad s, H(9)); 8.45 – 8.7 (2H, broad, H(13)); 8.41 (2H, d, J = 8.4 Hz, H(2,3)); 8.25 – 8.35 (2H, 2d, J = 7.7 Hz, H(5,8)); 7.68 – 7.83 (4H, m, H(1,4,6,7)); 2.93 (4H, broad t, H(10)); 2.35 (4H, broad t, H(11)); 2.12 (3H, s, H(12)). MALDI-TOF: m/z [MH^+] 451.1405 found, 451.1440 calcd.

*1,4-Diketo-3-((4-[N-(3-chloro-4-hydroxyphenyl)amino]sulfonyl)phenyl)-6-phenylpyrrolo[3,4-c]pyrrole (**3c**)*
The preparation of **3c** is described in chapter 4.

*N-(3,5-Dichloro-4-hydroxyphenyl)-N'-(2,6-diisopropylphenyl)-1,6,7,12-tetrachloroperylene-3,4:9,10-tertracarboxylic bisimide (**4a**)*
1,6,7,12-Tetrachloroperylene-3,4:9,10-tetracarboxylic bisanhydride (3 g, 5.66 mmol) was dissolved in 1-methyl-2-pyrrolidone (200 ml) at 110 °C. 4-Amino-2,6-dichlorophenol (1.04 g, 5.84 mmol), 2,6-diisopropylaniline (1.2 ml, 6.37 mmol) and propionic acid (100 ml) were added, the mixture was flushed with nitrogen and stirred at 110 °C for 22 h. 5 % aqueous NaCl (800 ml) was added, the orange precipitate was filtered, washed with water, dried and purified by column chromatography with methylene chloride / toluene 70 / 30 as eluent, yield 1.18 g (25 %).^{1}H NMR (300 MHz, $CDCl_3$, TMS): δ = 8.75 (4H, 2s, H(1)); 7.53 (1H, t, J = 7.7 Hz, H(3)); 7.39 (2H, d, J = 7.9 Hz, H(2)); 7.29 (2H, s, H(6)); 6.08 (1H, s, H(7)); 2.74 (2H, quint, J = 6.7 Hz, H(4)); 1.19 (12H, dd, J_1 = 6.9 Hz, J_2 = 3.6 Hz, H(5)). MALDI-TOF: m/z [M^+] 849.9963 found, 849.9949 calcd.

*N-(2,6-Diisopropylphenyl)-N'-(2-(dimethylamino)ethyl)-1,6,7,12-tetrachloroperylene-3,4:9,10-tertracarboxylic bisimide (**4b**)*

1,6,7,12-Tetrachloroperyl-2-pyrrolidone (200 ml) at 80 °C. The mixture was flushed with nitrogen and *N,N*-dimethylethylene diamine (0.65 ml, 5.89 mmol) was added. After 1 h, temperature was raised to 120°C, 2,6-diisopropylaniline (4.61 ml, 24.4 mmol) and propionic acid (70 ml) and the mixture was stirred for 20 h. 20 % aqueous NaCl (1 l) was added, the orange precipitate was filtered, washed with dilute aqueous $NaHCO_3$, dried and purified by column chromatography with methylene chloride / methanol 50 / 1 as eluent, yield 1.36 g (33 %).^{1}H NMR (300 MHz, $CDCl_3$, TMS): δ = 8.71 (4H, 2s, H(1)); 7.52 (1H, t, J = 7.6 Hz, H(3)); 7.38 (2H, d, J = 7.7 Hz, H(2)); 4.41 (2H, t, J = 5.7 Hz, H(6)); 2.76 (4H, m, H(4,7)); 2.42 (6H, s, H(8)); 1.18 (12H, dd, J_1 = 3.7 Hz, J_2 = 3.2 Hz, H(5)). MALDI-TOF: m/z [M-H$^+$] 760.1169 found, 760.1125 calcd.

*N-(3-Chloro-4-hydroxyphenyl)-N'-(2,6-diisopropylphenyl)-1,6,7,12-tetrachloroperylene-3,4:9,10-tertracarboxylic bisimide (**4c**)*

4c was prepared in the same way as **4a**, 4-Amino-2-chlorophenol (813 mg, 5.66 mmol) was used instead of the dichloro compound, yield 1.41 g (31 %). ^{1}H NMR (300 MHz, $CDCl_3$, TMS): δ = 8.75 (4H, 2s, H(1)); 7.53 (1H, t, J = 7.8 Hz, H(3)); 7.39 (2H, d, J = 7.8 Hz, H(2)); 7.33 (1H, d, J = 2.3 Hz, H(6)); 7.22 (1H, d, J = n.m. due to $CHCl_3$, H(8)); 7.17 (1H, dd, J_1 = 8.7 Hz, J_2 = 2.3 Hz, H(7)); 5.77 (1H, s, H(9)); 2.74 (2H, quint, J = 6.8 Hz, H(4)); 1.19 (12H, dd, J_1 = 6.6 Hz, J_2 = 3.6 Hz, H(5)). MALDI-TOF: m/z [M$^+$] 816.0355 found, 816.0340 calcd.

*N-(3,5-Dichloro-4-hydroxyphenyl)-N'-(2,6-diisopropylphenyl)-1,6,7,12-tetraphenoxy-perylene-3,4:9,10-tertracarboxylic bisimide (**5a**)*

A mixture of **4a** (70 mg, 0.082 mmol), 1-methyl-2-pyrrolidone (7 ml), phenol (77mg, 0.82 mmol) and potassium carbonate (91 mg, 0.66 mmol) was stirred at 110°C for 15 h. 50 ml of 20 % aqueous NaCl containing 0.7 M HCl were added, the purple precipitate was filtered, washed with water, dried and purified by column chromatography with toluene / ethanol 99 / 1 as eluent, yield 54 mg (61 %). ^{1}H NMR (300 MHz, $CDCl_3$, TMS): δ = 8.24 (4H, 2s, H(1)); 7.44 (1H, t, J = 8.4 Hz, H(3)); 7.23 – 7.34 (10H, m, H(2,8)); 7.21 (2H, s, H(6)); 7.12 (4H, m, H(9)); 6.98 (8H, t, J = 6.5 Hz, H(7)); 6.11 (1H, s, H(10)); 2.71 (2H, quint, J = 6.4 Hz , H(4)); 1.14 (12H, d, J = 6.6 Hz, H(5)). MALDI-TOF: m/z [M$^+$] 1080.248 found, 1080.258 calcd.

*N-(2,6-Diisopropylphenyl)-N'-(2-(dimethylamino)ethyl)-1,6,7,12-tetraphenoxyperylene-3,4:9,10-tertracarboxylic bisimide (**5b**)*

A mixture of **4b** (800 mg, 1.05 mmol), 1-methyl-2-pyrrolidone (50 ml), phenol (950 mg, 10.1 mmol) and potassium carbonate (1.1 g, 7.96 mmol) was stirred at 110°C for 3.5 h. 50 ml of 15 % aqueous NaCl containing 0.3 M HCl were added, the purple precipitate was filtered, washed with dilute aqueous $NaHCO_3$, dried and purified by column chromatography with methylene chloride / methanol 98 / 2 as eluent, yield 681mg (65 %). ^{1}H NMR (300 MHz, $CDCl_3$, TMS): δ = 8.21 (4H, 2s, H(1)); 7.42 (1H, t, J = 7.8 Hz, H(3)); 7.20 – 7.33 (10H, m, H(2,10)); 7.12 (4H, q, J = 7.8 Hz, H(11)); 6.96 (8H, q, J = 3.9 Hz, H(9)); 4.28 (2H, t, J = 6.8 Hz, H(6)); 2.58 – 2.75 (4H, m, (4,7)); 2.34 (6H, s, H(8)); 1.12 (12H, d, J = 6.8 Hz, H(5)). MALDI-TOF: m/z [M-H$^+$] 990.3752 found, 990.3754 calcd.

*N-(3-Chloro-4-hydroxyphenyl)-N'-(2,6-diisopropylphenyl)-1,6,7,12-tetraphenoxy-perylene-3,4:9,10-tertracarboxylic bisimide (**5c**)*

5c was prepared in the same way as **5a**, **4c** (70 mg, 0.086 mmol) was used as starting material, yield 40 mg (45 %). ^{1}H NMR (300 MHz, $CDCl_3$, TMS): δ = 8.24 (4H, 2s, H(1)); 7.44 (1H, t, J = 8.2 Hz, H(3)); 7.23 – 7.33 (11H, m, H(2,6,10)); 7.06 – 7.16 (6H, m, H(7,8,11)); 6.98 (4H, dd, J_1 = 5.1 Hz, J_2 = 7.5 Hz, H(9)); 5.73 (1H, s, H(12)); 2.71 (2H, quint, J = 6.3 Hz , H(4)); 1.12 (12H, d, J = 6.8 Hz, H(5)). MALDI-TOF: m/z [M-H$^+$] 1045.2913 found, 1045.2892 calcd.

*N-(3,5-Dichloro-4-hydroxyphenyl)-N'-(2,6-diisopropylphenyl)-1-(1-morpholinyl)-6,7,12-trichloroperylene-3,4:9,10-tertracarboxylic bisimide (**6a**)*

4a (175 mg, 0.24 mmol) was stirred in a mixture of morpholine (3 ml, 35 mmol) and 1-methyl-2-pyrrolidone (3 ml) at 40°C for 2 h. 50 ml 15 % aqueous NaCl containing 0.4 M HCl were added, the green precipitate was filtered, washed with water, dried and purified by column chromatography with methylene chloride / methanol 50 / 1 as eluent, yield 144 mg (75 %). ^{1}H NMR (300 MHz, $CDCl_3$, TMS): δ = 8.73 (2H, s, H(1)); 8.59 (1H, s, H(1)); 8.54 (1H, s, H(1)); 7.53 (1H, t, J = 7.8 Hz, H(3)); 7.38 (2H, d, J = 7.7 Hz, H(2)); 7.30 (2H, s, H(6)); 6.08 (1H, s, H(11)); 4.07 – 4.32 (3H, m, H(7,10)); 3.95 (1H, t, J = 8.9 Hz, H(10)); 3.58 (1H, d, J = 11.4 Hz, H(9)); 3.37 (1H, t, J = 8.8 Hz, H(9)); 2.65 – 2.90 (3H, m, H(4,8)); 2.17 (1H, d, J = 13.7 Hz, H(8)); 1.19 (12H, dd, J_1 = 6.5 Hz, J_2 = 11.8 Hz, H(5)). MALDI-TOF: m/z [M-H$^+$] 900.0797 found, 900.0790 calcd.

*N-(2,6-Diisopropylphenyl)-N'-(2-(dimethylamino)ethyl)-1-(1-morpholinyl)-6,7,12-trichloroperylene-3,4:9,10-tertracarboxylic bisimide (**6b**)*

6b was prepared in the same way as **6a**, **4b** (180 mg, 0.21 mmol) was used as starting material, eluent for column chromatography was methylene chloride / methanol 30 / 1, yield 132 mg (69 %). ^{1}H NMR (300 MHz, $CDCl_3$, TMS): δ = 8.61 (2H, m, H(1)); 8.45 (2H, m, H(1)); 7.44 (1H, t, J = 7.8 Hz, H(3)); 7.30 (2H, d, J = 7.6 Hz, H(2)); 7.30 (2H, d, J = 7.6 Hz, H(2)); 4.32 (2H, m, H(6)); 3.95 – 4.25 (3H, m, H(9,12)); 3.84 (1H, m, H(12)); 3.53 (1H, t, J = 12.3 Hz, H(11)); 3.28 (1H, t, J = 8.4 Hz, H(11)); 2.55 – 2.95 (5H, m, H(4,7,10)); 2.31 (6H, 2d, H(8)); 2.06 (1H, t, J = 13.5 Hz, H(10)); 1.10 (12H, m, H(5)). MALDI-TOF: m/z [M-H$^+$] 809.0286 found, 809.0264 calcd.

Acknowledgement

Financial support from the Austrian Science Fund FWF (project P 21192-N17) is gratefully acknowledged.

Chapter 6

Perylene Bisimides for FLIM-based pH Measurements in 2D and 3D Cell Models

Preface to Chapter 6

Now that the suitability and high flexibility of PET-based systems for optical pH-sensing has been shown, their practical applicability is to be demonstrated. One of the most scientifically relevant and exciting fields of application for fluorescent probes is live cell imaging. PET-based probes are not perfect candidates for this purpose since referencing is urgently required but not easy to perform. They are typically not useful in ratiometric imaging as they exhibit no pH-dependent spectral shift. However, fluorescence lifetime imaging (FLIM) has become more attractive in the recent years as confocal FLIM-microscopes have become more available. Those require pH-probes with different fluorescence lifetimes for acidic and basic forms. Examples are pH-probes undergoing partial quenching by PET, as has been revealed in chapter 5.

Among the probes capable of partial quenching, tetraphenoxy-PBIs carrying amines as PET groups have been selected for live cell FLIM because they are very bright, excellently photostable and accessible to further structural modification. Modification is necessary as tetraphenoxy-PBIs need to be made water-soluble and functionalities promoting cell permeability have to be provided. Chlorosulfonation at mild conditions allows the introduction of four groups at the phenoxy substituents. For delivery into cells, which is often promoted by cationic groups, two strategies are investigated: Attachment of sulfonate groups followed by physical entrapment into cationic nanoparticles (Eudragit RL100®) to yield pH-nanosensors and attachment of guanidine ethyl ester units to yield a molecular probe.

In agreement to previous results with Eudragit RL100, the nanoparticles are delivered into four different cell types with localisation predominantly in lysosomes. When cells are permeabilised to equilibrate to the buffer solution applied, a pH-induced lifetime change typically from 4.8 ns (pH 4.5) to 3.8 ns (pH 8) throughout the pH-range relevant in cells is observable. Bafilomycin A1, an inhibitor of lysosomal acidification, causes a decrease in observed lifetime which is in agreement with the increase in lysosomal pH expected. The nanosensors are also successfully employed in 3D models of neuronal tissue (“neurospheres”). These results underline that the nanoparticles are useful for live cell pH-imaging.

In contrast, the molecular probe based on tetraphenoxy-PBI shows effective cell staining but pH-response in all cell types is blurred by strong inhomogeneity in lifetimes over individual images. Those probes are not useful for reliable pH-measurement probably due to strong interactions with biological components which can be very critical in the absence of a protective polymer shell.

In chapter 1, tetraphenoxy-PBIs proved of little use for pH-sensors due to aggregation issues. However, the RL100 nanoparticles used in this chapter remained useful and stable for at least 14 days upon storage in buffer. Their stability is sufficient for imaging applications in which sensors are often used once and then discarded. The tetra-anionic PBI may be more stable against aggregation due to its tight binding to the cationic matrix, its more hydrophilic character and its high charge presumably inhibiting stacking.

Perylene Bisimides for FLIM-based pH Measurements in 2D and 3D Cell Models

This chapter has been submitted to **Journal of Materials Chemistry B**

Authors: **Daniel Aigner, Ruslan I Dmitriev, Sergey M Borisov, Dmitri B Papkovsky and Ingo Klimant**

New perylene bisimide based pH-sensitive probes for live cell fluorescence lifetime imaging (FLIM), represented by cationic hydrogel nanoparticles and guanidine-rich conjugates, are described. They were evaluated in high-resolution confocal FLIM-TCSPC (time-correlated single photon counting) studies with adherent mammalian cells (2D) and neurosphere (3D) models and compared with the conventional pH probe BCECF. We found that the nanoparticle probe provides stable pH calibration, with lifetime changes from 4.7 to 3.7 ns between pH 4.4 and 8, which are attributed to photoinduced electron transfer (PET). In contrast, the molecular probes lacking a protective polymer coat were affected by micro-environment and worked less reliably in quantitative FLIM. High brightness and excellent photostability, efficient staining of various cells and positive optical response to acidification are the major benefits of the new pH probes. Development of new derivatives with stronger PET effect can further improve the resolution of pH measurements.

Introduction

Intracellular pH in mammalian cells is tightly regulated in a complex manner [12]. Compartmentalised cells possess a considerable heterogeneity in pH. The cytosolic values 7.1 - 7.2 are essential for the function of intracellular organelles. The degradation of proteins in lysosomes requires an acidic pH (4.5 - 5.5) [83], the alkaline pH of the mitochondria (7.5 - 8) is crucial for oxidative phosphorylation [13,277]. The fluxes of other ions (Na^+, K^+, Ca^{2+}, Cl^-) also depend on pH gradients [12,278,279]. Intra- and extracellular pH gradients play important roles in cell proliferation, senescence and apoptosis [280], endo- and exocytosis, intracellular transport and organelle recycling [281,282] and muscle cell contractility [283]. Cellular pH is a useful biomarker for neuroscience [284-286] and cancer research, cell bioenergetics and metabolism [14].
Fluorescence imaging is an established method for investigating cells and cellular compartments, allowing the analysis of submicron-size objects in multiple dimensions (spatial, temporal, multicolour) [2,287]. Imaging techniques usually rely on fluorescent probes which can be genetically encoded fluorescent proteins, molecular probes or (polymeric) nanoparticles [108,288-290]. Synthetic intracellular fluorescent probes provide controlled concentration and brightness in the cell, fast and efficient loading and tuning of cell-permeating properties [291,292]. The main challenges with self-loading probes are in controlling their intracellular localisation and providing robust and specific response to pH minimally affected by environment. This can be addressed by the use of amphiphilic probes with specific charged groups and targeting "escort" moieties (e.g. antibody fragments or peptide sequences) and by encapsulation of reporter dyes in polymeric nanoparticles (pH-nanosensors) having sizes of 10 – 100 nm.

Current research on pH-nanosensors is focused on new indicator dyes and materials with improved operational performance, bio-distribution and reduced toxicity [18,293-297].
The main detection modalities for intracellular pH-probes are fluorescence intensity (ratiometric detection) [83] and lifetime (FLIM) measurements [298,299]. FLIM instrumentation is becoming more widely available and popular in biomedical research, since it can provide stable and absolute pH calibration and reliable quantitative measurements. The FLIM technique is compatible with laser-scanning one- and two-photon microscopy and facilitates multi-parametric measurements, as the fluorophores can also be distinguished by their lifetimes. Therefore, FLIM-based detection is also very attractive for quantitative and high-resolution pH analysis in cultured cells and 3D tissue models.
FLIM detection have been described for several pH-probes, including fluorescent proteins [110,111,300,301], quantum dots [106,295] and organic dyes (as molecular probes or embedded into nanosensors). 2',7'-Bis-(2-carboxyethyl)-5,6-carboxyfluorescein (BCECF) is one such organic dye but it has poor photostability [302-305]. BCECF and other probes [306-309] have demonstrated the promise of FLIM for quantitative pH measurements, but there is a clear need for development of new pH probes with improved brightness, photostability and staining properties for FLIM applications.
Perylene bisimides (PBI) are organic dyes exhibiting convenient spectral properties, bright fluorescence and high photostability [117,119,120]. They have been used for DNA, protein and membrane labelling [126,310,311], but not for intracellular pH measurement, to the best of our knowledge. Due to their high intrinsic hydrophobicity, PBI are often modified with branched hydrophilic groups to suppress aggregation and facilitate their use in biological systems [312-316].
In this work, we prepared new PBI derivatives for FLIM-based imaging of intracellular pH. As previously demonstrated [59,268,270], pH sensitivity can be introduced by attaching amino groups causing PET which leads to fluorescence quenching by the free amine, but not by the protonated form dominating at low pH (figure 6-1) [60,61]. We anticipated that PET should also reduce fluorescence lifetime of the basic form, thus enabling FLIM-based pH imaging. Moderate quenching would be ideal for our application since strong quenching would make the lifetime of the basic form hard to measure (low fluorescent signals). We therefore designed pH probes as tetraaryloxy-substituted PBI as we found previously that PET can cause their partial quenching [270]. In this work, we found that solubility, brightness and FLIM compatibility were gradually improved by incorporation into nanoparticles and by chemical modification of PBI with cell-penetrating guanidine groups. Both probe preparation strategies were relatively easy to perform. However, only incorporation of the dye in polymer nanoparticles was sufficient for reliable quantitative FLIM measurements, providing minimal effect of the environment on the calibration and making them superior compared with structurally similar PBI-based molecular probes and with BCECF.

Results and Discussion

Preparation and Evaluation of PBI pH Probes and Sensors

Nanosensor particles (**NSP**) and a molecular probe (**MP**) based on PBI were produced for FLIM-based pH measurement in live cells (figure 6-1). **NSP** consisted of a polyanionic PBI incorporated into cationic nanoparticles, made by precipitation of Eudragit RL-100®, a biocompatible acrylate hydrogel [19], which has been shown to facilitate cell penetration [317]. In **MP**, four arginine ethyl ester units have been introduced to obtain a polycationic PBI. The charged groups were attached by chlorosulfonation followed by either hydrolysis or reaction with a primary amine (arginine ethyl ester) [268]. The uncharged precursors were synthesised according to established procedures [69,270].

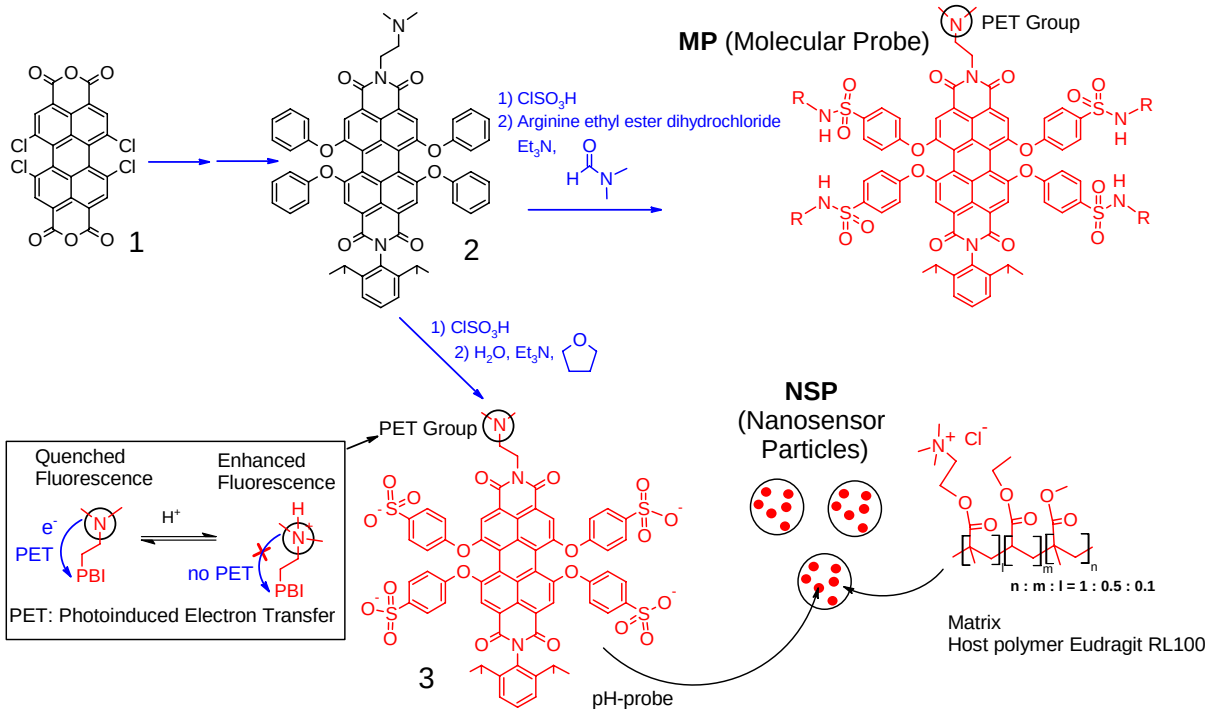

Figure 6-1: Structures of NSP and MP.

First, we evaluated the pH response of **NSP** and **MP** in aqueous buffer solution (figure 6-2). In agreement with the PET mechanism, partial fluorescence quenching was observed for **NSP**, with sigmoidal pH response and a pK_A value of 6.4, most likely corresponding to the (de)protonation equilibrium of the tertiary amino group. Furthermore, a clearly diminished fluorescence lifetime at basic pH was observed showing sufficient separation of lifetime values (≈ 2 ns) at the extreme physiological pH-values: pH 4.4 (lysosomes) and pH 8 (mitochondria) [12]. These results indicate that partial quenching by PET can lead to a decrease in fluorescence lifetime measureable by FLIM. Since different lifetimes for acidic and basic forms are expected, fluorescence decay should be bi-exponential at neutral and slightly basic pH. However, we found that with PBI producing relatively small changes in lifetime values, mono-exponential fits (with 1.2 ns shift, figure 6-S1)) were accurate and reproducible, allowing easier data processing. Therefore we used them in our study.

For **MP**, fluorescence intensity decreased over a broad pH range (5 – 9), and sigmoidal fits for pH calibration were not applicable. Fluorescence lifetime in solution underwent only minor changes which may be due to the low emission of the basic form. It is likely that pH-response was affected by aggregation, which was evident by diminished fluorescence quantum yield in water (0.33) and structureless absorption spectra which are untypical for tetraaryloxy-PBI [270]. In tetrahydrofuran/water 9:1, the quantum yield was much higher (0.93) and spectra of **MP** were typical for tetraaryloxy-PBI. On the contrary, **NSP** in water did not show those signs of dye aggregation. Thus, aggregation which complicates the pH response of **MP** does not occur in **NSP**.

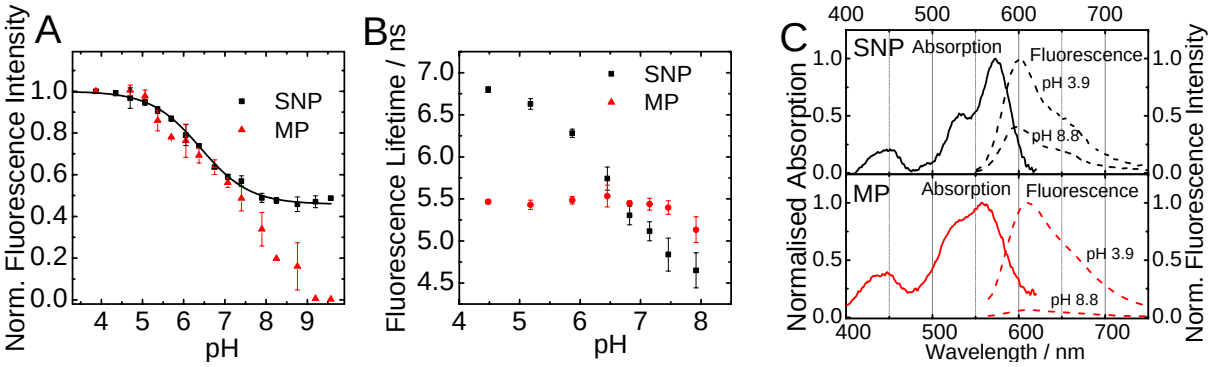

Figure 6-2: Photophysical properties of NSP (5 g l^{-1}) and MP (0.5 µM) in aqueous buffer at 25°C. A: pH calibration curves based on fluorescence intensity; B: Calibration based on fluorescence lifetime; C: Absorption and fluorescence emission (excited at 550 nm) spectra.

Cell Permeation Properties

Cell permeability of the pH-probes was first studied with mouse embryonic fibroblast (MEF) cells. We found efficient intracellular staining over 24 h incubation at concentrations of 5 µM (**MP**) and 10 g l^{-1} (**NSP,** equivalent to a dye concentration of 0.025 µM). **MP** showed faster cell staining, with maximal signals reached after 6 h and 35% of the maximum already after 1 h (figure 6-3). Interestingly, emission clearly weakened after 24 h staining. A possible explanation is hydrolysis of the ester groups in **MP** by cellular esterases which would dramatically change the net charge and therefore cause migration to a different microenvironment. Although cellular uptake was slower for **NSP**, stronger emission was reached after 24 h, compared to **MP**. Slower staining kinetics can be explained by different size and internalisation mechanism [318]. Notably, cells were even stained to some degree by the polyanionic pH probe used in **NSP** without any polymer shell. However, the fluorescent signal was much lower (> 10-fold, not shown) compared to **NSP** and fluorescence lifetime was only slightly dependent on pH ($\Delta\tau \approx 0.3$ ns in cells, compared to ≈ 1 ns for **NSP**, table 6-1), underlining the important role of polymer shell.

Both **NSP** and **MP** in MEF cells displayed punctuated intracellular localisation (figure 6-3), similar to endocytic compartments, in agreement with previous reported data for nanoparticle and guanidine-containing conjugates [294,319]. For **NSP** we studied intracellular localisation in detail (figure 6-3) and found a considerable overlap with transferrin (marker of clathrin-mediated endosomes including lysosomes) and no overlap with Dextran 10,000 (macropinosomes) or markers of nuclei and mitochondria (not shown). These results point at predominantly lysosomal localisation, previously reported for a RL100-based oxygen sensitive probe [317]. Indeed, when we counter-stained **NSP** with another RL100-based probe, PtTPTBPF (emitting in another spectral window) [320], we found a significant overlap (yellow colour), indicating a similar

pattern of intracellular localisation for RL100-based nanoparticles doped with different indicator dyes.

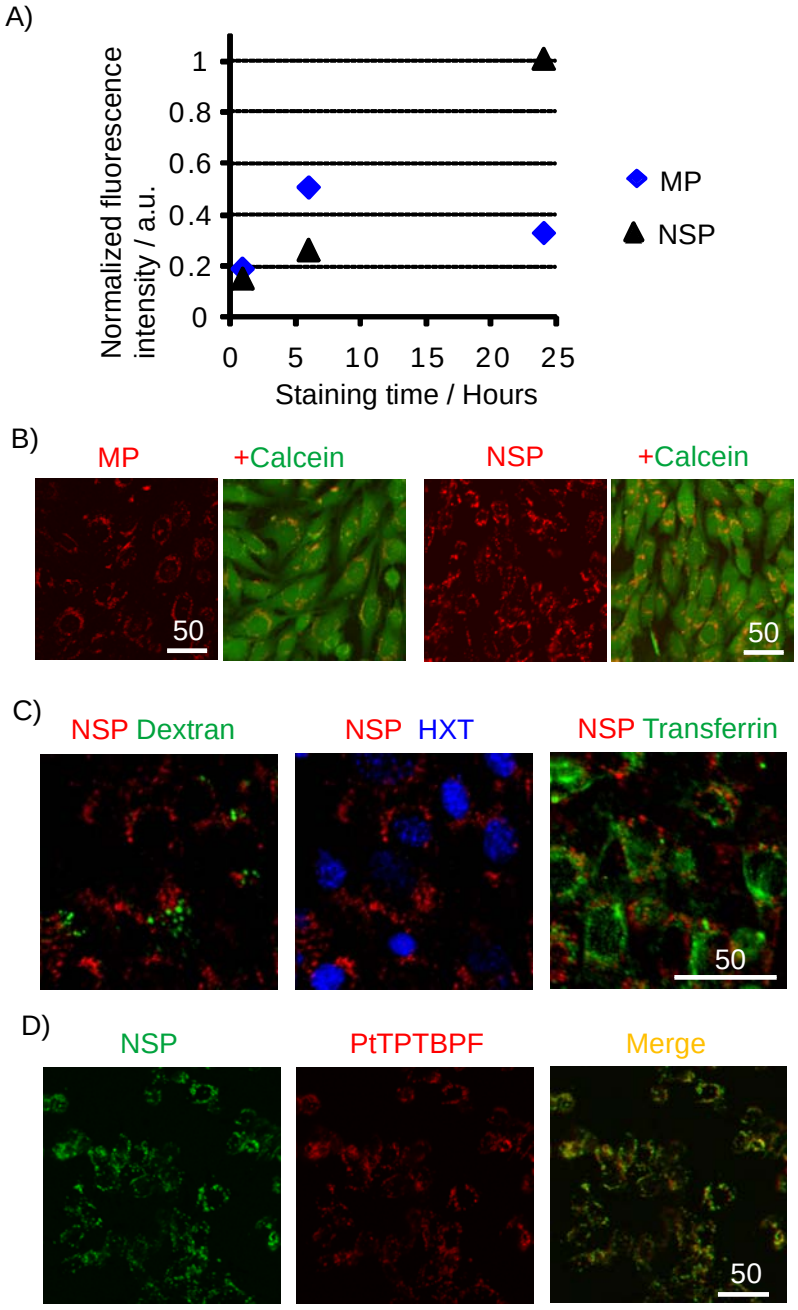

Figure 6-3: Cell staining properties with MEF cells. A: Kinetics of cell staining (0 – 24 h). Cells were incubated with probe, washed and imaged on fluorescence microscope and then their brightness in cells was quantified; B: Confocal images showing localisation of NSP and MP in the cell, counter-stained with Calcein Green(cytosolic stain); C: Co-localisation of NSP with markers of macropinosomes (Dextran 10,000), nuclei (Hoechst) and clathrin-mediated endosomes (transferrin); D: Co-localisation of NSP with platinum(II)-*meso*-tetra(4-fluorophenyl)tetrabenzoporphyrin (PtTPTBPF) in RL100. Scale bars are in μm.

Similarly, we observed that **NSP** and **MP** can provide intracellular staining of several other cell types (6 – 20 h staining time), including human colon cancer cells HCT116 (wild type and deficient on oxidative phosphorylation, SCO_2(-/-) [321]) and Caco-2. We observed no damaging or acute toxic effects upon staining. Cytotoxicity of the new probes tested by CellTox Green assay (membrane integrity) was found to be negligible: after staining for 24 h, viability of the cells

remained at 98 – 99% (not shown). This indicates that **NSP** and **MP** can be successfully used with different cell types.

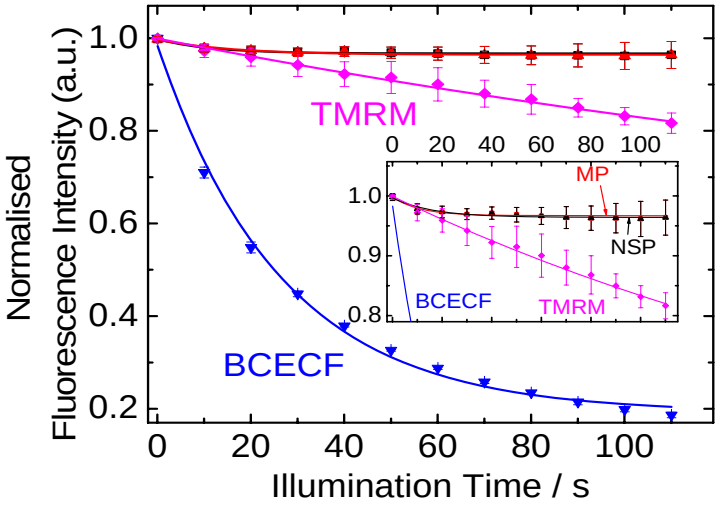

Figure 6-4: Photostability of NSP and MP (excited at 590 nm), compared to BCECF (470 nm exc.) and TMRM (590 nm exc.), obtained with MEF cells, under continuous illumination on a wide-field fluorescence microscope.

The photostability of **NSP** and **MP** upon live cell imaging was tested and found to be superior over the conventional FLIM pH-probe BCECF and spectrally similar rhodamine derivative TMRM (figure 6-4). Upon continuous LED illumination for 2 min, no decrease in fluorescent signal was found. A slight decrease within the first seconds can be due to a small, bleachable fraction, but after that, the signal remained constant. In contrast to that, the intensity of BCECF was diminished by 30% within the first 10 s.

pH Sensing and Imaging with Cultures of Adherent Cells.

Next we evaluated pH-sensing properties using FLIM microscopy and compared their performance with known pH-probe BCECF. Cells stained with **NSP** and **MP** were permeabilised with nigericin and equilibrated in buffer solutions of different pH (4.4 – 8). [12,83,110,322] Figures 6-5, 6-8 and table 6-1 summarise FLIM calibration experiments with different probes on four different cell lines. In all cases, fluorescence lifetime was reduced with increasing pH. For **NSP**, the pH-dependent change in lifetime ($\Delta\tau$) was less profound (around 1 ns), compared to data obtained in plain buffer ($\approx$ 2 ns). Lifetimes values in different cell lines varied only slightly (table 6-1), reflecting the shielding effect of the polymer matrix from the environment. Resolution of the FLIM method could be significantly limited by variations in fluorescence lifetime within individual images. Those can be due to actual pH gradients in cells, imperfections of measurement, data processing and analysis, or cross-sensitivity of the pH-probe to the environment. Though absolute lifetime distributions for **NSP** (half-width 0.3 – 0.6 ns) were broader than for BCECF (0.2 – 0.3 ns), relative to the total value they were narrower (25 – 65%, compared to 100 – 150% for BCECF, $\Delta\tau$ was 0.9 – 1.2 ns for **NSP** and $\approx$ 0.2 ns for BCECF). Hence, **NSP** can provide better resolution in pH measurements.
For **MP**, which lacks a protective polymer shell, $\Delta\tau$ found in cells (0.5 – 1 ns) was larger than in buffer (0.3 ns) and strongly dependent on the cell type, showing broad distributions of lifetimes

over the images (table 6-1, figures 6-5, 6-S2). Even though we could clearly see an effect of pH on probe lifetime, we were unable to perform pH calibrations reliably due to considerable effects of environment. However, due to its fast and efficient permeation, **MP** strategy may be used in future probe design.

It is important to mention that the $\Delta\tau$ observed for BCECF differed from published data where $\Delta\tau$ was typically 0.5 – 1 ns and absolute values for the acidic and basic forms varied [302-305]. A smaller $\Delta\tau$ was found by Hille et al [323]. The variations in $\Delta\tau$ and poor performance of BCECF in our FLIM-based pH sensing can be explained by its poor photostability (figure 6-4), strong concentration dependence of fluorescence properties and different measurement set-up used. Although BCECF emission intensity did change with pH (decreased at acidic pH, figure 6-S3), we could not use this probe in quantitative FLIM. **NSP** clearly allowed for a better resolution in intracellular pH imaging by FLIM than BCECF.

Table 6-1: Fluorescence lifetimes (calculated as stated in the experimental part) of pH-probes in different cell lines measured by FLIM microscopy at 25°C.

Probe	Environment	Average fluorescence lifetime [ns]		Half-width of lifetime distribution [ns]	
		pH 4.4	pH 8.0	pH 4.4	pH 8.0
NSP	MEF cells	4.73	3.68	0.56	0.32
	HCT116 wild type cells	4.58	3.68	0.53	0.41
	HCT116 SCO_2(-/-) cells	4.82	3.75	0.31	0.60
	Caco-2 cells	4.68	3.48	0.52	0.47
MP	MEF cells	3.86	2.82	1.43	0.55
	HCT116 wild type cells	4.31	3.19	0.73	0.85
	HCT116 SCO_2(-/-) cells	3.51	2.92	0.81	0.91
	Caco-2 cells	4.06	3.56	1.34	1.33
BCECF	MEF cells	3.79	3.64	0.22	0.29

Full FLIM pH calibrations for **NSP** with MEF and HCT116 SCO_2(-/-) cells are shown in figure 6-5C. We found clearly sigmoidal calibration curve behaviour at pH 6 – 8, with pK_A values (6.5 – 7.0) similarly to **NSP** in buffer. However, for the range pH 4.4 – 6, a linear fit seems equally or more accurate, indicating in that range other effects than PET may contribute to pH sensitivity of the probe.

In MEF cells at temperatures 25°C and 37°C the calibration curves were not identical (figure 6-S4) but linear fits were applicable at both temperatures for pH < 6, the typical pH for the found localisation of **NSP** (lysosomal), thus enabling uncomplicated calibration in the measurement range of interest. In buffer, lifetime-based calibration curves of **NSP** measured at 37°C and 25°C are very similar (figure 6-S4).

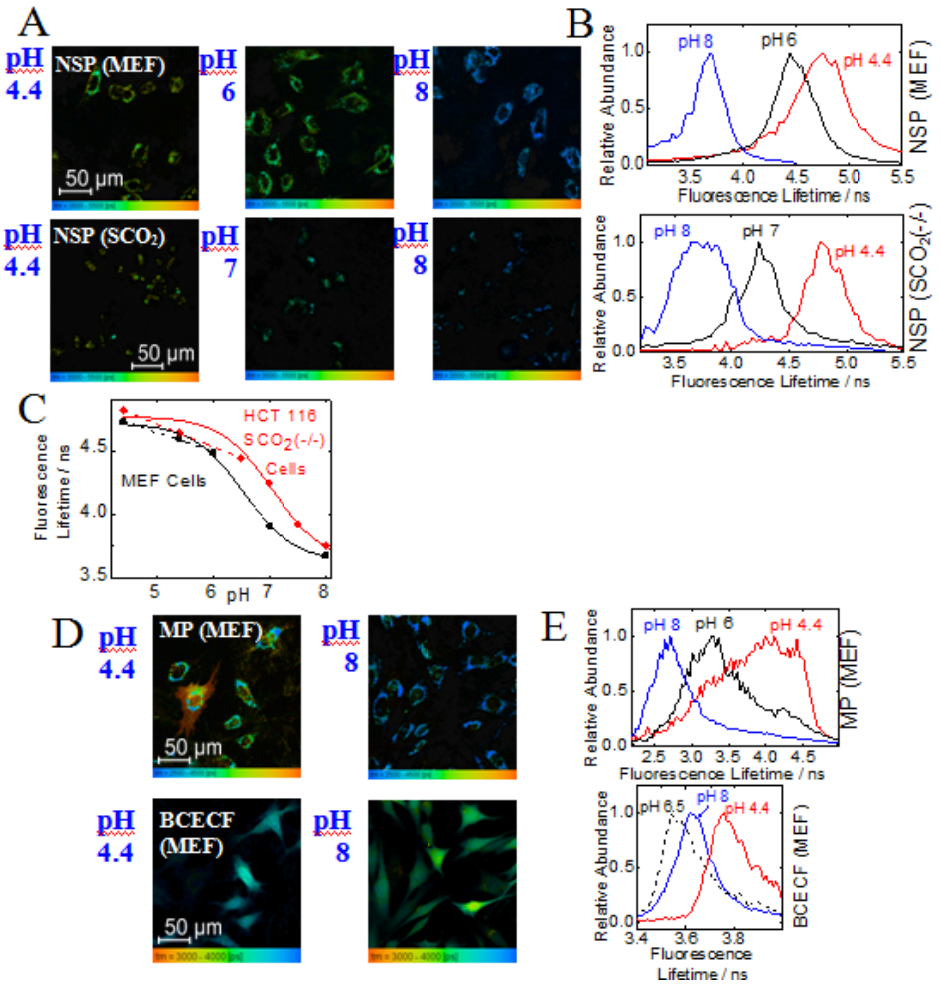

Figure 6-5: Confocal TCSPC FLIM of permeabilised cells (MEF and SCO_2(-/-)), performed at 25°C. A: False-colour images of cells stained with NSP, permeabilised with nigericin and exposed to buffers of different pH; B: Corresponding distributions of lifetimes within the images; C: pH calibration curves (sigmoidal and linear) calculated from the distributions shown in B; D: Images of cells stained with MP and BCECF; E: Corresponding lifetime distributions.

At 25°C, resting cells stained with **NSP** demonstrated lifetimes corresponding to low pH values (5.4 in MEF cells, 5.2 in HCT116 SCO2(-/-) cells, as calculated by linear fit), thus confirming probe localisation in acidic organelles. This makes **NSP** highly suitable for studying pH regulation within recycling endocytic compartments [324]. We therefore treated resting MEF cells with a drug affecting lysosomal acidification (bafilomycin A1) and monitored lifetime changes by live cell FLIM at 37°C. Treatment of cells with this drug leads to rapid (15 – 30 min) inhibition of V-ATPase and increase of lysosomal pH [325]. Indeed, we found disappearance of LysoTracker Red staining upon treatment (not shown) and consistent decrease of fluorescence lifetime of **NSP** for the same regions of interest (figure 6-S5). The decrease in lifetime observed (0.2 – 0.3 ns) can be associated with an increase in pH by 0.9 units, with respect to the initial value at 37°C (4.7). Collectively, our data indicates that **NSP** can be used for sensing pH in acidic organelles within conventional (2D) cell cultures.

Application of PBI Probes for FLIM Imaging of Multicellular Spheroid (3D) Models

The reliability and physiological significance of data obtained with cell cultures significantly increase when cells maintain cell-cell interactions within 3D environment and experience diffusion-limited supply of metabolites [326]. For evaluation of **NSP** and **MP** we selected neurosphere culture, representing heterogeneous multicellular spheroid aggregates with size distribution of 0.1 – 0.5 mm. The neurosphere model is useful for studying processes of neural cell development, cellular responses to various patho-physiological conditions and drugs in 3D [327-329].

Using a previously optimised procedure [330], we produced neurospheres from rat embryonic brain and performed their staining with the pH-probes BCECF, **NSP** and **MP**. Notably, both **NSP** and **MP** displayed efficient in-depth staining, while BCECF produced weak signals from neurosphere interior staining (figure 6-6). Similarly to our data obtained with adherent cells, **MP** showed the highest efficiency being able to stain spheroids in 24 h, while **NSP** needed a continuous staining protocol (>72 h). On average from 3 spheroids of 0.2 – 0.3 mm diameter, **MP** yielded 2.1-fold higher signals than **NSP** and 5.2-fold higher ones than BCECF.

As we could not reliably perform pH FLIM calibration for **MP**, **NSP**-stained neurospheres were selected for further experiments. The detailed analysis of probe distribution across the spheroids revealed extracellular patch-like localisation similar to the staining pattern of previously reported RL100-based probes [330]. However, the analysis of FLIM images revealed clear presence of micro-regions with decreased lifetime (~0.6 ns drop) inside the spheroids (figure 6-6B). The line profiles across the optical cross-sections clearly indicated the presence of regions corresponding to alkaline pH. This data contradicts to observed pH gradients in tumor spheroids [329], which might be argued by different nature of neurosphere-forming cells (neural stem cells), having cell metabolism distinctive from cancer cells [14]. Interestingly, these “alkaline pH” cores harbouring distinct pH gradients were of asymmetrical shape and sometimes were present in a number of copies per spheroid. They can also indicate functional cell heterogeneity of neurosphere- forming cells.

With BCECF we observed decreased fluorescent signals within the spheroid core. This could be a result of lower pH-values there or of poor in-depth probe accumulation.

In another set of experiments we performed neurosphere stimulation with sodium glutamate, a common neuromediator and excitotoxic stimulant [331]. Figure 6-6C shows that all analysed spheroids showed reproducible decrease of fluorescence lifetime upon stimulation with sodium glutamate within 15 – 30 min, implying alkalinisation of neurospheres. Thus, our experiments demonstrate that PBI can be used for pH mapping and time-lapse monitoring by FLIM within spheroid cultures.

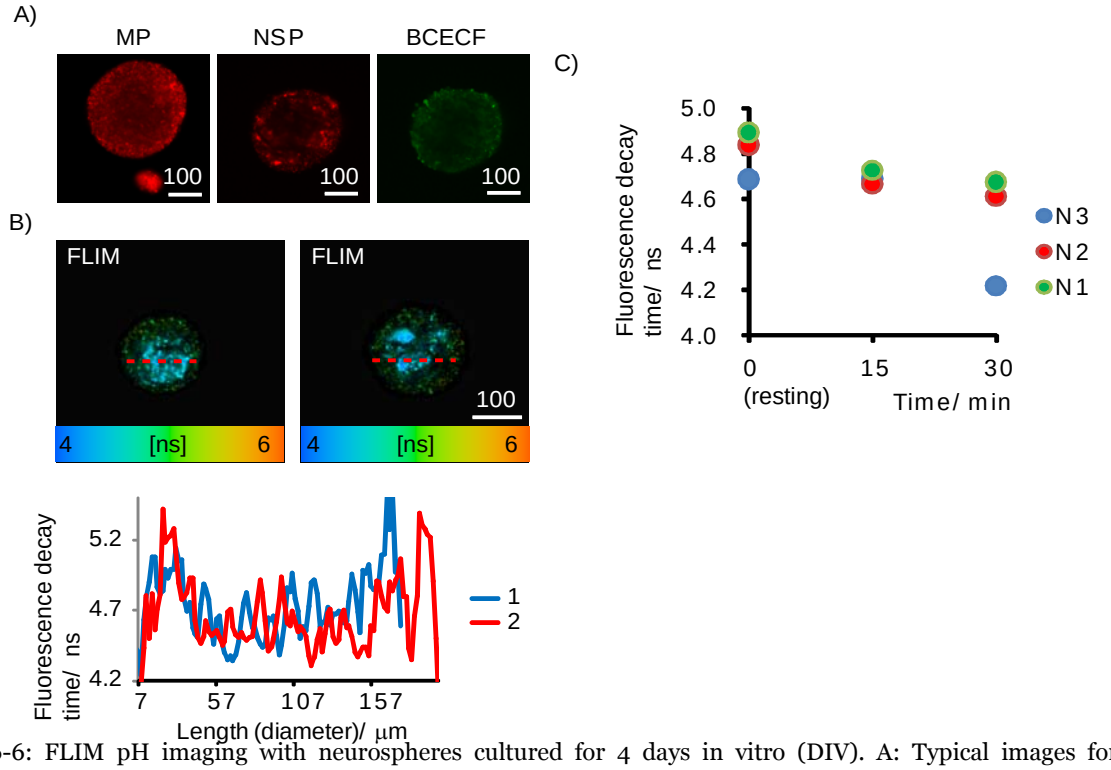

Figure 6-6: FLIM pH imaging with neurospheres cultured for 4 days in vitro (DIV). A: Typical images for neurospheres stained with NSP (5 mg l^{-1}, days 1, 3), MP (2 µM, 24 h) and BCECF (2 µM, 24 h). Each image represents a single optical section across selected spheroids; B: False-color FLIM images of neurospheres stained with NSP (top) and line profiles (indicated with red dashed lines) across the spheroids (bottom); C: Averaged lifetime values within cores of spheroid under resting (0) and stimulated conditions (15, 30 min, 2 mM sodium glutamate), for 3 different spheroids. Scale bar is in µm.

Conclusion

In conclusion, we have presented and evaluated new pH-probes based on perylene bisimides, immobilised in cationic hydrogel particles (**NSP**) or conjugated to cell-penetrating moieties (**MP**). We found that **NSP** is the most suitable probe for intracellular pH measurements by FLIM and provided efficient intracellular staining (predominantly lysosomes) within 6 – 24 h. Excellent photostability and high brightness are the clear advantages and when compared to a conventional FLIM pH-probe, BCECF, better pH-resolution was found. **NSP** was successfully applied for FLIM measurements in four different cell lines (2D cell culture) and with neurospheres prepared from primary neural cells (3D culture). For further optimisation, an improvement of pH-resolution by increasing the absolute pH-dependent lifetime change appears to be most relevant. That may be achieved by increasing the efficiency of the PET process by using different PET groups and/or different PBI structures.

In comparison to **NSP**, the small molecule **MP** was not very useful for intracellular pH-measurement by FLIM, probably due to aggregation and strong interaction with intracellular components. This indicates that nanoparticle structures can feature significant advantages for the development of FLIM-based pH-probes, compared to "unprotected" probes such as small molecule dyes or fluorescent proteins.

Experimental

Materials and Methods

Calcein Green AM, BCECF, tetramethylrhodamine methyl ester (TMRM), B27 serum-free supplement, Alexa Fluor488-dextran 10,000 and transferrin conjugates, MitoTracker Green were from Invitrogen (Biosciences, Dublin, Ireland). Epidermal growth (EGF) and fibroblast growth (FGF) factors were from Millipore (Cork, Ireland). PtTPTBPF-RL100 nanoparticles were prepared as described previously [332]. CellTox Green Cytotoxicity assay kit was form Promega (MyByo, Ireland). 1,6,7,12-Tetrachloroperylene-3,4:9,10-tertracarboxylic bisanhydride was from Beijing Wenhaiyang Industry and Traiding Co. Ltd (http://china.zhaoteng.com), 1-methyl-2-pyrrolidone from TCI Europe (http://www.tcichemicals.com). Deuterated solvents were obtained form Eurisotop (www.eurisotop.com), silica gel from Acros (www.fishersci.com). Eudragit® RL100 was from Evonik Industries (http://corporate.evonik.de). All other chemicals and reagents were form Sigma-Aldrich. Standard cell culture grade plasticware was from Sarstedt (Wexford, Ireland) and Corning (VWR, Ireland), glass bottom mini-dishes were from MatTek (Ashland, USA), glass bottom multiwell slides from Ibidi (Martinsried, Germany).
NMR spectra were recorded on a 300 MHz instrument (Bruker) with TMS as a standard. MALDI-TOF mass spectra were taken on a Micromass TofSpec 2E in reflectron mode at an accelerating voltage of +20 kV. Absorption measurements were performed on a Cary 50 UV-VIS spectrophotometer from Varian (www.varianinc.com). Fluorescence spectra were recorded on a Hitachi F-7000 spectrofluorimetre (www.hitachi.com). Relative fluorescence quantum yields were determined at 25 °C using rhodamine 101 (Φ_F = 0.98 in ethanol) as a standard.

Syntheses

*N-(2,6-Diisopropylphenyl)-N'-(2-dimethylaminoethyl)-1,6,7,12-tetraphenoxyperylene-3,4:9,10-tertracarboxylic bisimide (**2**):*
1,6,7,12-Tetrachloroperylene-3,4:9,10-tertracarboxylic bisanhydride (3 g, 5.66 mmol) was dissolved in 1-methyl-2-pyrrolidone (NMP; 210 ml) at 80°C. A solution of 648 µl (5.66 mmol) *N,N*-dimethylethylenediamine in NMP (10 ml) was added dropwise and the mixture stirred for 1 h. Temperature was increased to 120°C, 2,6-diisopropylaniline (4.61 ml, 22.7 mmol) and propionic acid (70 ml) were added and the mixture was stirred overnight. The crude product was precipitated with 20% aqueous sodium chloride solution, filtered, washed with water and dried. Purification by column chromatography (silica gel 40 – 63 µm) with dichloromethane/methanol 40:1 (V/V) as eluent afforded 1.58 g (37%) *N-(2,6-diisopropylphenyl)-N'-(2-dimethylaminoethyl)-1,6,7,12-tetrachloroperylene-3,4:9,10-tertracarboxylic bisimide*; ^{1}H NMR: (300 MHz, $CDCl_3$**,** δ): 8.71 (2s, 4H, ArH), 7.52 (t, J = 7.8 Hz, 1H, ArH), 7.38 (d, J = 7.7 Hz, 2H, ArH), 4.39 (t, J = 6.3 Hz, 2H, CH_2), 2.6 – 2.8 (m, 4H, CH_2 and CH_3), 2.37 (s, 6H, CH_3), 1.18 (dd, J_1 = 3.7 Hz, J_2 = 3.2 Hz, 12H, CH_3).
800 mg (1.05 mmol) of the obtained product, phenol (950 mg, 10.1 mmol), potassium carbonate (1.1 g, 7.96 mmol) and NMP (60 ml) were stirred at 115°C for 6 h. The crude product was precipitated with 20% aqueous sodium chloride solution containing 0.3 M HCl, filtered, washed with water, dried and purified by column chromatography (silica gel 40 – 63 µm) with dichloromethane / methanol 50:1 (V/V) as eluent, yield 0.78 g (75 %). ^{1}H NMR: (300 MHz,

$CDCl_3$, δ): 8.21 (2s, 4H, ArH), 7.42 (t, *J* = 7.8 Hz, 1H, ArH), 7.20 – 7.33 (m, 10H, ArH), 7.12 (q, *J* = 7.8 Hz, 4H, ArH), 6.96 (q, *J* = 3.9 Hz, 8H, ArH), 4.28 (t, *J* = 6.8 Hz, 2H, CH_2), 2.58 – 2.75 (m, 4H, CH_2 and CH), 2.34 (s, 6H, CH_3), 1.12 (d, *J* = 6.8 Hz, 12H, CH_3).

*N-(2,6-Diisopropyl-4-sulfophenyl)-N'-(2-dimethylaminoethyl)-1,6,7,12-tetra(4-sulfophenoxy)perylene-3,4:9,10-tertracarboxylic bisimide (**3**)*
and *N-(2,6-Diisopropyl-4-([N-(1-ethoxycarbonyl-4-guanidinylbutyl)amino]sulfonyl)phenyl)-N'-(2-dimethylaminoethyl)-1,6,7,12-tetra(4-([N-(1-ethoxycarbonyl-4-guanidinylbutyl)amino]sulfonyl)phenoxy)perylene-3,4:9,10-tertracarboxylic bisimide (**MP**):*
Compound **2** (200 mg, 0.202 mmol) in 3 ml chlorosulfonic acid was stirred at 0°C for 50 min, added dropwise onto ice cubes, filtered, washed with cold water and dried under vacuum at RT to yield the sulfochloride intermediate (298 mg), which was used without further purification.
For the preparation of **3**, 150 mg of the sulfochloride was stirred overnight in a mixture of tetrahydrofuran (8 ml), water (2 ml) and triethylamine (200 µl, 1.43 mmol). The mixture was concentrated under vacuum and purified by column chromatography (silica gel 40 – 63 µm) with dichloromethane/methanol 3:1 (V/V) as eluent. The product was re-dissolved in a mixture of methanol (0.5 ml) and water (0.1 ml) and precipitated with a mixture of methylene chloride, toluene and n-hexane (1 ml each) to yield 68 mg (52 %) of deep red powder after drying. ^{1}H NMR: (300 MHz, $(CD_3)_2SO$:D_2O 20:1 (V/V), δ): 7.98 (s, 2H, ArH), 7.84 (s, 2H, ArH), 7.68 (d, *J* = 8.7Hz, 4H, ArH), 7.59 (d, *J* = 8.4Hz, 4H, ArH), 7.42 (t, *J* = 7.6 Hz, 1H, ArH), 7.28 (d, *J* = 7.5 Hz, 2H, ArH), 6.98 (2d, *J* = 7.4 Hz, 8H, ArH), 4.27 (broad s, 2H, CH_2), 3.25 – 3.4 (broad s, 2H, CH_2), 2.6 – 2.9 (m, 8H, CH_2 and CH), 1.01 (d, *J* = 6.6Hz, 12H, CH_3). UV–vis (H_2O): λ_{max} (ε) = 567 (32000), 536 (32000), 454 nm (17000). HRMS: *m/z* 1310.20 ([MH^+], 1310.20 calcd.); 1332.19 ([MNa^+], 1332.18 calcd.); 1348.16 ([$MNaK^+$], 1348.16 calcd.).
For the preparation of **MP**, the rest of the sulfochloride was added to a solution of arginine ethyl ester dihydrochloride (275 mg, 1.00 mmol) and triethylamine (290µl, 2.07 mmol) in dry *N,N*-dimethylformamide (10 ml) and stirred overnight at RT. The crude product was precipitated and washed with 20% aqueous sodium chloride solution, dried and purified by HPLC chromatography (column NUCLEODUR® 100-5 C18 ec, 125 mm × 21mm ID, Macherey-Nagel, on a Dionex™ UltiMate™ 3000 semi-preparative system) as stated in detail in table A-7, appendix, yield 19 mg (8%). ^{1}H NMR: (300 MHz, CD_3OD, δ): 8.19 (d, *J* = 8.4Hz, 4H, ArH), 7.81 (dd, J_1 = 6.2Hz, J_2 = 8.5Hz, 8H, ArH), 7.45 (t, *J* = 7.8Hz, 1H, ArH), 7.30 (d, *J* = 7.6Hz, 2H, ArH), 7.12 (dd, J_1 = 8.6Hz, J_2 = 16.5Hz, 8H, ArH), 4.50 (broad s, 2H, CH_2), 3.85 – 4.10 (m, 12H, CH and CH_2), 3.51 (broad s, 2H, CH_2), 3.22 (m, 8H, CH_2), 2.97 (s, 6H, CH_3), 2.69 (p, *J* = 6.8Hz, 2H, CH), 1.6 – 1.9 (m, 16H, CH_2), 1.0 – 1.23 (m, 24H, CH_3). UV–vis (H_2O): λ_{max} (ε) = 557 (42000), 447 nm (17000). HRMS: *m/z* 2046.72 ([MH^+], 2046.73 calcd.).

*Preparation of nanosensor particles (**NSP**)*
This was done accordingly to previously described procedure [332]. Briefly, a solution of RL100 polymer (200 mg) and **3** (0.5 mg) in acetone (80 ml) was prepared and water (500 ml) was added quickly (5 s). The nanoparticle suspension (typical average size 30 nm) was concentrated in vacuum to reach a concentration of 5 g l^{-1} and was stored at 4°C (1 month). Prior the use, it was filtered through 0.2 µm filter.
Cell Culture

Mouse embryonic fibroblast (MEF), human colon carcinoma HCT116 and human colorectal adenocarcinoma Caco-2 cells were from ATCC (Manassas, VA, USA) and were handled as described previously [319,333]. For fluorescence microscopy and confocal imaging, cells were seeded for onto Cell$^+$ (confocal upright microscope) or glass bottom (inverted microscope) collagen-poly-D-lysine coated mini-dishes to reach 50 – 75% confluence. Staining with fluorescent probes was performed by addition of medium containing probe, incubation (0.5 – 24 h) and 1 – 2 cycles of washing. Typical staining concentrations/times for fluorescent probes were 2.5 μM/ 0.5 h (BCECF), 20 nM/ 10 min (TMRM), 1 μM/ 0.5 h (Hoechst 33342, Calcein Green AM), 0.01%/ 10 min (CellTox Green), 25 μg ml^{-1}/ 0.5 h (Dextran 10,000-Alexa Fluor488), 40 μg ml^{-1}/ 0.5 h (Transferrin-AlexaFluor488), 100 nM/ 0.5h (MitoTracker Green), 10 μg ml^{-1} / 16 h (PtTPTBPF in RL100).

Neurosphere Culture

All procedures with animals were performed under a licence issued by the Irish Government Department of Health and Children (Ireland) and in accordance with the Directive 2010/63/EU adopted by the European Parliament and the Council of the European Union. Neurospheres from cortices of embryonic (E18) rat brain were prepared as described before [330] and cultured in DMEM/ F12 Ham medium supplemented with FGF (20 ng ml^{-1}), EGF (20 ng ml^{-1}), B27 (2%) and penicillin-streptomycin for 4 days in vitro (DIV), to reach a size of 0.1 – 0.5 mm. For microscopy, neurospheres were collected, washed with medium and plated on poly-D-lysine coated 35 mm dishes and allowed to adhere for 30 min.

Microscopy

Analysis of cell staining kinetics, cell viability and photostability experiments were performed on wide-field fluorescence microscope Axiovert 200 (Zeiss) equipped with custom made pulsed LED (390, 470 and 590 nm excitation), fluorescence emission filter cubes and integrated temperature and CO_2/O_2 control as described previously [330].
FLIM imaging was performed on upright Axio Examiner Z1 (Zeiss) microscope, equipped with 20x/1.0 W Apochromat objective, heated stage (Z-axis control), integrated TCSPC (time-correlated single photon counting) confocal scanning module DCS-120 (Becker & Hickl, Germany), an R10467U-40 and 50 photon counting detectors (Hamamatsu Photonics K.K.) and TCSPC hardware (Becker & Hickl) [330]. The PBI and TMRM probes were excited with picosecond supercontinuum laser SC400-4 (Fianium, UK) at 540 nm (561 nm longpass filter, emission 565 – 605 nm), while BCECF, Calcein Green, Alexa Fluor488-conjugates and MitoTracker Green at 488 nm (495 nm longpass filter, emission 512 – 536 nm). Hoechst 33342 probe was excited at 405 nm (435 nm longpass filter, emission 438 – 458 nm). PtTPTBPF in RL100 was excited at 614 nm (665 nm longpass filter, emission 750-810 nm).
Buffers for pH titrations used were composed of 10 mM buffer salt (sodium acetate, MES, MOPS or HEPES), 135 mM KCl, 2 mM $CaCl_2$, 1 mM $MgCl_2$ and 20 mM Sucrose. Prior to calibration, nigericin (10 μM) was added with 15 – 30 min pre-incubation time. The following equation was used for sigmoidal calibration:

Data processing
The wide-field microscopy imaging data were processed in ImSpector pro software (La Vision BioTec, Germany), and exported in ASCII (line profiles) or RGB Tif (images) format. FLIM data obtained from 256x256 regions of interest were fit using mono-exponential decay function, delay parameter t_1=42, binning factor 1 in SPCImage software (Becker & Hickl). Fit curves in each pixel, excluding dark regions, yielded a lifetime distribution over the whole image, with lifetime being displayed on the x-axis and the abundance of each lifetime on the y-axis. From the distribution curve were calculated the average lifetime (50% of the total integral is reached) and half-width (difference between lifetimes at which half-maximal abundance is reached).

Acknowledgement

This work was supported by Science Foundation Ireland (SFI) grants 12/TIDA/B2413 and 12/RC/2276 and by Graz University of Technology travel grant “Förderungsstipendium für wissenschaftliche Arbeiten 2013”. We thank Alina Kondrashina (University College Cork) for preparation of PtTPTBPF nanoparticles and Tara Foley (University College Cork) for help with isolation of primary neurons, as well as Becker & Hickl GmbH for providing software licenses, the Nano-optics Department, Institute of Physics, Karl-Franzens University Graz, for help with preliminary TCSPC experiments, Robert Saf (Institute of Chemistry and Technology of Materials, Graz University of Technology) for HRMS-measurements and Gernot Strohmeier (Institute of Organic Chemistry, Graz University of Technology) for help with HPLC purification.

Supplementary Information

to *Perylene Bisimides for FLIM-based pH Measurements in 2D and 3D Cell Models*

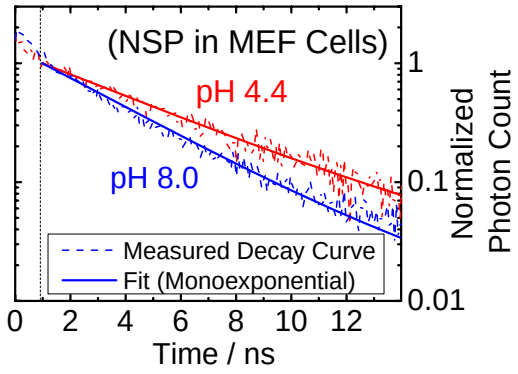

Figure 6-S1: Typical fluorescence decay curves in MEF cells stained with NSP, permeabilised with nigericin and exposed to buffer as indicated, obtained by confocal TCSPC-FLIM.

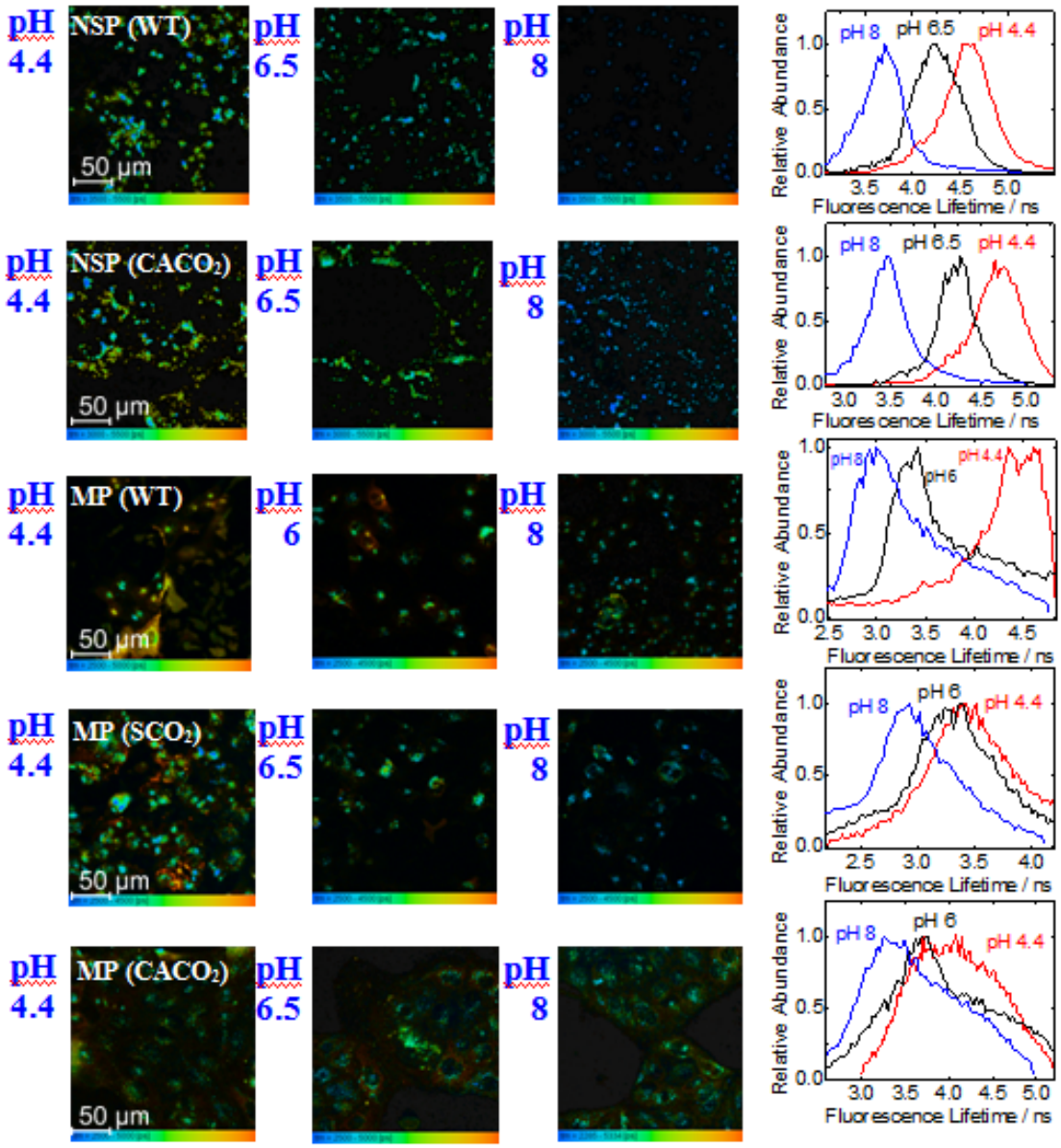

Figure 6-S2: Confocal TCSPC-FLIM of permeabilised cells stained with NSP or MP, permeabilised with nigericin and exposed to buffer as indicated, performed at 25°C. Left: False-colour images of cells exposed to buffers with different pH; Right: Corresponding distributions of lifetimes within the images.

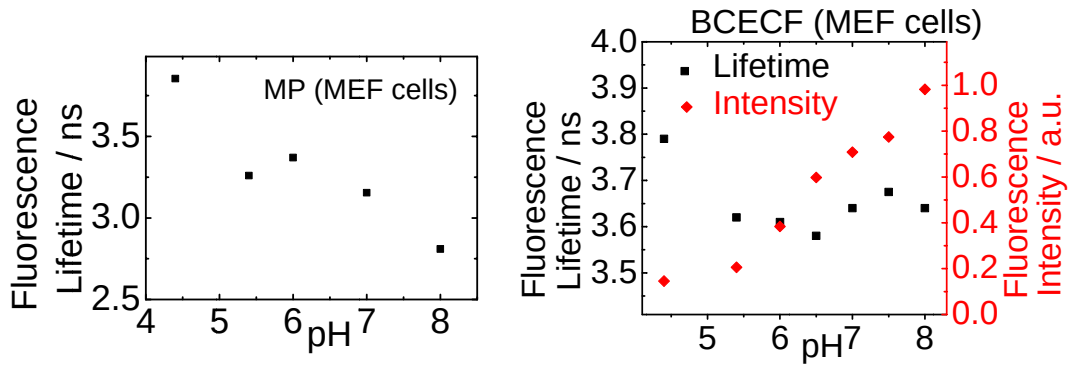

Figure 6-S3: pH calibration curves in MEF cells stained with NSP or BCECF, permeabilised with nigericin and exposed to buffer as indicated, obtained by confocal TCSPC-FLIM.

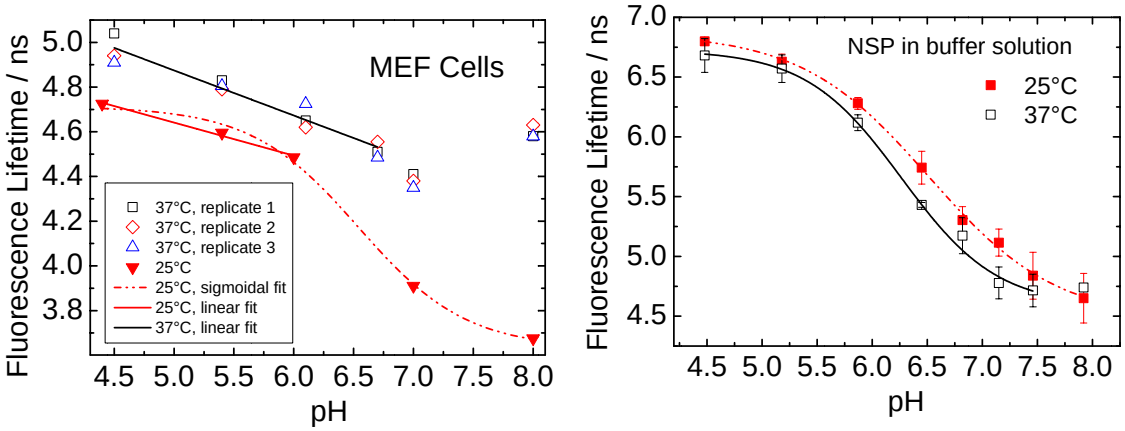

Figure 6-S4: pH calibration curves of NSP based on fluorescence lifetime in MEF cells (left) and aqueous buffer (right), obtained by confocal TCSPC-FLIM.

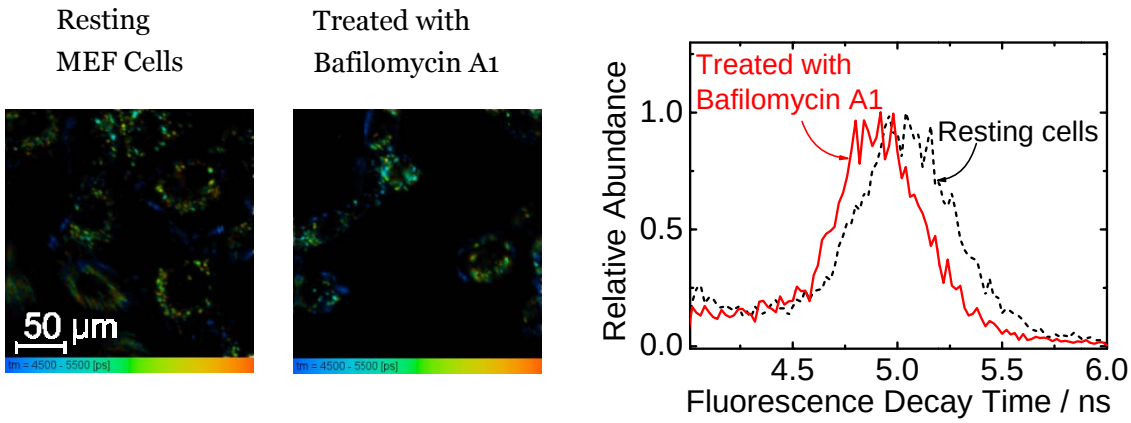

Figure 6-S5: Monitoring of intracellular acidification with NSP, obtained by confocal FLIM microscopy. A: false-color images of MEF cells before (resting) and after stimulation with bafilomycin A1 (0.25 µM); B: Corresponding lifetime distributions over the images.

Part C

Conclusion and Outlook

The attachment of groups causing photoinduced electron transfer (PET) has enabled the preparation of optical pH-sensors based on intrinsically insensitive fluorophores, namely perylene bisimides (PBIs), rhodamine and diketopyrrolo[3,4-c]pyrroles (DPPs). Spectral properties and other parameters mainly determined by the indicator dye such as photostability can therefore be chosen depending on the application. Selection of the PET group enables effective tuning of the sensitive pH-range, for instance by using secondary and tertiary amines or phenols with different halogenation patterns. Proper selection of the immobilisation matrix can additionally contribute to the tunability. Those facts underline that PET is a highly versatile concept for the design of pH-sensors. Note that the PET-based probes and sensors in this thesis can generally be prepared in a comparatively simple way. Because probes with different pK_A-values but virtually identical spectral properties are accessible, the PET-concept is also optimal for designing sensors with a broad sensitive pH-range, as was experimentally confirmed. Furthermore, sensors with minimal (< 0.1 pH-units between 50 and 500 mM) cross-sensitivity to ionic strength could be obtained, underlining that PET helps to deal with many of the most critical limitations of optical pH-sensors. The dual lifetime referencing (DLR) concept was successfully employed in several examples, underlining that even though intrinsic ratiometric referencing is not possible for the PET-based sensors, referencing is still unproblematic at least for sensors in the layer format. Very notably, we found that phenoxide groups systematically cause more effective PET than the more frequently employed amines, thus making a wider selection of fluorophores accessible to pH-sensing.

For sensors based on PBIs, severe issues in long-term stability above all due to aggregation were found. However, those can be overcome by performing covalent dye coupling. Furthermore, preparation of 1-aminoPBIs makes the sensors near infra-red emissive. Sensors based on the red-light emitting tetraphenoxyPBIs offer high brightness and excellent photostability and were successfully employed in live cell imaging. For DPP-based sensors, similar problems in sensor signal stability were found. Covalent immobilisation is difficult for those, but they were successfully applied in the bead format for microfluidic imaging where typical application times are short. Rhodamines are highly water-soluble and obviously require covalent immobilisation which could be accomplished by “click” chemistry. They yield very bright sensors potentially useful in fluorescence imaging or biotechnological process monitoring. Consequently, covalent dye coupling is often the key tool required to make a good pH-probe a good pH-sensor.

While valuable tools for preparing high-performance fluorescence pH-sensors have been presented, a system offering high brightness, near infra-red emission and excellent photostability in combination is still to be found. For this purpose, improved fluorophores are required. A class of pH-sensors already meeting those criteria to a comparatively high extent based on tetraarylazadipyrromethene (Aza-BODIPY) dyes has been presented by Jokic et al [145]. Further optimisation may be possible employing high-performance near infra-red emitting fluorophores as outlined in section 4.1. That may be a challenge with PBIs as 1-aminoPBIs are of limited brightness and core-enlarged PBIs are presumably too hydrophobic. However, bisimidazoloPBIs recently presented by Langhals et al [131] have promise. Pyrrolopyrrole cyanines[136] and some BODIPY [147] and Aza-BODIPY [146] dyes have great potential as well due to their extraordinary spectral properties. All of those dyes are yet to be tested as PET-based pH-probes. Testing their quenchability by PET groups – preferentially phenoxides – is the first step towards future pH-optrodes with optimal performance.

Part D

Appendix

References

1. Valeur, B. *Molecular Fluorescence - Principles and Applications*. (Wiley-VCH, 2001).
2. Lakowicz, J. R. *Principles of Fluorescence Spectroscopy*. (Springer,2006).
3. Klauk, H. *Organic Electronics: Materials, Manufacturing, and Applications*. (John Wiley & Sons, 2006).
4. Marquette, C. A. & Blum, L. J. in *Chemilumin. Biolumin.* (2010). at <http://pubs.rsc.org/en/content/chapter/bk9781847558121-00488/978-1-84755-812-1>
5. Turner, A. P. F. Biosensors: sense and sensibility. *Chem. Soc. Rev.* **42,** 3184–3196 (2013).
6. Dorota Wencel & Colette McDonagh. in *Optochemical Nanosensors* 51–96 (Taylor & Francis, 2012). at <http://www.crcnetbase.com/doi/abs/10.1201/b13065-5>
7. Lobnik, A. in *Opt. Chem. Sens.* (Baldini, F., Chester, A. N., Homola, J. & Martellucci, S.) 77–98 (Springer Netherlands, 2006). at <http://link.springer.com/chapter/10.1007/1-4020-4611-1_5>
8. Jiang, S. *et al.* Surface-functionalized nanoparticles for biosensing and imaging-guided therapeutics. *Nanoscale* **5,** 3127–3148 (2013).
9. Homola, J. Surface Plasmon Resonance Sensors for Detection of Chemical and Biological Species. *Chem. Rev.* **108,** 462–493 (2008).
10. Stoddart, P. R. & White, D. J. Optical fibre SERS sensors. *Anal. Bioanal. Chem.* **394,** 1761–1774 (2009).
11. http://www.merckmanuals.com/professional/endocrine_and_metabolic_disorders/acid-base_regulation_and_disorders/acid-base_disorders.html. (2014).
12. Casey, J. R., Grinstein, S. & Orlowski, J. Sensors and regulators of intracellular pH. *Nat. Rev. Mol. Cell Biol.* **11,** 50–61 (2010).
13. Abad, M. F. C., Benedetto, G. D., Magalhães, P. J., Filippin, L. & Pozzan, T. Mitochondrial pH Monitored by a New Engineered Green Fluorescent Protein Mutant. *J. Biol. Chem.* **279,** 11521–11529 (2004).
14. Webb, B. A., Chimenti, M., Jacobson, M. P. & Barber, D. L. Dysregulated pH: a perfect storm for cancer progression. *Nat. Rev. Cancer* **11,** 671–677 (2011).
15. Schroder, C. R., Weidgans, B. M. & Klimant, I. pH Fluorosensors for use in marine systems. *The Analyst* **130,** 907–916 (2005).
16. Huber, C., Klimant, I., Krause, C. & Wolfbeis, O. S. Dual Lifetime Referencing as Applied to a Chloride Optical Sensor. *Anal Chem* **73,** 2097–2103 (2001).
17. Liebsch, G., Klimant, I., Krause, C. & Wolfbeis, O. S. Fluorescent Imaging of pH with Optical Sensors Using Time Domain Dual Lifetime Referencing. *Anal Chem* **73,** 4354–4363 (2001).
18. Borisov, S. M. & Klimant, I. Optical nanosensors-smart tools in bioanalytics. *The Analyst* **133,** 1302–1307 (2008).
19. Borisov, S. M. *et al.* Precipitation as a simple and versatile method for preparation of optical nanochemosensors. *Talanta* **79,** 1322–1330 (2009).
20. Munkholm, C., Walt, D. R., Milanovich, F. P. & Klainer, S. M. Polymer modification of fiber optic chemical sensors as a method of enhancing fluorescence signal for pH measurement. *Anal. Chem.* **58,** 1427–1430 (1986).
21. Mcdonagh, C. & Wencel, D. Sol-Gel- Derived Materials for Optical Fluorescent Ph Sensing. (2009).
22. Waich, K., Borisov, S., Mayr, T. & Klimant, I. Dual lifetime referenced trace ammonia sensors. *Sens. Actuators B Chem.* **139,** 132–138 (2009).
23. Wolfbeis, O. S., Weis, L. J., Leiner, M. J. P. & Ziegler, W. E. Fiber-optic fluorosensor for oxygen and carbon dioxide. *Anal. Chem.* **60,** 2028–2030 (1988).

24. Schutting, S., Borisov, S. M. & Klimant, I. Diketo-Pyrrolo-Pyrrole Dyes as New Colorimetric and Fluorescent pH Indicators for Optical Carbon Dioxide Sensors. *Anal. Chem.* **85,** 3271–3279 (2013).

25. Morf, W. E., Seiler, K., Rusterholz, B. & Simon, W. Design of a novel calcium-selective optode membrane based on neutral ionophores. *Anal. Chem.* **62,** 738–742 (1990).

26. De Silva, A. P. *et al.* Signaling Recognition Events with Fluorescent Sensors and Switches. *Chem. Rev.* **97,** 1515–1566 (1997).

27. Weidgans, B. M., Krause, C., Klimant, I. & Wolfbeis, O. S. Fluorescent pH sensors with negligible sensitivity to ionic strength. *The Analyst* **129,** 645–650 (2004).

28. Rink, T. J., Tsien, R. Y. & Pozzan, T. Cytoplasmic pH and free Mg2+ in lymphocytes. *J. Cell Biol.* **95,** 189–196 (1982).

29. Speake, T. & Elliott, A. C. Modulation of calcium signals by intracellular pH in isolated rat pancreatic acinar cells. *J. Physiol.* **506,** 415–430 (1998).

30. Donoso, P., Beltrán, M. & Hidalgo, C. Luminal pH Regulates Calcium Release Kinetics in Sarcoplasmic Reticulum Vesicles. *Biochemistry (Mosc.)* **35,** 13419–13425 (1996).

31. Probes Useful at Acidic pH—Section 20.3. at <http://www.lifetechnologies.com/at/en/home/references/molecular-probes-the-handbook/ph-indicators/probes-useful-at-acidic-ph.html#head2>

32. Probes Useful at Near Neutral pH—Section 20.2. at <http://www.lifetechnologies.com/at/en/home/references/molecular-probes-the-handbook/ph-indicators/probes-useful-at-near-neutral-ph.html>

33. Hirano, T., Kikuchi, K., Urano, Y., Higuchi, T. & Nagano, T. Novel Zinc Fluorescent Probes Excitable with Visible Light for Biological Applications13. *Angew. Chem. Int. Ed.* **39,** 1052–1054 (2000).

34. Tsien, R. Y. New calcium indicators and buffers with high selectivity against magnesium and protons: design, synthesis, and properties of prototype structures. *Biochemistry (Mosc.)* **19,** 2396–2404 (1980).

35. The Alexa Fluor Dye Series—Note 1.1. at <http://www.lifetechnologies.com/at/en/home/references/molecular-probes-the-handbook/technical-notes-and-product-highlights/the-alexa-fluor-dye-series.html>

36. Beija, M., Afonso, C. A. M. & Martinho, J. M. G. Synthesis and applications of Rhodamine derivatives as fluorescent probes. *Chem. Soc. Rev.* **38,** 2410–2433 (2009).

37. Kim, H. N., Lee, M. H., Kim, H. J., Kim, J. S. & Yoon, J. A new trend in rhodamine-based chemosensors: application of spirolactam ring-opening to sensing ions. *Chem. Soc. Rev.* **37,** 1465 (2008).

38. Wu, S., Li, Z., Han, J. & Han, S. Dual colored mesoporous silica nanoparticles with pH activable rhodamine-lactam for ratiometric sensing of lysosomal acidity. *Chem. Commun.* **47,** 11276–11278 (2011).

39. Yuan, L., Lin, W. & Feng, Y. A rational approach to tuning the pKa values of rhodamines for living cell fluorescence imaging. *Org. Biomol. Chem.* **9,** 1723–1726 (2011).

40. Best, Q. A., Xu, R., McCarroll, M. E., Wang, L. & Dyer, D. J. Design and Investigation of a Series of Rhodamine-Based Fluorescent Probes for Optical Measurements of pH. *Org Lett* **12,** 3219–3221 (2010).

41. Koide, Y., Urano, Y., Hanaoka, K., Terai, T. & Nagano, T. Evolution of Group 14 Rhodamines as Platforms for Near-Infrared Fluorescence Probes Utilizing Photoinduced Electron Transfer. *ACS Chem Biol* **6,** 600–608 (2011).

42. Wu, L. & Burgess, K. Synthesis and Spectroscopic Properties of Rosamines with Cyclic Amine Substituents. *J. Org. Chem.* **73,** 8711–8718 (2008).

43. Bossi, M. *et al.* Multicolor Far-Field Fluorescence Nanoscopy through Isolated Detection of Distinct Molecular Species. *Nano Lett* **8,** 2463–2468 (2008).

44. Crosby, G. A. & Demas, J. N. Measurement of photoluminescence quantum yields. Review. *J. Phys. Chem.* **75,** 991–1024 (1971).

45. Whitaker, J. E., Haugland, R. P. & Prendergast, F. G. Spectral and photophysical studies of benzo[c]xanthene dyes: Dual emission pH sensors. *Anal. Biochem.* **194,** 330–344 (1991).

46. Liu, J., Diwu, Z. & Leung, W.-Y. Synthesis and photophysical properties of new fluorinated benzo[c]xanthene dyes as intracellular pH indicators. *Bioorg. Med. Chem. Lett.* **11,** 2903–2905 (2001).

47. Grant, S. A. & Glass, R. S. A sol-gel based fiber optic sensor for local blood pH measurements. *Sens. Actuators B Chem.* **45,** 35–42 (1997).

48. Zhang, F. *et al.* Ion and pH Sensing with Colloidal Nanoparticles: Influence of Surface Charge on Sensing and Colloidal Properties. *ChemPhysChem* **11,** 730–735 (2010).

49. Borisov, S. M., Gatterer, K. & Klimant, I. Red light-excitable dual lifetime referenced optical pH sensors with intrinsic temperature compensation. *Analyst* **135,** 1711–1717 (2010).

50. Schulman, S. G. *et al.* Dependence of the fluorescence of immobilized 1-hydroxypyrene-3,6,8-trisulfonate on solution pH: Extension of the range of applicability of a pH fluorosensor. *Anal. Chim. Acta* **304,** 165–170 (1995).

51. Hakonen, A. & Hulth, S. A high-precision ratiometric fluorosensor for pH: Implementing time-dependent non-linear calibration protocols for drift compensation. *Anal. Chim. Acta* **606,** 63–71 (2008).

52. Kocincova, A. S., Borisov, S. M., Krause, C. & Wolfbeis, O. S. Fiber-Optic Microsensors for Simultaneous Sensing of Oxygen and pH, and of Oxygen and Temperature. *Anal. Chem.* **79,** 8486–8493 (2007).

53. Neurauter, G., Klimant, I. & Wolfbeis, O. S. Fiber-optic microsensor for high resolution pCO2 sensing in marine environment. *Fresenius J. Anal. Chem.* **366,** 481–487 (2000).

54. Mohr, G. J., Werner, T. & Wolfbeis, O. S. Application of a novel lipophilized fluorescent dye in an optical nitrate sensor. *J. Fluoresc.* **5,** 135–138 (1995).

55. Saleh, N., Alsoud, Y. & Nau, W. Novel fluorescent pH sensor based on coumarin with piperazine and imidazole substituents. *Spectrochim. Acta. A. Mol. Biomol. Spectrosc.* **71,** 818–822 (2008).

56. Vasylevska, A., Karasyov, A., Borisov, S. & Krause, C. Novel coumarin-based fluorescent pH indicators, probes and membranes covering a broad pH range. *Anal. Bioanal. Chem.* **387,** 2131–2141 (2007).

57. Weller, A. Electron-transfer and complex formation in the excited state. *Pure Appl. Chem.* **16,** 115–124 (1968).

58. Silva, A. P. de & Rupasinghe, R. A. D. D. A new class of fluorescent pH indicators based on photo-induced electron transfer. *J. Chem. Soc. Chem. Commun.* 1669–1670 (1985).

59. Daffy, L. M. *et al.* Arenedicarboximide Building Blocks for Fluorescent Photoinduced Electron Transfer pH Sensors Applicable with Different Media and Communication Wavelengths. *Chem. – Eur. J.* **4,** 1810–1815 (1998).

60. Silva, A. P. de, Vance, T. P., West, M. E. S. & Wright, G. D. Bright molecules with sense, logic, numeracy and utility. *Org. Biomol. Chem.* **6,** 2468–2480 (2008).

61. Bissell, R. A. *et al.* Molecular fluorescent signalling with 'fluor-spacer-receptor' systems: approaches to sensing and switching devices via supramolecular photophysics. *Chem. Soc. Rev.* **21,** 187–195 (1992).

62. Silva, A. P. de, Gunnlaugsson, T. & Rice, T. E. Recent evolution of luminescent photoinduced electron transfer sensors. A review. *The Analyst* **121,** 1759–1762 (1996).

63. Silva, A. P. de, Silva, S. A. de, Dissanayake, A. S. & Sandanayake, K. R. A. S. Compartmental fluorescent pH indicators with nearly complete predictability of indicator parameters; molecular engineering of pH sensors. *J. Chem. Soc. Chem. Commun.* 1054–1056 (1989).

64. Bissell, R. A. *et al.* Luminescence and charge transfer. Part 2. Aminomethyl anthracene derivatives as fluorescent PET (photoinduced electron transfer) sensors for protons. *J. Chem. Soc. Perkin Trans. 2* 1559–1564 (1992).

65. Silva, A. P. de *et al.* New Fluorescent Model Compounds for the Study of Photoinduced Electron Transfer: The Influence of a Molecular Electric Field in the Excited State. *Angew. Chem. Int. Ed. Engl.* **34,** 1728–1731 (1995).

66. Gareis, T., Huber, C., Wolfbeis, O. S. & Daub, J. Phenol/phenolate-dependent on/off switching of the luminescence of4,4-difluoro-4-bora-3a,4a-diaza-s-indacenes. *Chem. Commun.* 1717–1718 (1997).

67. Zhang, X.-F. Fluorescence Properties of Phenol-Modified Zinc Phthalocyanine that Tuned by Photoinduced Intra-Molecular Electron Transfer and pH Values. *J. Fluoresc.* **21,** 1559–1564 (2011).

68. Yokoi, H., Nakano, T., Fujita, W., Ishiguro, K. & Sawaki, Y. In-Cage Formation of Carbanions in Photoinduced Electron-Transfer Reaction of Carboxylate Ions. *J. Am. Chem. Soc.* **120,** 12453–12458 (1998).

69. Kohl, C., Weil, T., Qu, J. & Müllen, K. Towards Highly Fluorescent and Water-Soluble Perylene Dyes. *Chem. - Eur. J.* **10,** 5297–5310 (2004).

70. Closs, G. L. & Miller, J. R. Intramolecular Long-Distance Electron Transfer in Organic Molecules. *Science* **240,** 440–447 (1988).

71. Lewis, F. D. & Burch, E. L. Amide Conformation-Dependent Intramolecular Photoinduced Electron Transfer. *J. Am. Chem. Soc.* **116,** 1159–1160 (1994).

72. Bissell, R. A. *et al.* Fluorescent PET (photoinduced electron transfer) indicators for solvent polarity with quasi-step functional response. *Tetrahedron Lett.* **32,** 425–428 (1991).

73. Murtagh, J., Frimannsson, D. O. & O'Shea, D. F. Azide Conjugatable and pH Responsive Near-Infrared Fluorescent Imaging Probes. *Org. Lett.* **11,** 5386–5389 (2009).

74. Ireland, J. F. & Wyatt, P. A. H. in *Adv. Phys. Org. Chem.* (V. Gold) **Volume 12,** 131–221 (Academic Press, 1976).

75. Kano, K., Takenoshita, I. & Ogawa, T. Fluorescence quenching of pyrene and naphthalene in aqueous cyclodextrin solutions. Evidence of three-component complex formation. *J. Phys. Chem.* **86,** 1833–1838 (1982).

76. Baruah, M., Qin, W., Basarić, N., De Borggraeve, W. M. & Boens, N. BODIPY-Based Hydroxyaryl Derivatives as Fluorescent pH Probes. *J. Org. Chem.* **70,** 4152–4157 (2005).

77. Werner, T. *et al.* Novel optical pH-sensor based on a boradiaza-indacene derivative. *Fresenius J. Anal. Chem.* **359,** 150–154 (1997).

78. Boens, N., Leen, V. & Dehaen, W. Fluorescent indicators based on BODIPY. *Chem. Soc. Rev.* **41,** 1130–1172 (2012).

79. BODIPY Dye Series—Section 1.4. at <http://www.lifetechnologies.com/gr/en/home/references/molecular-probes-the-handbook/fluorophores-and-their-amine-reactive-derivatives/bodipy-dye-series.html>

80. Yin, L. *et al.* A dual pH and temperature responsive polymeric fluorescent sensor and its imaging application in living cells. *Chem. Commun.* **48,** 4486–4488 (2012).

81. Shen, L., Lu, X., Tian, H. & Zhu, W. A Long Wavelength Fluorescent Hydrophilic Copolymer Based on Naphthalenediimide as pH Sensor with Broad Linear Response Range. *Macromolecules* **44,** 5612–5618 (2011).

82. Tian, Y. *et al.* A series of naphthalimide derivatives as intra and extracellular pH sensors. *Biomaterials* **31,** 7411–7422 (2010).

83. Han, J. & Burgess, K. Fluorescent Indicators for Intracellular pH. *Chem. Rev.* **110,** 2709–2728 (2010).

84. Probes for Lysosomes, Peroxisomes and Yeast Vacuoles—Section 12.3. at <http://www.lifetechnologies.com/gr/en/home/references/molecular-probes-the-

handbook/probes-for-organelles/probes-for-lysosomes-peroxisomes-and-yeast-vacuoles.html>

85. Kang, J. S. & Kostov, Y. Ratiometric pH measurements using LysoSensor DND-192. *J. Biochem. Mol. Biol.* **35,** 384–388 (2002).

86. Sakai, N., Mareda, J., Vauthey, E. & Matile, S. Core-substituted naphthalenediimides. *Chem. Commun.* **46,** 4225–4237 (2010).

87. Bhosale, S. V., Jani, C. H. & Langford, S. J. Chemistry of naphthalene diimides. *Chem. Soc. Rev.* **37,** 331 (2008).

88. Banerjee, S. *et al.* Recent advances in the development of 1,8-naphthalimide based DNA targeting binders, anticancer and fluorescent cellular imaging agents. *Chem. Soc. Rev.* **42,** 1601 (2013).

89. Thalacker, C., Röger, C. & Würthner, F. Synthesis and Optical and Redox Properties of Core-Substituted Naphthalene Diimide Dyes. *J Org Chem* **71,** 8098–8105 (2006).

90. Mujumdar, R. B., Ernst, L. A., Mujumdar, S. R., Lewis, C. J. & Waggoner, A. S. Cyanine dye labeling reagents: Sulfoindocyanine succinimidyl esters. *Bioconjug. Chem.* **4,** 105–111 (1993).

91. Tang, B. *et al.* A Near-Infrared Neutral pH Fluorescent Probe for Monitoring Minor pH Changes: Imaging in Living HepG2 and HL-7702 Cells. *J. Am. Chem. Soc.* **131,** 3016–3023 (2009).

92. Song, F. *et al.* Tuning the photoinduced electron transfer in near-infrared heptamethine cyanine dyes. *Tetrahedron Lett.* **46,** 4817–4820 (2005).

93. Lee, H. *et al.* Near-Infrared pH-Activatable Fluorescent Probes for Imaging Primary and Metastatic Breast Tumors. *Bioconjug. Chem.* **22,** 777–784 (2011).

94. Xu, Y., Liu, Y. & Qian, X. Novel cyanine dyes as fluorescent pH sensors: PET, ICT mechanism or resonance effect? *J. Photochem. Photobiol. Chem.* **190,** 1–8 (2007).

95. Silva, A. P. de & Gunaratne, H. Q. N. Fluorescent PET (photoinduced electron transfer) sensors selective for submicromolar calcium with quantitatively predictable spectral and ion-binding properties. *J. Chem. Soc. Chem. Commun.* 186–188 (1990).

96. Kubo, K. & Mori, A. PET fluoroionophores for Zn2+ and Cu2+: complexation and fluorescence behavior of anthracene derivatives having diethylamine, N-methylpiperazine and N,N-bis(2-picolyl)amine units. *J. Mater. Chem.* **15,** 2902 (2005).

97. Ozmen, B. & Akkaya, E. U. Infrared fluorescence sensing of submicromolar calcium: pushing the limits of photoinduced electron transfer. *Tetrahedron Lett.* **41,** 9185–9188 (2000).

98. He, H. *et al.* A Fluorescent Chemosensor for Sodium Based on Photoinduced Electron Transfer. *Anal. Chem.* **75,** 549–555 (2003).

99. Schäferling, M. The Art of Fluorescence Imaging with Chemical Sensors. *Angew. Chem. Int. Ed.* **51,** 3532–3554 (2012).

100. Silva, A. P. de & Sandanayake, K. R. A. S. Fluorescent PET (photo-induced electron transfer) sensors for alkali metal ions with improved selectivity against protons and with predictable binding constants. *J. Chem. Soc. Chem. Commun.* 1183–1185 (1989).

101. Almutairi, A., Guillaudeu, S. J., Berezin, M. Y., Achilefu, S. & Fréchet, J. M. J. Biodegradable pH-Sensing Dendritic Nanoprobes for Near-Infrared Fluorescence Lifetime and Intensity Imaging. *J. Am. Chem. Soc.* **130,** 444–445 (2008).

102. Zhou, K. *et al.* Tunable, Ultrasensitive pH-Responsive Nanoparticles Targeting Specific Endocytic Organelles in Living Cells. *Angew. Chem. Int. Ed.* **50,** 6109–6114 (2011).

103. Langhals, H. & Pust, T. Fluorescent nano pH indicators based on supramolecular interactions. *Z. Fuer Naturforschung B J. Chem. Sci.* **65,** 291–294 (2010).

104. Schäfer, H., Ptacek, P., Kömpe, K. & Haase, M. Lanthanide-Doped NaYF4 Nanocrystals in Aqueous Solution Displaying Strong Up-Conversion Emission. *Chem. Mater.* **19,** 1396–1400 (2007).

105. Sun, L.-N., Peng, H., Stich, M. I. J., Achatz, D. & Wolfbeis, O. S. pH sensor based on upconverting luminescent lanthanide nanorods. *Chem. Commun.* 5000–5002 (2009).

106. Orte, A., Alvarez-Pez, J. M. & Ruedas-Rama, M. J. Fluorescence Lifetime Imaging Microscopy for the Detection of Intracellular pH with Quantum Dot Nanosensors. *ACS Nano* **7,** 6387–6395 (2013).

107. Tang, R., Lee, H. & Achilefu, S. Induction of pH Sensitivity on the Fluorescence Lifetime of Quantum Dots by NIR Fluorescent Dyes. *J. Am. Chem. Soc.* **134,** 4545–4548 (2012).

108. Dedecker, P., De Schryver, F. C. & Hofkens, J. Fluorescent Proteins: Shine on, You Crazy Diamond. *J. Am. Chem. Soc.* **135,** 2387–2402 (2013).

109. Tsien, R. Y. The Green Fluorescent Protein. *Annu. Rev. Biochem.* **67,** 509–544 (1998).

110. Tantama, M., Hung, Y. P. & Yellen, G. Imaging Intracellular pH in Live Cells with a Genetically Encoded Red Fluorescent Protein Sensor. *J. Am. Chem. Soc.* **133,** 10034–10037 (2011).

111. Nakabayashi, T. *et al.* pH dependence of the fluorescence lifetime of enhanced yellow fluorescent protein in solution and cells. *J. Photochem. Photobiol. Chem.* **235,** 65–71 (2012).

112. Antje Kriltz, C. L. Covalent immobilization of a fluorescent pH-sensitive naphthalimide dye in sol–gel films. *J. Sol-Gel Sci. Technol.* **63,**

113. Brown, G. J. *et al.* Solid-bound, proton-driven, fluorescent 'off–on–off' switches based on PET (photoinduced electron transfer). *Tetrahedron* **64,** 8301–8306 (2008).

114. Doussineau, T., Trupp, S. & Mohr, G. J. Ratiometric pH-nanosensors based on rhodamine-doped silica nanoparticles functionalized with a naphthalimide derivative. *J. Colloid Interface Sci.* **339,** 266–270 (2009).

115. Shi, W., He, S., Wei, M., Evans, D. G. & Duan, X. Optical pH Sensor with Rapid Response Based on a Fluorescein-Intercalated Layered Double Hydroxide. *Adv. Funct. Mater.* **20,** 3856–3863 (2010).

116. Zhang, X., Rehm, S., Safont-Sempere, M. M. & Würthner, F. Vesicular perylene dye nanocapsules as supramolecular fluorescent pH sensor systems. *Nat. Chem.* **1,** 623–629 (2009).

117. Rademacher, A., Märkle, S. & Langhals, H. Lösliche Perylen-Fluoreszenzfarbstoffe mit hoher Photostabilität. *Chem. Ber.* **115,** 2927–2934 (1982).

118. Li, C. & Wonneberger, H. Perylene Imides for Organic Photovoltaics: Yesterday, Today, and Tomorrow. *Adv. Mater.* **24,** 613–636 (2012).

119. Muellen, K., Peneva, K., Weil, T., Vosch, T. & Hofkens, J. The Rylene Colorant Family—Tailored Nanoemitters for Photonics Research and Applications. *Angew Chem Int Ed* **49,** 2–28 (2010).

120. Würthner, F. Perylene bisimide dyes as versatile building blocks for functional supramolecular architectures. *Chem. Commun.* 1564 (2004). doi:10.1039/b401630k

121. Görl, D., Zhang, X. & Würthner, F. Molecular Assemblies of Perylene Bisimide Dyes in Water. *Angew. Chem. Int. Ed.* **51,** 6328–6348 (2012).

122. Grimsdale, A. C. & Müllen, K. The Chemistry of Organic Nanomaterials. *Angew. Chem. Int. Ed.* **44,** 5592–5629 (2005).

123. Holman, M. W., Liu, R. & Adams, D. M. Single-Molecule Spectroscopy of Interfacial Electron Transfer. *J. Am. Chem. Soc.* **125,** 12649–12654 (2003).

124. Baumstark, D. & Wagenknecht, H.-A. Perylene Bisimide Dimers as Fluorescent 'Glue' for DNA and for Base-Mismatch Detection. *Angew. Chem. Int. Ed.* **47,** 2612–2614 (2008).

125. Qu, J., Kohl, C., Pottek, M. & Müllen, K. Ionic Perylenetetracarboxdiimides: Highly Fluorescent and Water-Soluble Dyes for Biolabeling. *Angew. Chem. Int. Ed.* **43,** 1528–1531 (2004).

126. Peneva, K. *et al.* Water-Soluble Monofunctional Perylene and Terrylene Dyes: Powerful Labels for Single-Enzyme Tracking. *Angew. Chem.* **120,** 3420–3423 (2008).

127. Wurthner, F. *et al.* Preparation and Characterization of Regioisomerically Pure 1,7-Disubstituted Perylene Bisimide Dyes. *J. Org. Chem.* **69,** 7933–7939 (2004).

128. Fan, L., Xu, Y. & Tian, H. 1,6-Disubstituted perylene bisimides: concise synthesis and characterization as near-infrared fluorescent dyes. *Tetrahedron Lett.* **46,** 4443–4447 (2005).

129. Avlasevich, Y., Li, C. & Mullen, K. Synthesis and applications of core-enlarged perylene dyes. *J. Mater. Chem.* **20,** 3814–3826 (2010).

130. Nolde, F. *et al.* Synthesis and Modification of Terrylenediimides as High-Performance Fluorescent Dyes. *Chem. - Eur. J.* **11,** 3959–3967 (2005).

131. Langhals, H., Esterbauer, A. J. & Kinzel, S. Red shining silica: macroscopic pigments and nanoparticles by silylation. *New J. Chem.* **33,** 1829 (2009).

132. Hao, Z. & Iqbal, A. Some aspects of organic pigments. *Chem. Soc. Rev.* **26,** 203–213 (1997).

133. Bijleveld, J. C. *et al.* Poly(diketopyrrolopyrrole–terthiophene) for Ambipolar Logic and Photovoltaics. *J. Am. Chem. Soc.* **131,** 16616–16617 (2009).

134. Walker, B. *et al.* Nanoscale Phase Separation and High Photovoltaic Efficiency in Solution-Processed, Small-Molecule Bulk Heterojunction Solar Cells. *Adv. Funct. Mater.* **19,** 3063–3069 (2009).

135. Guo, E. Q., Ren, P. H., Zhang, Y. L., Zhang, H. C. & Yang, W. J. Diphenylamine end-capped 1,4-diketo-3,6-diphenylpyrrolo[3,4-c]pyrrole (DPP) derivatives with large two-photon absorption cross-sections and strong two-photon excitation red fluorescence. *Chem. Commun.* 5859–5861 (2009).

136. Fischer, G. M., Daltrozzo, E. & Zumbusch, A. Selektive Nah-Infrarot-Chromophore: Bis(pyrrolopyrrol)-Cyanine. *Angew. Chem.* **123,** 1442–1445 (2011).

137. Fischer, G. M., Isomäki-Krondahl, M., Göttker-Schnetmann, I., Daltrozzo, E. & Zumbusch, A. Pyrrolopyrrole Cyanine Dyes: A New Class of Near-Infrared Dyes and Fluorophores. *Chem. - Eur. J.* **15,** 4857–4864 (2009).

138. Sreejith, S., Carol, P., Chithra, P. & Ajayaghosh, A. Squaraine dyes: a mine of molecular materials. *J. Mater. Chem.* **18,** 264–274 (2008).

139. Sprenger, H.-E. & Ziegenbein, W. Cyclobutendiylium-Farbstoffe. *Angew. Chem.* **80,** 541–546 (1968).

140. Law, K.-Y. & Bailey, F. C. Squaraine Chemistry: Synthesis, Characterization and Xerographic Properties of Bis(4-methylbenzylaminophenyl)-squaraine and Its Derivatives. *Dyes Pigments* **9,** 85–107 (1988).

141. Law, K.-Y. Squaraine Chemistry. Absorption, Fluorescence Emission, and Photophysics of Unsymmetrical Squaraines. *J. Phys. Chem.* **99,** 9818–9824 (1995).

142. Isgor, Y. G. & Akkaya, E. U. Chemosensing in deep red: A squaraine-based fluorescent chemosensor for pH. *Tetrahedron Lett.* **38,** 7417–7420 (1997).

143. Xue, L. *et al.* Carboxylate-modified squaraine dye doped silica fluorescent pH nanosensors. *Nanotechnology* **21,** 215502 (2010).

144. McDonnell, S. O. & O'Shea, D. F. Near-Infrared Sensing Properties of Dimethlyamino-Substituted BF2–Azadipyrromethenes. *Org. Lett.* **8,** 3493–3496 (2006).

145. Jokic, T. *et al.* Highly Photostable Near-Infrared Fluorescent pH Indicators and Sensors Based on BF2-Chelated Tetraarylazadipyrromethene Dyes. *Anal. Chem.* **84,** 6723–6730 (2012).

146. Zhao, W. & Carreira, E. M. Conformationally Restricted Aza-BODIPY: Highly Fluorescent, Stable Near-Infrared Absorbing Dyes. *Chem. – Eur. J.* **12,** 7254–7263 (2006).

147. Umezawa, K., Nakamura, Y., Makino, H., Citterio, D. & Suzuki, K. Bright, Color-Tunable Fluorescent Dyes in the Visible–Near-Infrared Region. *J. Am. Chem. Soc.* **130,** 1550–1551 (2008).

148. Awuah, S. G., Polreis, J., Biradar, V. & You, Y. Singlet Oxygen Generation by Novel NIR BODIPY Dyes. *Org. Lett.* **13,** 3884–3887 (2011).

149. Jagdeo, J. R., Adams, L. E., Brody, N. I. & Siegel, D. M. Transcranial red and near infrared light transmission in a cadaveric model. *PloS One* **7,** e47460 (2012).

150. Allard, E. & Larpent, C. Core-shell type dually fluorescent polymer nanoparticles for ratiometric pH-sensing. *J. Polym. Sci. Part Polym. Chem.* **46,** 6206–6213 (2008).

151. McNamara, K. P. *et al.* Synthesis, Characterization, and Application of Fluorescence Sensing Lipobeads for Intracellular pH Measurements. *Anal. Chem.* **73,** 3240–3246 (2001).

152. Strömberg, N., Mattsson, E. & Hakonen, A. An imaging pH optode for cell studies based on covalent attachment of 8-hydroxypyrene-1,3,6-trisulfonate to amino cellulose acetate films. *Anal. Chim. Acta* **636,** 89–94 (2009).

153. Borisov, S. M., Herrod, D. L. & Klimant, I. Fluorescent poly(styrene-block-vinylpyrrolidone) nanobeads for optical sensing of pH. *Sens. Actuators B Chem.* **139,** 52–58 (2009).

154. Opitz, N. & Lübbers, D. W. New fluorescence photometrical techniques for simultaneous and continuous measurements of ionic strength and hydrogen ion activities. *Sens. Actuators* **4,** 473–479 (1983).

155. Parker, J. W. *et al.* Fiber-optic sensors for pH and carbon dioxide using a self-referencing dye. *Anal. Chem.* **65,** 2329–2334 (1993).

156. Xu, Z., Rollins, A., Alcala, R. & Marchant, R. E. A novel fiber-optic pH sensor incorporating carboxy SNAFL-2 and fluorescent wavelength-ratiometric detection. *J. Biomed. Mater. Res.* **39,** 9–15 (1998).

157. Kuwana, E., Liang, F. & Sevick-Muraca, E. M. Fluorescence Lifetime Spectroscopy of a pH-Sensitive Dye Encapsulated in Hydrogel Beads. *Biotechnol. Prog.* **20,** 1561–1566 (2004).

158. Mes, G. F., Van Ramesdonk, H. J. & Verhoeven, J. W. Photoinduced electron transfer in polychromophoric systems. 2. Protonation directed switching between tri- and bichromophoric interaction. *J. Am. Chem. Soc.* **106,** 1335–1340 (1984).

159. Li, Z.-Z. *et al.* A novel fluorescence ratiometric pH sensor based on covalently immobilized piperazinyl-1,8-napthalimide and benzothioxanthene. *Sens. Actuators B Chem.* **114,** 308–315 (2006).

160. Trupp, S., Hoffmann, P., Henkel, T. & Mohr, G. J. Novel pH indicator dyes for array preparation via NHS ester activation or solid-phase organic synthesis. *Org. Biomol. Chem.* **6,** 4319 (2008).

161. Niu, C.-G., Zeng, G.-M., Chen, L.-X., Shen, G.-L. & Yu, R.-Q. Proton 'off-on' behaviour of methylpiperazinyl derivative of naphthalimide: a pH sensor based on fluorescence enhancement. *Analyst* **129,** 20–24 (2004).

162. Golchini, K. *et al.* Synthesis and characterization of a new fluorescent probe for measuring potassium. *Amer J Phys* **258,** 438–443 (1990).

163. Pearson, A. J. & Xiao, W. Fluorescence and NMR Binding Studies of N-Aryl-N'-(9-methylanthryl)diaza-18-crown-6 Derivatives. *J. Org. Chem.* **68,** 5369–5376 (2003).

164. Zhang, Z. *et al.* Visible Study of Mercuric Ion and Its Conjugate in Living Cells of Mammals and Plants. *Chem. Res. Toxicol.* **18,** 1814–1820 (2005).

165. Lee, J. H., Jeong, A. R., Shin, I.-S., Kim, H.-J. & Hong, J.-I. Fluorescence Turn-On Sensor for Cyanide Based on a Cobalt(II)–Coumarinylsalen Complex. *Org. Lett.* **12,** 764–767 (2010).

166. Langhals, H., Ismael, R. & Yürük, O. Persistent Fluorescence of Perylene Dyes by Steric Inhibition of Aggregation. *Tetrahedron* **56,** 5435–5441 (2000).

167. Seybold, G. & Wagenblast, G. New perylene and violanthrone dyestuffs for fluorescent collectors. *Dyes Pigments* **11,** 303–317 (1989).

168. Chiu, T.-L. *et al.* Low reflection and photo-sensitive organic light-emitting device with perylene diimide and double-metal structure. *Thin Solid Films* **517,** 3712–3716 (2009).

169. Breeze, A. J. *et al.* Polymer---perylene diimide heterojunction solar cells. *Appl. Phys. Lett.* **81,** 3085–3087 (2002).

170. Reisfeld, R., Yariv, E. & Minti, H. New developments in solid state lasers. *Opt. Mater.* **8,** 31–36 (1997).

171. Qiu, W., Chen, S., Sun, X., Liu, Y. & Zhu, D. Suzuki Coupling Reaction of 1,6,7,12-Tetrabromoperylene Bisimide. *Org. Lett.* **8,** 867–870 (2006).

172. Rehm, S., Stepanenko, V., Zhang, X., Rehm, T. H. & Würthner, F. Spermine-Functionalized Perylene Bisimide Dyes-Highly Fluorescent Bola-Amphiphiles in Water. *Chem. - Eur. J.* **16,** 3372–3382 (2010).

173. Schnurpfeil, G., Stark, J. & Wöhrle, D. Syntheses of uncharged, positively and negatively charged 3,4,9,10-perylene-bis(dicarboximides). *Dyes Pigments* **27,** 339–350 (1995).

174. Avlasevich, Y., Müller, S., Erk, P. & Müllen, K. Novel Core-Expanded Rylenebis(Dicarboximide) Dyes Bearing Pentacene Units: Facile Synthesis and Photophysical Properties. *Chem. - Eur. J.* **13,** 6555–6561 (2007).

175. Weil, T., Abdalla, M. A., Jatzke, C., Hengstler, J. & Mullen, K. Water-Soluble Rylene Dyes as High-Performance Colorants for the Staining of Cells. *Biomacromolecules* **6,** 68–79 (2005).

176. Ren, T. *et al.* A Simple and Versatile Route to Stable Quantum Dot–Dye Hybrids in Nonaqueous and Aqueous Solutions. *J. Am. Chem. Soc.* **130,** 17242–17243 (2008).

177. Wang, E. *et al.* Optical films for protamine detection with lipophilic dichlorofluorescein derivatives. *Anal. Chim. Acta* **334,** 139–147 (1996).

178. Langhals, H., Demmig, S. & Huber, H. Rotational barriers in perylene fluorescent dyes. *Spectrochim. Acta Part Mol. Spectrosc.* **44,** 1189–1193 (1988).

179. Kaiser, H., Lindner, J. & Langhals, H. Synthese von nichtsymmetrisch substituierten Perylen-Fluoreszenzfarbstoffen. *Chem. Ber.* **124,** 529–535 (1991).

180. Tröster, H. Untersuchungen zur Protonierung von Perylen-3,4,9,10-tetracarbonsäurealkalisalzen. *Dyes Pigments* **4,** 171–177 (1983).

181. Baffreau, J., Leroy-Lhez, S., Vân Anh, N., Williams, R. M. & Hudhomme, P. Fullerene C_{60}-Perylene-3,4:9,10-bis(dicarboximide) Light-Harvesting Dyads: Spacer-Length and Bay-Substituent Effects on Intramolecular Singlet and Triplet Energy Transfer. *Chem. - Eur. J.* **14,** 4974–4992 (2008).

182. Langhals, H., Jaschke, H., Bastani-Oskoui, H. & Speckbacher, M. Perylene Dyes with High Resistance to Alkali. *Eur. J. Org. Chem.* **2005,** 4313–4321 (2005).

183. Langhals, H., Krotz, O., Polborn, K. & Mayer, P. A Novel Fluorescent Dye with Strong, Anisotropic Solid-State Fluorescence, Small Stokes Shift, and High Photostability. *Angew. Chem. Int. Ed.* **44,** 2427–2428 (2005).

184. Holtrup, F. O. *et al.* Terrylenimides: New NIR Fluorescent Dyes. *Chem. - Eur. J.* **3,** 219–225 (1997).

185. Avlasevich, Y. & Müllen, K. Dibenzopentarylenebis(dicarboximide)s: Novel near-infrared absorbing dyes. *Chem. Commun.* 4440 (2006).

186. Queste, M., Cadiou, C., Pagoaga, B., Giraudet, L. & Hoffmann, N. Synthesis and characterization of 1,7-disubstituted and 1,6,7,12-tetrasubstituted perylenetetracarboxy-3,4:9,10-diimide derivatives. *New J. Chem.* **34,** 2537 (2010).

187. Quante, H., Geerts, Y. & Mullen, K. Synthesis of Soluble Perylenebisamidine Derivatives. Novel Long-Wavelength Absorbing and Fluorescent Dyes. *Chem. Mater.* **9,** 495–500 (1997).

188. Oh, S. H. *et al.* The synthesis of symmetric and asymmetric perylene derivatives and their optical properties. *Dyes Pigments* **85,** 37–42 (2010).

189. Cox, R. P. *et al.* A new fluorescent H+ sensor based on core-substituted naphthalene diimide. *Chem. Phys. Lett.* **521,** 59–63 (2012).

190. Zhao, Y. & Wasielewski, M. R. 3,4:9,10-Perylenebis(dicarboximide) chromophores that function as both electron donors and acceptors. *Tetrahedron Lett.* **40,** 7047–7050 (1999).

191. Feng, J. *et al.* Structural and property comparison between the di-piperidinyl- and di-pyrrolidinyl-substituted perylene tetracarboxylic diimides. *J. Phys. Org. Chem.* **24,** 621–629 (2011).

192. Dubey, R. K., Efimov, A. & Lemmetyinen, H. 1,7- And 1,6-Regioisomers of Diphenoxy and Dipyrrolidinyl Substituted Perylene Diimides: Synthesis, Separation, Characterization, and Comparison of Electrochemical and Optical Properties. *Chem. Mater.* **23,** 778–788 (2011).

193. Alvino, A. *et al.* Synthesis and spectroscopic properties of highly water-soluble perylene derivatives. *Tetrahedron* **63,** 7858–7865 (2007).

194. Tsai, H.-Y. & Chen, K.-Y. 1,7-Diaminoperylene bisimides: Synthesis, optical and electrochemical properties. *Dyes Pigments* **96,** 319–327 (2013).

195. Husár, B. & Liska, R. Vinyl carbonates, vinyl carbamates, and related monomers: synthesis, polymerization, and application. *Chem. Soc. Rev.* **41,** 2395 (2012).

196. Borisov, S. M., Gatterer, K., Bitschnau, B. & Klimant, I. Preparation and Characterization of Chromium(III)-Activated Yttrium Aluminum Borate: A New Thermographic Phosphor for Optical Sensing and Imaging at Ambient Temperatures. *J. Phys. Chem. C* **114,** 9118–9124 (2010).

197. Sens, R. & Drexhage, K. H. Fluorescence quantum yield of oxazine and carbazine laser dyes. *J. Lumin.* **24–25, Part 2,** 709–712 (1981).

198. Kermis, H. R., Kostov, Y. & Rao, G. Rapid method for the preparation of a robust optical pH sensor. *Analyst* **128,** 1181–1186 (2003).

199. Chan, Y.-H. *et al.* Development of Ultrabright Semiconducting Polymer Dots for Ratiometric pH Sensing. *Anal Chem* **83,** 1448–1455 (2011).

200. Medina-Castillo, A. L., Fernandez-Sanchez, J. F., Segura-Carretero, A. & Fernandez-Gutierrez, A. Design and synthesis by ATRP of novel, water-insoluble, lineal copolymers and their application in the development of fluorescent and pH-sensing nanofibres made by electrospinning. *J. Mater. Chem.* **21,** 6742–6750 (2011).

201. Aslan, K., Lakowicz, J. R., Szmacinski, H. & Geddes, C. D. Enhanced Ratiometric pH Sensing Using SNAFL-2 on Silver Island Films: Metal-enhanced Fluorescence Sensing. *J. Fluoresc.* **15,** 37–40 (2005).

202. Yang, H. *et al.* Silica-Coated Manganese Oxide Nanoparticles as a Platform for Targeted Magnetic Resonance and Fluorescence Imaging of Cancer Cells. *Adv. Funct. Mater.* **20,** 1733–1741 (2010).

203. Wang, H. *et al.* Rhodamine-based highly sensitive colorimetric off-on fluorescent chemosensor for Hg2+ in aqueous solution and for live cell imaging. *Org. Biomol. Chem.* **9,** 2850–2855 (2011).

204. Li, L. *et al.* Quantitative Counting of Single Fluorescent Molecules by Combined Electrochemical Adsorption Accumulation and Total Internal Reflection Fluorescence Microscopy. *Anal Chem* **80,** 3999–4006 (2008).

205. Quitevis, E. L., Marcus, A. H. & Fayer, M. D. Dynamics of ionic lipophilic probes in micelles: picosecond fluorescence depolarization measurements. *J Phys Chem* **97,** 5762–5769 (1993).

206. Prazeres, T. J. V., Fedorov, A. & Martinho, J. M. G. Dynamics of Oligonucleotides Adsorbed on Thermosensitive Core–Shell Latex Particles. *J Phys Chem B* **108,** 9032–9041 (2004).

207. Bossi, M., Belov, V., Polyakova, S. & Hell, S. W. Reversible Red Fluorescent Molecular Switches. *Angew. Chem. Int. Ed.* **45,** 7462–7465 (2006).

208. Shiraishi, Y., Miyamoto, R., Zhang, X. & Hirai, T. Rhodamine-Based Fluorescent Thermometer Exhibiting Selective Emission Enhancement at a Specific Temperature Range. *Org Lett* **9,** 3921–3924 (2007).

209. Soh, J. H. *et al.* Rhodamine urea derivatives as fluorescent chemosensors for Hg2+. *Tetrahedron Lett.* **48,** 5966–5969 (2007).

210. Yang, Y.-K., Yook, K.-J. & Tae, J. A Rhodamine-Based Fluorescent and Colorimetric Chemodosimeter for the Rapid Detection of Hg2+ Ions in Aqueous Media. *J Am Chem Soc* **127,** 16760–16761 (2005).

211. Dujols, V., Ford, F. & Czarnik, A. W. A Long-Wavelength Fluorescent Chemodosimeter Selective for Cu(II) Ion in Water. *J Am Chem Soc* **119,** 7386–7387 (1997).

212. Xiang, Y. & Tong, A. A New Rhodamine-Based Chemosensor Exhibiting Selective FeIII-Amplified Fluorescence. *Org Lett* **8,** 1549–1552 (2006).

213. Kwon, J. Y. *et al.* A Highly Selective Fluorescent Chemosensor for Pb2+. *J Am Chem Soc* **127,** 10107–10111 (2005).

214. Tang, B. *et al.* A Rhodamine-Based Fluorescent Probe Containing a Se–N Bond for Detecting Thiols and Its Application in Living Cells. *J Am Chem Soc* **129,** 11666–11667 (2007).

215. Li, Z., Wu, S., Han, J. & Han, S. Imaging of intracellular acidic compartments with a sensitive rhodamine based fluorogenic pH sensor. *Analyst* **136,** 3698–3706 (2011).

216. Wu, S., Li, Z., Han, J. & Han, S. Dual colored mesoporous silica nanoparticles with pH activable rhodamine-lactam for ratiometric sensing of lysosomal acidity. *Chem. Commun.* **47,** 11276–11278 (2011).

217. Zhang, W. *et al.* A highly sensitive acidic pH fluorescent probe and its application to HepG2 cells. *Analyst* **134,** 367–371 (2009).

218. Misra, V., Mishra, H., Joshi, H. C. & Pant, T. C. An optical pH sensor based on excitation energy transfer in Nafion® film. *Sens. Actuators B Chem.* **82,** 133–141 (2002).

219. Misra, V., Mishra, H., Joshi, H. C. & Pant, T. C. Excitation energy transfer between acriflavine and rhodamine 6G as a pH sensor. *Sens. Actuators B Chem.* **63,** 18–23 (2000).

220. Becer, C. R. *et al.* Clicking Pentafluorostyrene Copolymers: Synthesis, Nanoprecipitation, and Glycosylation. *Macromolecules* **42,** 2387–2394 (2009).

221. Becer, C. R., Hoogenboom, R. & Schubert, U. S. Click Chemistry beyond Metal-Catalyzed Cycloaddition. *Angew. Chem. Int. Ed.* **48,** 4900–4908 (2009).

222. Samaroo, D., Vinodu, M., Chen, X. & Drain, C. M. meso-Tetra(pentafluorophenyl)porphyrin as an Efficient Platform for Combinatorial Synthesis and the Selection of New Photodynamic Therapeutics using a Cancer Cell Line. *J Comb Chem* **9,** 998–1011 (2007).

223. Vives, G. *et al.* Facile functionalization of a fully fluorescent perfluorophenyl BODIPY: photostable thiol and amine conjugates. *Chem. Commun.* (2011).

224. Figueira, A. C. B., de Oliveira, K. T. & Serra, O. A. New porphyrins tailored as biodiesel fluorescent markers. *Dyes Pigments* **91,** 383–388 (2011).

225. Kubin, R. F. & Fletcher, A. N. Fluorescence quantum yields of some rhodamine dyes. *J. Lumin.* **27,** 455–462 (1982).

226. Öztürk, N., Akgöl, S., ArIsoy, M. & Denizli, A. Reversible adsorption of lipase on novel hydrophobic nanospheres. *Sep. Purif. Technol.* **58,** 83–90 (2007).

227. Janata, J. Do optical sensors really measure pH? *Anal. Chem.* **59,** 1351–1356 (1987).

228. Gao, F., Wang, L., Tang, L. & Zhu, C. A Novel Nano-Sensor Based on Rhodamine-β-Isothiocyanate – Doped Silica Nanoparticle for pH Measurement. *Microchim. Acta* **152,** 131–135 (2005).

229. Kühl, M. & Polerecky, L. Functional and structural imaging of phototrophic microbial communities and symbioses. *Aquat. Microb. Ecol.* **53,** 99–118 (2008).

230. Stahl, H. *et al.* Time-resolved pH imaging in marine sediments with a luminescent planar optode. *Limnol. Oceanogr. Methods* **4,** 336–345 (2006).

231. Hulth, S., Aller, R. C., Engström, P. & Selander, E. A pH plate fluorosensor (optode) for early diagenetic studies of marine sediments. *Limnol. Oceanogr.* **47,** 212–220 (2002).

232. Baki, C. N. & Akkaya, E. U. Boradiazaindacene-Appended Calix[4]arene: Fluorescence Sensing of pH Near Neutrality. *J. Org. Chem.* **66,** 1512–1513 (2001).

233. Potrawa, T. & Langhals, H. Fluoreszenzfarbstoffe mit großen Stokes-Shifts – lösliche Dihydropyrrolopyrroldione. *Chem. Ber.* **120,** 1075–1078 (1987).

234. Herbst, W. & Hunger, K. *Industrial Organic Pigments*. (Wiley VCH, 2004).

235. Luňák Jr., S. *et al.* Absorption and fluorescence of soluble polar diketo-pyrrolo-pyrroles. *Dyes Pigments* **91,** 269–278 (2011).

236. Luňák Jr., S., Vyňuchal, J., Vala, M., Havel, L. & Hrdina, R. The synthesis, absorption and fluorescence of polar diketo-pyrrolo-pyrroles. *Dyes Pigments* **82,** 102–108 (2009).

237. Zambounis, J. S., Hao, Z. & Iqbal, A. Latent pigments activated by heat. *Nature* **388,** 131–132 (1997).

238. Zhu, Y., Rabindranath, A. R., Beyerlein, T. & Tieke, B. Highly Luminescent 1,4-Diketo-3,6-diphenylpyrrolo[3,4-c]pyrrole- (DPP-) Based Conjugated Polymers Prepared Upon Suzuki Coupling. *Macromolecules* **40,** 6981–6989 (2007).

239. Zhang, K. & Tieke, B. Highly Luminescent Polymers Containing the 2,3,5,6-Tetraarylated Pyrrolo[3,4-c]pyrrole-1,4-dione (N-Aryl DPP) Chromophore in the Main Chain. *Macromolecules* **41,** 7287–7295 (2008).

240. Tantiwiwat, M., Tamayo, A., Luu, N., Dang, X.-D. & Nguyen, T.-Q. Oligothiophene Derivatives Functionalized with a Diketopyrrolopyrrolo Core for Solution-Processed Field Effect Transistors: Effect of Alkyl Substituents and Thermal Annealing. *J. Phys. Chem. C* **112,** 17402–17407 (2008).

241. Bürgi, L. *et al.* High-Mobility Ambipolar Near-Infrared Light-Emitting Polymer Field-Effect Transistors. *Adv. Mater.* **20,** 2217–2224 (2008).

242. Wienk, M. M., Turbiez, M., Gilot, J. & Janssen, R. A. J. Narrow-Bandgap Diketo-Pyrrolo-Pyrrole Polymer Solar Cells: The Effect of Processing on the Performance. *Adv. Mater.* **20,** 2556–2560 (2008).

243. Zou, Y. *et al.* A High-Mobility Low-Bandgap Poly(2,7-carbazole) Derivative for Photovoltaic Applications. *Macromolecules* **42,** 2891–2894 (2009).

244. Jiang, Y. *et al.* Synthesis and two-photon absorption properties of hyperbranched diketo-pyrrolo-pyrrole polymer with triphenylamine as the core. *J. Polym. Sci. Part Polym. Chem.* **47,** 4400–4408 (2009).

245. Qu, Y., Hua, J. & Tian, H. Colorimetric and Ratiometric Red Fluorescent Chemosensor for Fluoride Ion Based on Diketopyrrolopyrrole. *Org. Lett.* **12,** 3320–3323 (2010).

246. Jeong, Y.-H., Lee, C.-H. & Jang, W.-D. A Diketopyrrolopyrrole-Based Colorimetric and Fluorescent Probe for Cyanide Detection. *Chem. – Asian J.* **7,** 1562–1566 (2012).

247. Deng, L. *et al.* Colorimetric and Ratiometric Fluorescent Chemosensor Based on Diketopyrrolopyrrole for Selective Detection of Thiols: An Experimental and Theoretical Study. *J. Org. Chem.* **76,** 9294–9304 (2011).

248. Mizuguchi, J., Imoda, T., Takahashi, H. & Yamakami, H. Polymorph of 1,4-diketo-3,6-bis-(4′-dipyridyl)-pyrrolo-[3,4-c]pyrrole and their hydrogen bond network: A material for H2 gas sensor. *Dyes Pigments* **68,** 47–52 (2006).

249. Yamagata, T., Kuwabara, J. & Kanbara, T. Synthesis of highly fluorescent diketopyrrolopyrrole derivative and two-step response of fluorescence to acid. *Tetrahedron Lett.* **51,** 1596–1599 (2010).

250. Thakur, M., Thakur, A., Khadikar, P. V. & Supuran, C. T. QSAR study on pKa vis-à-vis physiological activity of sulfonamides: a dominating role of surface tension (inverse steric parameter). *Bioorg. Med. Chem. Lett.* **15,** 203–209 (2005).

251. Caltagirone, C., Bates, G. W., Gale, P. A. & Light, M. E. Anion binding vs. sulfonamide deprotonation in functionalised ureas. *Chem. Commun.* 61–63 (2007).

252. Larsen, M., Borisov, S. M., Grunwald, B., Klimant, I. & Glud, R. N. A simple and inexpensive high resolution color ratiometric planar optode imaging approach: application to oxygen and pH sensing. *Limnol. Oceanogr. METHODS* **9,** 348–360 (2011).

253. Meier, R. J., Fischer, L. H., Wolfbeis, O. S. & Schäferling, M. Referenced luminescent sensing and imaging with digital color cameras: A comparative study. *Sens. Actuators B Chem.* **177,** 500–506 (2013).

254. Wang, X. *et al.* Self-referenced RGB colour imaging of intracellular oxygen. *Chem. Sci.* **2,** 901 (2011).

255. Jezierski, S., Belder, D. & Nagl, S. Microfluidic free-flow electrophoresis chips with an integrated fluorescent sensor layer for real time pH imaging in isoelectric focusing. *Chem. Commun.* **49,** 904–906 (2013).

256. Pischel, U. Chemical Approaches to Molecular Logic Elements for Addition and Subtraction. *Angew. Chem. Int. Ed.* **46,** 4026–4040 (2007).

257. Silva, A. P. de & Uchiyama, S. Molecular logic and computing. *Nat. Nanotechnol.* **2,** 399–410 (2007).

258. Credi, A. Molecules That Make Decisions. *Angew. Chem. Int. Ed.* **46,** 5472–5475 (2007).

259. Kaake, L. G. *et al.* Photoinduced Charge Generation in a Molecular Bulk Heterojunction Material. *J. Am. Chem. Soc.* **134,** 19828–19838 (2012).

260. Grätzel, M. Recent Advances in Sensitized Mesoscopic Solar Cells. *Acc. Chem. Res.* **42,** 1788–1798 (2009).

261. Jeong, Y. & Yoon, J. Recent progress on fluorescent chemosensors for metal ions. *Inorganica Chim. Acta* **381,** 2–14 (2012).

262. Bozdemir, O. A. *et al.* Selective Manipulation of ICT and PET Processes in Styryl-Bodipy Derivatives: Applications in Molecular Logic and Fluorescence Sensing of Metal Ions. *J. Am. Chem. Soc.* **132,** 8029–8036 (2010).

263. Mbatia, H. W. & Burdette, S. C. Photochemical Tools for Studying Metal Ion Signaling and Homeostasis. *Biochemistry (Mosc.)* **51,** 7212–7224 (2012).

264. Qin, W., Baruah, M., De Borggraeve, W. M. & Boens, N. Photophysical properties of an on/off fluorescent pH indicator excitable with visible light based on a borondipyrromethene-linked phenol. *J. Photochem. Photobiol. Chem.* **183,** 190–197 (2006).

265. Sun, K. M., McLaughlin, C. K., Lantero, D. R. & Manderville, R. A. Biomarkers for Phenol Carcinogen Exposure Act as pH-Sensing Fluorescent Probes. *J. Am. Chem. Soc.* **129,** 1894–1895 (2007).

266. Aigner, D. *et al.* Fluorescent materials for pH sensing and imaging based on novel 1,4-diketopyrrolo-[3,4-c]pyrrole dyes. *J. Mater. Chem. C* **1,** 5685–5693 (2013).

267. Aigner, D., Dmitriev, R. I., Borisov, S. M., Papkovsyky, D. B. & Klimant, I. Perylene Bisimides for FLIM-based pH Measurements in 2D and 3D Cell Models. *J Mater Chem B* **In preparation,**

268. Aigner, D., Borisov, S. M., Petritsch, P. & Klimant, I. Novel near infra-red fluorescent pH sensors based on 1-aminoperylene bisimides covalently grafted onto poly(acryloylmorpholine). *Chem. Commun.* **49,** 2139–2141 (2013).

269. Lin, H.-J., Herman, P., Kang, J. S. & Lakowicz, J. R. Fluorescence Lifetime Characterization of Novel Low-pH Probes. *Anal. Biochem.* **294,** 118–125 (2001).

270. Aigner, D., Borisov, S. M. & Klimant, I. New fluorescent perylene bisimide indicators—a platform for broadband pH optodes. *Anal. Bioanal. Chem.* **400,** 2475–2485 (2011).

271. Mills, A., Lepre, A. & Wild, L. Breath-by-breath measurement of carbon dioxide using a plastic film optical sensor. *Sens. Actuators B Chem.* **39,** 419–425 (März).

272. Walkup, G. K., Burdette, S. C., Lippard, S. J. & Tsien, R. Y. A New Cell-Permeable Fluorescent Probe for Zn $^{2+}$. *J. Am. Chem. Soc.* **122,** 5644–5645 (2000).

273. Ford, W. E. & Kamat, P. V. Photochemistry of 3,4,9,10-perylenetetracarboxylic dianhydride dyes. 3. Singlet and triplet excited-state properties of the bis(2,5-di-tert-butylphenyl)imide derivative. *J. Phys. Chem.* **91,** 6373–6380 (1987).

274. Graboski, Z. R. & Dobkowski, J. Twisted intramolecular charge transfer (TICT) excited states: Energy and molecular structure. *Pure Appl. Chem.* **55,** 245 (1983).

275. Aigner, D. *et al.* New fluorescent pH sensors based on covalently linkable PET rhodamines. *Talanta* **99,** 194–201 (2012).

276. Bard, A. J. & Faulkner, L. R. *Electrochemical Methods: Fundamentals and Applications.* (John Wiley & Sons, 2001).

277. Llopis, J., McCaffery, J. M., Miyawaki, A., Farquhar, M. G. & Tsien, R. Y. Measurement of cytosolic, mitochondrial, and Golgi pH in single living cells with green fluorescent proteins. *Proc. Natl. Acad. Sci.* **95,** 6803–6808 (1998).

278. Shin, J. M., Munson, K., Vagin, O. & Sachs, G. The gastric HK-ATPase: structure, function, and inhibition. *Pflugers Arch.* **457,** 609–622 (2009).

279. Numata, M. & Orlowski, J. Molecular Cloning and Characterization of a Novel (Na+,K+)/H+ Exchanger Localized to the trans-Golgi Network. *J. Biol. Chem.* **276,** 17387–17394 (2001).

280. Pérez-Sala, D., Collado-Escobar, D. & Mollinedo, F. Intracellular Alkalinization Suppresses Lovastatin-induced Apoptosis in HL-60 Cells through the Inactivation of a pH-dependent Endonuclease. *J. Biol. Chem.* **270,** 6235–6242 (1995).

281. Maxfield, F. R. & McGraw, T. E. Endocytic recycling. *Nat. Rev. Mol. Cell Biol.* **5,** 121–132 (2004).

282. Gruenberg, J. & Stenmark, H. The biogenesis of multivesicular endosomes. *Nat. Rev. Mol. Cell Biol.* **5,** 317–323 (2004).

283. Chin, E. R. & Allen, D. G. The contribution of pH-dependent mechanisms to fatigue at different intensities in mammalian single muscle fibres. *J. Physiol.* **512,** 831–840 (1998).

284. Chesler, M. Regulation and Modulation of pH in the Brain. *Physiol. Rev.* **83,** 1183–1221 (2003).

285. Deitmer, J. W. & Rose, C. R. pH regulation and proton signalling by glial cells. *Prog. Neurobiol.* **48,** 73–103 (1996).

286. Wang, W., Bradley, S. R. & Richerson, G. B. Quantification of the response of rat medullary raphe neurones to independent changes in pH and PCO2. *J. Physiol.* **540,** 951–970 (2002).

287. Powe, A. M. *et al.* Molecular Fluorescence, Phosphorescence, and Chemiluminescence Spectrometry. *Anal. Chem.* **82,** 4865–4894 (2010).

288. Shcherbakova, D. M., Subach, O. M. & Verkhusha, V. V. Red Fluorescent Proteins: Advanced Imaging Applications and Future Design. *Angew. Chem. Int. Ed.* **51,** 10724–10738 (2012).

289. Nienhaus, K. & Nienhaus, G. U. Fluorescent proteins for live-cell imaging with super-resolution. *Chem. Soc. Rev.* (2013).

290. Burns, A., Sengupta, P., Zedayko, T., Baird, B. & Wiesner, U. Core/Shell Fluorescent Silica Nanoparticles for Chemical Sensing: Towards Single-Particle Laboratories13. *Small* **2,** 723–726 (2006).

291. Jensen, E. C. Use of Fluorescent Probes: Their Effect on Cell Biology and Limitations. *Anat. Rec. Adv. Integr. Anat. Evol. Biol.* **295,** 2031–2036 (2012).

292. Giepmans, B. N. G., Adams, S. R., Ellisman, M. H. & Tsien, R. Y. The Fluorescent Toolbox for Assessing Protein Location and Function. *Science* **312,** 217–224 (2006).

293. Singh, R. & Nalwa, H. S. Medical Applications of Nanoparticles in Biological Imaging, Cell Labeling, Antimicrobial Agents, and Anticancer Nanodrugs. *J. Biomed. Nanotechnol.* **7,** 489–503 (2011).

294. Benjaminsen, R. V. *et al.* Evaluating Nanoparticle Sensor Design for Intracellular pH Measurements. *ACS Nano* **5,** 5864–5873 (2011).

295. Dennis, A. M., Rhee, W. J., Sotto, D., Dublin, S. N. & Bao, G. Quantum Dot–Fluorescent Protein FRET Probes for Sensing Intracellular pH. *ACS Nano* **6,** 2917–2924 (2012).

296. Ray, A., Lee, Y.-E. K., Kim, G. & Kopelman, R. Two-Photon Fluorescence Imaging Super-Enhanced by Multishell Nanophotonic Particles, with Application to Subcellular pH. *Small* **8,** 2213–2221 (2012).

297. Esipova, T. V. *et al.* Dendritic upconverting nanoparticles enable in vivo multiphoton microscopy with low-power continuous wave sources. *Proc. Natl. Acad. Sci.* **109,** 20826–20831 (2012).

298. Berezin, M. Y. & Achilefu, S. Fluorescence Lifetime Measurements and Biological Imaging. *Chem. Rev.* **110,** 2641–2684 (2010).

299. Becker, W. Fluorescence lifetime imaging – techniques and applications. *J. Microsc.* **247,** 119–136 (2012).

300. Battisti, A. *et al.* Intracellular pH measurements made simple by fluorescent protein probes and the phasor approach to fluorescence lifetime imaging. *Chem. Commun.* **48,** 5127–5129 (2012).

301. Esposito, A., Gralle, M., Dani, M. A. C., Lange, D. & Wouters, F. S. pHlameleons: A Family of FRET-Based Protein Sensors for Quantitative pH Imaging†. *Biochemistry (Mosc.)* **47,** 13115–13126 (2008).

302. Niesner, R. *et al.* 3D-Resolved Investigation of the pH Gradient in Artificial Skin Constructs by Means of Fluorescence Lifetime Imaging. *Pharm. Res.* **22,** 1079–1087 (2005).

303. Wang, H.-P. *et al.* Fluorescence lifetime image of a single halobacterium. *Chem. Phys. Lett.* **442,** 441–444 (2007).

304. Hille, C. *et al.* Time-domain fluorescence lifetime imaging for intracellular pH sensing in living tissues. *Anal. Bioanal. Chem.* **391,** 1871–1879 (2008).

305. Hanson, K. M. *et al.* Two-Photon Fluorescence Lifetime Imaging of the Skin Stratum Corneum pH Gradient. *Biophys. J.* **83,** 1682–1690 (2002).

306. Lin, H.-J., Herman, P. & Lakowicz, J. R. Fluorescence lifetime-resolved pH imaging of living cells. *Cytom. Part J. Int. Soc. Anal. Cytol.* **52,** 77–89 (2003).

307. Szmacinski, H. & Lakowicz, J. R. Optical measurements of pH using fluorescence lifetimes and phase-modulation fluorometry. *Anal. Chem.* **65,** 1668–1674 (1993).

308. Hassan, M. *et al.* Fluorescence Lifetime Imaging System for In Vivo Studies. *Mol. Imaging* **6,** 229–236 (2007).

309. Ray, A., Yoon, H. K., Lee, Y. E. K., Kopelman, R. & Wang, X. Sonophoric nanoprobe aided pH measurement in vivo using photoacoustic spectroscopy. *Analyst* **138,** 3126–3130 (2013).

310. Jung, C. *et al.* A New Photostable Terrylene Diimide Dye for Applications in Single Molecule Studies and Membrane Labeling. *J. Am. Chem. Soc.* **128,** 5283–5291 (2006).

311. Peneva, K. *et al.* Exploiting the Nitrilotriacetic Acid Moiety for Biolabeling with Ultrastable Perylene Dyes. *J. Am. Chem. Soc.* **130,** 5398–5399 (2008).

312. Liu, H. *et al.* Fluorescent water-soluble probes based on dendritic PEG substituted perylene bisimides: synthesis, photophysical properties, and live cell images. *J. Mater. Chem.* **22,** 6176 (2012).

313. Yang, S. K. *et al.* Monovalent, Clickable, Uncharged, Water-Soluble Perylenediimide-Cored Dendrimers for Target-Specific Fluorescent Biolabeling. *J. Am. Chem. Soc.* **133,** 9964–9967 (2011).

314. Yin, M. *et al.* Fluorescent Core/Shell Nanoparticles for Specific Cell-Nucleus Staining. *Small* **4,** 894–898 (2008).

315. Schmidt, C. D., Böttcher, C. & Hirsch, A. Chiral Water-Soluble Perylenediimides. *Eur. J. Org. Chem.* **2009,** 5337–5349 (2009).

316. Heek, T. *et al.* Highly fluorescent water-soluble polyglycerol-dendronized perylene bisimide dyes. *Chem. Commun.* **46,** 1884–1886 (2010).

317. Dmitriev, R. I., Zhdanov, A. V., Jasionek, G. & Papkovsky, D. B. Assessment of Cellular Oxygen Gradients with a Panel of Phosphorescent Oxygen-Sensitive Probes. *Anal. Chem.* **84,** 2930–2938 (2012).

318. Fercher, A., Borisov, S. M., Zhdanov, A. V., Klimant, I. & Papkovsky, D. B. Intracellular O2 Sensing Probe Based on Cell-Penetrating Phosphorescent Nanoparticles. *ACS Nano* **5,** 5499–5508 (2011).

319. Koren, K., Dmitriev, R. I., Borisov, S. M., Papkovsky, D. B. & Klimant, I. Complexes of IrIII-Octaethylporphyrin with Peptides as Probes for Sensing Cellular O2. *ChemBioChem* **13,** 1184–1190 (2012).

320. Borisov, S. M. *et al.* New NIR-emitting complexes of platinum(II) and palladium(II) with fluorinated benzoporphyrins. *J. Photochem. Photobiol. Chem.* **201,** 128–135 (2009).

321. Sung, H. J. *et al.* Mitochondrial respiration protects against oxygen-associated DNA damage. *Nat. Commun.* **1,** 5 (2010).

322. Thomas, J. A., Buchsbaum, R. N., Zimniak, A. & Racker, E. Intracellular pH measurements in Ehrlich ascites tumor cells utilizing spectroscopic probes generated in situ. *Biochemistry (Mosc.)* **18,** 2210–2218 (1979).

323. Hille, C., Lahn, M., Dosche, C. & Koberling, F. Two-photon fluorescence lifetime imaging (2P-FLIM) for ion sensing in living cells. (2008).

324. Canton, I. & Battaglia, G. Endocytosis at the nanoscale. *Chem. Soc. Rev.* **41,** 2718 (2012).

325. Yoshimori, T., Yamamoto, A., Moriyama, Y., Futai, M. & Tashiro, Y. Bafilomycin A1, a specific inhibitor of vacuolar-type H(+)-ATPase, inhibits acidification and protein degradation in lysosomes of cultured cells. *J. Biol. Chem.* **266,** 17707–17712 (1991).

326. Pampaloni, F., Reynaud, E. G. & Stelzer, E. H. K. The third dimension bridges the gap between cell culture and live tissue. *Nat. Rev. Mol. Cell Biol.* **8,** 839–845 (2007).

327. Reynolds, B. A. & Weiss, S. Generation of neurons and astrocytes from isolated cells of the adult mammalian central nervous system. *Science* **255,** 1707–1710 (1992).

328. Filippis, L. D. & Delia, D. Hypoxia in the regulation of neural stem cells. *Cell. Mol. Life Sci.* **68,** 2831–2844 (2011).

329. Mehta, G., Hsiao, A. Y., Ingram, M., Luker, G. D. & Takayama, S. Opportunities and challenges for use of tumor spheroids as models to test drug delivery and efficacy. *J. Controlled Release* **164,** 192–204 (2012).

330. Dmitriev, R. I., Zhdanov, A. V., Nolan, Y. M. & Papkovsky, D. B. Imaging of neurosphere oxygenation with phosphorescent probes. *Biomaterials* **34,** 9307–9317 (2013).

331. Lau, A. & Tymianski, M. Glutamate receptors, neurotoxicity and neurodegeneration. *Pflüg. Arch. - Eur. J. Physiol.* **460,** 525–542 (2010).

332. Kondrashina, A. V. *et al.* A Phosphorescent Nanoparticle-Based Probe for Sensing and Imaging of (Intra)Cellular Oxygen in Multiple Detection Modalities. *Adv. Funct. Mater.* **22,** 4931–4939 (2012).

333. Zhdanov, A. V., Dmitriev, R. I. & Papkovsky, D. B. Bafilomycin A1 activates HIF-dependent signalling in human colon cancer cells via mitochondrial uncoupling. *Biosci. Rep.* **32,** 587–595 (2012).

Structure Analyses

Chapter 1

New Fluorescent Perylene Bisimide Indicators – a Platform for Broadband pH Optodes

NMR Spectroscopy

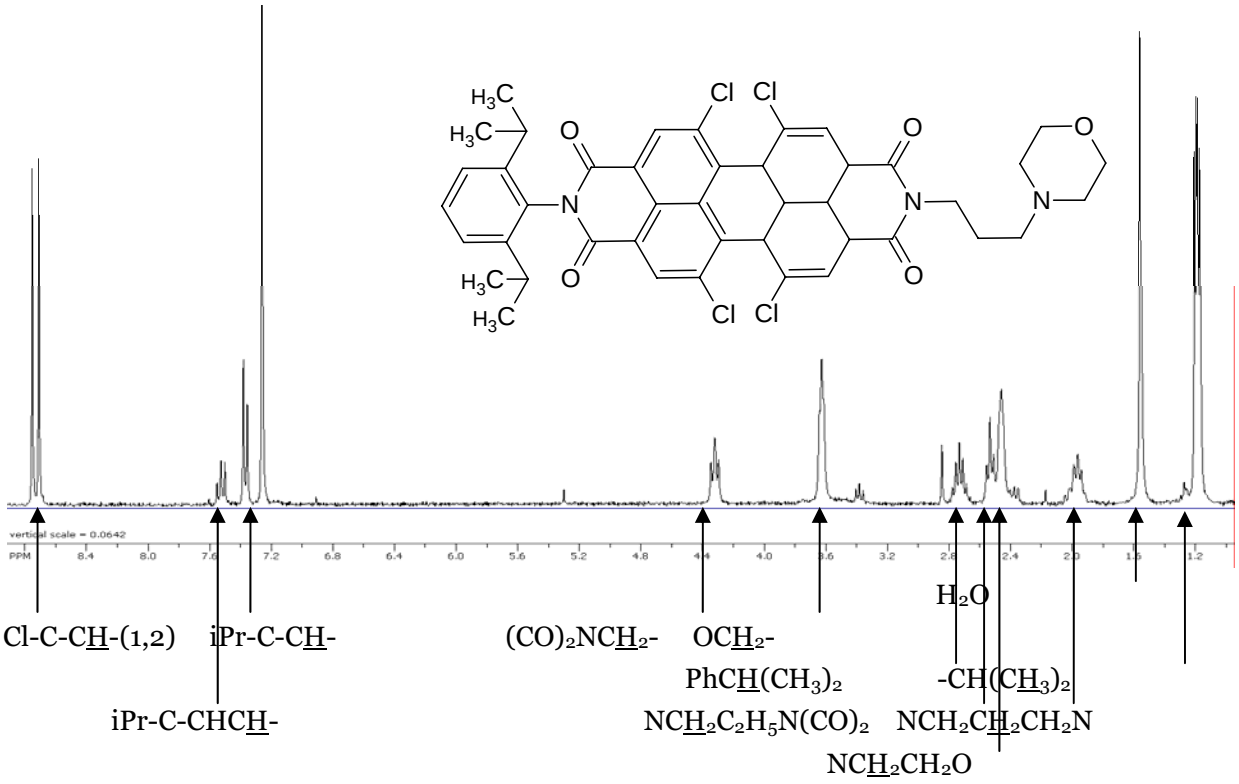

Figure A-1: ^{1}H-NMR spectrum of **2a**

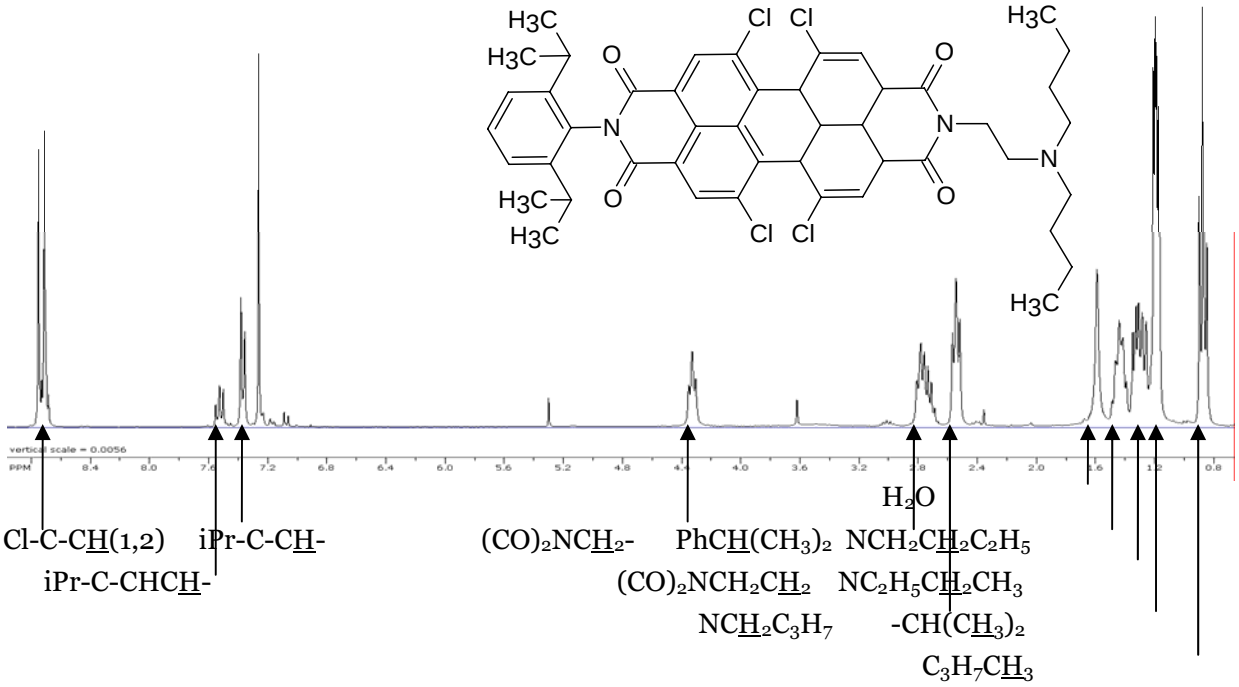

Figure A-2: ^{1}H-NMR spectrum of **2b**

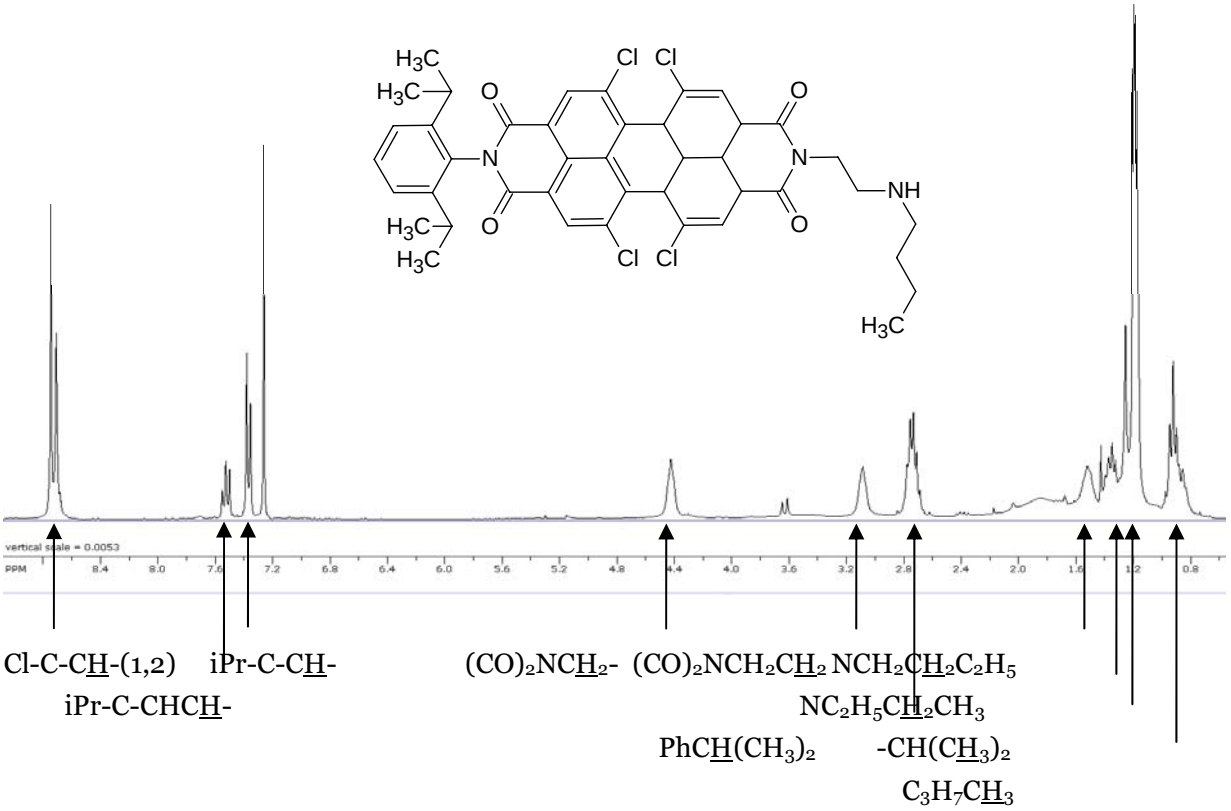

Figure A-3: ^{1}H-NMR spectrum of **2c**

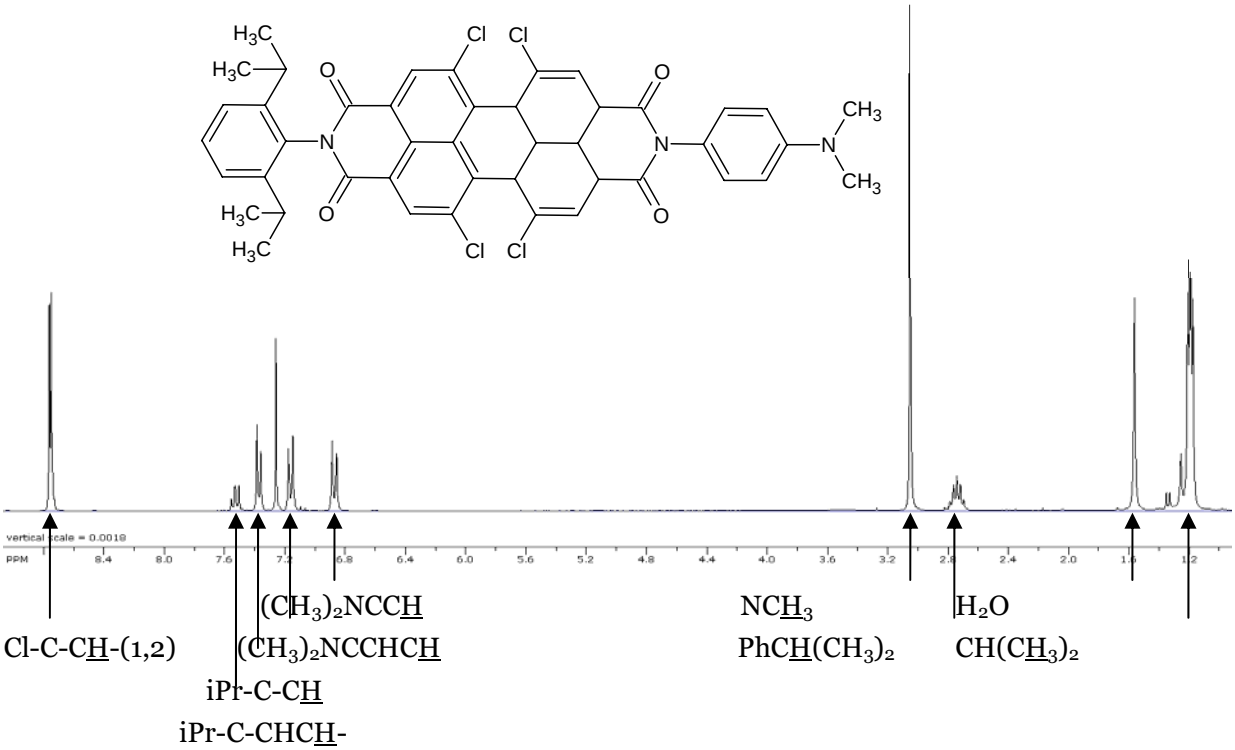

Figure A-4: ^{1}H-NMR spectrum of **2d**

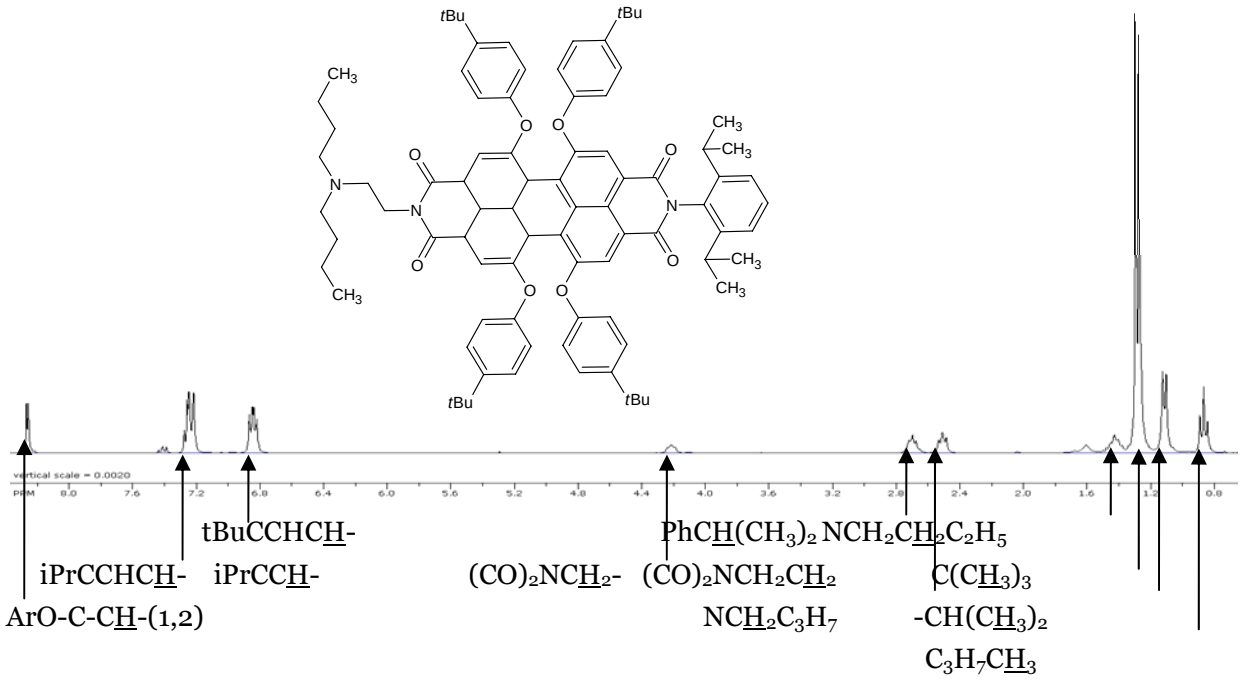

Figure A-5: ^{1}H-NMR spectrum of **3**

MALDI-TOF Mass Spectroscopy

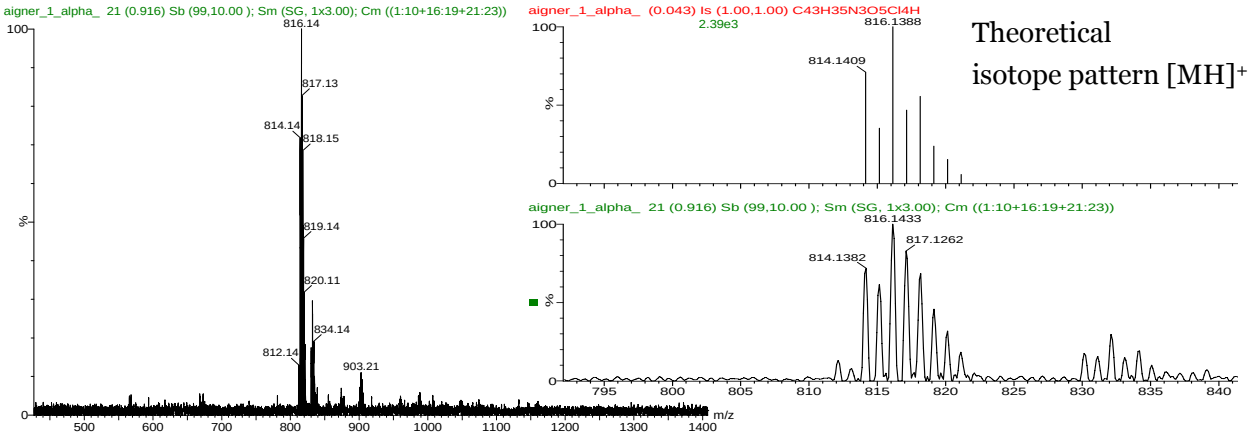

Figure A-6: MALDI-TOF spectrum of **2a**

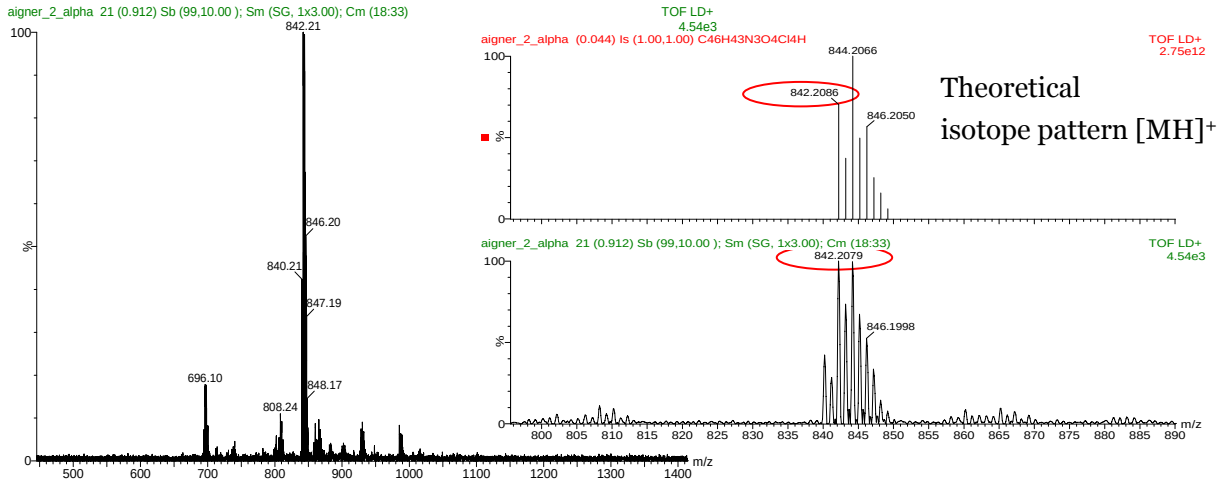

Figure A-7: MALDI-TOF spectrum of **2b**

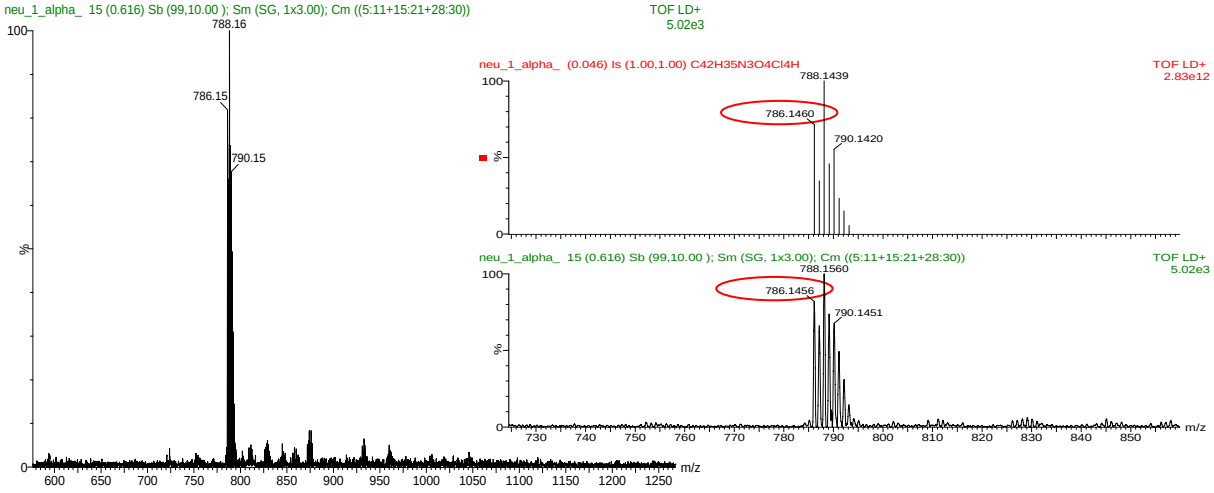

Figure A-8: MALDI-TOF spectrum of **2c**

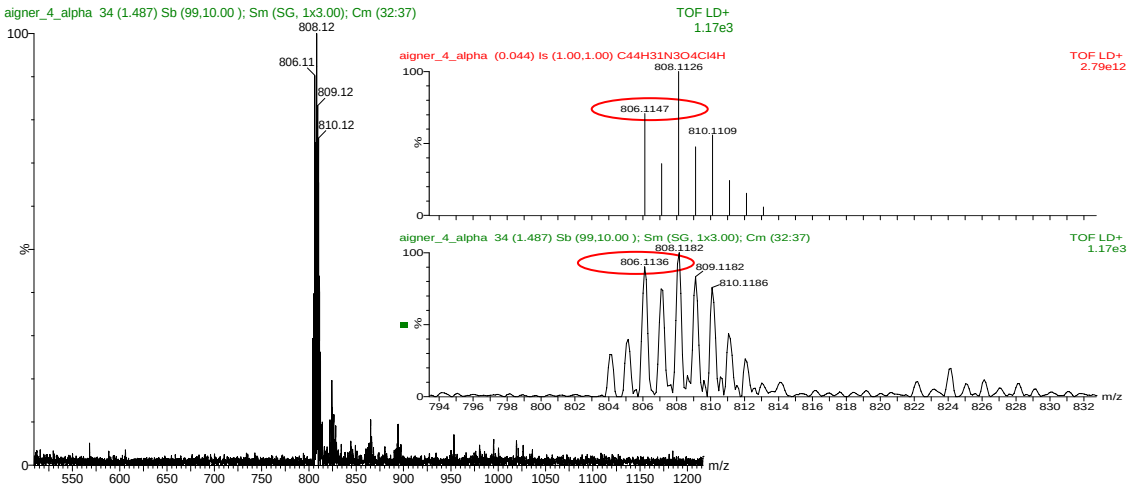

Figure A-9: MALDI-TOF spectrum of **2d**

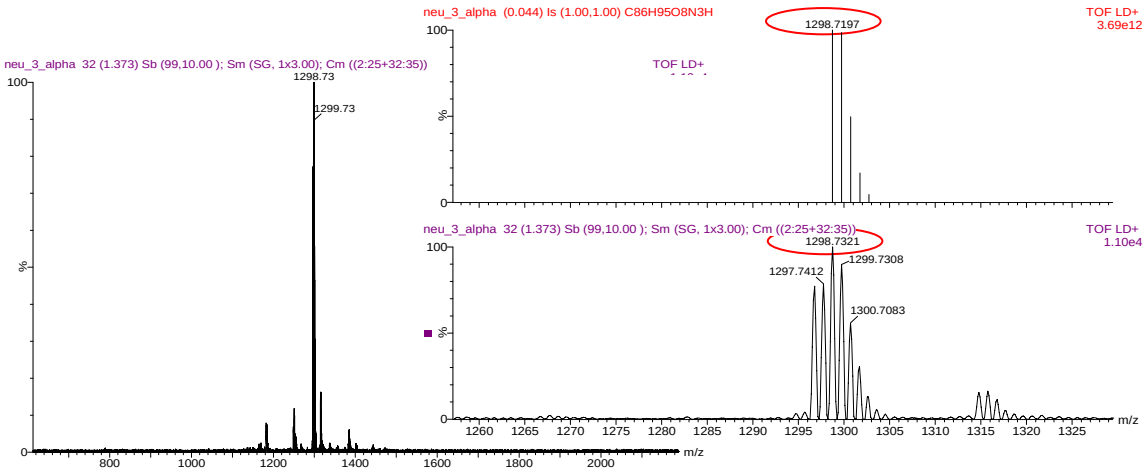

Figure A-10: MALDI-TOF spectrum of **3**

Chapter 2

Novel Near Infra-red Fluorescenct pH-Sensors Based on 1-Aminoperylene Bisimides Covalently Grafted to Poly(acryloylmorpholine)

NMR Spectroscopy

The structures of **1** and **2** are unequivocally confirmed by ^{1}H- and ^{13}C-NMR, as well as two-dimensional NMR (HH-COSY and HSQC). The 2D spectra have been included since the 4-methyl-1-piperazinyl and the 4-morpholinyl substituent show relatively broad ^{1}H-resonances and cause complicated ^{1}H-spectra. The 2D-methods provide a further proof for the accuracy of the assigned fine structures.

For **3**, limited solubility and the large number of different carbons (67 carbons none of which are fully equivalent) made it impossible to obtain a useful ^{13}C-spectrum. **3** is a mixture of different isomers which differ in the exact substitution pattern of the *N*-aryl substituents after chlorosulfonation, as will be discussed in more detail near figure ESI18. Nevertheless, the following ^{1}H- and two-dimensional NMR spectra without a doubt confirm that **3** carries two polymerisable groups, while the structure of the perylene bisimide centre is equal to **1** - that is further confirmed by mass spectroscopy as shown in fig. ESI25 and ESI30. The exact substitution pattern of the *N*-aryl group, which essentially acts as a linker between the chromophore centre and the polymerisable groups, is not of major importance to the presented concept.

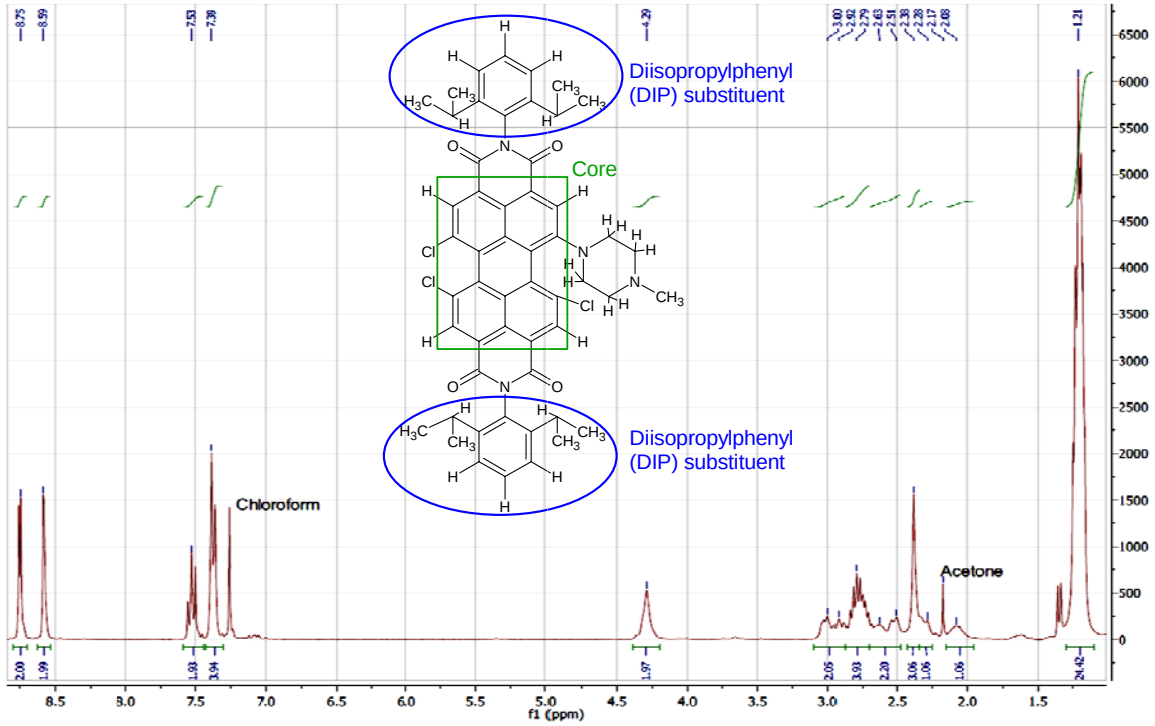

Figure A-11: ^{1}H-NMR of **1**: δ_H (300 MHz, $CDCl_3$) 8.75 (2 H, d, ArH (Core)), 8.59 (2 H, d, ArH (Core)), 7.53 (2 H, t, *J* 7.8, ArH (DIP)), 7.38 (4 H, d, *J* 7.8, ArH (DIP)); 4.29 (2 H, br s, NCH_2), 2.87-3.10 (2 H, m, NCH_2), 2.70-2.87 (4 H, m, ArCH), 2.48-2.70 (2 H, m, NCH_2), 2.38 (3 H, s, NCH_3), 2.25-2.34 (1 H, br s, NCH_2), 1.96-2.15 (1 H, br s, NCH_2), 1.21 (24 H, m, ArCHC<u>H</u>$_3$).

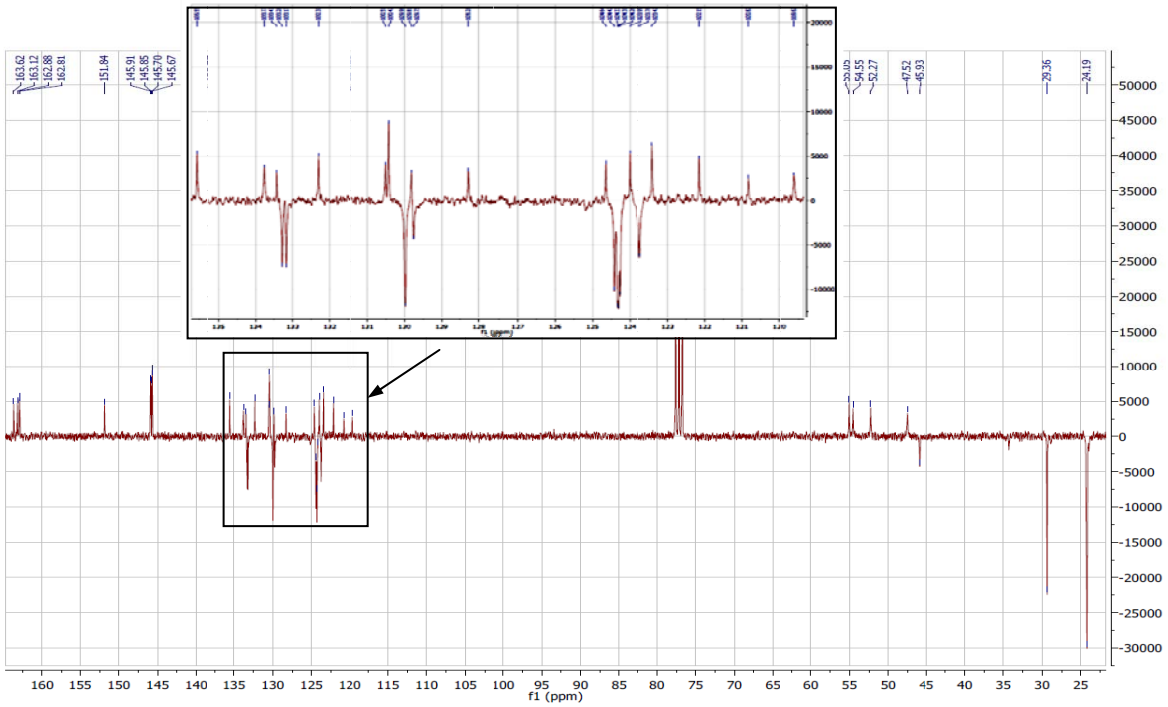

Figure A-12:: ^{13}C-APT-NMR of **1**: *δc* (300 MHz, $CDCl_3$) 163.6, 163.1, 162.9, 162.8 (C=O); 151.8; 145.9 (2 C), 145.7 (2 C), 135.6, 133.8 (2 C), 133.4, *133.3*, *133.2*, 132.3, 130.5, 130.4, *130.0* (2 C), 129.8, *129.7*, 128.3, 124.6, *124.3-124.4* (4 C), 124.0, 123.8, *123.4*, 122.1, 120.8, 119.6 (aromatic); 55.1, 54.6, 52.3, 47.5, *45.9* (NCH_2); *29.3-29.5* (multiple C, ArCH); *24.1-24.4* (multiple C, $ArCHCH_3$). Underlined peaks are of negative intensity (CH or CH_3), those in italics can be found in the HSQC spectrum.

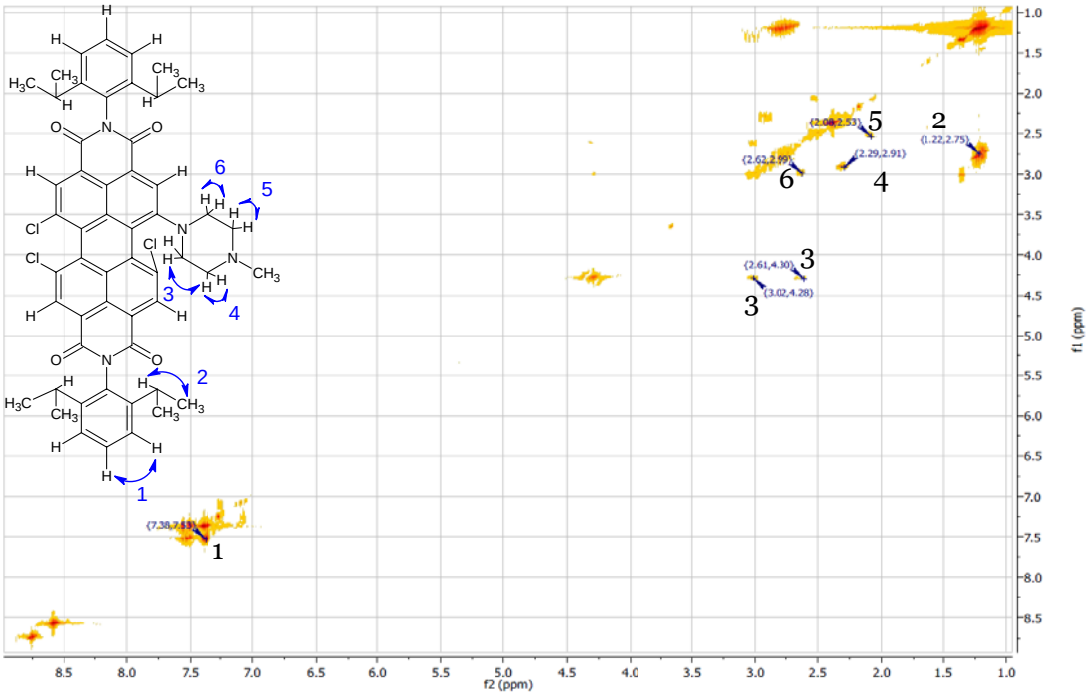

Figure A-13: HH COSY-NMR of **1** (300 MHz, CDCl3).

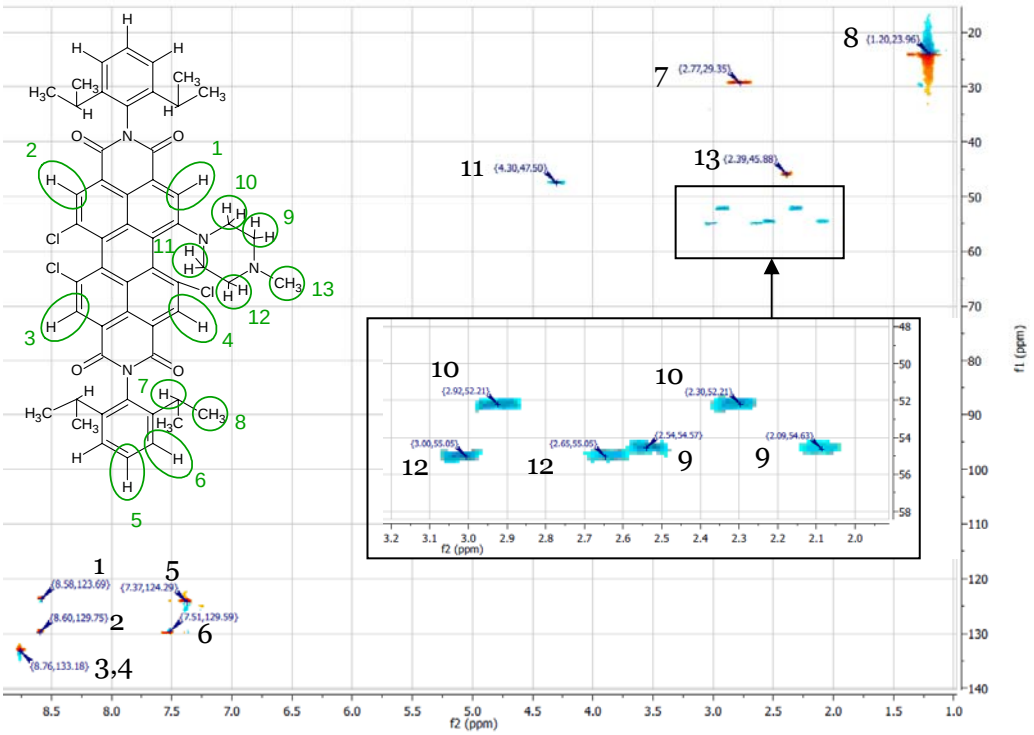

Figure A-14: HSQC-NMR of **1** (300 MHz, CDCl3). All unmarked carbons carrying protons are undistinguishable in signal from a marked one due to molecular symmetry.

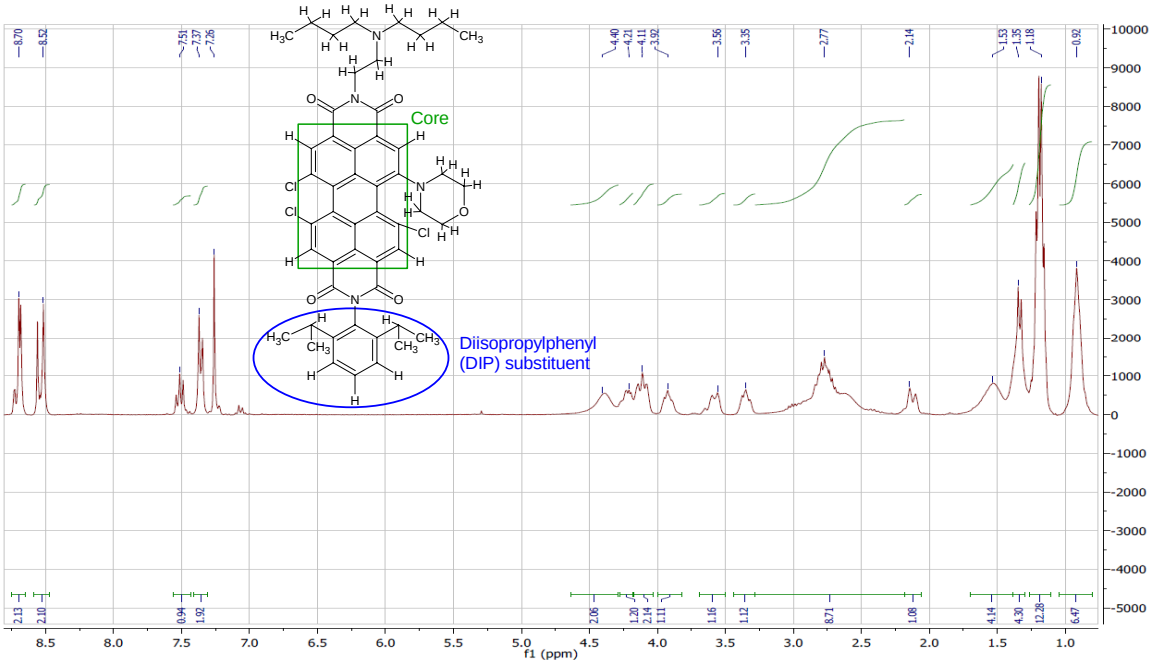

Figure A-15:: ^{1}H-NMR of **2**: δ_H (300 MHz, $CDCl_3$) 8.70 (2 H, d, ArH (Core)), 8.52 (2 H, d, ArH (Core)), 7.51 (1 H, t, *J* 7.8, ArH(DIP)), 7.37 (2 H, d, *J* 7.8, ArH(DIP)), 4.40 (2 H, br s, $(CO)_2NCH_2$), 4.18-4.28 (1 H, m, $NC\underline{H}_2CH_2O$), 4.04-4.18 (2 H, m, $NC\underline{H}_2CH_2O$ (1 H) and OCH_2 (1 H)), 3.82-4.00 (1 H, m, OCH_2), 3.50-3.69 (1 H, m, OCH_2), 3.28-3.43 (1 H, m, OCH_2), 2.18-3-28 (9 H, m, $(CO)_2NCH_2C\underline{H}_2N$ (2 H) and $NC\underline{H}_2$ (4 H) and $NC\underline{H}_2CH_2O$ (1 H) and ArCH (2 H)), 2.06-2.18 (1 H, m, $NC\underline{H}_2CH_2O$), 1.38-1.69 (4 H, br s, $NCH_2C\underline{H}_2$), 1.30-1.38 (4 H, m, $NCH_2CH_2C\underline{H}_2$), 1.11-1.27 (12 H, q, *J* 5.9, $ArCHC\underline{H}_3$), 0.92 (6 H, t, $NCH_2CH_2CH_2C\underline{H}_3$).

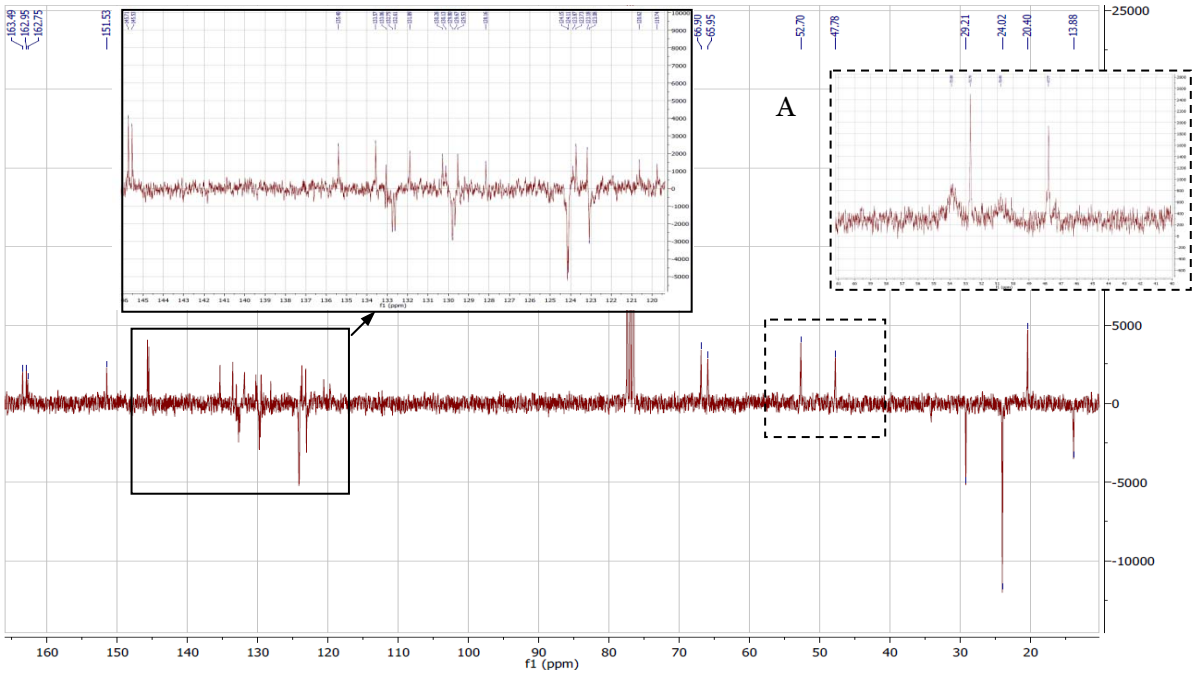

Figure A-16:: ^{13}C-APT-NMR of **2**: *δc* (300 MHz, $CDCl_3$) 163.5, 162.9, 162.7 (2 C) (C=O); 151.5, 145.7, 145.5, 135.4, 133.6, 133.1, *132.7*, *132.6*, 131.9, 130.3, 130.1 (2 C), *129.8*, *129.7*, 129.5, 128.1, *124.2*, *124.1*, 123.9, 123.7, 123.2, *123.1*, 120.6, 119.8 (aromatic); *66.9*, *66.0* (OCH_2); *53.9 (broad)*^{A}, *52.7*, *50.8 (broad)*^{A}, *47.8* (NCH_2); *29.2* (ArCH); *24.0* ($ArCHCH_3$); *20.4*, *13.9* (Alkyl). Underlined peaks are of negative intensity (CH or CH_3), those in italics can be found in the HSQC spectrum. Box **A**: Detail of a standard (not APT) ^{13}C spectrum. The broad peaks cannot be found in the ^{13}C-APT spectrum, however they were found in HSQC (figure ESI13, peaks 14 and 15).

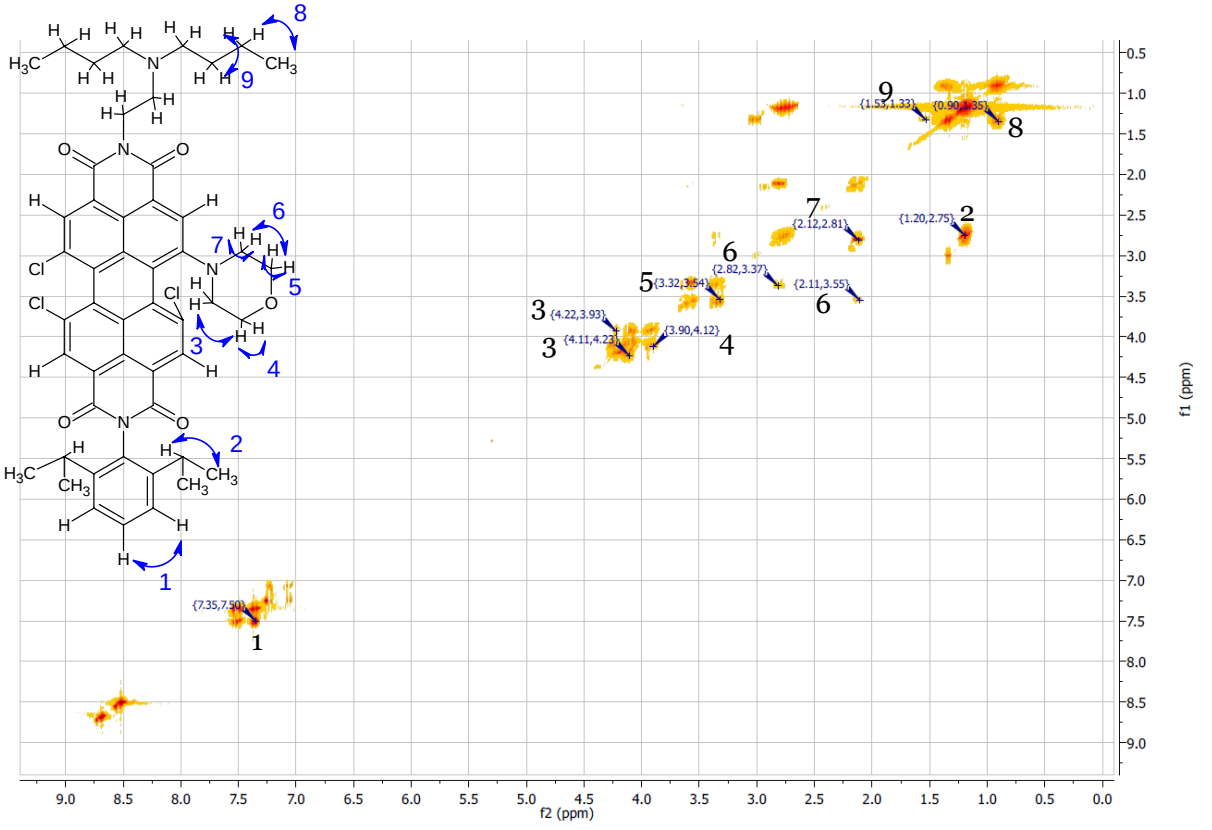

Figure A-17: HH COSY-NMR of **2** (300 MHz, CDCl3).

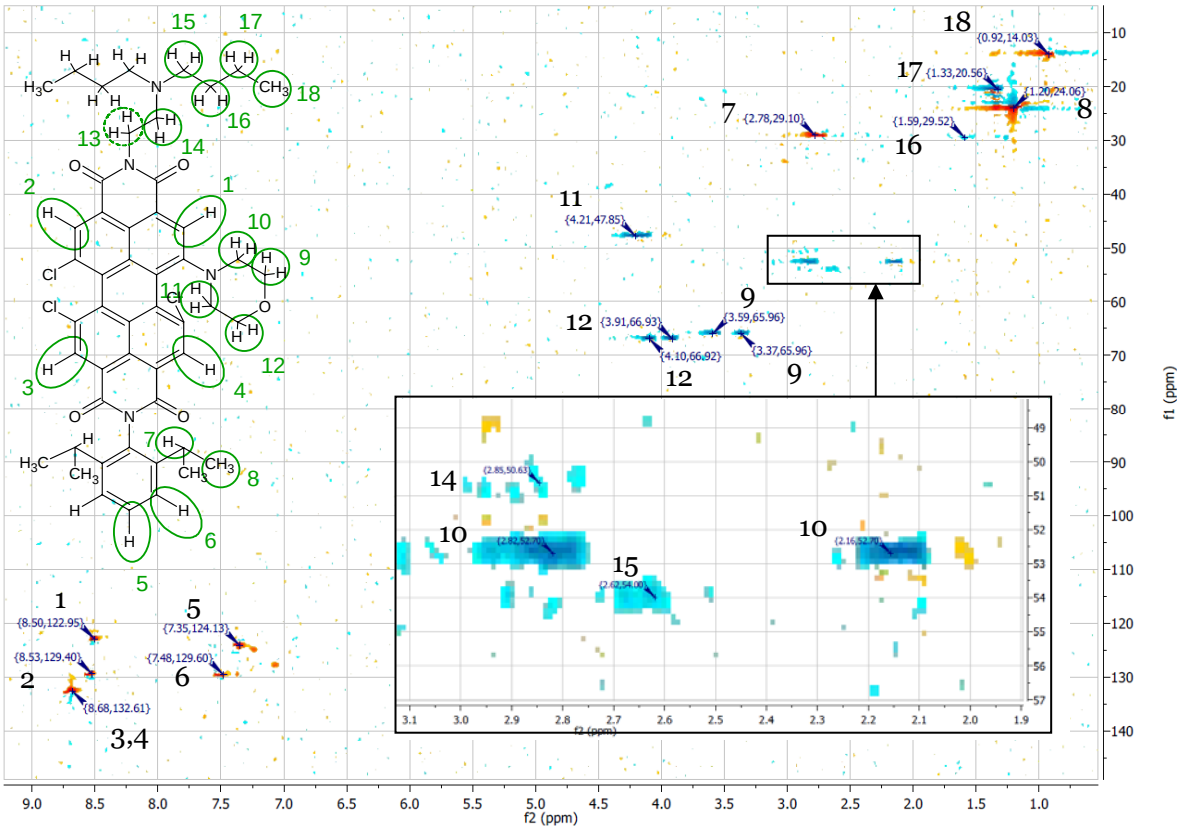

Figure A-18: HSQC-NMR of **2** (300 MHz, CDCl3). All unmarked carbons carrying protons are undistinguishable in signal from a marked one due to molecular symmetry.

In dye **3,** NMR spectroscopy reveals that the chlorosulfonation of the 2,6-diisopropylphenyl group can lead to substitution in the 3,5- and in the 4-position. That is expected since steric effects (vicinity of the relatively bulky isopropyl group) here favour 4-substitution while electronic (*o,p*-directing influence of the isopropyl group) and statistic (superior number of positions) effects favour 3,5-substitution. The signals of the unsubstituted group (7.51 ppm, 1 H, t and 7.37 ppm, 2 H, d) have been replaced by signals corresponding to 4-substitution (7.84 ppm, 2 H, s) and to 3,5-substitution (7.49 ppm, 1 H, d and 8.14 ppm, 1 H, d) in an approximate ratio of 1:1 (integral areas). For the sake of clarity, the assumed product structure here carries two differently substituted 2,6-diisopropylphenyl rings. The product may in reality also contain products where both rings are 4-substituted or both are 3,5-substituted. Other signals with low integrals (e.g. those at 7.55-7.75 ppm) are due to other products with even different substitution patterns, since under the acidic conditions of chlorosulfonation the isopropyl groups may migrate to others than the 2,6-positions. However, the exact substitution pattern of the diisopropylphenyl groups is not expected to have any significant impact on the investigated spectral and pH-dependent properties, since they are fully electronically separated from both the chromophore and the piperazinyl (pH receptor) moieties. MALDI-TOF mass spectroscopy (fig. ESI25) and LCMS (fig. ESI30) confirm that **3** contains only the isomers.

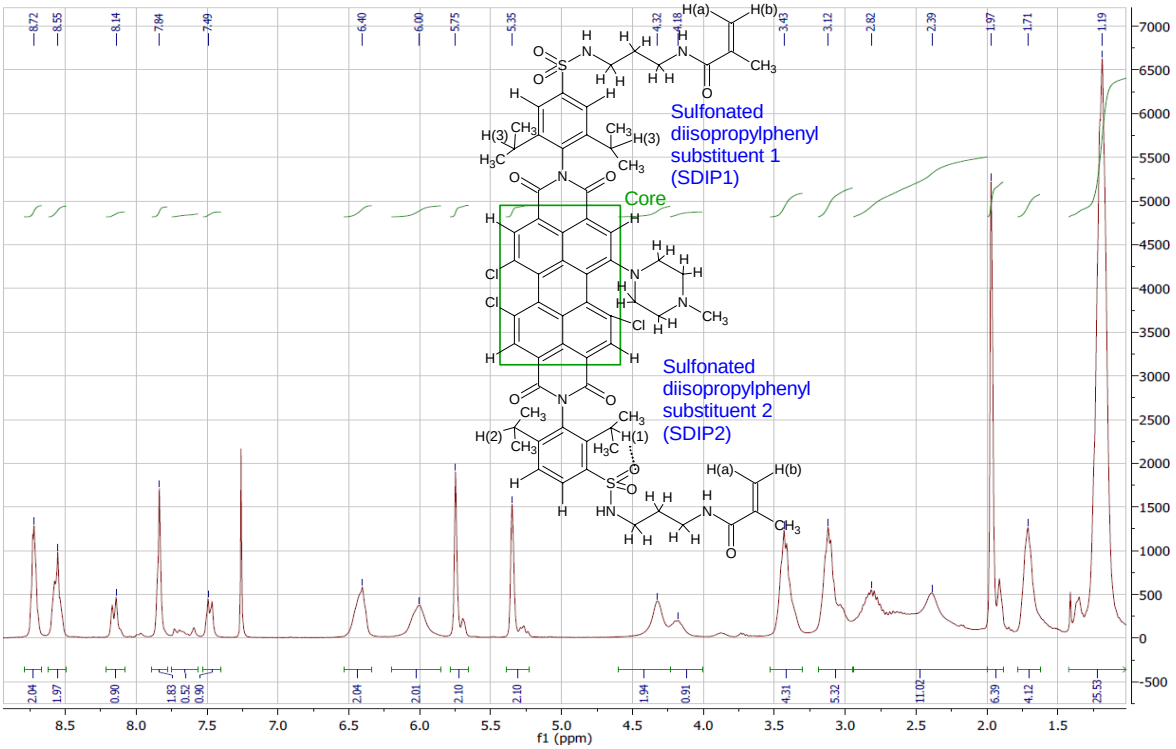

Figure A-19: ^{1}H-NMR of **3**: δ_H (300 MHz, $CDCl_3$) 8.66-8.78 (2 H, m, ArH (Core)), 8.49-8.62 (2 H, m, ArH (Core)), 8.14 (1 H, d, *J* 8.2, ArH(SDIP2)), 7.84 (2 H, s, ArH(SDIP1)), 7.49 (1 H, d, *J* 8.2, ArH(SDIP2)), 6.40 (2 H, br s, SO_2NH), 6.00 (2 H, br s, CONH), 5.75 (2 H, s, C=CH(a)), 5.35 (2 H, s, C=CH(b)), 4.32 (2 H, br s, $NC\underline{H}_2CH_2N$), 4.18 (1 H, m, ArCH(1)), 3.30-3.53 (4 H, m, SO_2NCH_2), 2.95-3.20 (5 H, m, $CONCH_2$ (4 H) and $NC\underline{H}_2CH_2N$ (1 H)), 1.99-2.95 (11 H, m, $NC\underline{H}_2CH_2N$ (5 H) and ArCH (3 H) and NCH_3 (3 H)), 1.87-1.99 (6 H, s, $C=CCH_3$), 1.71 (4 H, m, $SONCH_2C\underline{H}_2CH_2N$), 1.19 (24 H, m, $ArCHC\underline{H}_3$).

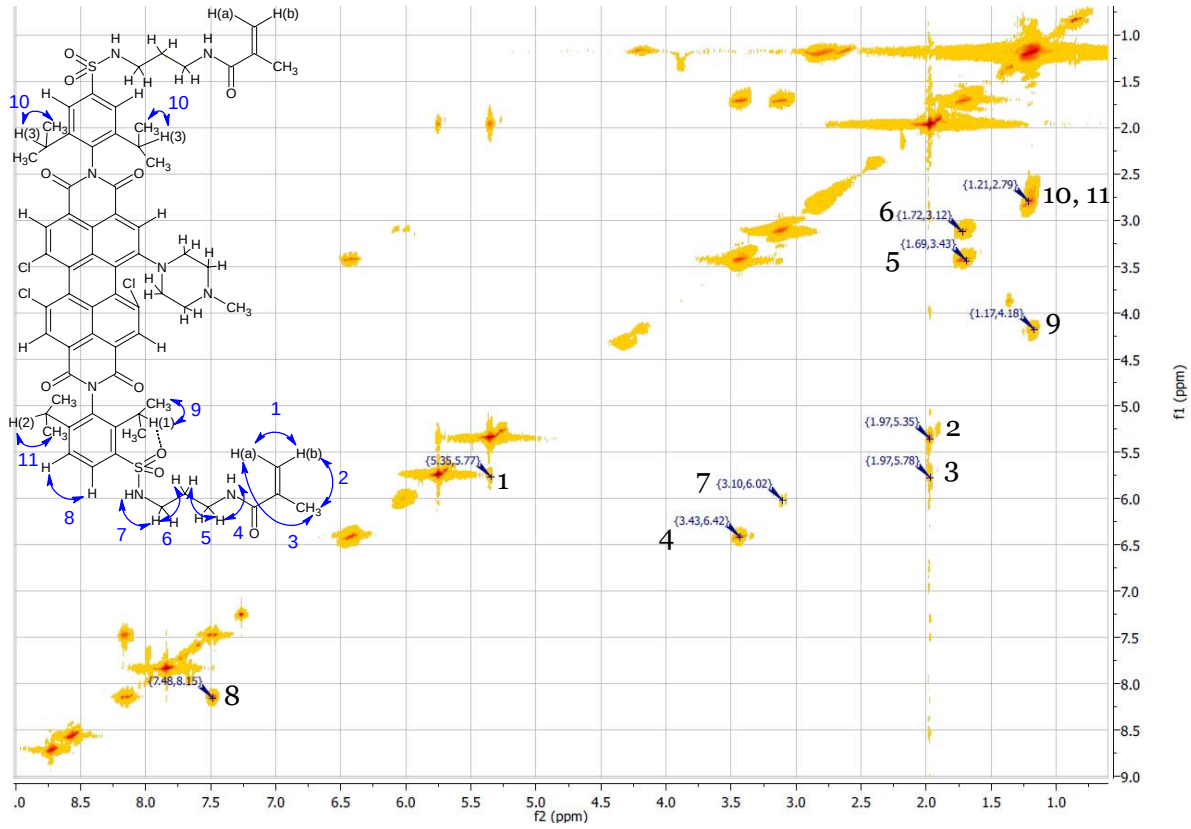

Figure A-20: HH COSY NMR of **3** (300 MHz, CDCl3).

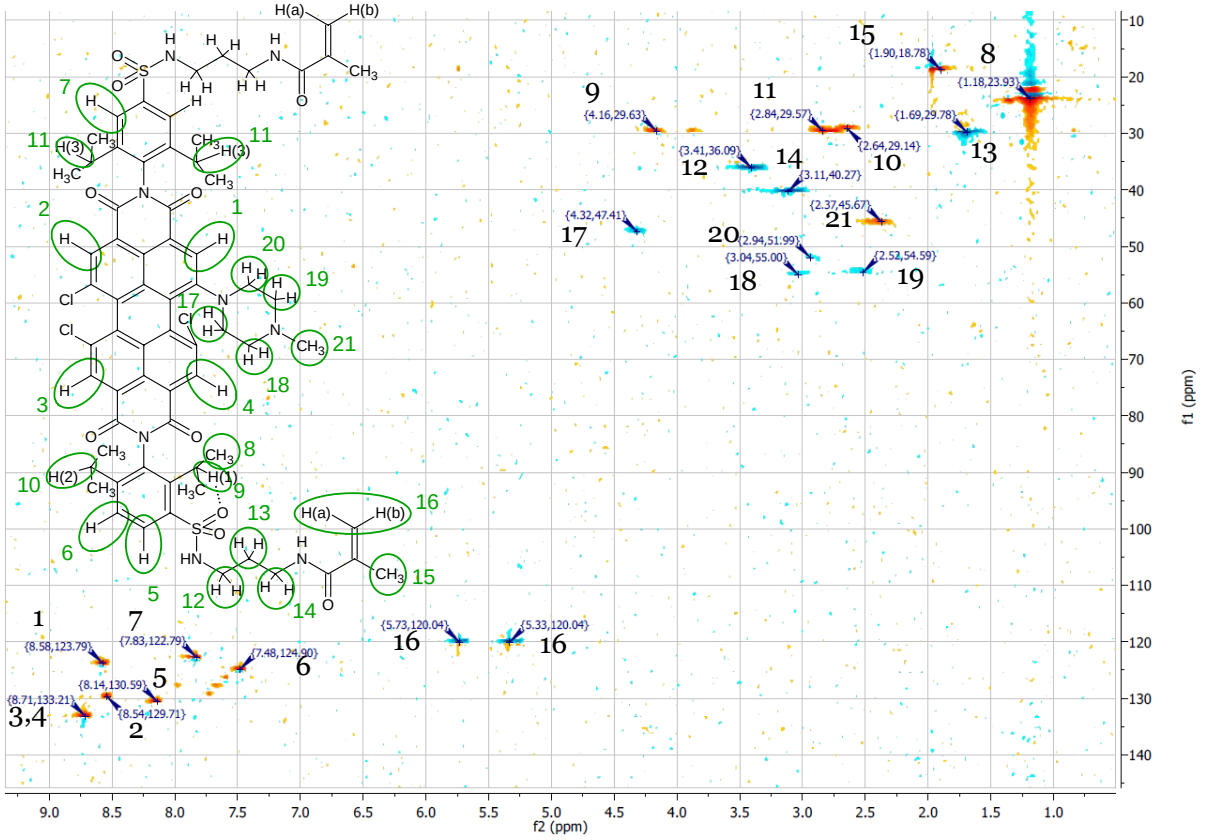

Figure A-21: HSQC NMR of **3** (300 MHz, CDCl3). All unmarked carbons carrying protons are undistinguishable in signal from a marked one due to molecular symmetry.

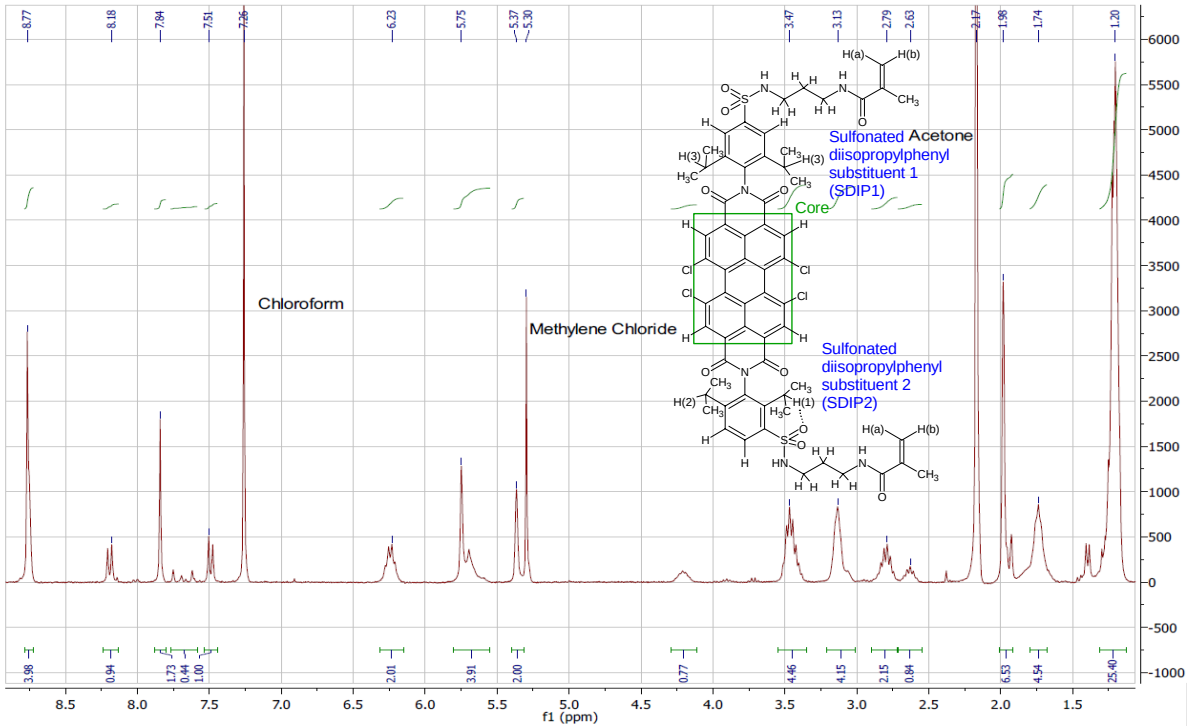

Figure A-22: ^{1}H-NMR of **4b**: δ_H (300 MHz, $CDCl_3$) 8.67 (4 H, s, ArH (Core)), 8.18 (1 H, d, *J* 8.4, ArH(SDIP2)), 7.84 (2 H, s, ArH(SDIP1)), 7.51 (1 H, d, *J* 8.4, ArH(SDIP2)), 6.23 (2 H, q, *J* 6.7, SO_2NH), 5.55-5.80 (4 H, s and br s, C=CH(a) (2 H) and CONH (2 H)), 5.37 (2 H, s, C=CH(b)), 4.20 (1 H, p, *J* 6.2, ArCH(1)), 3.47 (4 H, m, SO_2NCH_2), 3.13 (4 H, br s, $CONCH_2$), 2.79 (2 H, hex, *J* 6.6, ArCH(3)), 2.63 (1 H, p, *J* 6.5, ArCH(2)), 1.98 (6 H, s, $C=CCH_3$), 1.74 (4 H, p, *J* 6.9, $SONCH_2C\underline{H}_2CH_2N$), 1.20 (24 H, m, $ArCHCH_3$).

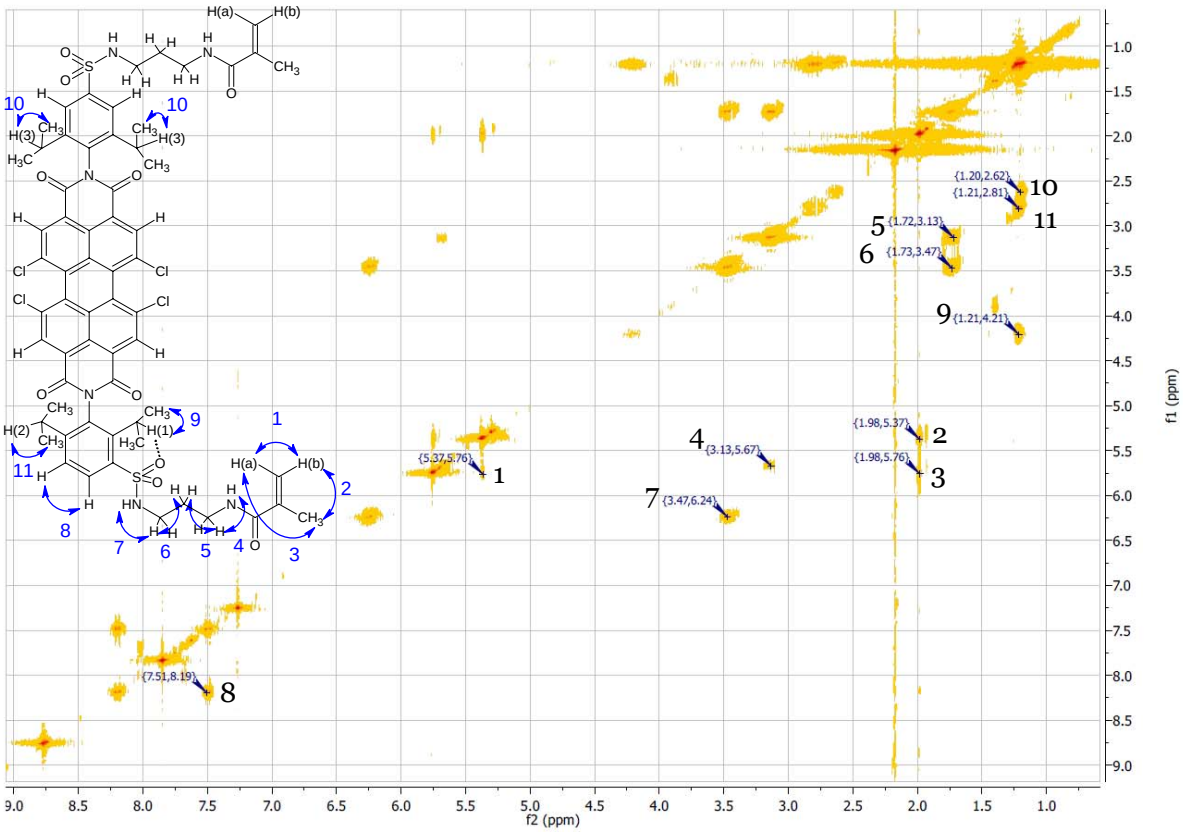

Figure A-23: HH COSY NMR of **4b** (300 MHz, CDCl3).

MALDI-TOF Mass Spectroscopy

MALDI-TOF mass spectroscopy clearly shows exact masses that are in agreement with the product structures. Other signals, which correspond to $[M\text{-}HCl]^+$ and $[M\text{-}HCl\text{-}2H]^+$, are formed upon MALDI (possibly by a photoreaction) and are not present in the products in significant amounts. That is confirmed by several facts - their formation is strongly enhanced if the laser energy used in MALDI is increased (fig. ESI27); NMR do not show a significant contamination with dechlorinated products (would require further signals in the aromatic range); if electrospray ionisation is employed (fig. ESI28-30), only product masses but no $[M\text{-}HCl]^+$ nor $[M\text{-}HCl\text{-}2H]^+$ are detected.

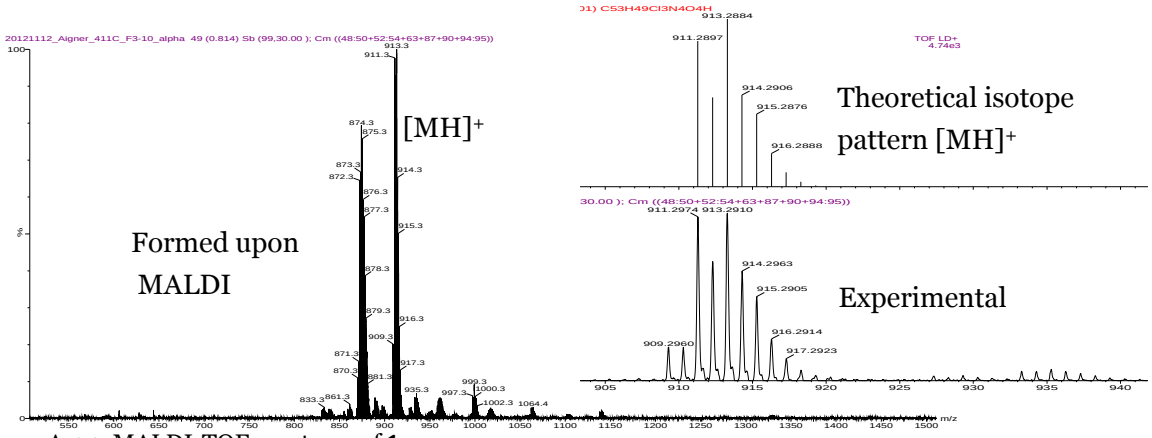

Figure A-24: MALDI-TOF spectrum of **1**.

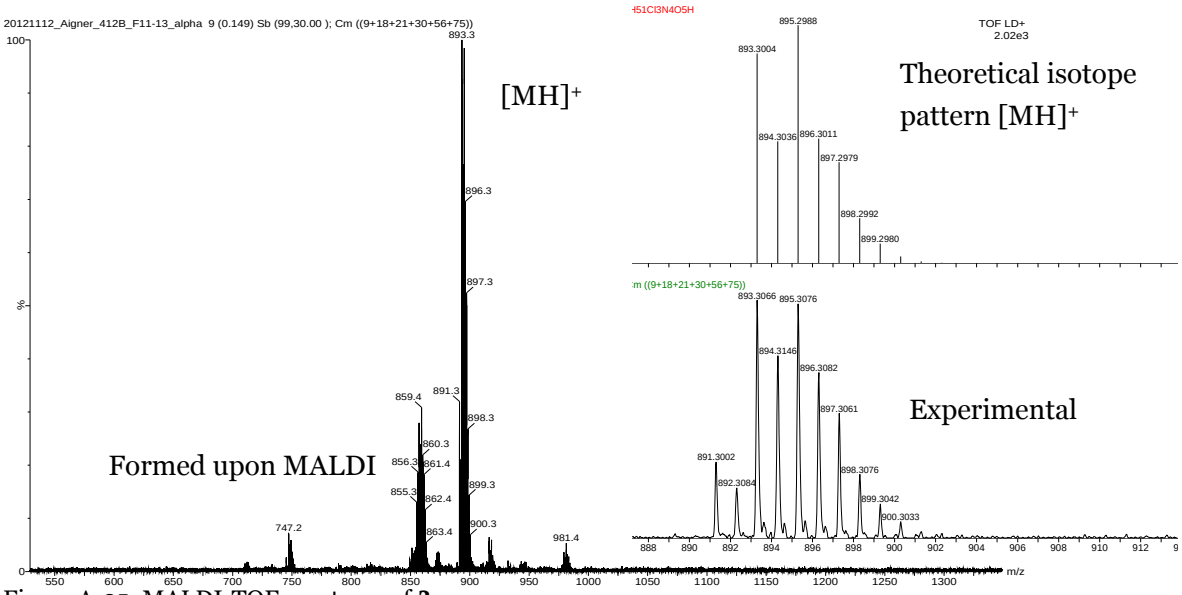

Figure A-25: MALDI-TOF spectrum of **2**.

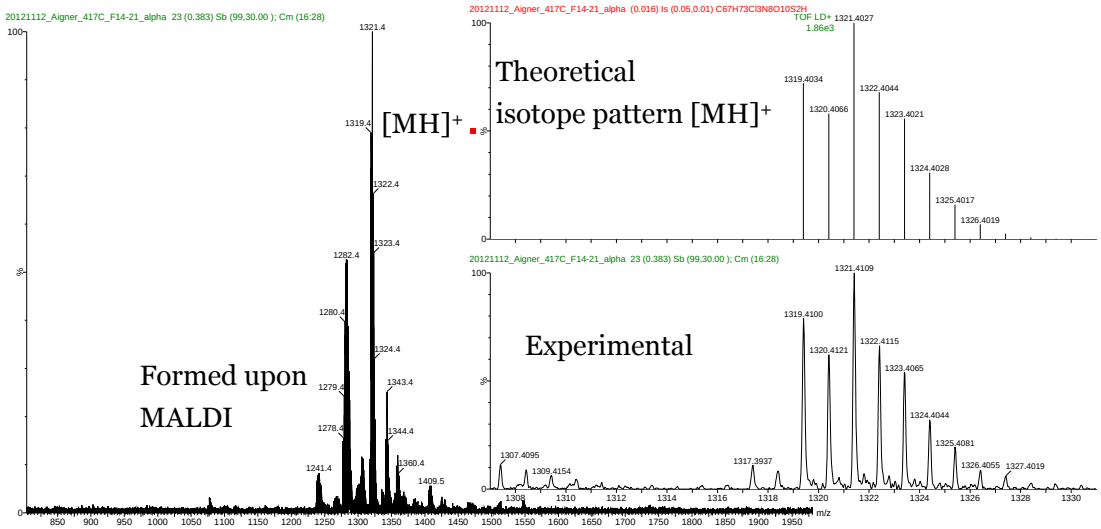

Figure A-26: MALDI-TOF spectrum of **3**.

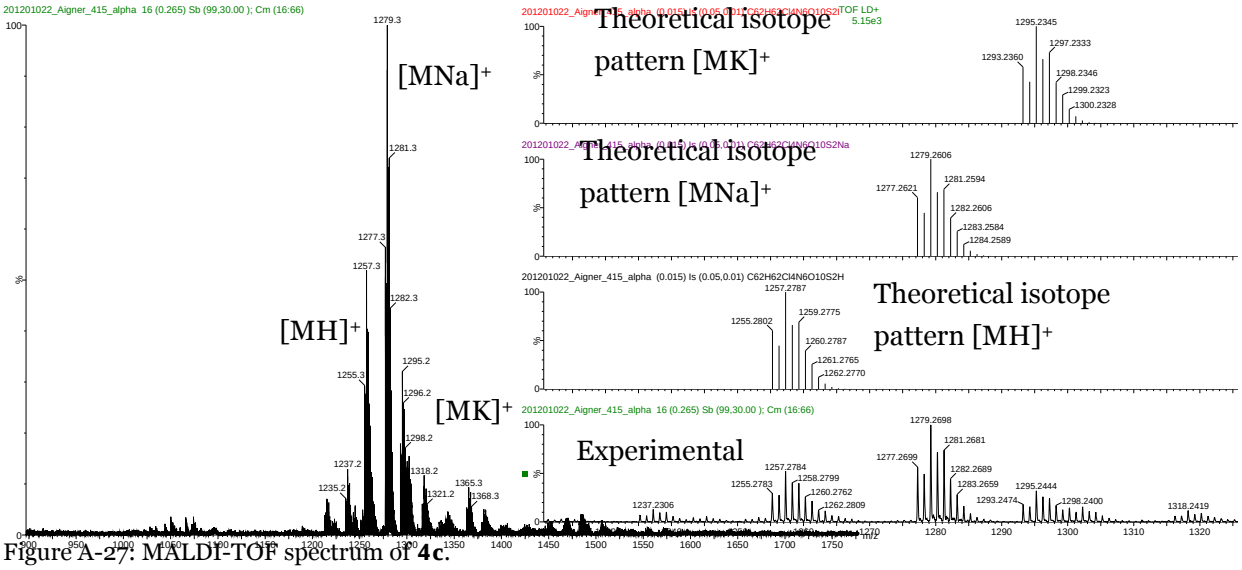

Figure A-27: MALDI-TOF spectrum of **4c**.

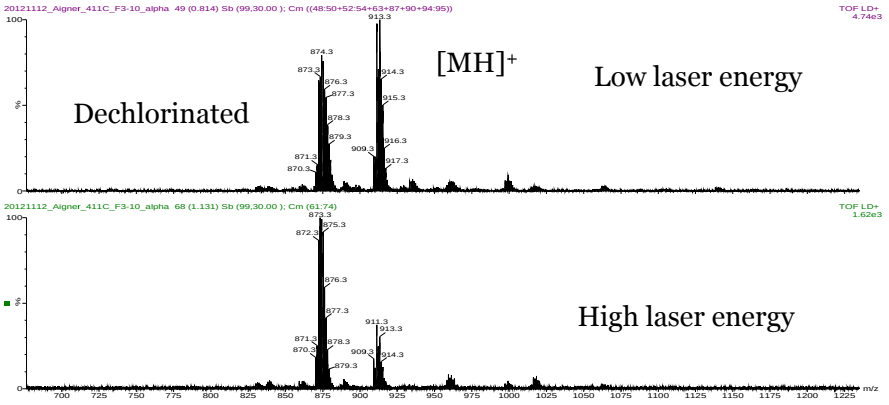

Figure A-28: MALDI-TOF spectra of **1**, acquired applying different laser energies. The formation of the dechlorinated product is significantly enhanced when higher laser energies are applied, which points out that it could be formed by a photoreaction upon MALDI.

LCMS Measurements

In the following LCMS (electrospray ionisation) measurements, the shown mass spectra are fully representative for the whole measurement. No others masses were detected at any time. All chromatograms were measured with a diode array detector set to 640 nm (reference 360 nm substracted). Gradients are stated in tables ESI1 and ESI2, following fig. ESI30.

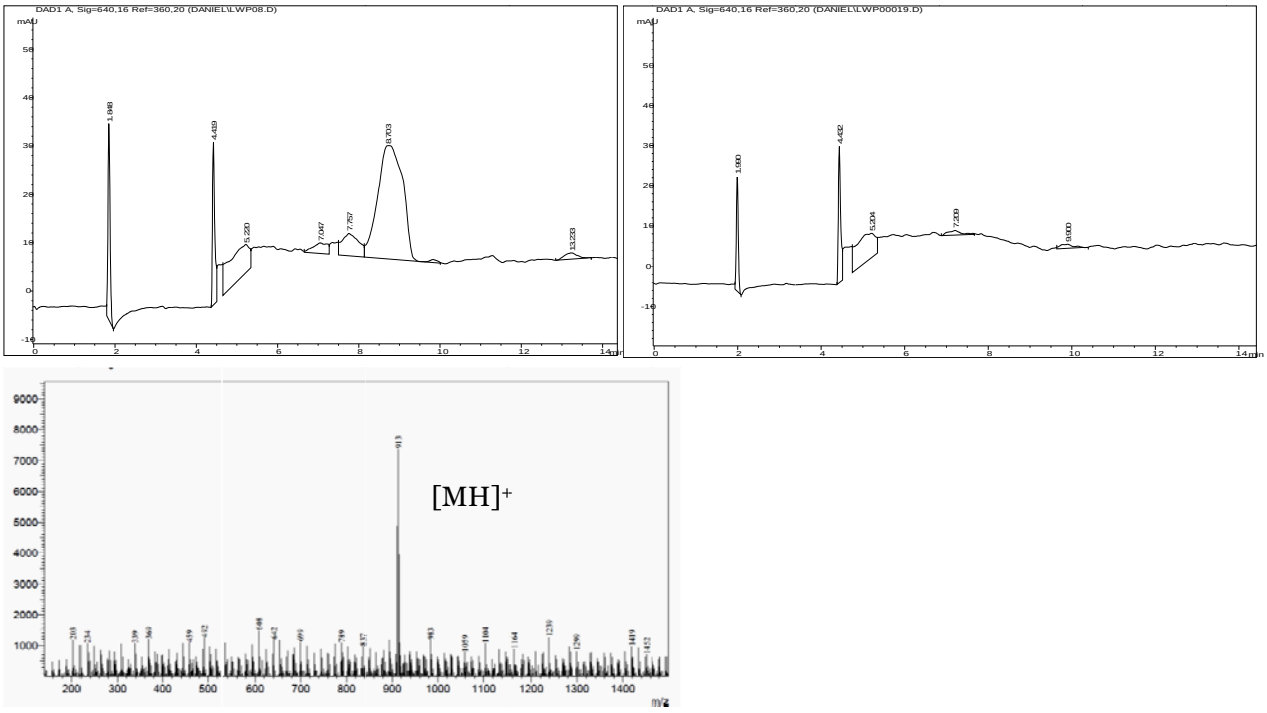

Figure A-29: HPLC-chromatogram of **1** (top, left), blank run under the same settings (top, right) and mass spectrum obtained by electrospray ionisation (bottom).

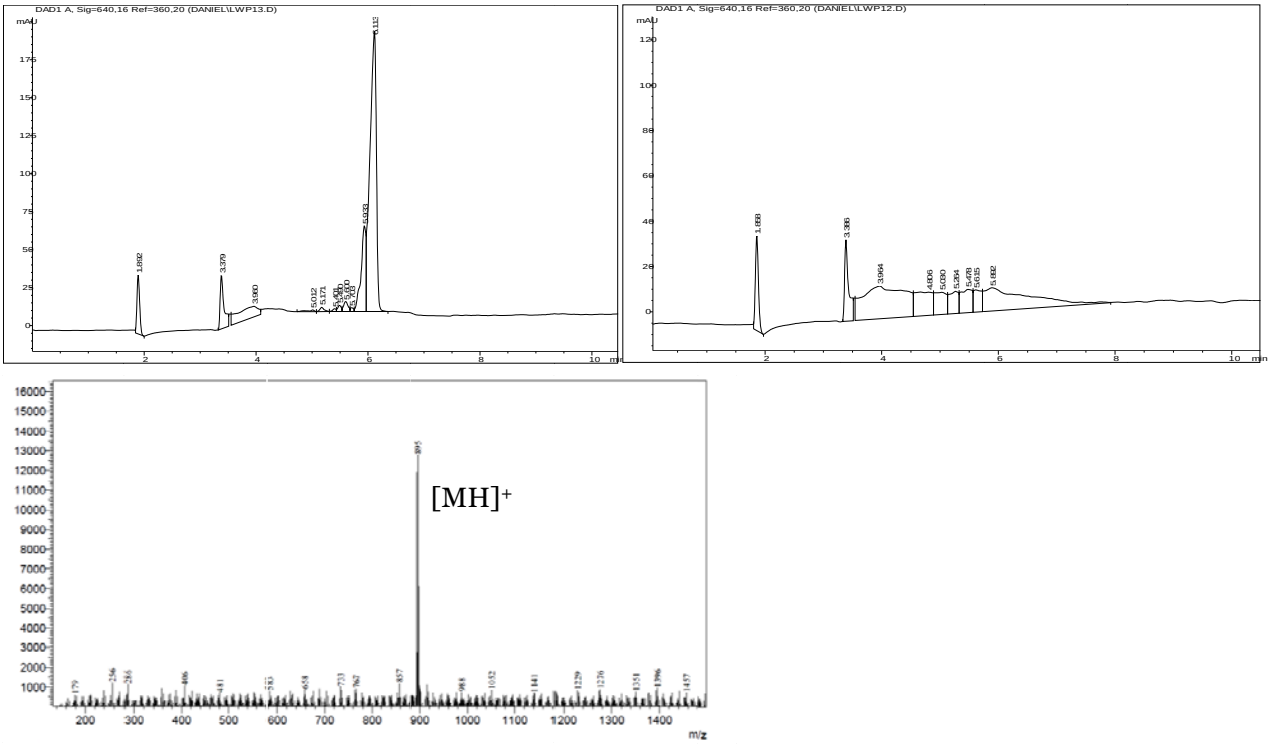

Figure A-30: HPLC-chromatogram of **2** (top, left), blank run under the same settings (top, right) and mass spectrum obtained by electrospray ionisation (bottom).

As discussed ealier, **3** is an isomeric mixture due to different sbstitution pattern formed upon chlorosulfonation. Note that no other masses than $[MNa]^+$ were detected in the whole sample.

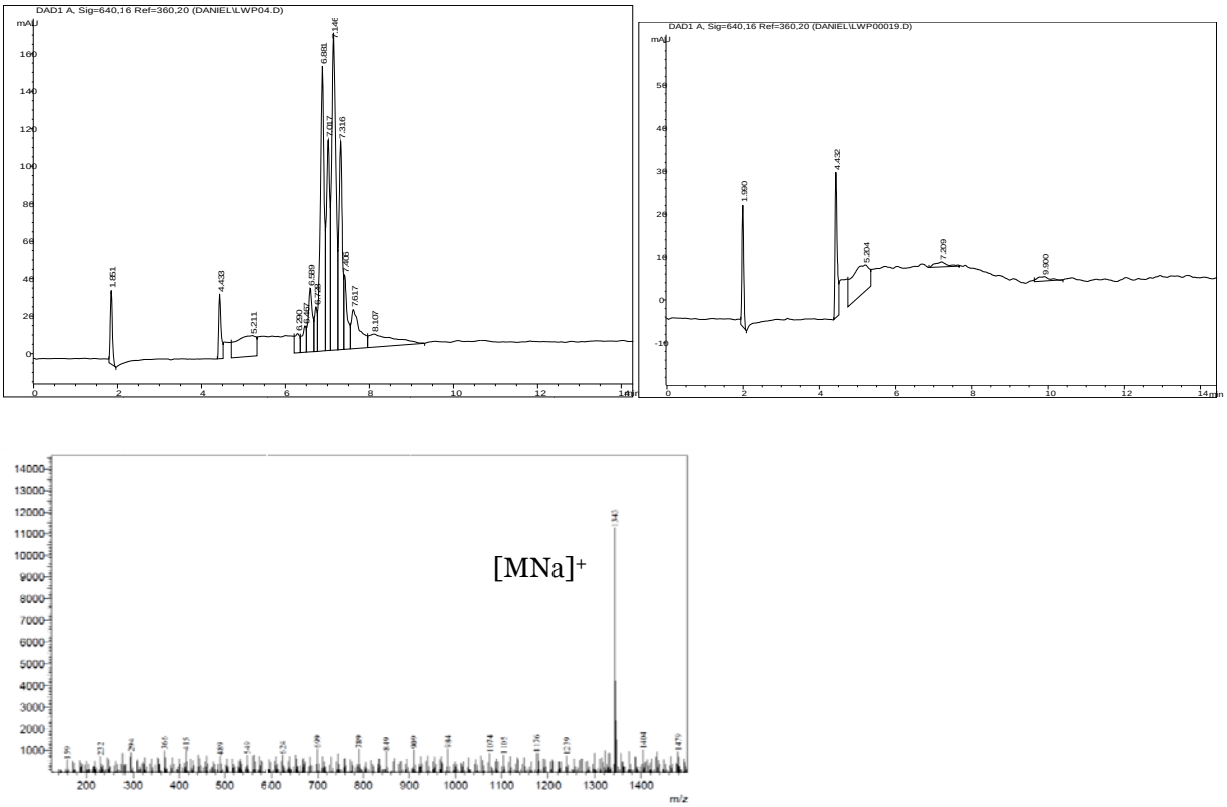

Figure A-31: HPLC-chromatogram of **3** (top, left), blank run under the same settings (top, right) and mass spectrum obtained by electrospray ionisation (bottom).

Table A-1: Elution gradient used for LCMS characterisation of **1** and **2**

Time/min	Ratio CH_3CN/%	Ratio 0.1% aqueous HOAc/%	Flow rate/ml·min^{-1}
0	0	100	1
5	100	0	1
10	100	0	1
11	0	100	1
15	0	100	1

Table A-2: Elution gradient used for LCMS characterisation of **3**

Time/min	Ratio CH_3CN/%	Ratio 0.1% aqueous HOAc/%	Flow rate/ml·min^{-1}
0	0	100	1
1	40	60	1
8	75	25	1
9	100	0	1
11	100	0	1
12	0	100	1
16	0	100	1

Chapter 3

New Fluorescent pH Optrodes Based on Covalently Linkable PET Rhodamines

NMR Spectra

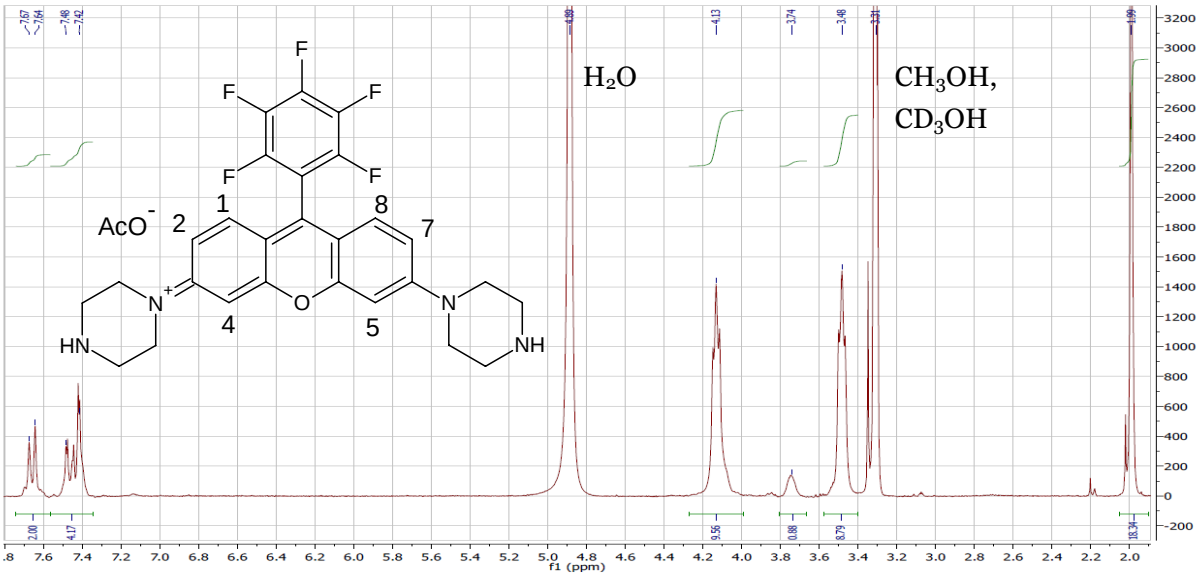

Figure A-32: ^{1}H-NMR spectrum of **1** in CD_3OD containing 0.1% HOAc and 0.1% CF_3COOH. Before addition of HOAc the integral of acetate hydrogen (1.99ppm) was 2.9 (spectrum not shown here). δ = 7.65ppm (2H, d, Ar-H(positions 1,8), $J_{ArH12,78}$ = 9.6 Hz); δ = 7.46 (2H, dd, Ar-H(2,7), $J_{ArH24,57}$ = 2.5 Hz); δ = 7.42 (2H, d, Ar-H(4,5)); δ = 4.13 (8H, t, $ArNCH_2$, J = 5.2 Hz); δ = 3.48 (8H, t, $HNC\underline{H}_2$); δ = 1.99 (3H, s, $H_{acetate}$).

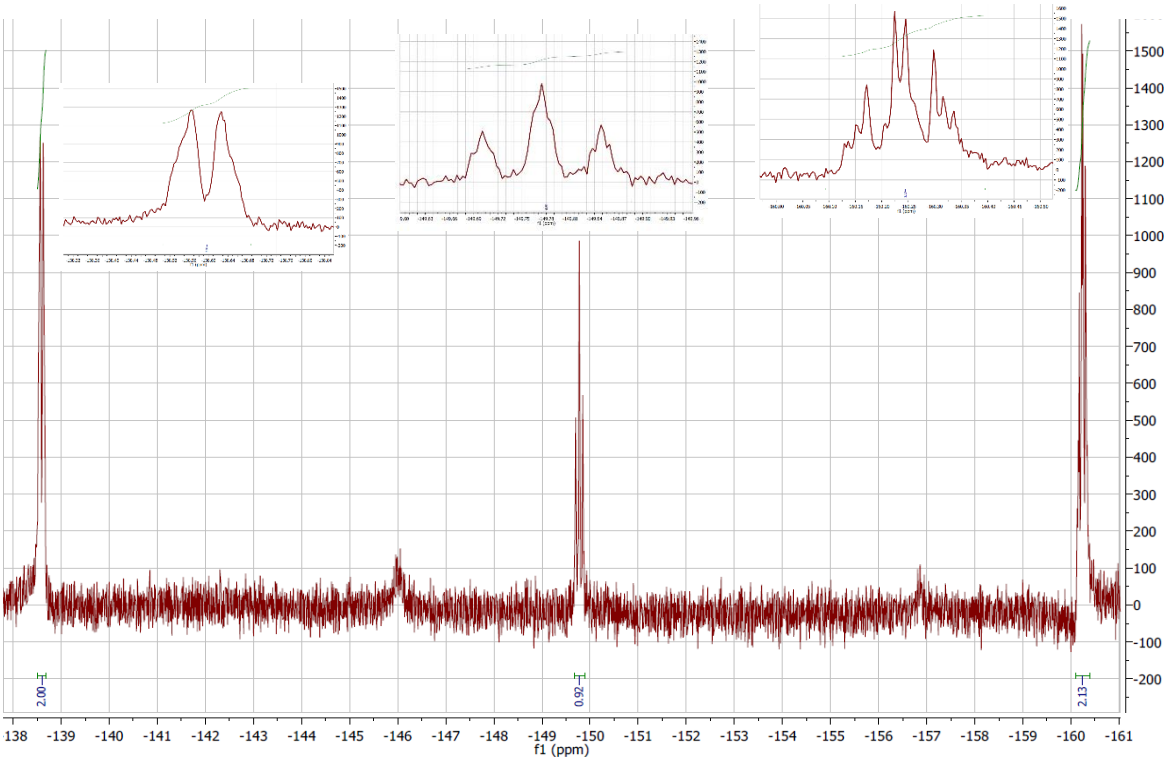

Figure A-33: ^{19}F-NMR spectrum of 1. δ = -139ppm (2F, d, J = 20 Hz); δ = -150 (1F, t, J = 21 Hz); δ = -160 (2F, dt, J_1 = 6 Hz, J_2 = 21 Hz).

Compound **2**

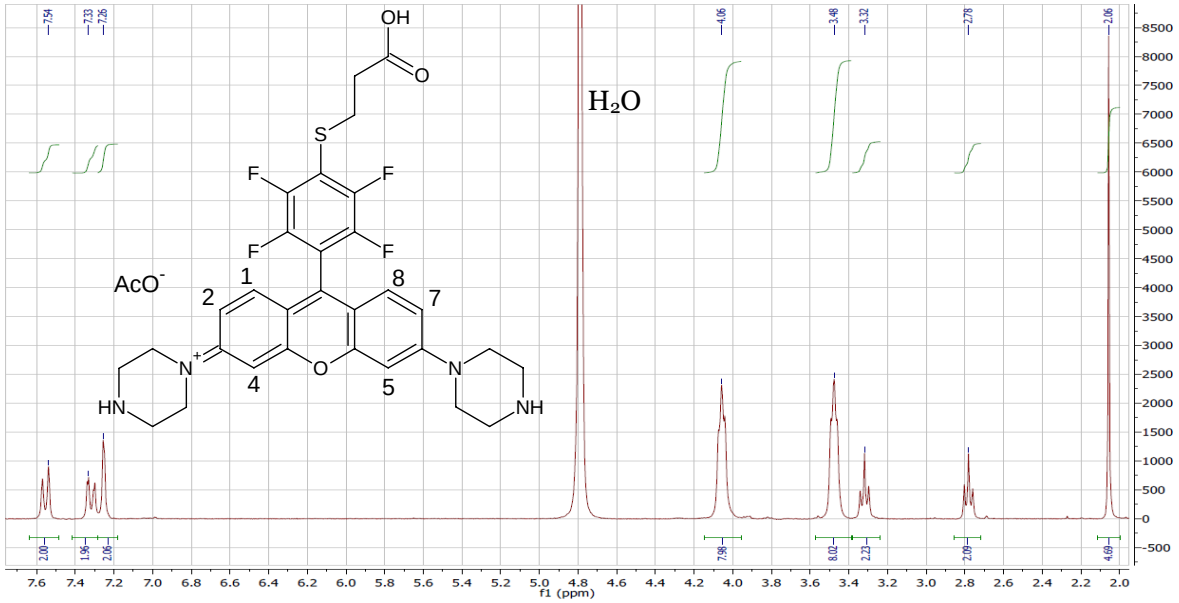

Figure A-34: ^{1}H-NMR spectrum of **2** in D_2O containing 0.1% CF_3COOH. δ = 7.55ppm (2H, d, Ar-H(positions 1,8), $J_{ArH12,78}$ = 9.6 Hz); δ = 7.32 (2H, dd, Ar-H(2,7), $J_{ArH24,57}$ = 2.3 Hz); δ = 7.26 (2H, d, Ar-H(4,5)); δ = 4.06 (8H, t, $ArNCH_2$, J = 4.9 Hz); δ = 3.48 (8H, t, $HNCH_2$); δ = 3.32 (2H, t, $ArSCH_2$, J = 6.7 Hz); δ = 2.76 (2H, t, CH_2COOH); δ = 2.06 (4.7H, s, $H_{acetate}$).

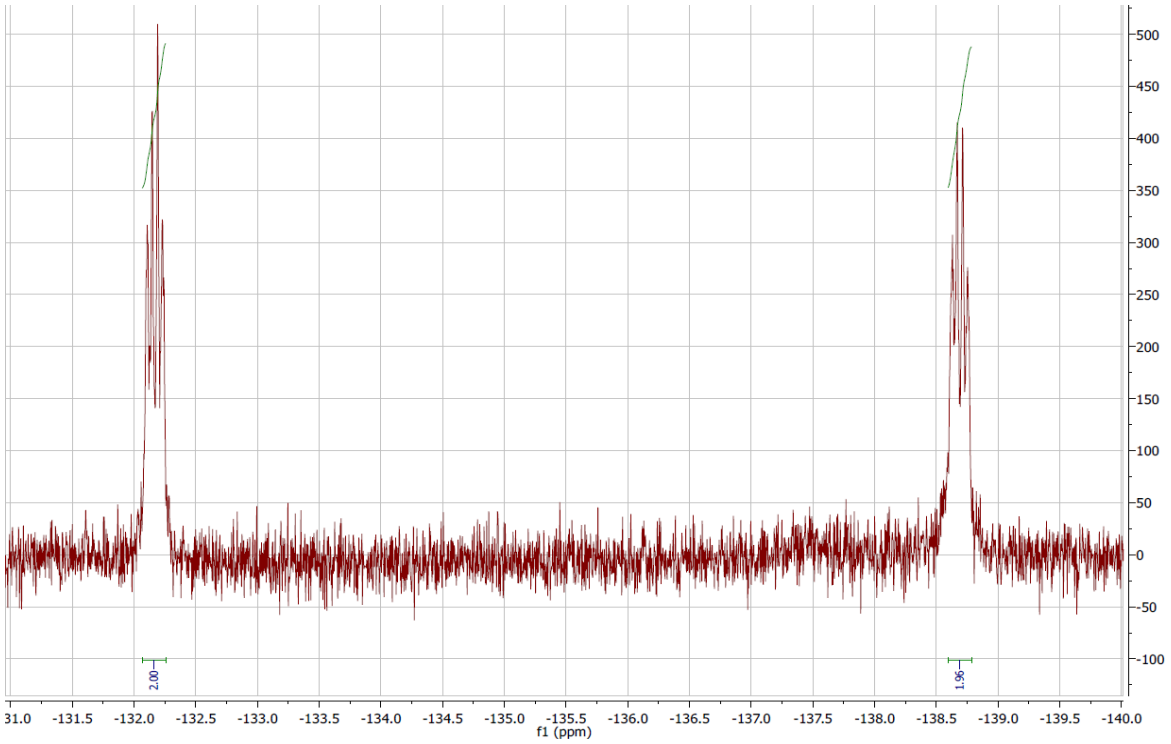

Figure A-35: ^{19}F-NMR spectrum of 2. δ = -132ppm (2F, q, J = 11 Hz); δ = -139 (2F, q, J = 11 Hz).

Compound **3**

Compound **3** could be identified as the pure 4'-carboxy regioisomer (figure S9). For comparison, the spectrum of the 5'-carboxy regioisomer (figure S10), which was also obtained upon HPLC purification of crude **3**, is shown. Resonance at >7.9ppm is can be attributed to the protons in the dicarboxyphenyl ring which are in ortho-position to a carboxy group. The 4'-isomer contains only two such protons, while three can be found for the 5'-isomer.

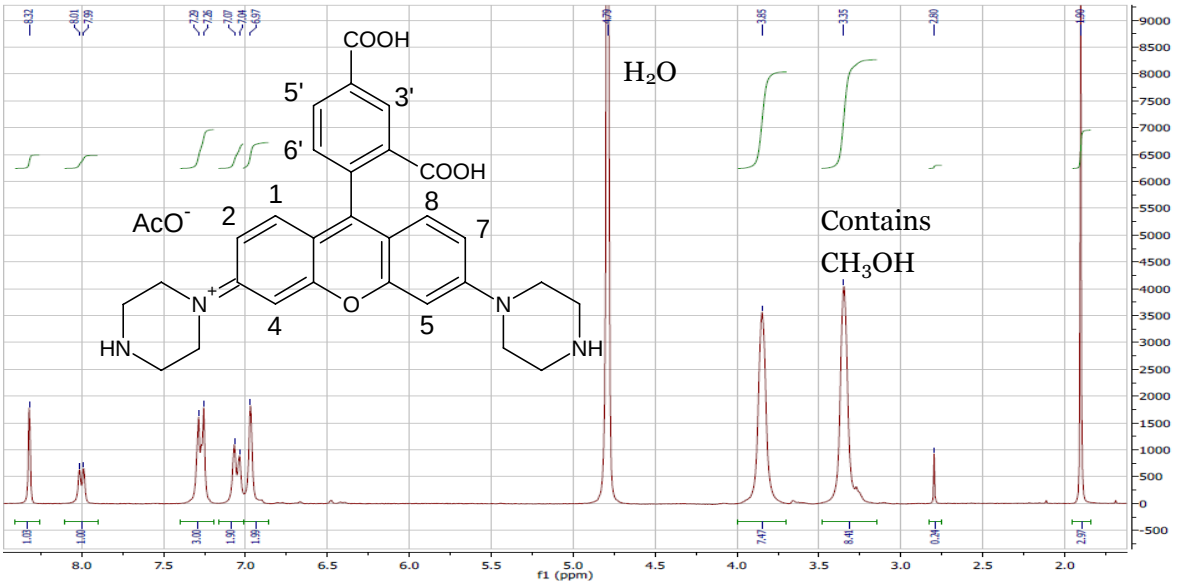

Figure A-36: ^{1}H-NMR spectrum of **3** (4'-carboxy regioisomer) in D_2O. δ = 8.32ppm (1H, s, Ar-H(position 3')); δ = 8.00 (1H, d, Ar-H(5'), $J_{ArH5'6'}$ = 7.5 Hz); δ = 7.27 (3H, d, Ar-H(6',1,8), $J_{ArH12,78}$ = 9.3 Hz); δ = 7.06 (2H, d, Ar-H(2,7)); δ = 6.97 (2H, s, Ar-H(4,5)); δ = 3.85 (8H, broad s, $ArNCH_2$); δ = 3.35 (8H, broad s, $HNCH_2$); δ = 1.90 (3H, s, $H_{acetate}$).

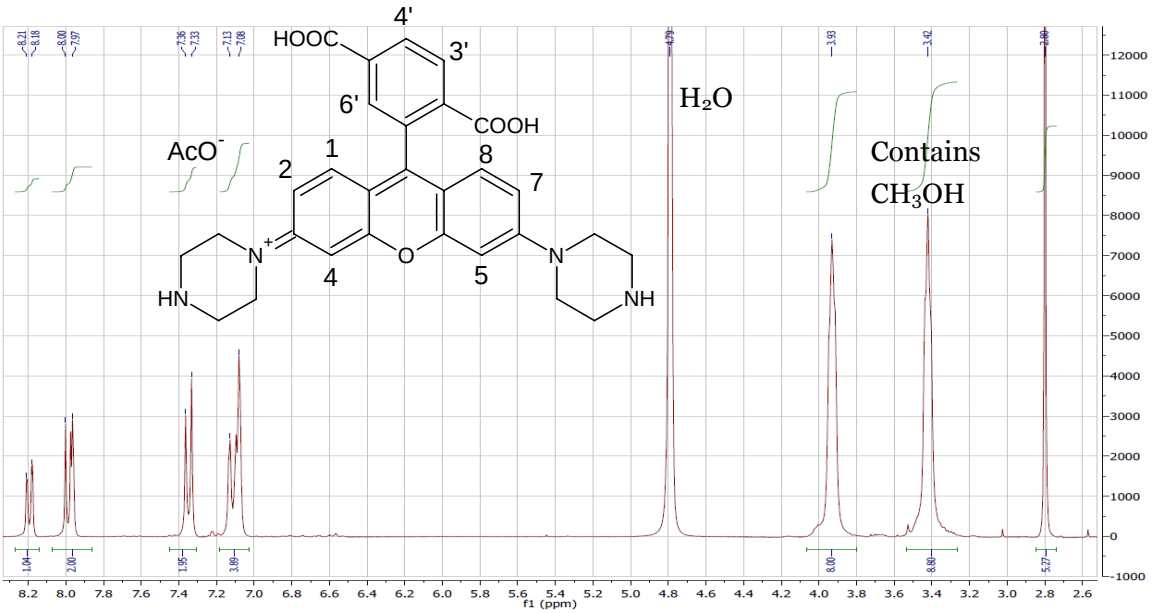

Figure A-37: ^{1}H-NMR spectrum of the 5'-carboxy regioisomer to **3** in D_2O. δ = 8.20 (1H, dd, Ar-H(4'), $J_{ArH3'4'}$ = 8.1Hz, $J_{ArH4'6'}$ = 1.7 Hz); δ = 7.99 (1H, d, Ar-H(3')); δ = 7.97 (1H, d, Ar-H(6')); δ = 7.35 (2H, dd, Ar-H(1,8), $J_{ArH12,78}$ = 9.4 Hz, $J_{ArH24,57}$ = 1.6 Hz); δ = 7.11 (2H, d, Ar-H(2,7)); δ = 7.08 (2H, d, Ar-H(4,5)); δ = 3.93 (8H, t, $ArNCH_2$, J = 4.6 Hz); δ = 3.42 (8H, t, $HNCH_2$); δ = 2.80 (5.3H, s, $H_{acetate}$).

LC-MS Measurements:

Compound **1** after HPLC purification

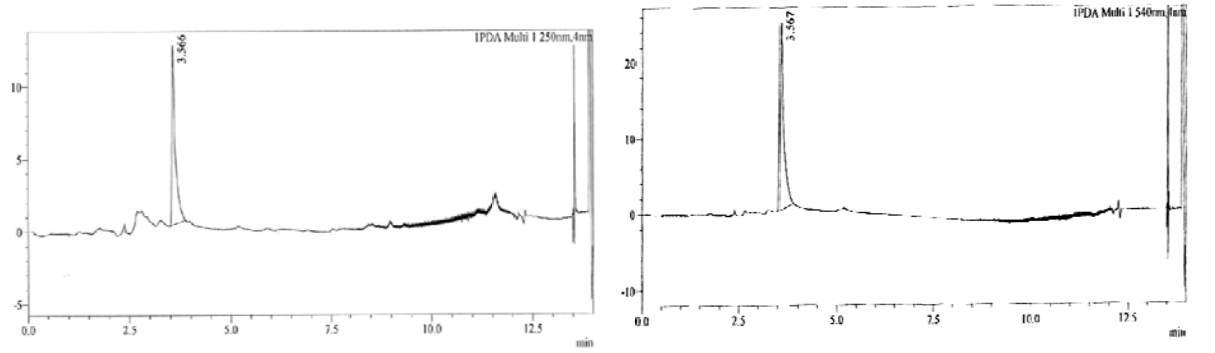

Figure A-38: Chromatogram of **1** after HPLC purification, recorded with an UV/VIS detector set to 250nm (left) and 540nm (right), bandwidth 4nm each.

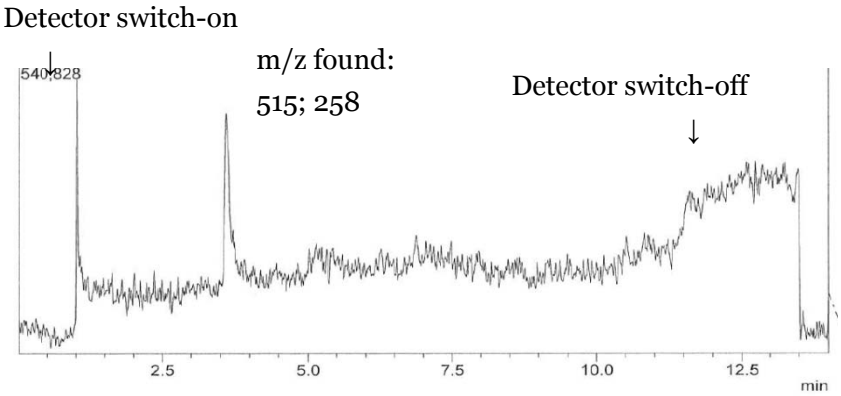

Figure A-39: Total ion current chromatogram of **1** after HPLC purification, recorded with an ESI-quadruple MS detector.

Compound **1** (crude)

LC-MS characterisation of crude **1** reveals an interesting side-product which shows a slightly higher mass than the main product but no absorption typical for rhodamines. This could be the product of a reduction (formal addition of H^- to the chinoid form of the rhodamine) which results in disruption of the xanthene chromophore.

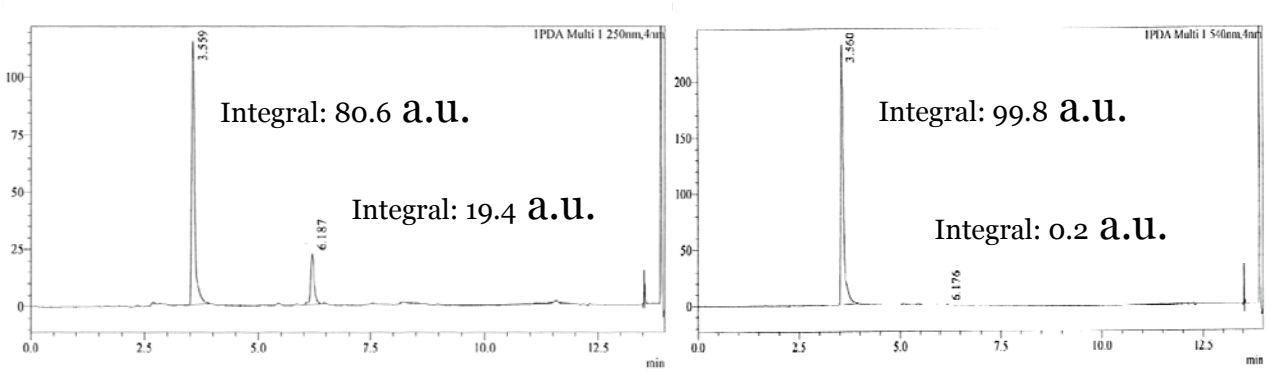

Figure A-40: Chromatogram of crude **1**, recorded with an UV/VIS detector set to 250nm (left) and 540nm (right), bandwidth 4nm each.

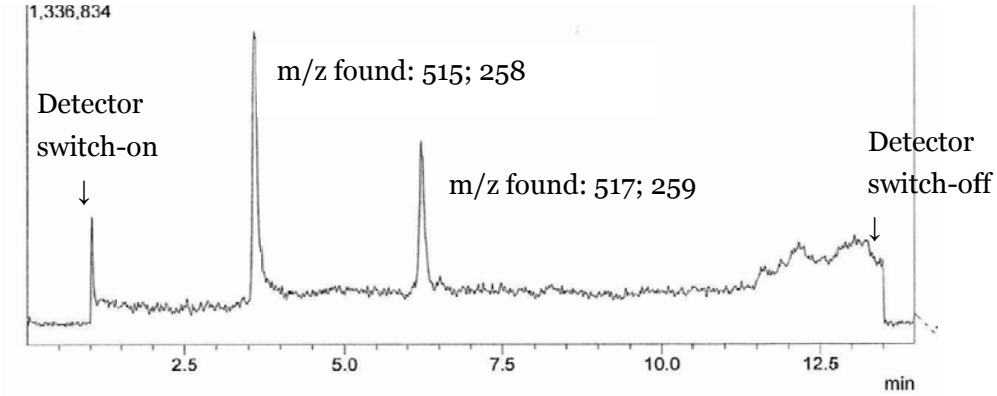

Figure A-41: Total ion current chromatogram of crude **1**, recorded with an ESI-quadruple MS detector.

Compound **2** after HPLC purification

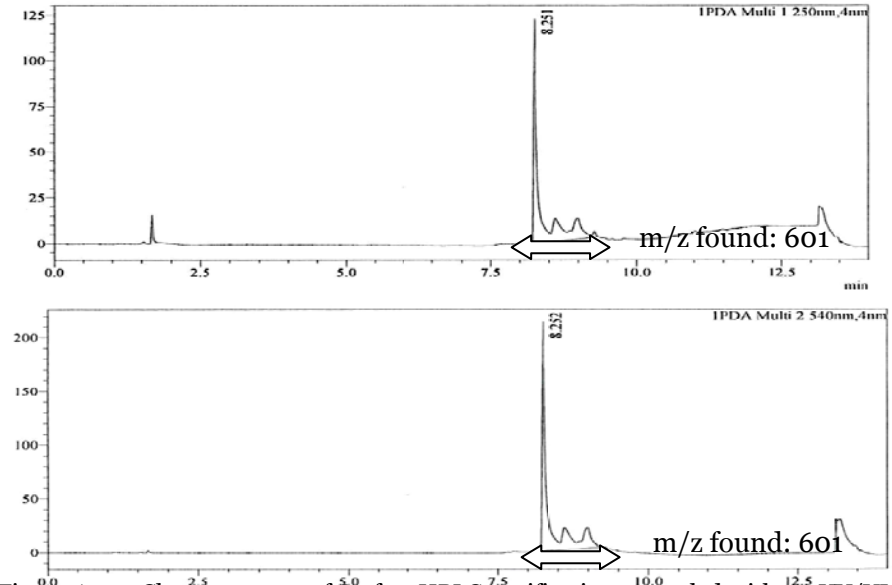

Figure A-42: Chromatogram of **2** after HPLC purification, recorded with an UV/VIS detector set to 250nm (top) and 540nm (bottom), bandwidth 4nm each. m/z=601 was found over the whole indicated time (ESI-quadruple MS detector).

Compound **3** after HPLC purification

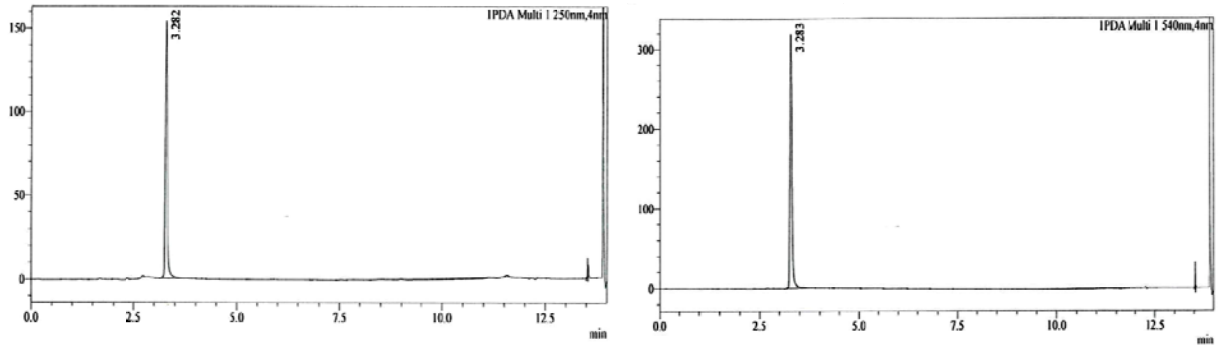

Figure A-43: Chromatogram of **3** after HPLC purification, recorded with an UV/VIS detector set to 250nm (left) and 540nm (right), bandwidth 4nm each.

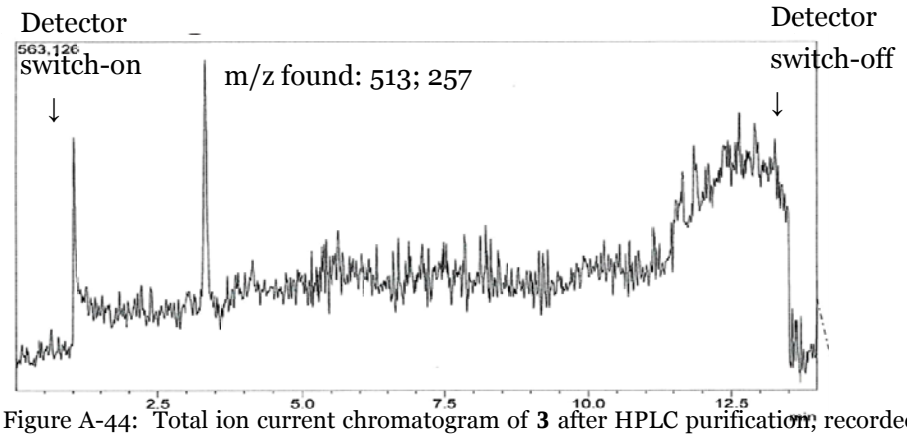

Figure A-44: Total ion current chromatogram of **3** after HPLC purification, recorded with an ESI-quadruple MS detector.

Compound **3** (crude)

LC-MS characterisation shows that crude **3** is composed of four different rhodamines which have been formed in an approximate ratio of 1:1:0.3:0.3. The two main components which are eluted earlier have been isolated and identified by NMR spectroscopy as the 5'-carboxy and the 4'-carboxy regioisomers of the target structure. The 4'-isomer (i.e. compound **3**) was used for characterisation. The two components eluted later have higher molecular masses and could be the result of methylation by methanesulfonic acid upon preparation.

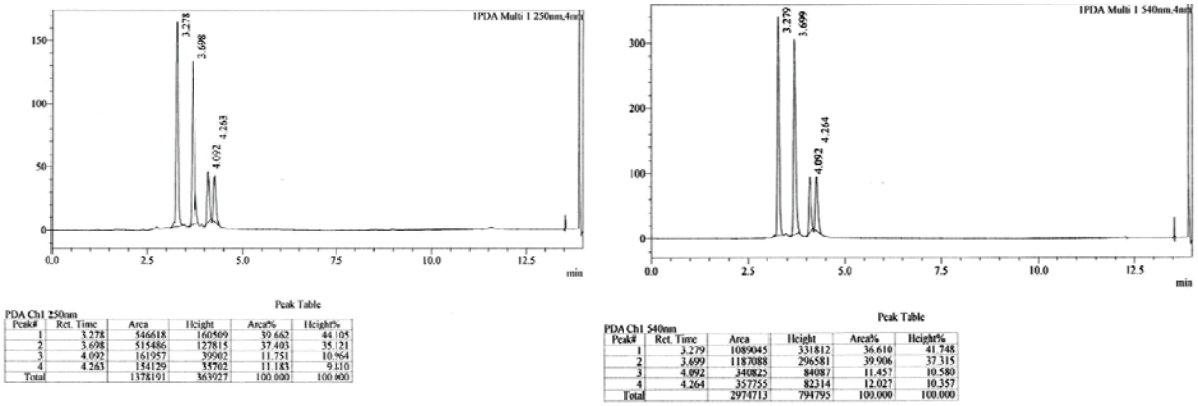

Peak Table

PDA Ch1 250nm

Peak#	Ret. Time	Area	Height	Area%	Height%
1	3.278	546618	160569	39.662	44.105
2	3.698	515486	127815	37.403	35.121
3	4.092	161957	39902	11.751	10.964
4	4.263	154129	35702	11.183	9.810
Total		1378191	363927	100.000	100.000

Peak Table

PDA Ch1 540nm

Peak#	Ret. Time	Area	Height	Area%	Height%
1	3.279	1089045	331812	36.610	41.748
2	3.699	1187088	296581	39.906	37.315
3	4.092	340825	84087	11.457	10.580
4	4.264	357755	82314	12.027	10.357
Total		2974713	794795	100.000	100.000

Figure A-45: Chromatogram of crude **3**, recorded with an UV/VIS detector set to 250nm (left) and 540nm (right), bandwidth 4nm each. The corresponding peak integrals are listed in the peak tables.

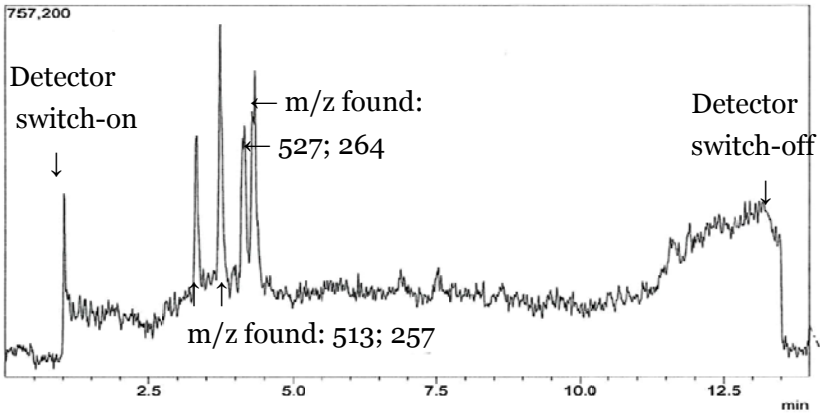

Figure A-46: Total ion current chromatogram of crude **3**, recorded with an ESI-quadruple MS detector.

Gradients used for HPLC purification:

Table A-3: HPLC gradient used for the purification of **1**.

Time/min	Ratio MeOH/%	Ratio 0.1% aqueous HOAc/%	Flow rate/ml·min^{-1}
0	0	100	4
10	30	70	4
11	100	0	4
16	100	0	4
17	0	100	4
22	0	100	4

Table A-4: HPLC gradient used for the purification of **2**.

Time/min	Ratio MeOH/%	Ratio 0.1% aqueous HOAc/%	Flow rate/ml·min^{-1}
0	10	90	16
30	25	75	16
32	100	0	16
40	100	0	16

Table A-5: HPLC gradient used for the purification of **3**.

Time/min	Ratio MeOH/%	Ratio 0.1% aqueous HOAc/%	Flow rate/ml·min^{-1}
0	0	100	4
12	30	70	4
12.5	100	0	4
16.5	100	0	4
17	0	100	4
21	0	100	4

Gradient used for LC-MS characterisation

Table A-6: Gradient used for LC-MS characterisation of **1**-**3**.

Time/min	Ratio MeOH/%	Ratio 0.01% aqueous HCOOH/%	Flow rate/ml·min^{-1}
0	2	98	0.7
5	2	98	0.7
10	100	0	0.7
12	100	0	0.7
13	2	98	0.7

Chapter 4

Fluorescent Materials for pH Sensing and Imaging Based on Novel 1,4-Diketopyrrolo-[3,4-c]pyrrole dyes

NMR spectra

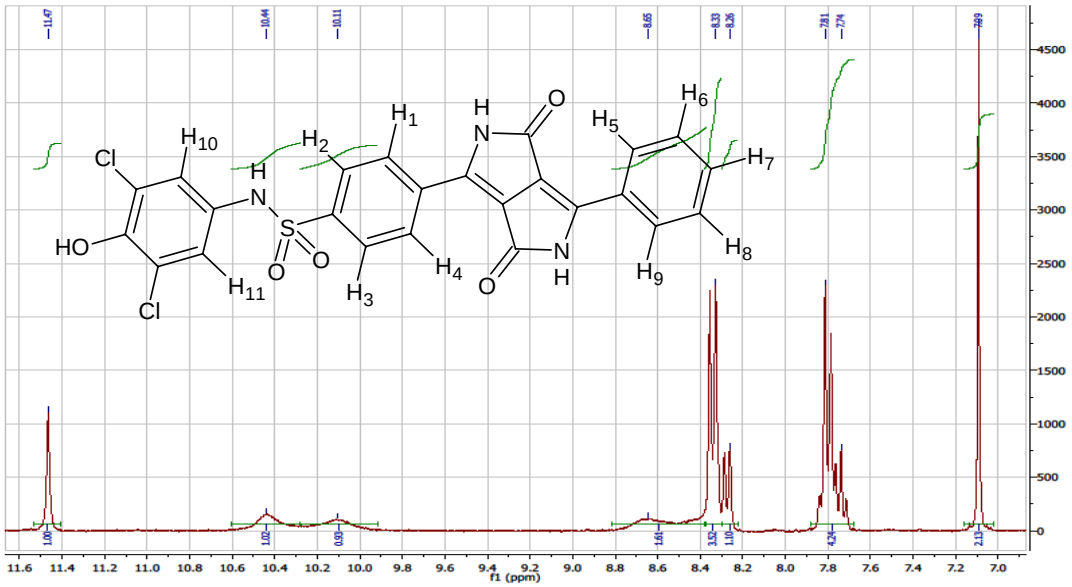

Figure A-47: ^{1}H-NMR spectrum of **2** (300 MHz, DMSO-*d6*, TMS): δ_H = 11.47 (1 H, s, Ar-H(9)), 10.44 (1 H, s, ArOH), 10.11 (1 H, s, SO_2NH), 8.3 - 8.7 (2 H, CONH), 8.33 (3 H, d, J = 8.4 Hz, Ar-H(2,3,5)), 8.26 (1 H, dd, J_1 = 7.7 Hz, J_2 = 1.1 Hz, Ar-H(8)), 7.70 - 7.86 (4 H, m, Ar-H(1,4,6,7)), 7.09 (2 H, s, Ar-H(10,11)).

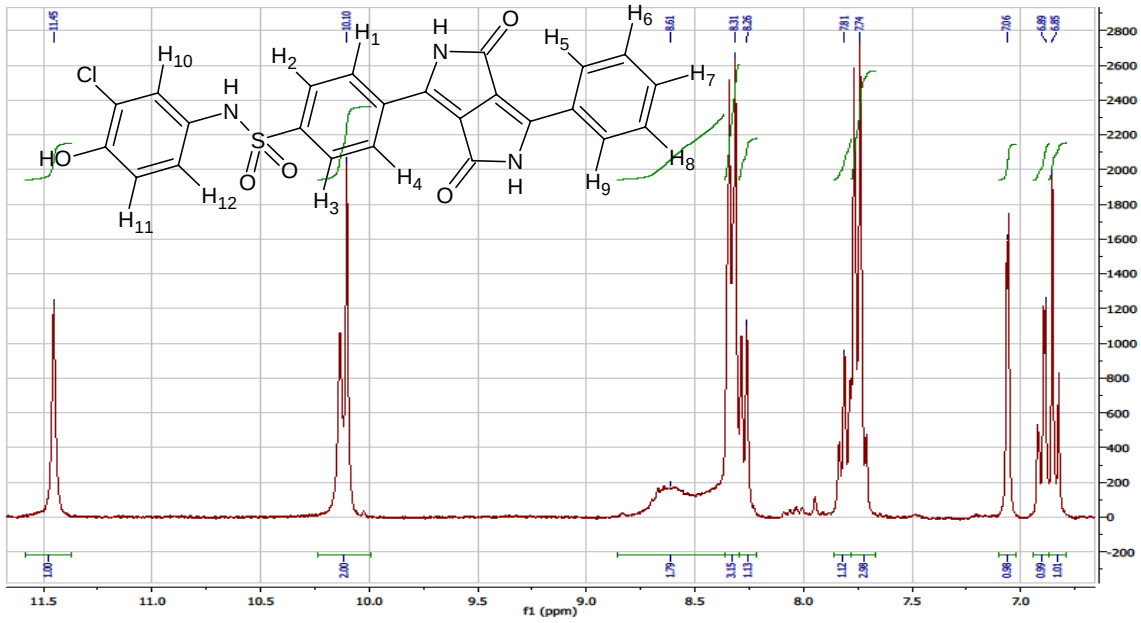

Figure A-48: ^{1}H-NMR spectrum of **3** (300 MHz, DMSO-*d6*, TMS): δ_H = 11.45 (1 H, s, Ar-H(9)), 10.10 (2 H, d, ArOH, SO_2NH), 8.3 - 8.7 (2 H, CONH), 8.31 (3 H, dd, J_1 = 8.1 Hz, J_2 = 2.1 Hz, Ar-H(2,3,5)), 8.26 (1 H, dd, J_1 = 7.7 Hz, J_2 = 1.4 Hz, Ar-H(8)), 7.70 - 7.86 (4 H, m, Ar-H(1,4,6,7)), 7.06 (1 H, d, J = 2.3 Hz, Ar-H(10)), 6.89 (1 H, dd, J_1 = 8.7 Hz, J_2 = 2.4 Hz, Ar-H(12)), 6.85 (1 H, d, J = 8.5 Hz, Ar-H(11)).

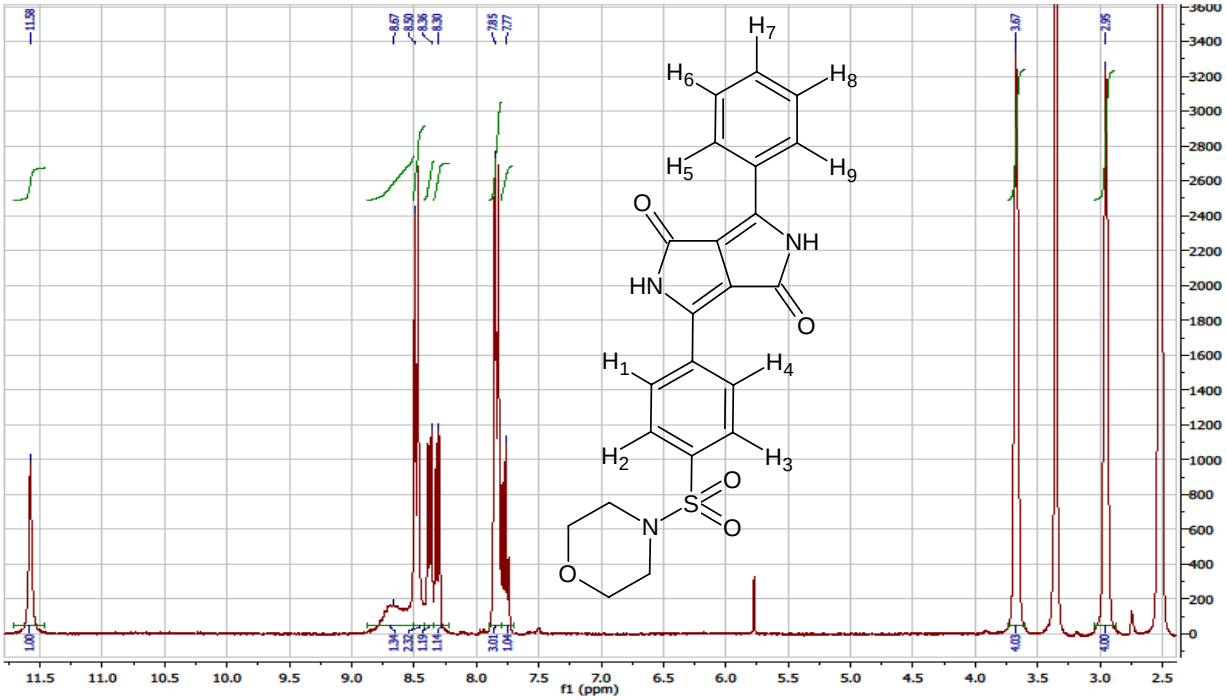

Figure A-49: ^{1}H-NMR spectrum of **4** (300 MHz, DMSO-*d6*, TMS): δ_H = 11.58 (1 H, s, Ar-H(9)), 8.3 - 8.8 (2 H, CONH), 8.50 (2 H, d, J = 8.7 Hz, Ar-H(2,3)), 8.36 (1 H, d, J = 7.8 Hz, Ar-H(5)), 8.30 (1 H, dd, J_1 = 7.8 Hz, J_2 = 1.1 Hz, Ar-H(8)), 7.85 (3 H, dt, J_1 = 8.4 Hz, J_2 = 1.9 Hz, Ar-H(1,4,6)), 7.77 (1 H, t, J = 7.5 Hz, Ar-H(7)), 3.67 (4 H, t, J = 4.2 Hz, OCH_2), 2.95 (4 H, t, J = 4.1 Hz, $ArNCH_2$).

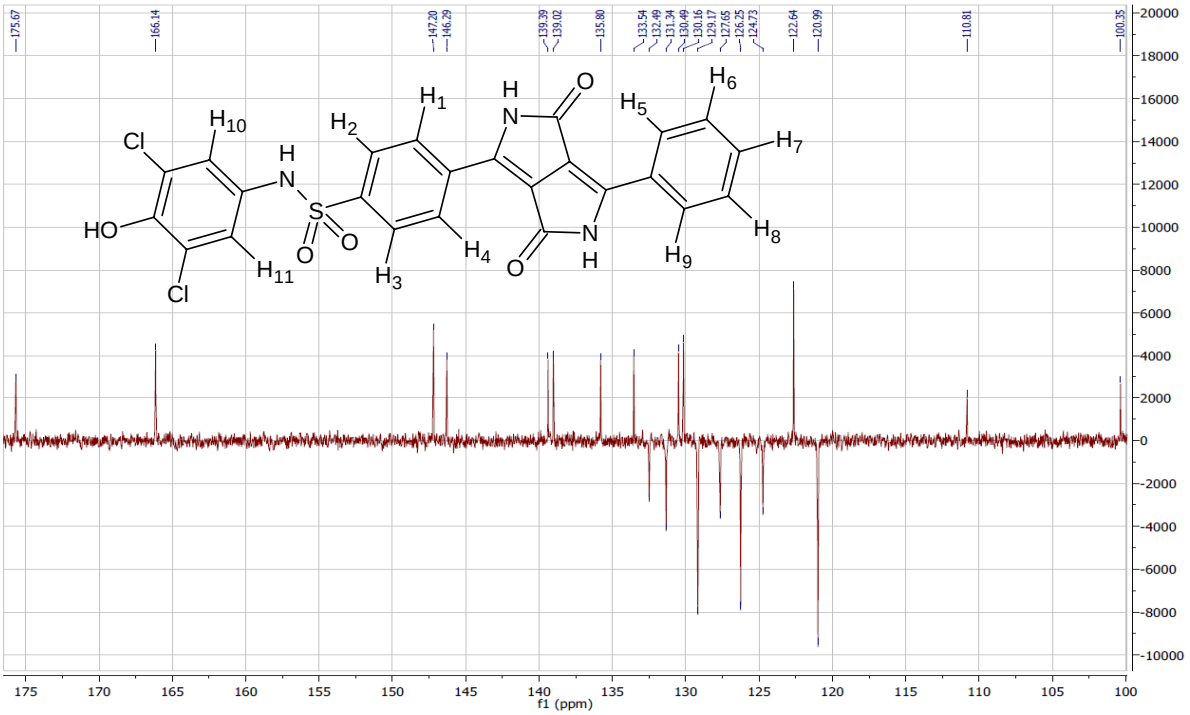

Figure A-50: ^{13}C-APT-NMR spectrum of **2** (300 MHz, DMSO-*d6*, TMS): δ_C = 175.67, 166.14 (C=O); 147.20, 146.29, 139.39, 139.02, 135.80, 133.54 (C_{Ar}); 132.49 (C_{Ar}-H_6), 131.34 (C_{Ar}-H_7); 130.49, 130.16 (C_{Ar}); 129.17 (2C, C_{Ar}-H_2, C_{Ar}-H_3), 127.65 (C_{Ar}-H_8), 126.25 (2C, C_{Ar}-H_1, C_{Ar}-H_4), 124.73 (C_{Ar}-H_5); 122.64 (2C, C_{Ar}); 120.99 (2C, C_{Ar}-H_{10}, C_{Ar}-H_{11}); 110.81, 100.35 (C_{Ar}).

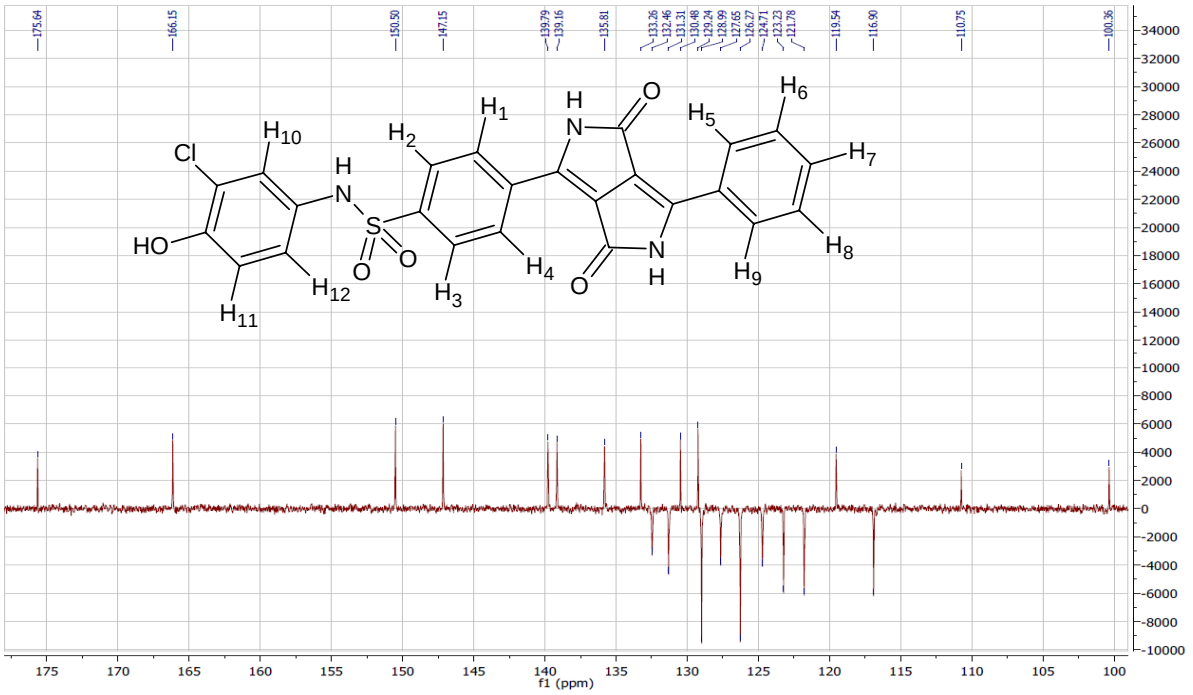

Figure A-51: ^{13}C-APT-NMR spectrum of **3** (300 MHz, DMSO-*d6*, TMS): δ_C = 175.64, 166.15 (C=O); 150.50, 147.15, 139.79, 139.16, 135.81, 133.26 (C_{Ar}); 132.46 (C_{Ar}-H_6), 131.31 (C_{Ar}-H_7); 130.48, 129.24 (C_{Ar}); 128.99 (2C, C_{Ar}-H_2, C_{Ar}-H_3), 127.65 (C_{Ar}-H_8), 126.67 (2C, C_{Ar}-H_1, C_{Ar}-H_4), 124.71 (C_{Ar}-H_5), 123.23 (C_{Ar}-H_{10}), 121.78 (C_{Ar}-H_{12}); 119.54 (C_{Ar}); 116.90 (C_{Ar}-H_{11}); 110.75, 100.36 (C_{Ar}).

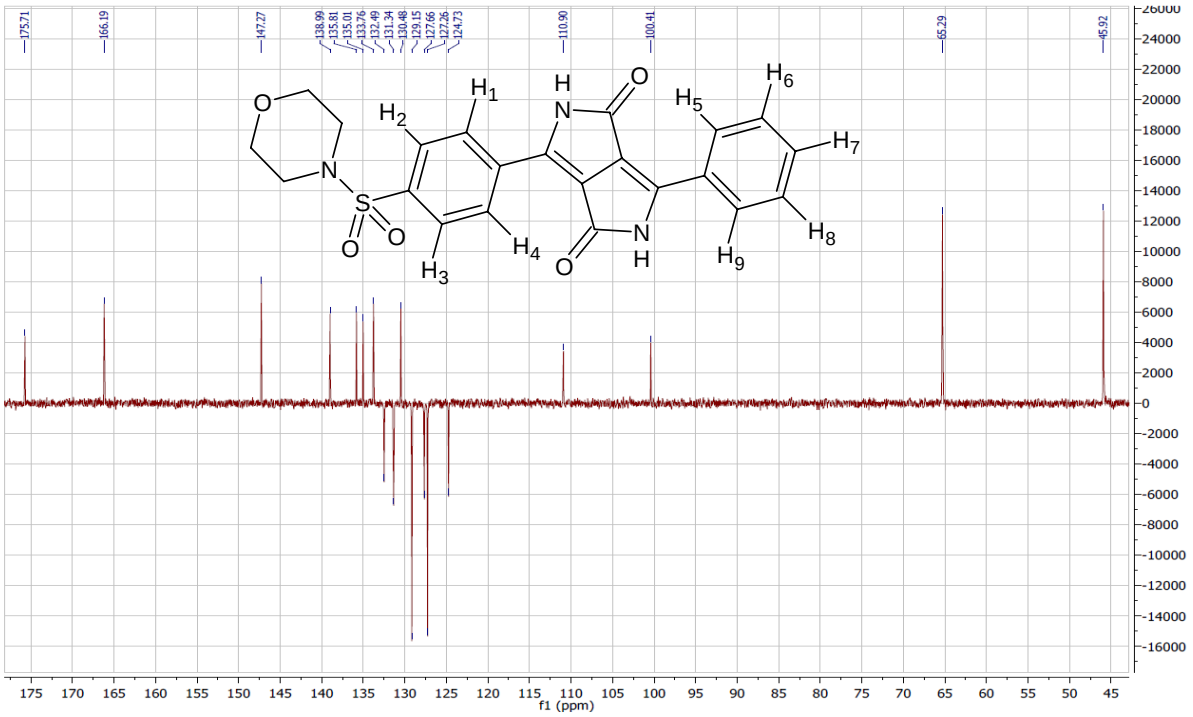

Figure A-52: ^{13}C-APT-NMR spectrum of **4** (300 MHz, DMSO-*d6*, TMS): δ_C = 175.71, 166.19 (C=O); 147.27, 138.99, 135.81, 135.01, 133.76 (C_{Ar}); 132.49 (C_{Ar}-H_6), 131.34 (C_{Ar}-H_7); 130.48, (C_{Ar}); 129.15 (2C, C_{Ar}-H_2, C_{Ar}-H_3), 127.66 (C_{Ar}-H_8), 127.26 (2C, C_{Ar}-H_1, C_{Ar}-H_4), 124.73 (C_{Ar}-H_5); 110.90, 100.41 (C_{Ar}); 65.29 (C-O); 45.92 (C-N).

MALDI-TOF Spectra:

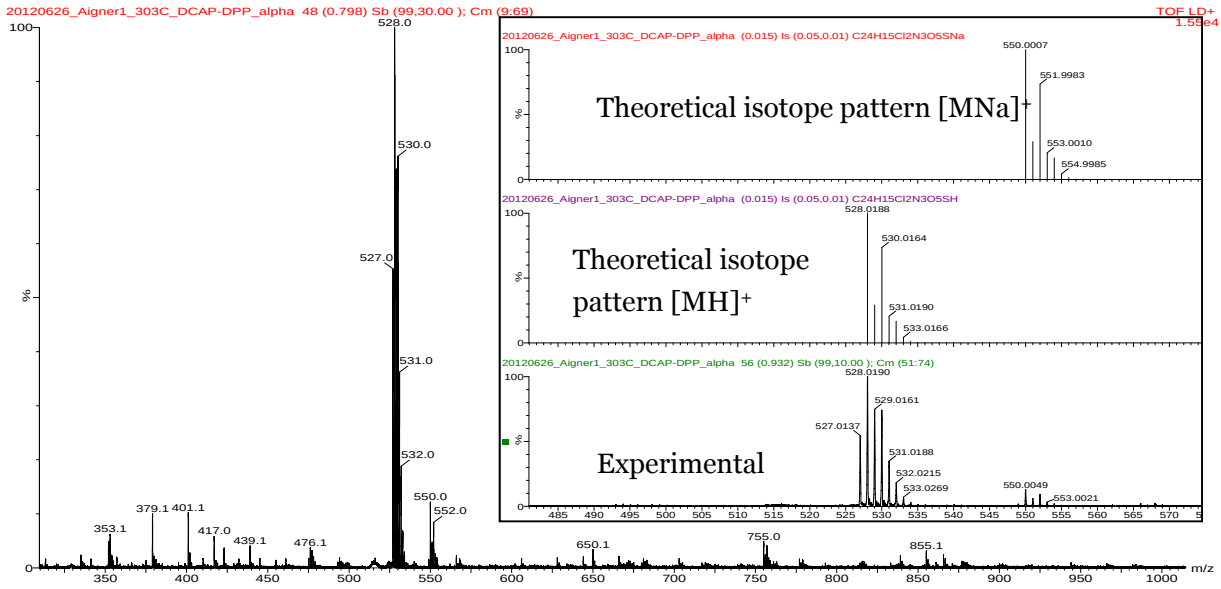

Figure A-53: MALDI-TOF spectrum of **2**

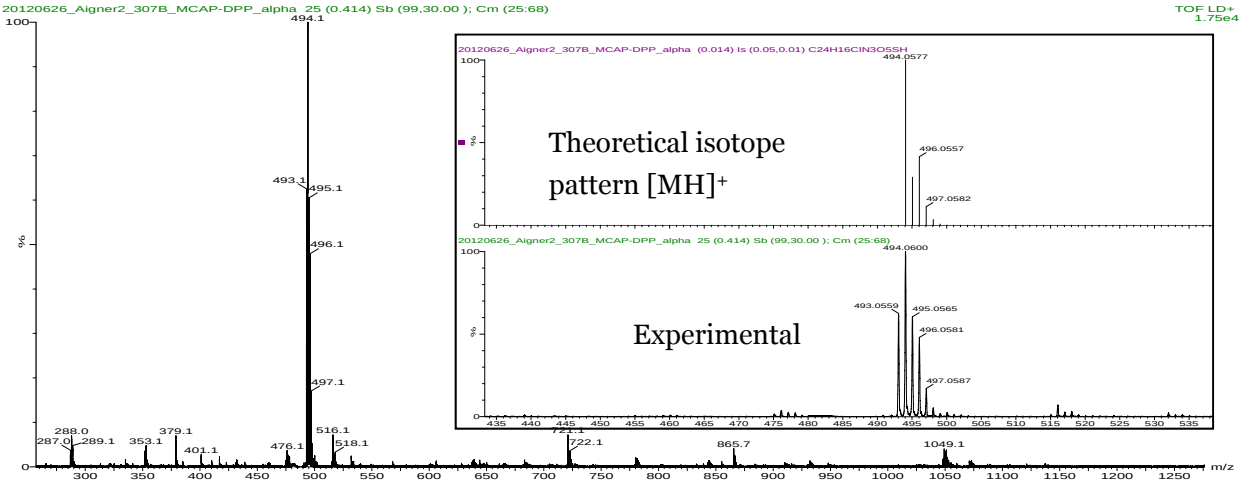

Figure A-54: MALDI-TOF spectrum of **3**

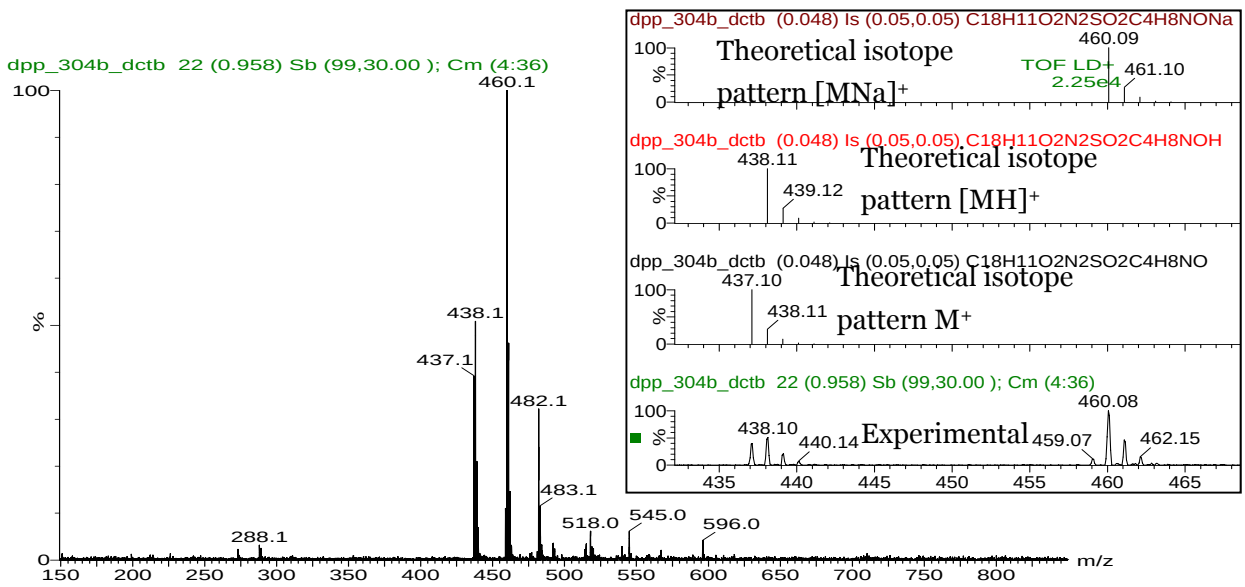

Figure A-55:: MALDI-TOF spectrum of **4**

Full UV/VIS absorption spectra (230 – 1000 nm) and IR spectra:

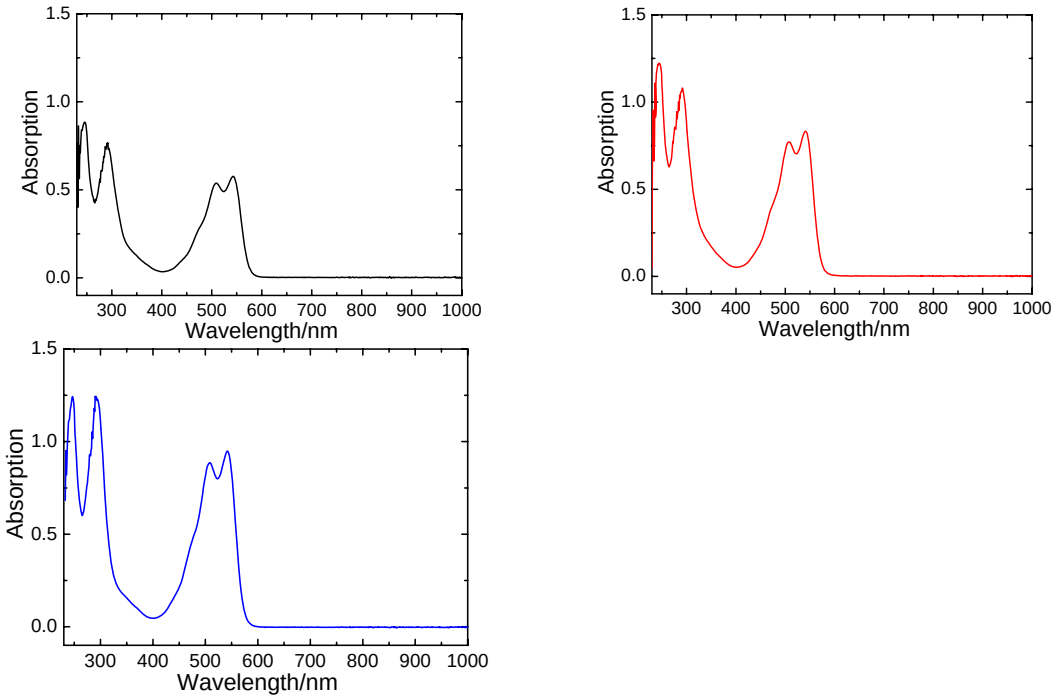

Figure A-56: UV/VIS absorption spectra of **2** (top, left), **3** (top, right) and **4** (bottom) in tetrahydrofuran

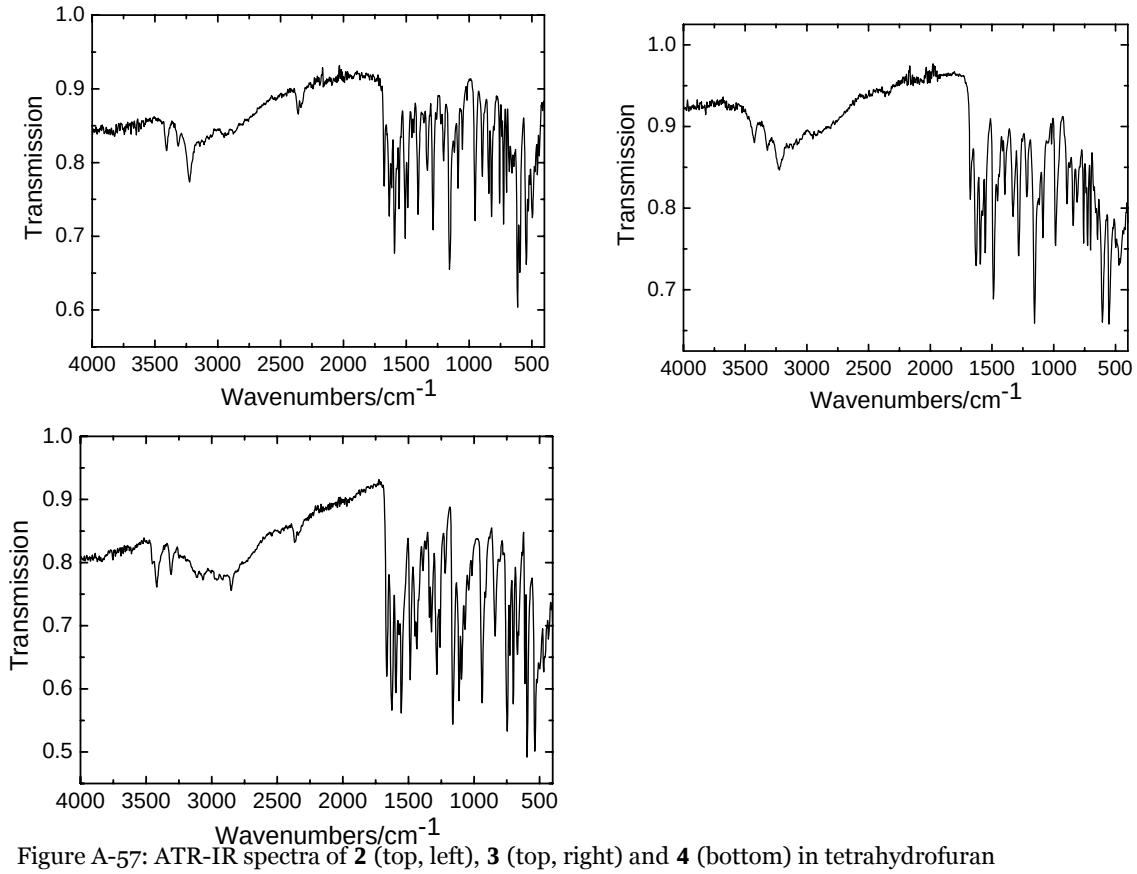

Figure A-57: ATR-IR spectra of **2** (top, left), **3** (top, right) and **4** (bottom) in tetrahydrofuran

Chapter 5

Enhancing Photoinduced Electron Transfer Efficiency of Fluorescent pH-probes with Halogenated Phenols

Electrochemical measurements

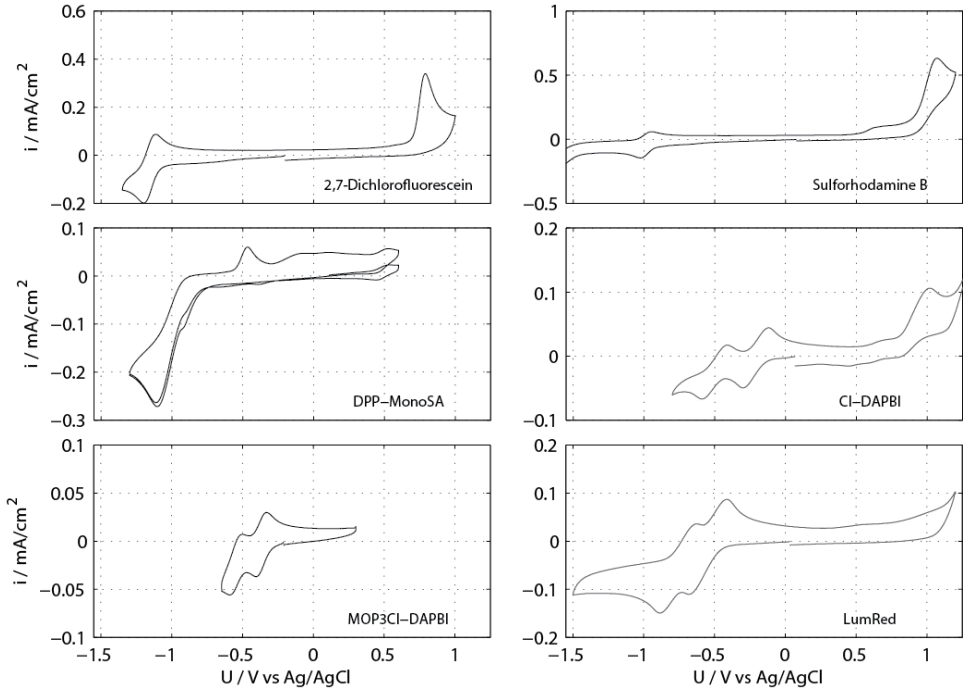

Figure A-58: Cyclic voltammograms of model compounds for fluorophores, denominated as stated in table 5-3 (main text). LumRed stands for LumogenRed (1,6,7,12-Tetraphenoxy-*N,N'*-di(2,6-diisopropylphenyl)perylene-3,4:9,10-tertracarboxylic bisimide) which is a model compound for 5A-C for which a very similar first reduction potential (-0.55 V) was found. %a-C are shown in the following figure.

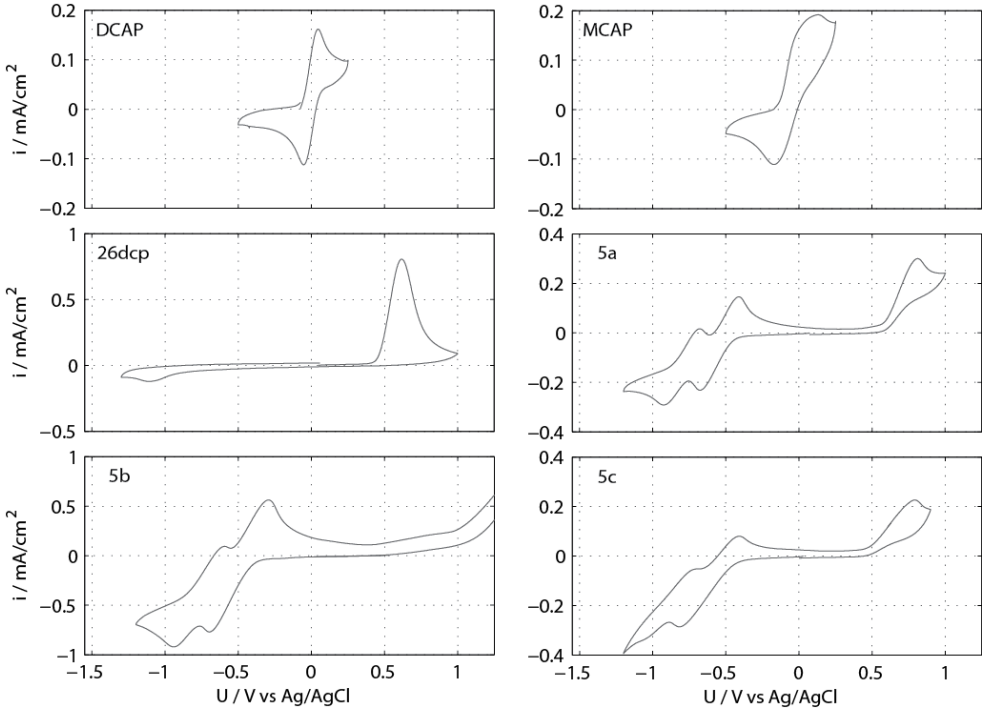

Figure A-59: Cyclic voltammograms of model compounds for PET groups; DCAP stands for 4-amino-2,6-dichlorophenol, MCAP for 4-amino-2-dichlorophenol and 26dcp for 2,6-dichlorophenol.

NMR Spectroscopy

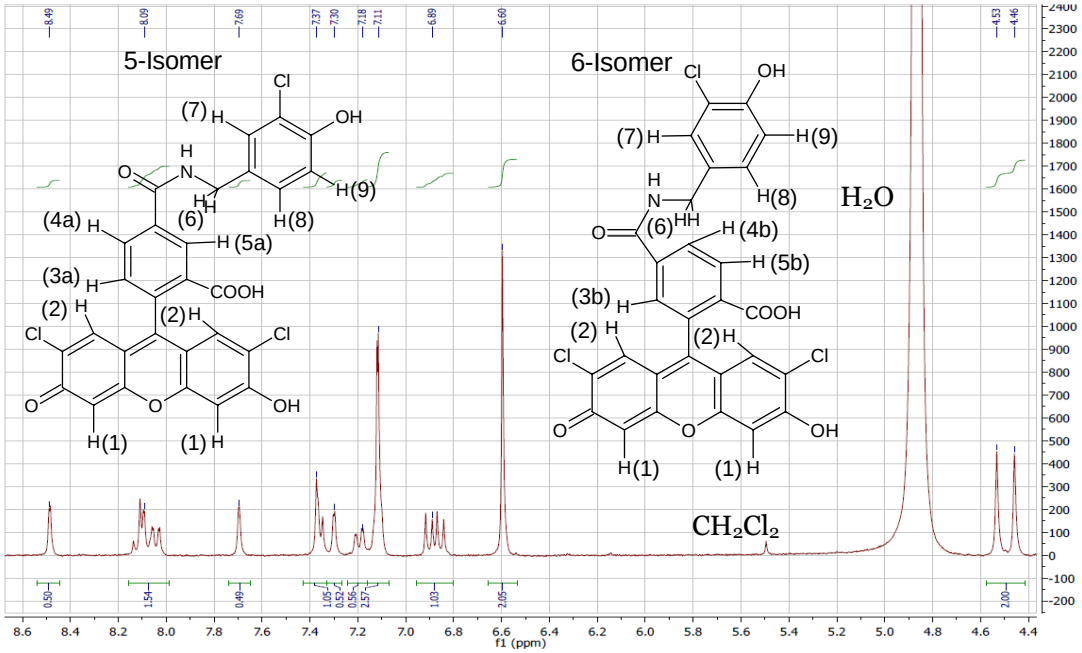

Figure A-60: ^{1}H NMR of **1a** (300 MHz, CD_3OD containing 0.02 M NH_3, TMS): δ = 8.49 (d, 0.5H, J = 1.3 Hz, H(5a)); 8.01 – 8.15 (m, 1.5H, H(4a,4b,5b)); 7.69 (d, 0.5H, J = 1.0 Hz, H(3b)); 7.33 – 7.39 (m, 1H, H(3a,7)); 7.30 (d, 0.5H, J = 1.8 Hz, H(7)); 7.16 – 7.22 (dd, 0.5H, J_1 = 8.2 Hz, J_2 = 2.0 Hz, H(9)); 7.11 (d, 2.5H, J = 1.6 Hz, H(2,9)); 6.82 – 6.93 (dd, 1H, J_1 = 8.3 Hz, J_2 = 14.2 Hz, H(8)); 6.60 (s, 2H, H(1)); 4.43 – 4.56 (d, 2H, H(6)).

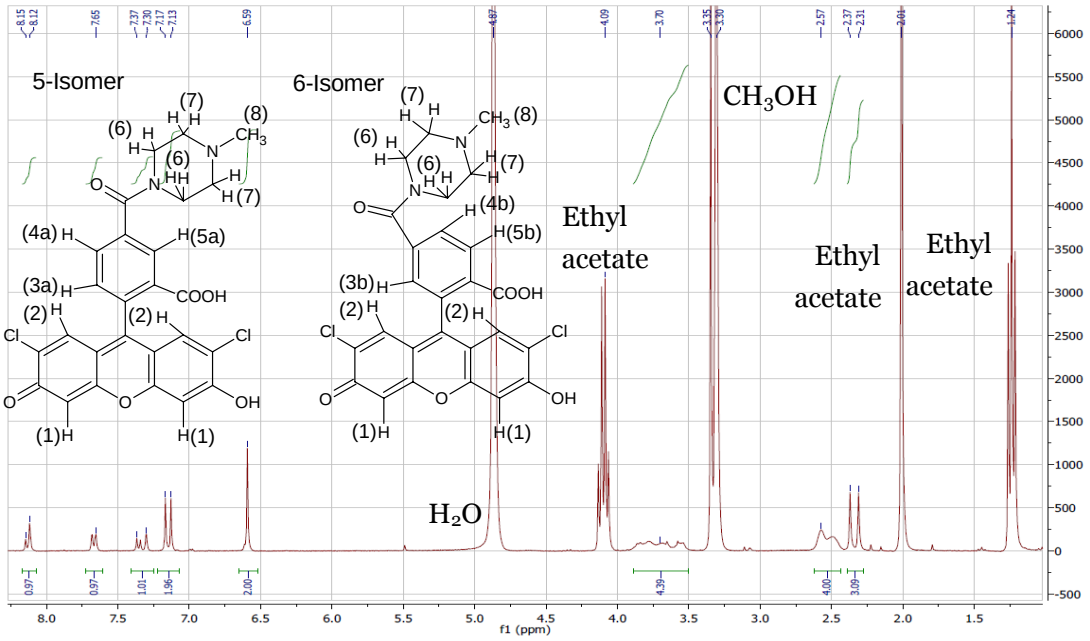

Figure A-61: ^{1}H NMR of **1b** (300 MHz, CD_3OD containing 0.02 M NH_3, TMS): δ = 8.09 – 8.17 (s + d, 1H, H(5a,5b); 7.65 (dd, 1H, J_1 = 7.8 Hz, J_2 = 1.1 Hz, H(4a,4b)); 7.27 – 7.39 (2d, 1H, J_1 = 7.7 Hz, J_2 = 1.2 Hz, H(3a,3b)); 7.10 – 7.19 (2s, 2H, H(2)); 6.59 (s, 2H, H(1)); 7.10 – 7.19 (2s, 2H, H(2)); 3.5 – 3.9 (m, 4H, H(6)); 2.44 – 3.64 (m, 4H, H(7)); 2.28 – 2.39 (2s, 3H, H(8)).

3-Chloro-4-hydroxybenzylamine

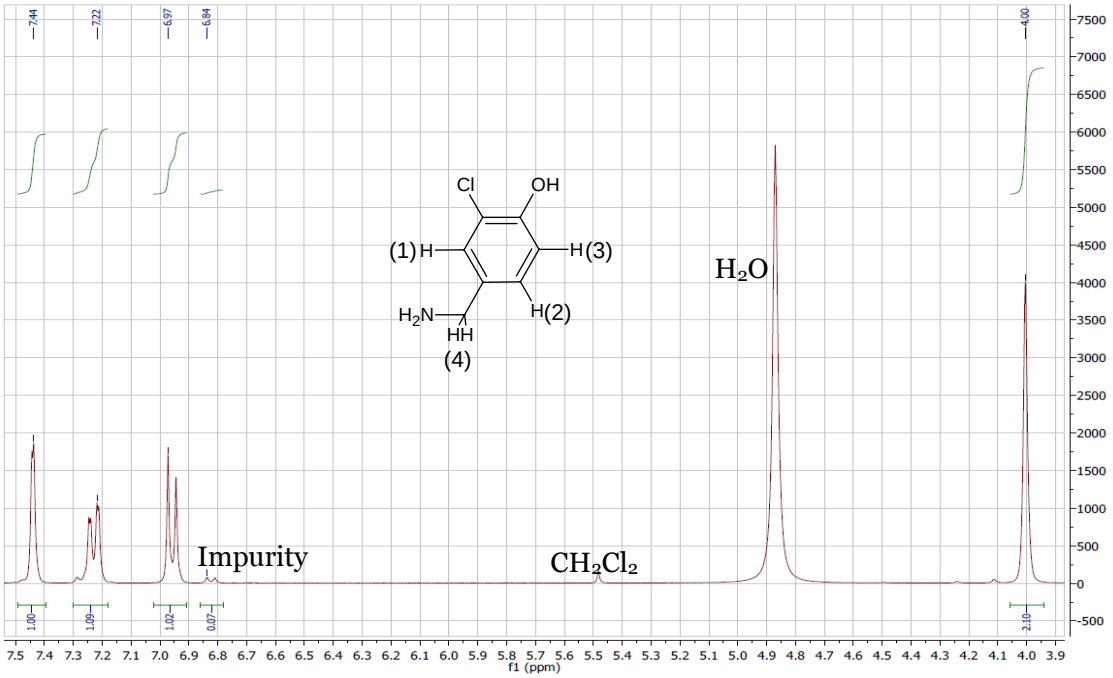

Figure A-62: ^{1}H NMR of 3-Chloro-4-hydroxybenzylamine (300 MHz, CD_3OD, TMS): δ = 7.44 (d, 1H, J = 1.9 Hz, H(1)); 7.22 (dd, 1H, J_1 = 8.3 Hz, J_2 = 1.8 Hz, H(2); 6.97 (d, 1H, J = 8.4 Hz, H(1); 4.00 (s, 2H, H(4)).

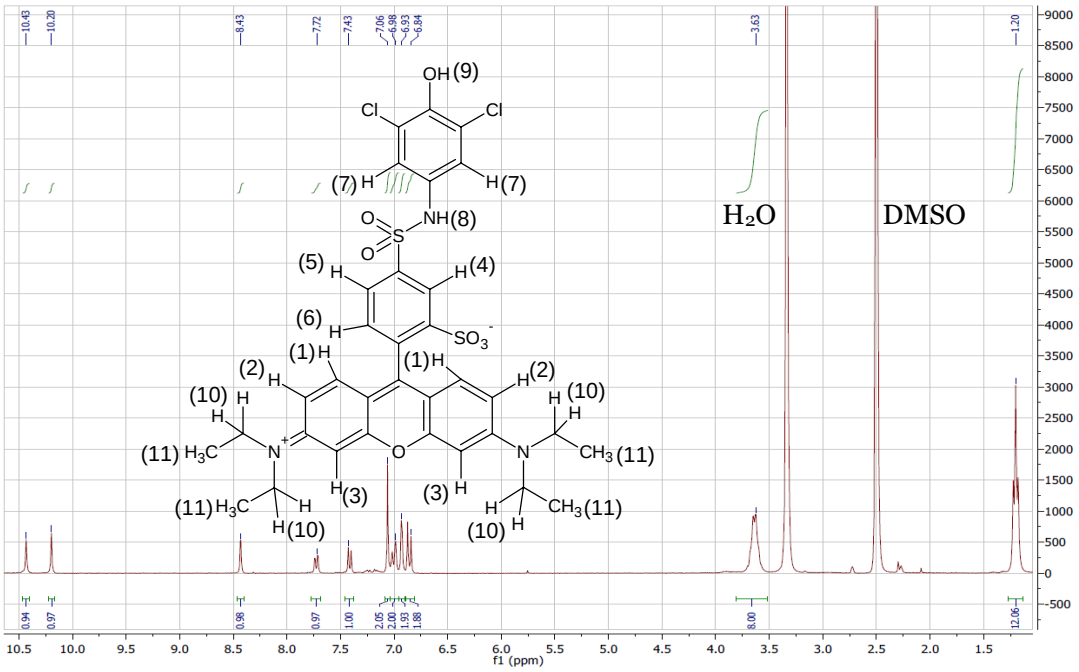

Figure A-63: ^{1}H NMR of **2a** (300 MHz, $(CD_3)_2SO$, TMS): δ = 10.43 (1H, s, H(9)); 10.20 (1H, s, H(8)); 8.43 (1H, d, J = 1.7 Hz, H(4)); 7.72 (1H, dd, J_1 = 8.0 Hz, J_2 = 1.8 Hz, H(5)); 7.43 (2H, d, J = 7.9 Hz, H(6)); 7.06 (2H, s, H(7)); 6.98 (2H, dd, J_1 = 9.5 Hz, J_2 = 1.8 Hz , H(2)); 6.93 (2H, d, J = 1.9 Hz, H(3)); 6.84 (2H, d, J = 9.3 Hz , H(1)); 3.63 (8H, q, J = 7.1 Hz , H(10)); 1.20 (12H, t, J = 6.9 Hz , H(11)).

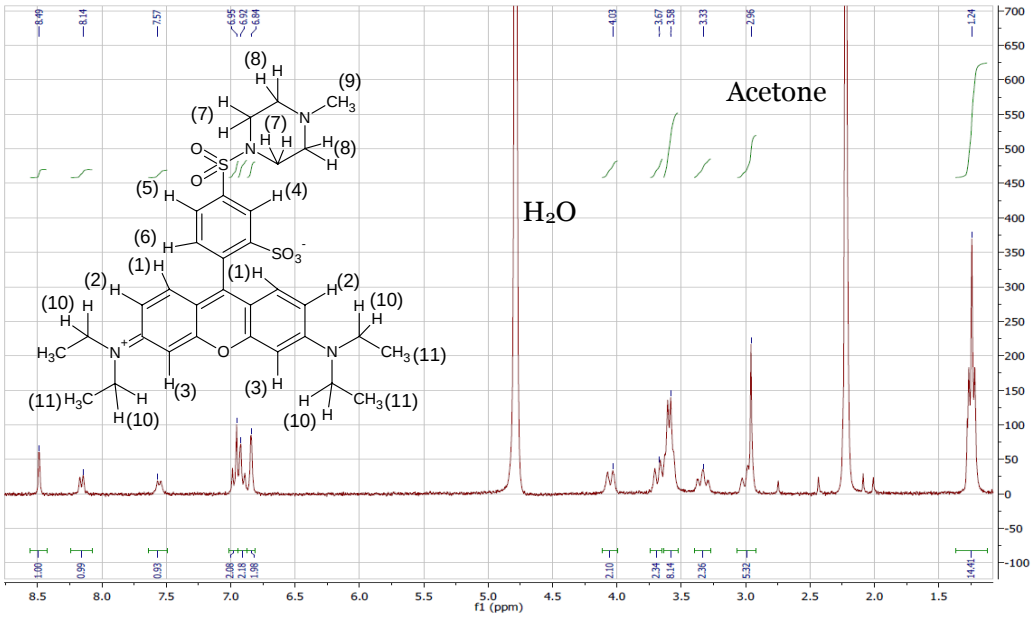

Figure A-64: ^{1}H NMR of **2b** (300 MHz, D_2O, 0.1% HCl conc., TMS): δ = 8.49 (1H, d, J = 1.5 Hz, H(4)); 8.14 (1H, broad d, J = 7.8 Hz, H(5)); 7.57 (1H, d, J = 7.6 Hz, H(6)); 6.95 (2H, d, J = 9.7 Hz, H(1)); 6.92 (2H, dd, J_1 = 10.0 Hz, J_2 = 1.2 Hz , H(2)); 6.84 (2H, d, J = 1.1 Hz, H(3)); 4.03 (2H, d, J = 12.6 Hz, H(7)); 3.64 – 3.73 (2H, d, J = 12.3 Hz, H(7)); 3.53 – 3.64 (8H, q, J = 7.1 Hz, H(10)); 3.33 (3H, d, J = 12.6 Hz, H(8)); 2.92 – 3.06 (5H, m, H(8,9)); 1.24 (12H, 7, J = 6.9 Hz, H(11)).

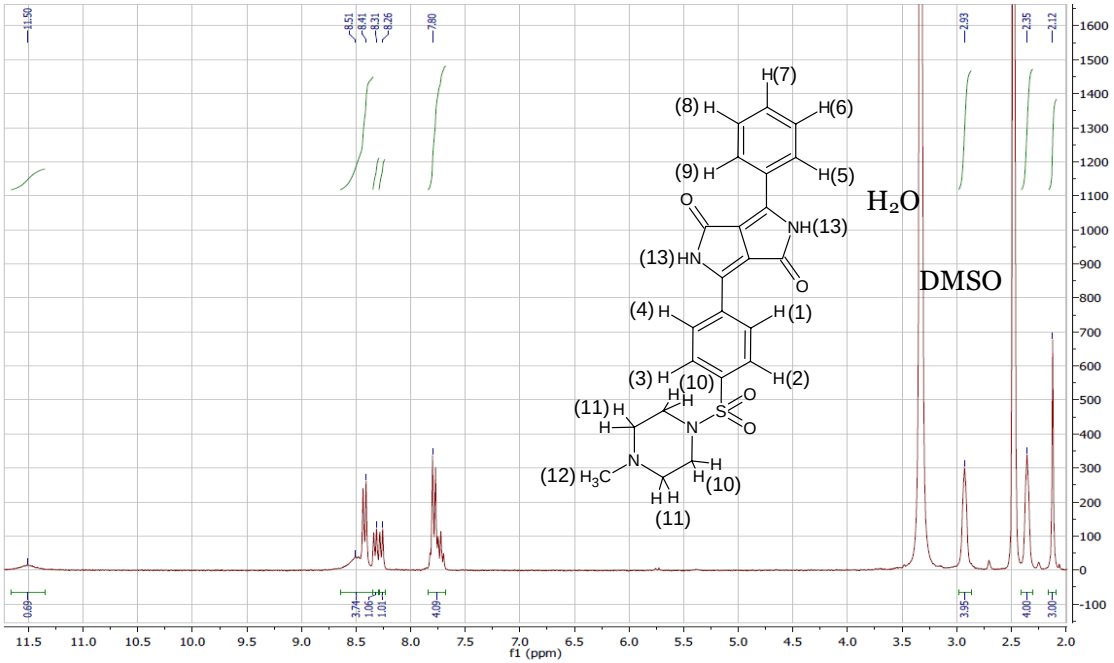

Figure A-65: ^{1}H NMR of **3b** (300 MHz, $(CD_3)_2SO$, TMS): δ = 11.50 (1H, broad s, H(9)); 8.45 – 8.7 (2H, broad, H(13)); 8.41 (2H, d, J = 8.4 Hz, H(2,3)); 8.25 – 8.35 (2H, 2d, J = 7.7 Hz, H(5,8)); 7.68 – 7.83 (4H, m, H(1,4,6,7)); 2.93 (4H, broad t, H(10)); 2.35 (4H, broad t, H(11)); 2.12 (3H, s, H(12)).

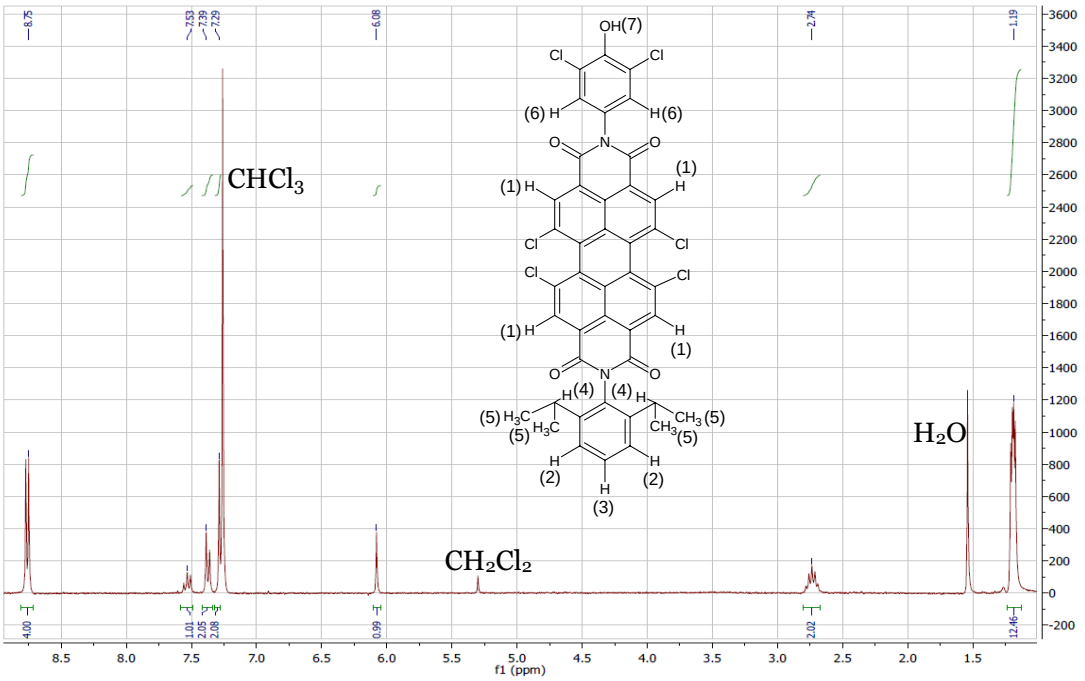

Figure A-66: ^{1}H NMR of **4a** (300 MHz, $CDCl_3$, TMS): δ = 8.75 (4H, 2s, H(1)); 7.53 (1H, t, J = 7.7 Hz, H(3)); 7.39 (2H, d, J = 7.9 Hz, H(2)); 7.29 (2H, s, H(6)); 6.08 (1H, s, H(7)); 2.74 (2H, quint, J = 6.7 Hz, H(4)); 1.19 (12H, dd, J_1 = 6.9 Hz, J_2 = 3.6 Hz, H(5)).

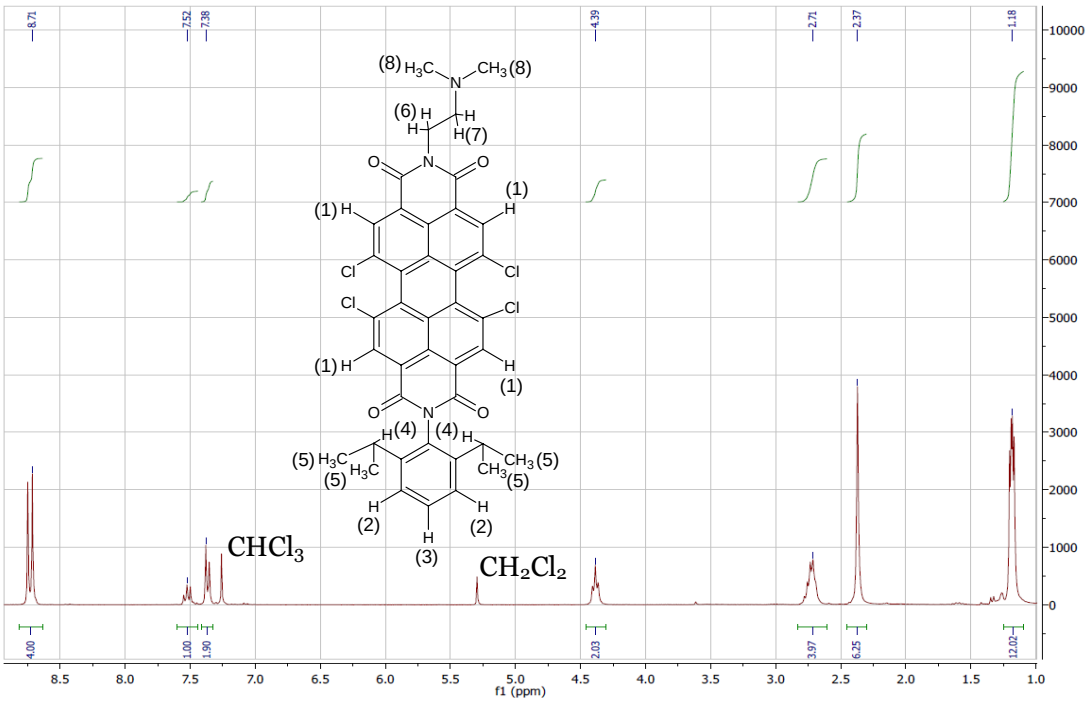

Figure A-67: ^{1}H NMR of **4b** (300 MHz, $CDCl_3$, TMS): δ = 8.71 (4H, 2s, H(1)); 7.52 (1H, t, J = 7.6 Hz, H(3)); 7.38 (2H, d, J = 7.7 Hz, H(2)); 4.41 (2H, t, J = 5.7 Hz, H(6)); 2.76 (4H, m, H(4,7)); 2.42 (6H, s, H(8)); 1.18 (12H, dd, J_1 = 3.7 Hz, J_2 = 3.2 Hz, H(5)).

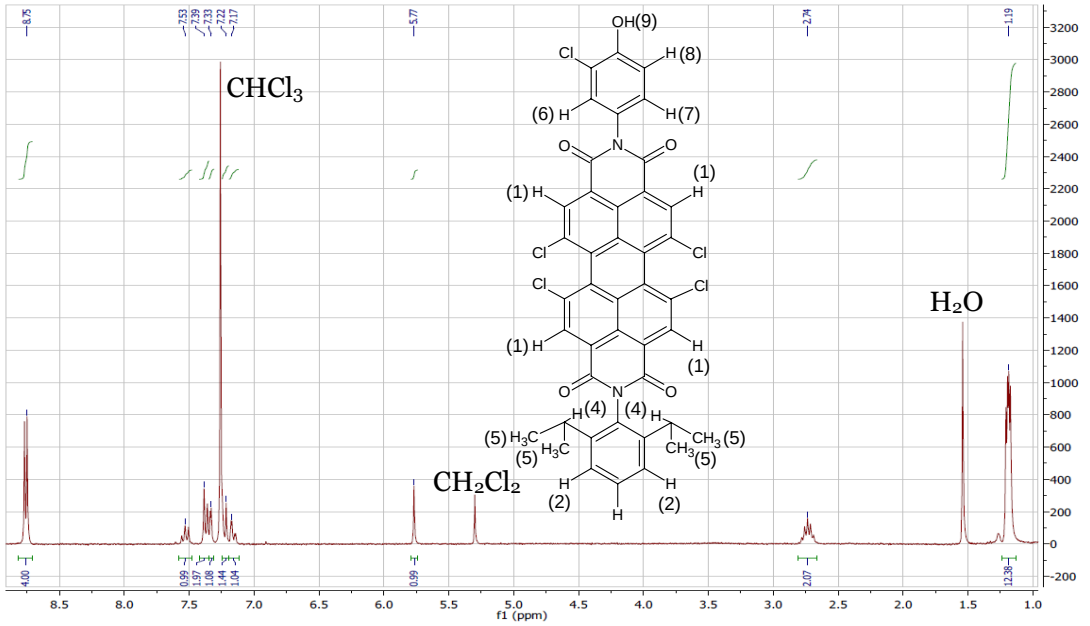

Figure A-68: ^{1}H NMR of **4c** (300 MHz, $CDCl_3$, TMS): δ = 8.75 (4H, 2s, H(1)); 7.53 (1H, t, J = 7.8 Hz, H(3)); 7.39 (2H, d, J = 7.8 Hz, H(2)); 7.33 (1H, d, J = 2.3 Hz, H(6)); 7.22 (1H, d, J = n.m. due to $CHCl_3$, H(8)); 7.17 (1H, dd, J_1 = 8.7 Hz, J_2 = 2.3 Hz, H(7)); 5.77 (1H, s, H(9)); 2.74 (2H, quint, J = 6.8 Hz, H(4)); 1.19 (12H, dd, J_1 = 6.6 Hz, J_2 = 3.6 Hz, H(5)).

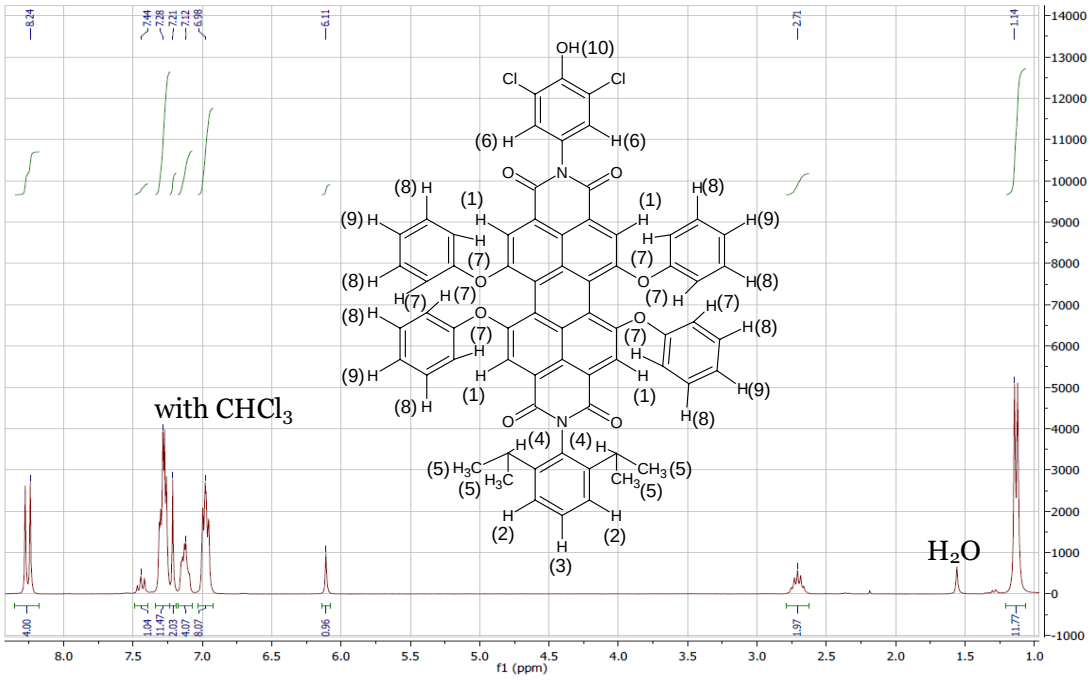

Figure A-69: ^{1}H NMR of **5a** (300 MHz, $CDCl_3$, TMS): δ = 8.24 (4H, 2s, H(1)); 7.44 (1H, t, J = 8.4 Hz, H(3)); 7.23 – 7.34 (10H, m, H(2,8)); 7.21 (2H, s, H(6)); 7.12 (4H, m, H(9)); 6.98 (8H, t, J = 6.5 Hz, H(7)); 6.11 (1H, s, H(10)); 2.71 (2H, quint, J = 6.4 Hz , H(4)); 1.14 (12H, d, J = 6.6 Hz, H(5)).

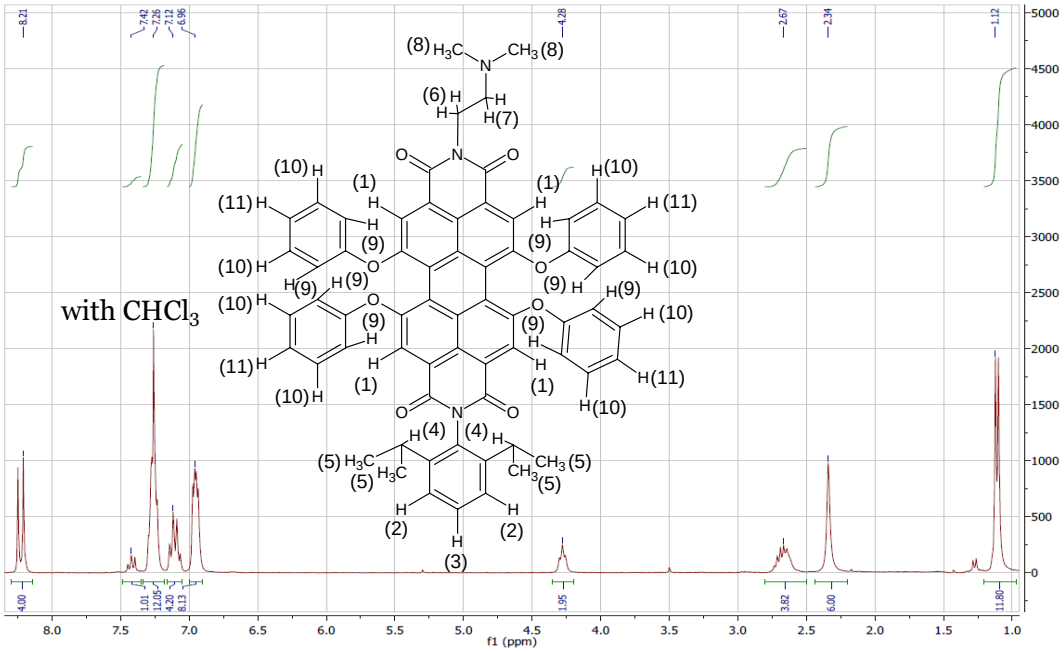

Figure A-70: ^{1}H NMR of **5b** (300 MHz, $CDCl_3$, TMS): δ = 8.21 (4H, 2s, H(1)); 7.42 (1H, t, J = 7.8 Hz, H(3)); 7.20 – 7.33 (10H, m, H(2,10)); 7.12 (4H, q, J = 7.8 Hz, H(11)); 6.96 (8H, q, J = 3.9 Hz, H(9)); 4.28 (2H, t, J = 6.8 Hz, H(6)); 2.58 – 2.75 (4H, m, (4,7)); 2.34 (6H, s, H(8)); 1.12 (12H, d, J = 6.8 Hz, H(5)).

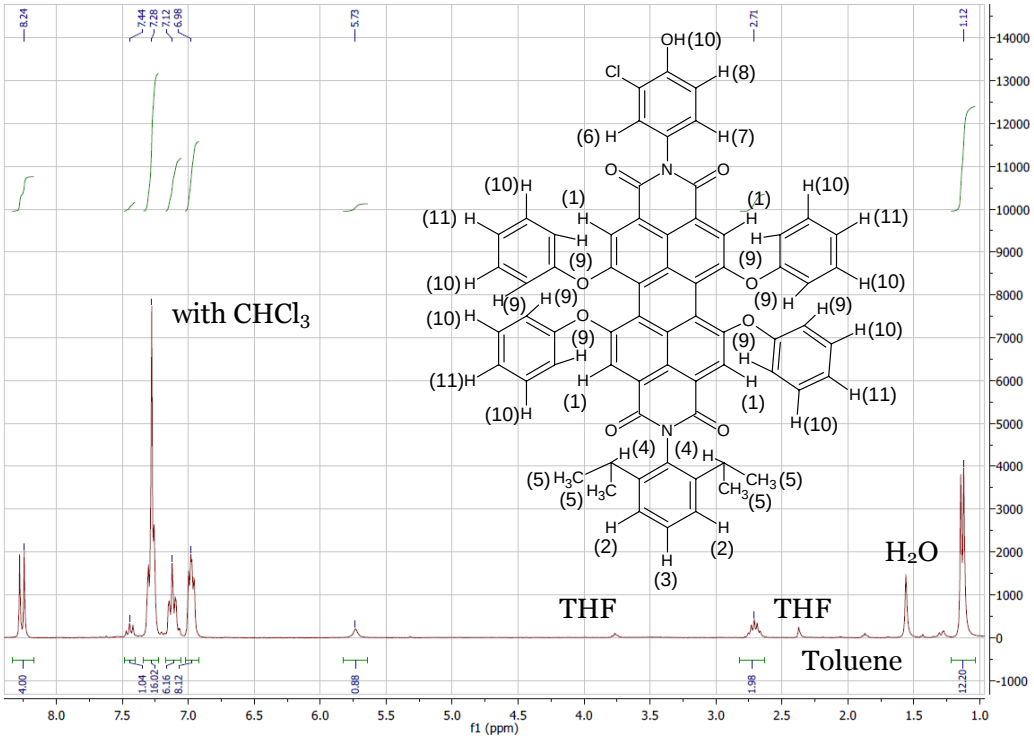

Figure A-71: ^{1}H NMR of **5c** (300 MHz, $CDCl_3$, TMS): δ = 8.24 (4H, 2s, H(1)); 7.44 (1H, t, J = 8.2 Hz, H(3)); 7.23 – 7.33 (11H, m, H(2,6,10)); 7.06 – 7.16 (6H, m, H(7,8,11)); 6.98 (4H, dd, J_1 = 5.1 Hz, J_2 = 7.5 Hz, H(9)); 5.73 (1H, s, H(12)); 2.71 (2H, quint, J = 6.3 Hz , H(4)); 1.12 (12H, d, J = 6.8 Hz, H(5)).

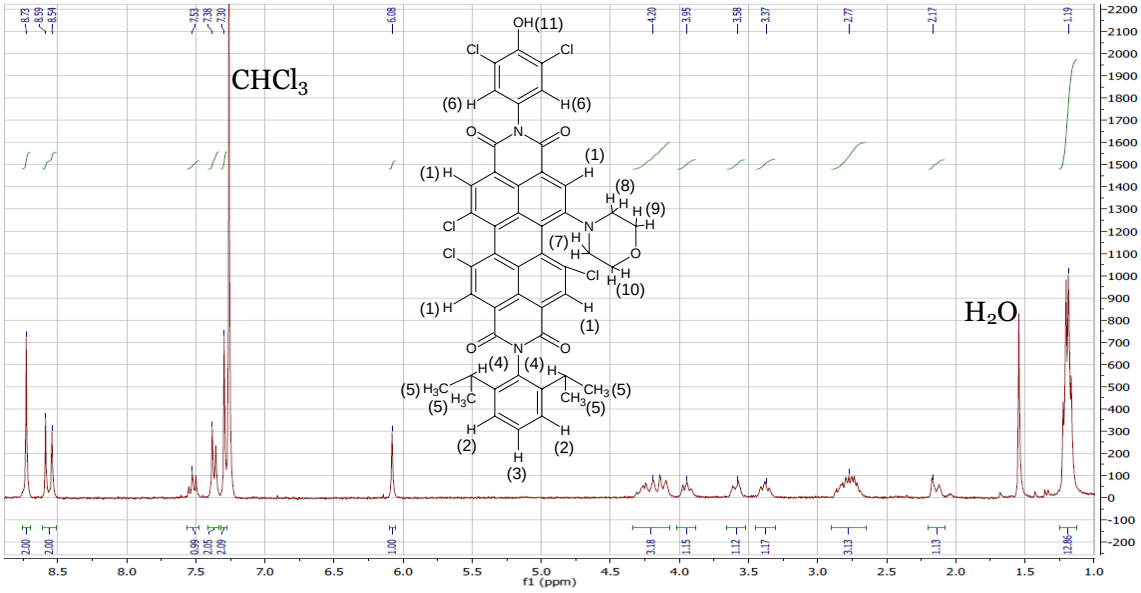

Figure A-72: ^{1}H NMR of **6a** (300 MHz, $CDCl_3$, TMS): δ = 8.73 (2H, s, H(1)); 8.59 (1H, s, H(1)); 8.54 (1H, s, H(1)); 7.53 (1H, t, J = 7.8 Hz, H(3)); 7.38 (2H, d, J = 7.7 Hz, H(2)); 7.30 (2H, s, H(6)); 6.08 (1H, s, H(11)); 4.07 – 4.32 (3H, m, H(7,10)); 3.95 (1H, t, J = 8.9 Hz, H(10)); 3.58 (1H, d, J = 11.4 Hz, H(9)); 3.37 (1H, t, J = 8.8 Hz, H(9)); 2.65 – 2.90 (3H, m, H(4,8)); 2.17 (1H, d, J = 13.7 Hz, H(8)); 1.19 (12H, dd, J_1 = 6.5 Hz, J_2 = 11.8 Hz, H(5)).

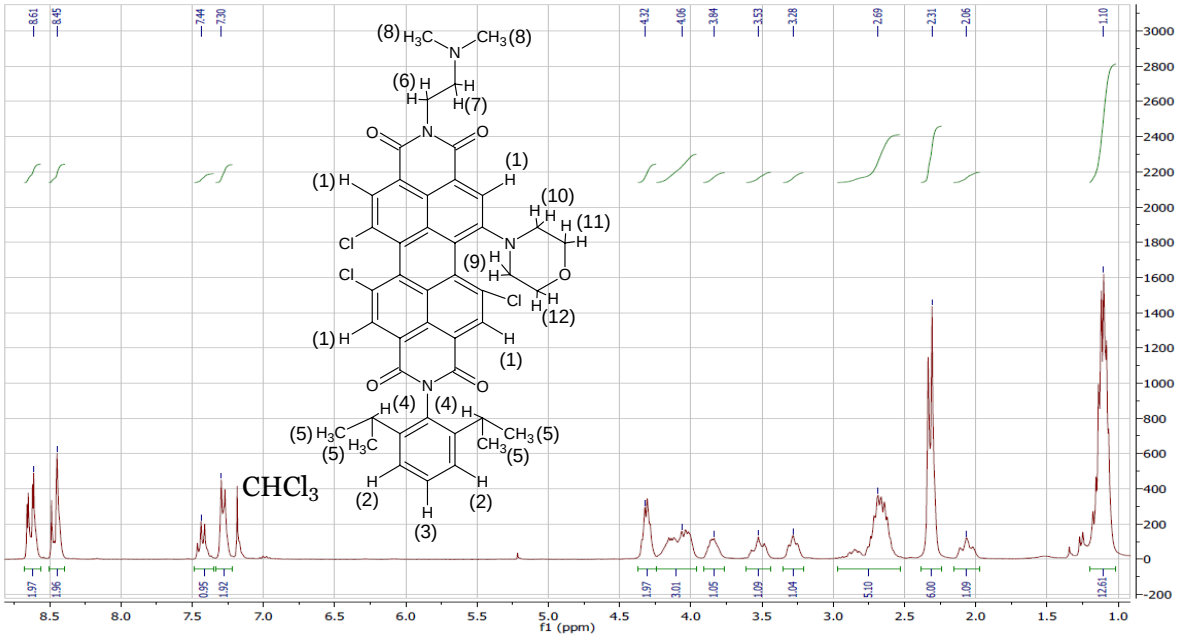

Figure A-73: ^{1}H NMR of **6b** (300 MHz, $CDCl_3$, TMS): δ = 8.61 (2H, m, H(1)); 8.45 (2H, m, H(1)); 7.44 (1H, t, J = 7.8 Hz, H(3)); 7.30 (2H, d, J = 7.6 Hz, H(2)); 7.30 (2H, d, J = 7.6 Hz, H(2)); 4.32 (2H, m, H(6)); 3.95 – 4.25 (3H, m, H(9,12)); 3.84 (1H, m, H(12)); 3.53 (1H, t, J = 12.3 Hz, H(11)); 3.28 (1H, t, J = 8.4 Hz, H(11)); 2.55 – 2.95 (5H, m, H(4,7,10)); 2.31 (6H, 2d, H(8)); 2.06 (1H, t, J = 13.5 Hz, H(10)); 1.10 (12H, m, H(5)).

MALDI-TOF Mass Spectroscopy

For the products 4-6, in addition to $[MH]^+$ and $[MNa]^+$, M^+ $[M - H]^+$ and $[M - 2H]^+$ (products of photoionization) were in some cases detected

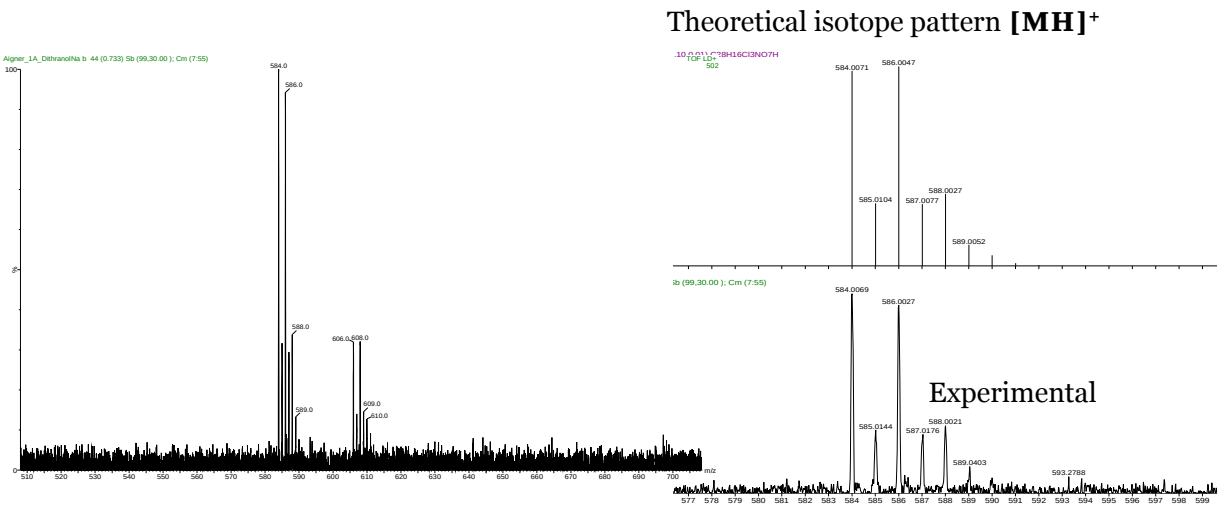

Figure A-74: MALDI-TOF spectrum of **1a**

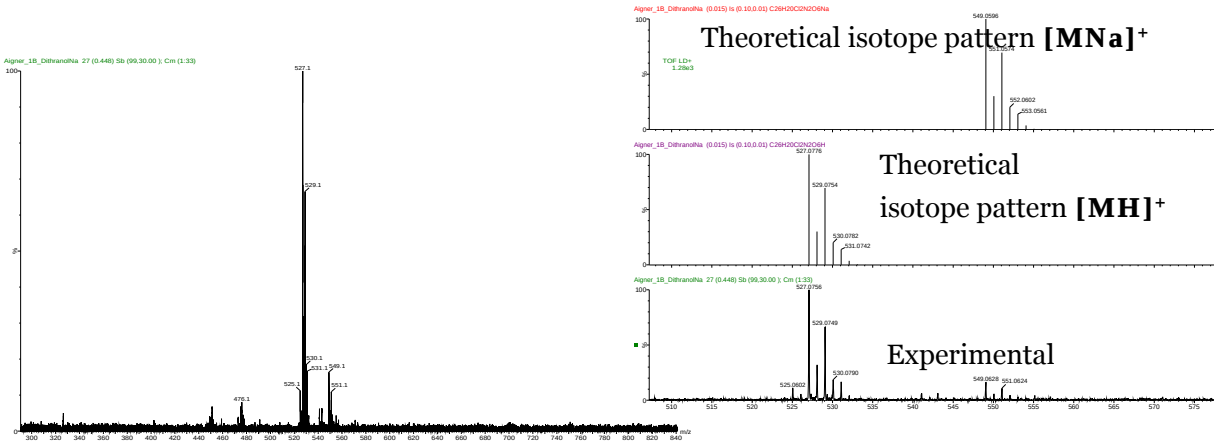

Figure A-75: MALDI-TOF spectrum of **1b**

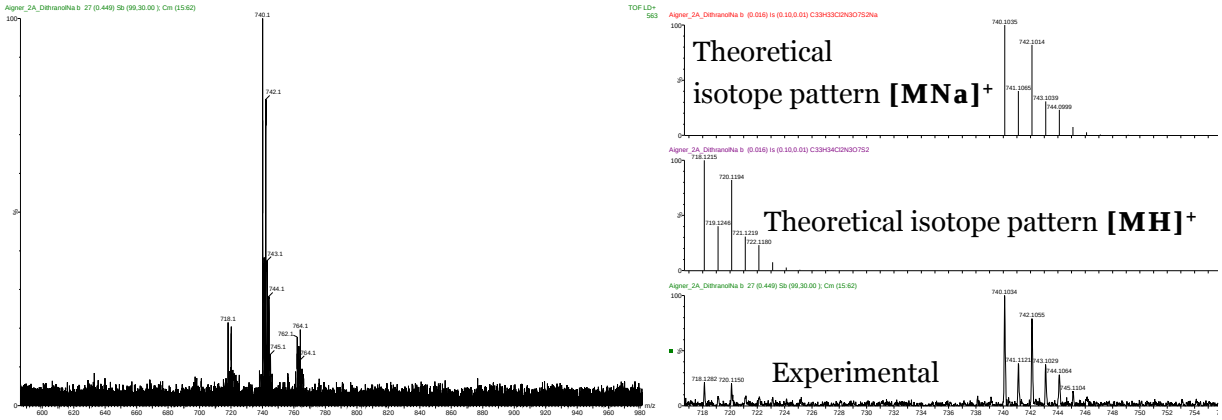

Figure A-76: MALDI-TOF spectrum of **2a**

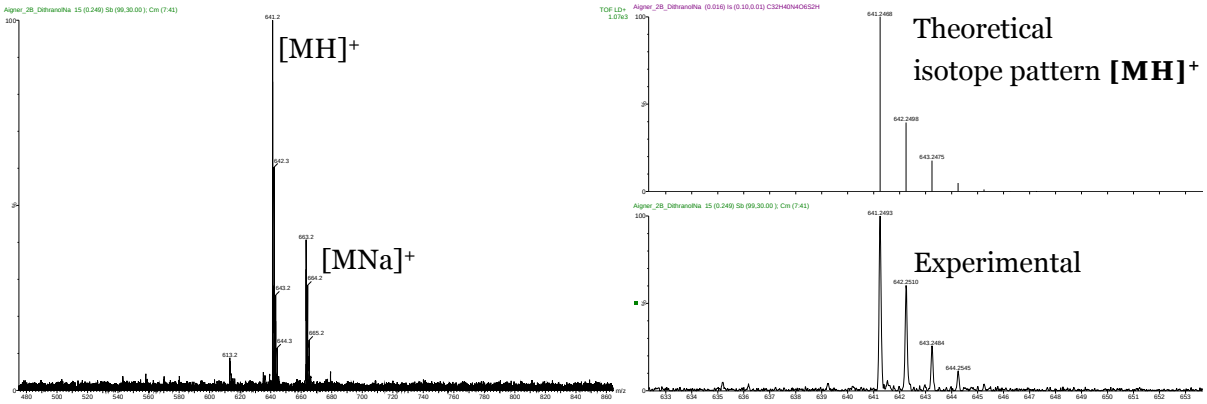

Figure A-77: MALDI-TOF spectrum of **2b**

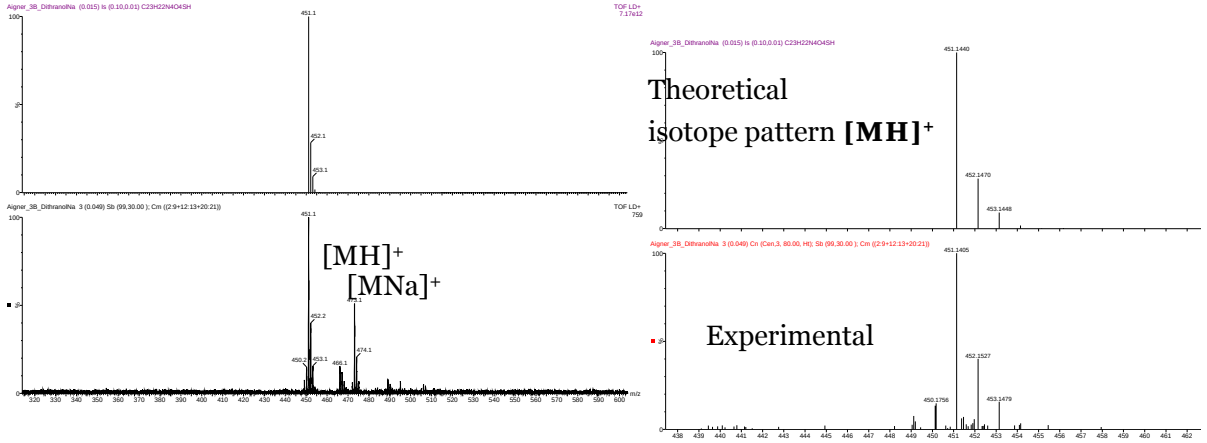

Figure A-78: MALDI-TOF spectrum of **3b**

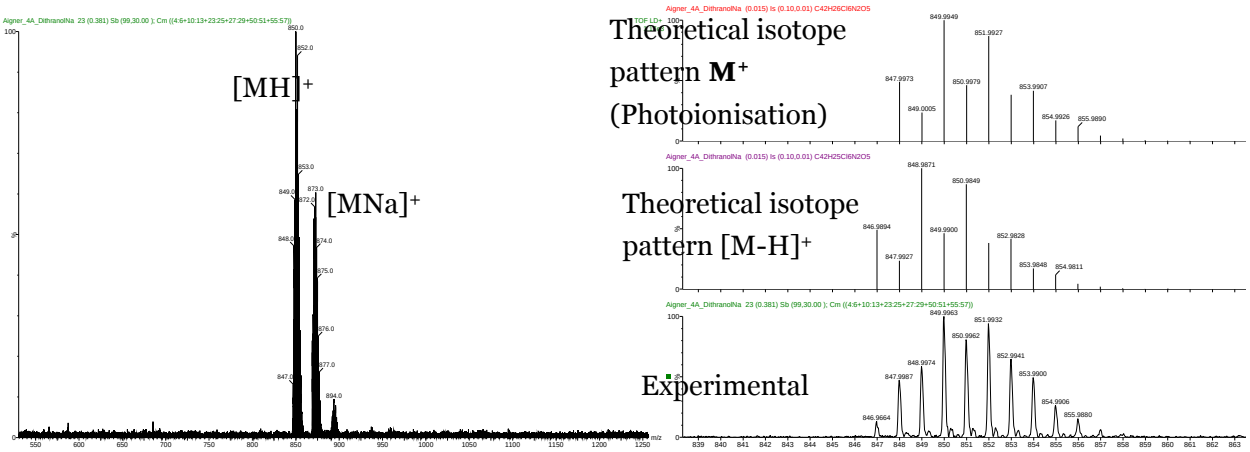

Figure A-79: MALDI-TOF spectrum of **4a**

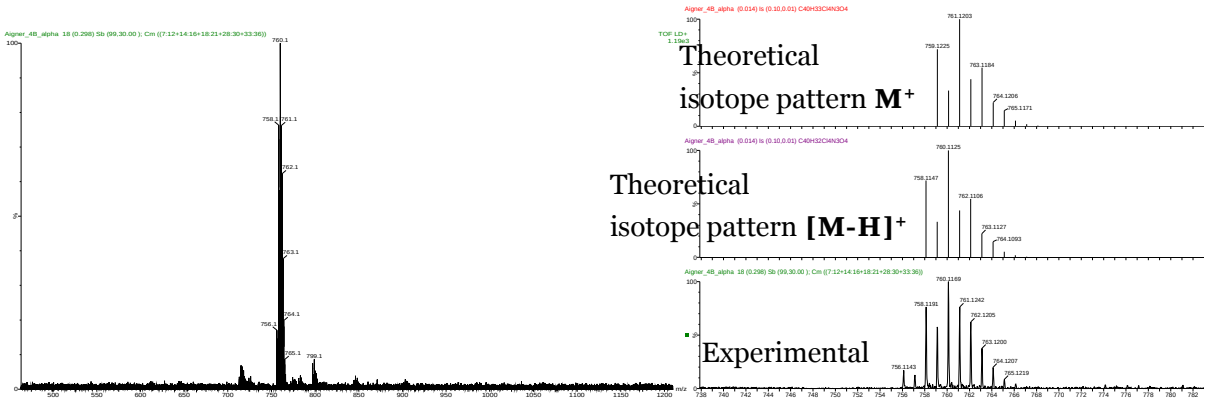

Figure A-80: MALDI-TOF spectrum of **4b**

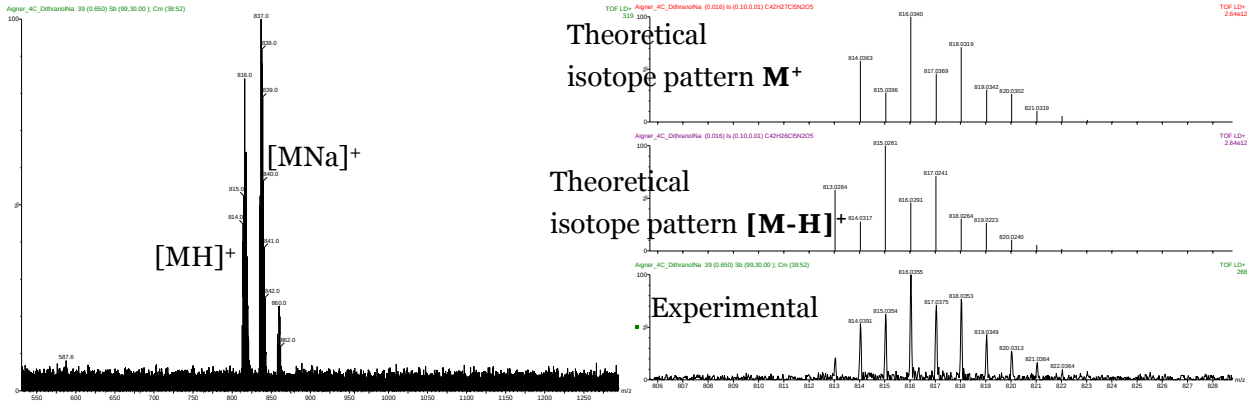

Figure A-81: MALDI-TOF spectrum of **4c**

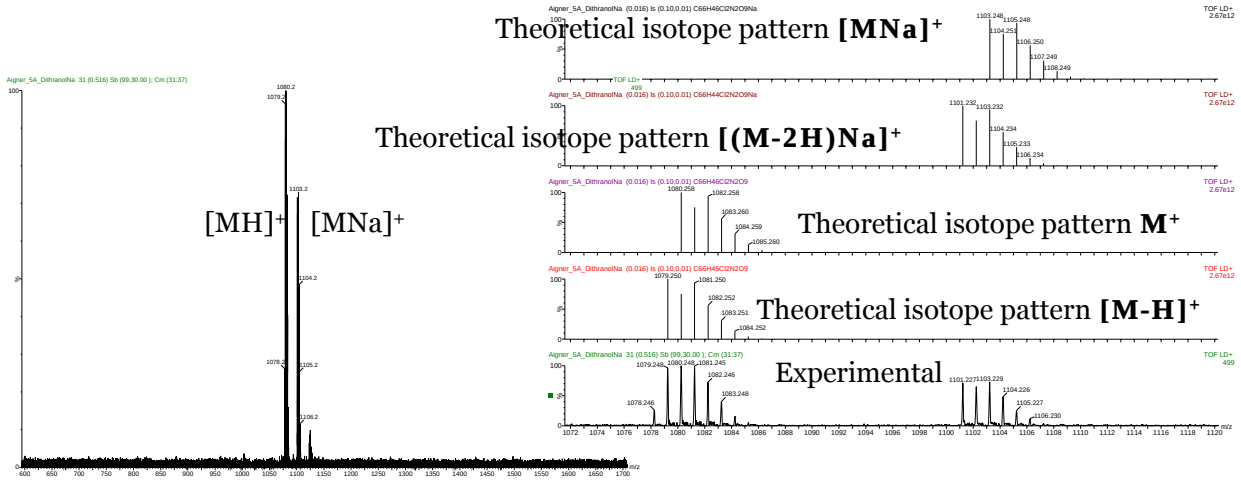

Figure A-82: MALDI-TOF spectrum of **5a**

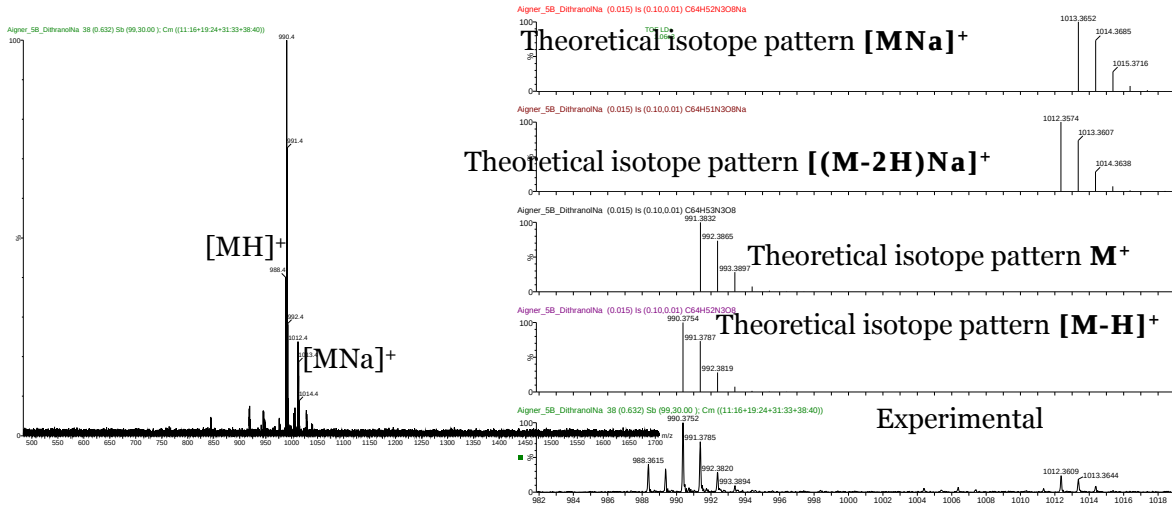

Figure A-83: MALDI-TOF spectrum of **5b**

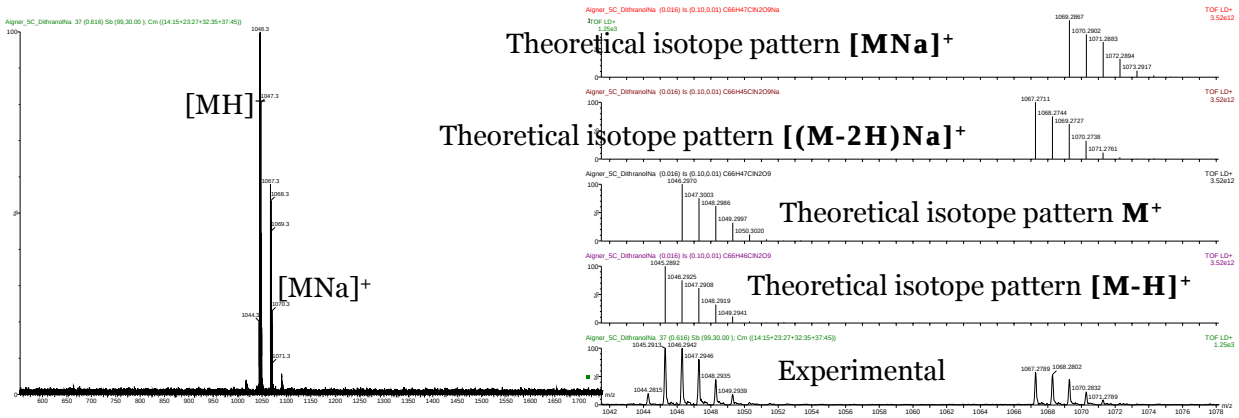

Figure A-84: MALDI-TOF spectrum of **5c**

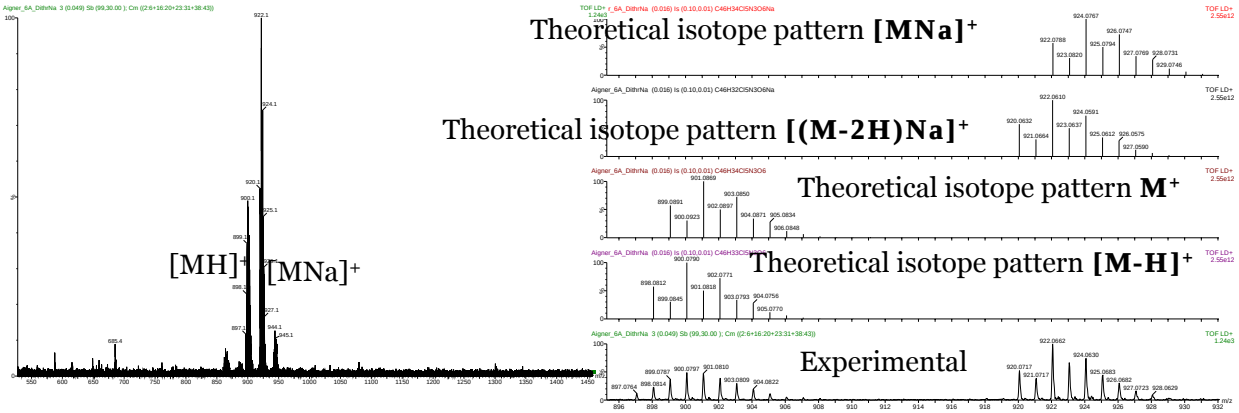

Figure A-85: MALDI-TOF spectrum of **6a**

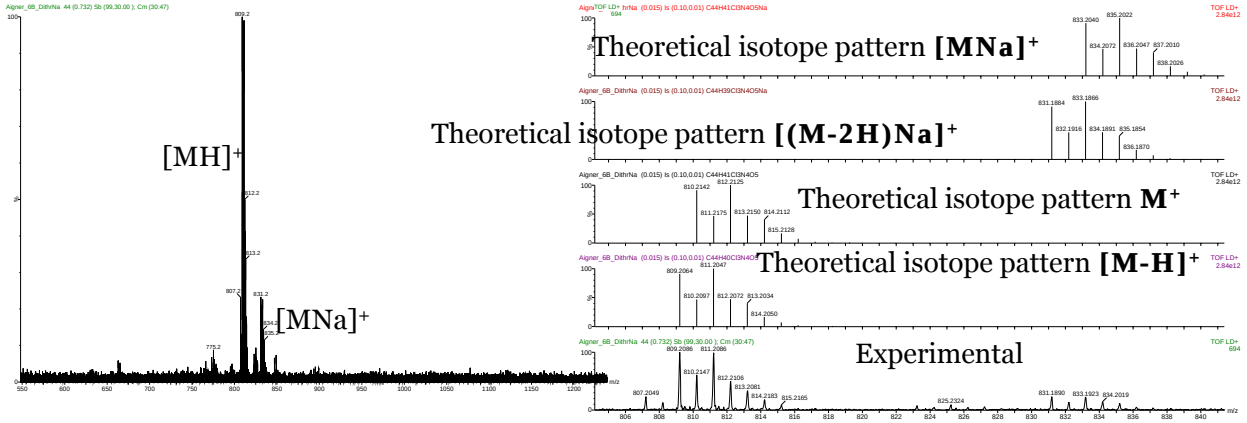

Figure A-86: MALDI-TOF spectrum of **6b**

Chapter 6

Perylene Bisimides for FLIM-based pH Measurements in 2D and 3D Cell Models

NMR Spectra:

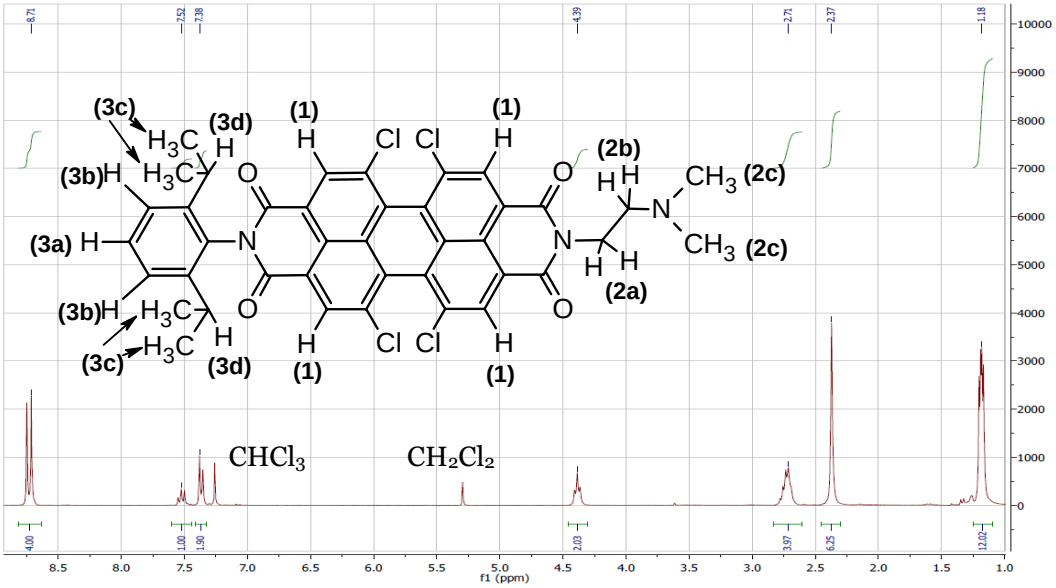

Figure A-87: ^{1}H NMR-spectrum (300MHz, CDCl3, TMS) of *N*-(2,6-Diisopropylphenyl)-*N'*-(2-dimethylaminoethyl)-1,6,7,12-tetrachloroperylene-3,4:9,10-tertracarboxylic bisimide; δ = 8.71 (4H, 2s, H(1)), 7.52 (1H, t, H(3a)), 7.38 (2H, d, J = 7.7Hz, H(3b)), 4.39 (2H, t, J = 6.3Hz, H(2a)), 2.6 – 2.8 (4H, m, H(2b) and H(3d), 2.37 (6H, s, H(2c)), 1.18 (12H, dd, J_1 = 3.7 Hz, J_2 = 3.2 Hz, H(3c)).

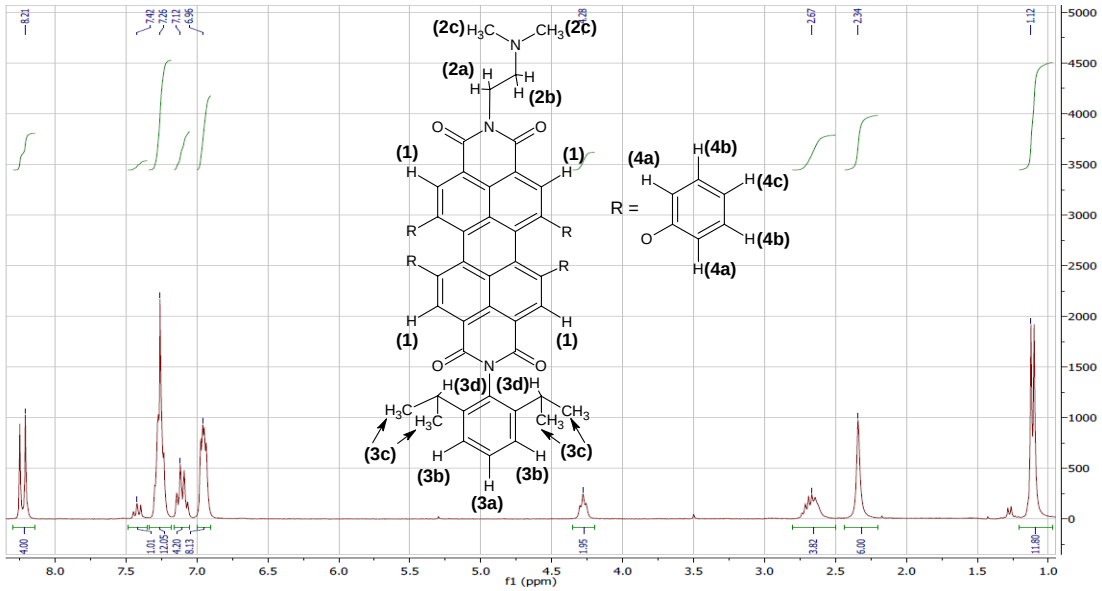

Figure A-88: ^{1}H NMR-spectrum (300MHz, CDCl3, TMS) of **2**; δ = 8.21 (4H, 2s, H(1)); 7.42 (1H, t, J = 7.8 Hz, H(3a)); 7.20 – 7.33 (10H, m, H(3b,4b)); 7.12 (4H, q, J = 7.8 Hz, H(4c)); 6.96 (8H, q, J = 3.9 Hz, H(4a)); 4.28 (2H, t, J = 6.8 Hz, H(2a)); 2.58 – 2.75 (4H, m, (2b,3d)); 2.34 (6H, s, H(2c)); 1.12 (12H, d, J = 6.8 Hz, H(3c)).

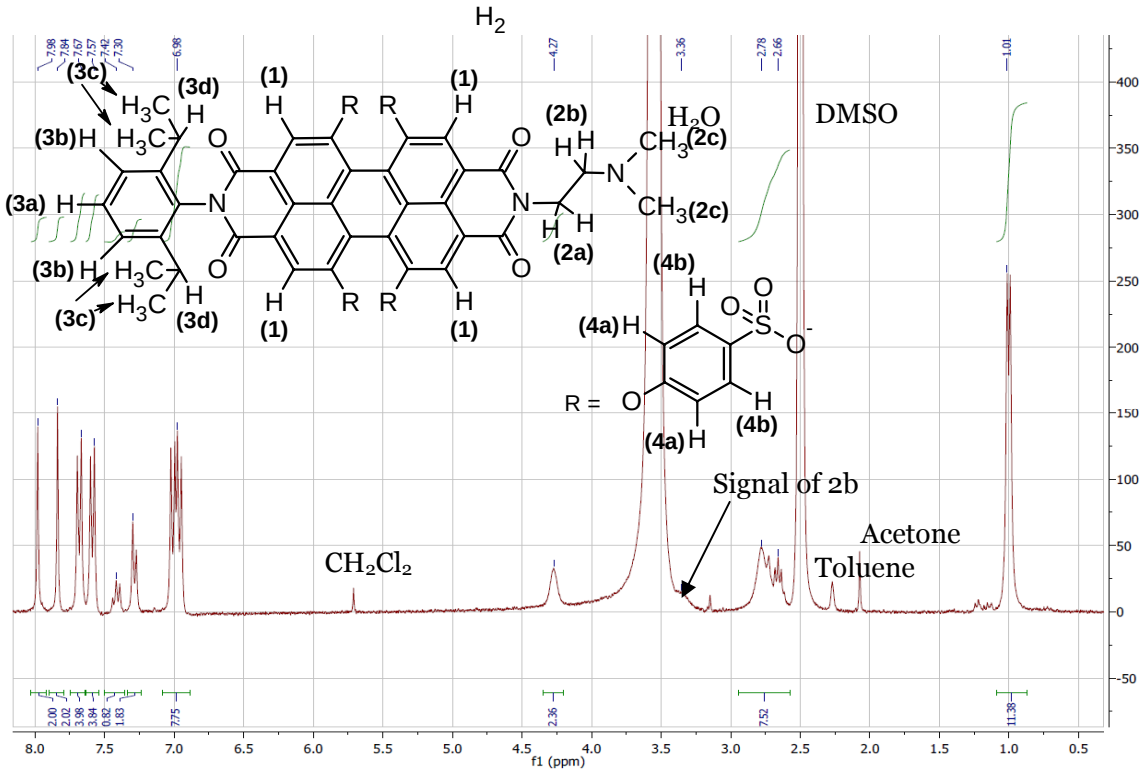

Figure A-89: ^{1}H NMR-spectrum (300MHz, $(CD_3)_2SO$:D_2O 20:1 (V/V), TMS) of **3**; δ = 7.98 (2H, s, H(1)), 7.84 (2H, s, H(1)), 7.68 (4H, d, J = 8.7Hz, H(4b)), 7.59 (4H, d, J = 8.4Hz, H(4b)), 7.42 (1H, t, J = 7.6Hz, H(3a)), 7.28 (2H, d, H(3b)), 6.98 (8H, 2d, H(4a)), 4.27 (2H, broad s, H(2a)), 3.25 – 3.4 (2H, broad s, H(2b)), 2.6 – 2.9 (8H, m, H(2c) and H(3d)), 1.01 (12H, d, J = 6.6Hz, H(3c)). An unusual shift for H_2O (3.5 instead of 3.3 ppm) is probably caused by difficulties upon shimming, as 5% of D_2O had to be added to DMSO-d6 to provide sufficient solubility of the dye.

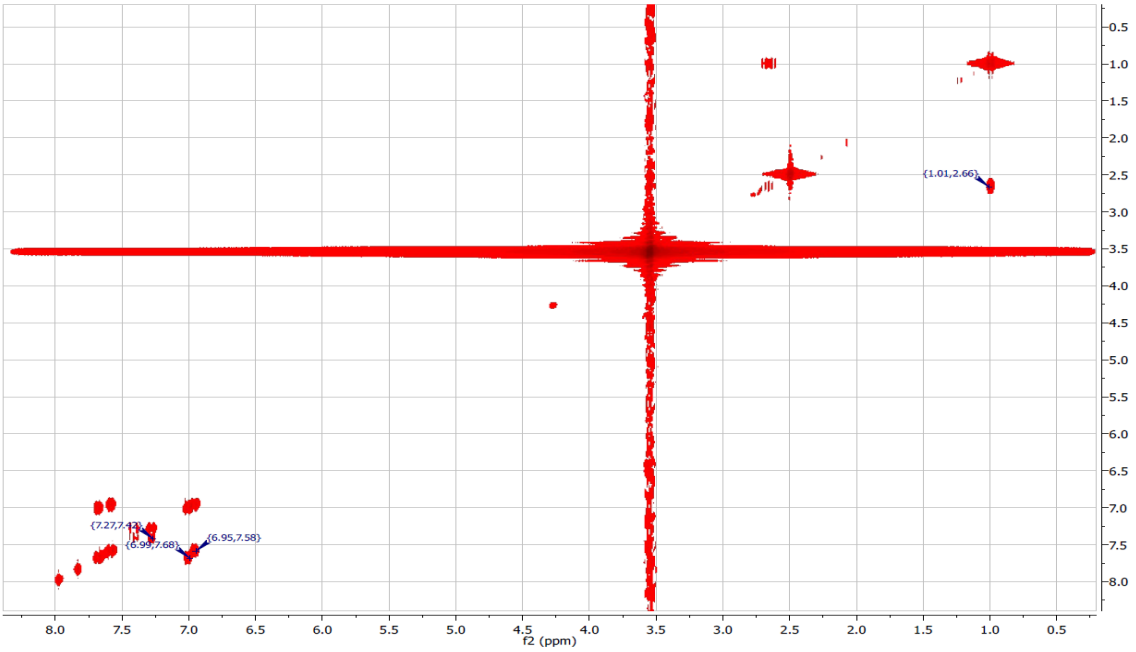

Figure A-90: HH-COSY NMR-spectrum (300MHz, $(CD_3)_2SO$:D_2O 20:1 (V/V), TMS) of **3**.

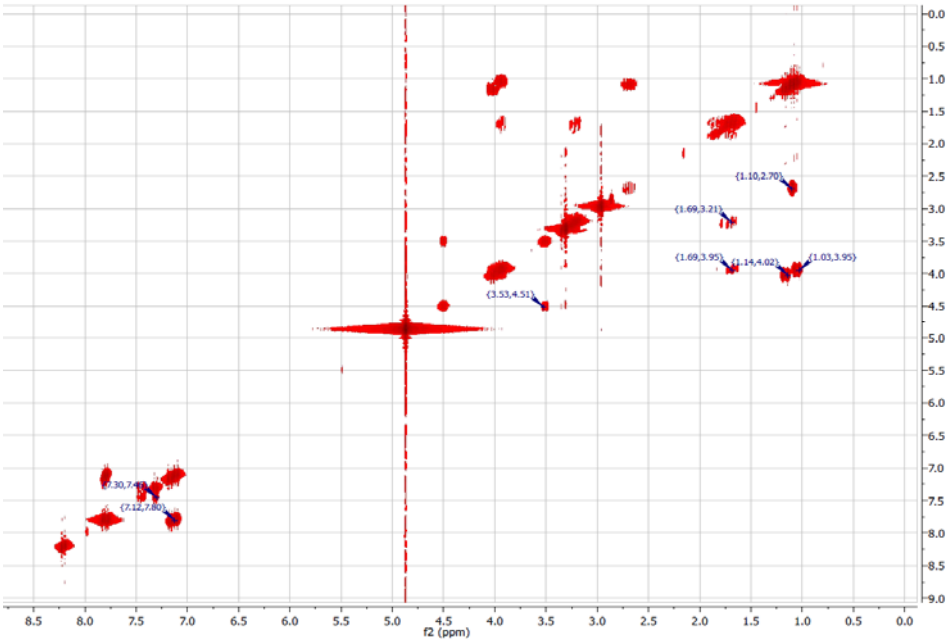

Figure A-91: HH-COSY-NMR-spectrum (300MHz, CD_3OD, TMS) of **MP**.

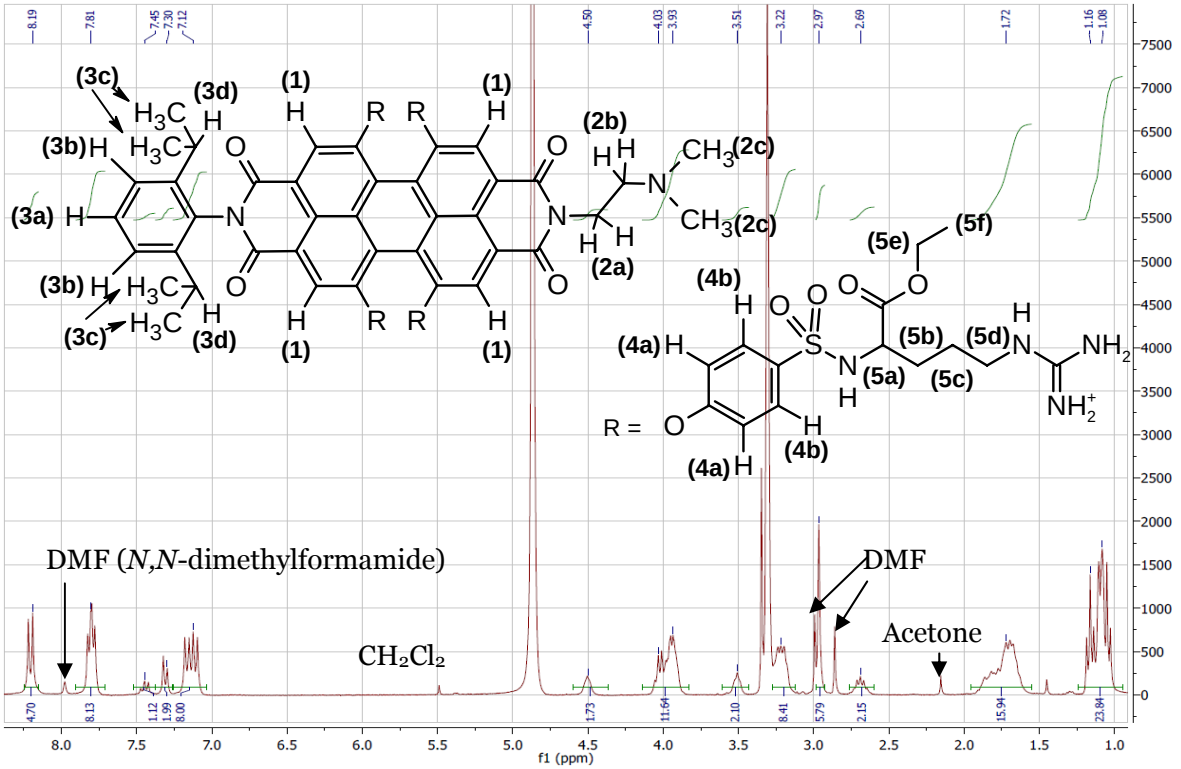

Figure A-92: ^{1}H NMR-spectrum (300MHz, CD_3OD, TMS) of **MP**; δ = 8.19 (4H, d, H(1)), J = 8.4Hz), 7.81 (8H, dd, J_1 = 6.2Hz, J_2 = 8.5Hz, H(4b)), 7.45 (1H, t, J = 7.8Hz, H(3a)), 7.30 (2H, d, J = 7.6Hz, H(3b)), 7.12 (8H, dd, J_1 = 8.6Hz, J_2 = 16.5Hz, H(4a)), 4.50 (2H, broad s, H(2a)), 3.85 – 4.10 (12H, m, H(5a) and H(5e)), 3.51 (2H, broad s, H(2b)), 3.22 (8H, m, H(5d)), 2.97 (6H, s, H(2c)), 2.69 (2H, p, J = 6.8Hz, H(3d)), 1.6 – 1.9 (16H, m, H(5b) and H(5c)), 1.0 – 1.23 (24H, m, H(3c) and H(5f)).

MALDI-TOF Spectra:

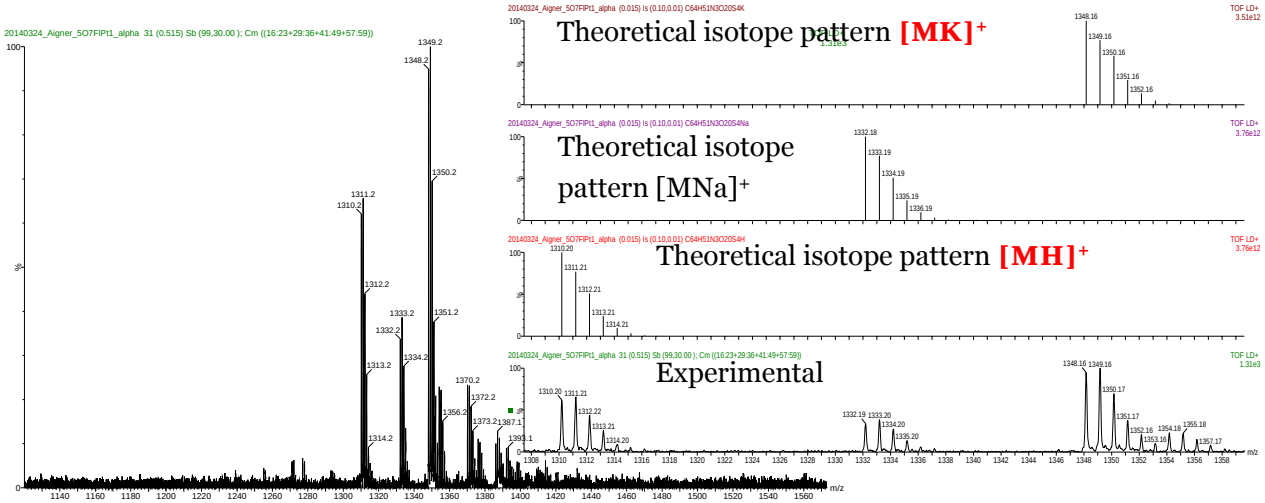

Figure A-93: MALDI-TOF-spectrum of **3.** Maxima at *m/z* = 1270-1272 and 1287.1 correspond to [MNa_2K^+] and to [$MNaK_2^+$], respectively.

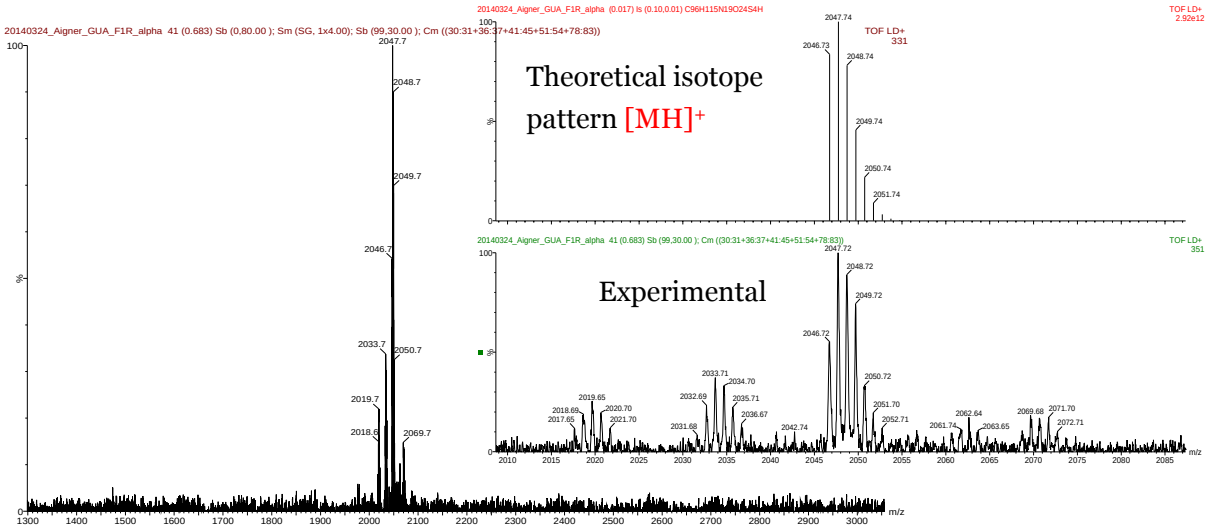

Figure A-94: MALDI-TOF-spectrum of **MP**. Maxima at *m/z* = 2061 – 2064 and 2069 – 2073. Correspond to [MNa^+] and to [MNK^+], respectively. *m/z* = Those around 2033.71 and 2019.65 most likely originate from small amounts of **MP** monomethylester and **MP** monocarboxylate (transesterification or hydrolysis of one of the four ethyl ester groups in **MP** which can occur during HPLC-chromotography or concentration after purification, catalyzed by formic acid.

HPLC Purification Details for **MP**:

Table A-7: HPLC gradient used for the purification of MP (Temperature 30°C).

Time/min	Ratio MeOH/%	Ratio 0.01% aqueous formic acid/%	Flow rate/ml·min^{-1}
0	35	65	20
35	70	70	20
35.1	100	0	20
39	100	0	20